DNA Assisted Ordered Assembly of Small Amphiphilic Molecules via Non-covalent Interactions

By

ANJALI B. R.

10CC16A39005

A thesis submitted to the
Academy of Scientific and Innovative Research
for the award of the degree of
DOCTOR OF PHILOSOPHY
in
SCIENCE

Under the supervision of
Dr. JOSHY JOSEPH

CSIR-National Institute for Interdisciplinary Science and Technology (CSIR-NIIST), Thiruvananthapuram – 695 019, India

Academy of Scientific and Innovative Research
AcSIR Headquarters, CSIR-HRDC campus
Sector 19, Kamla Nehru Nagar,
Ghaziabad, U.P. – 201 002, India

June 2022

Dedicated to

Arju... ❤️

Achan, Amma

&

Ashi

National Institute for Interdisciplinary Science and Technology (CSIR-NIIST)

Council of Scientific & Industrial Research (CSIR)
Industrial Estate P. O., Trivandrum - 695 019
Kerala, INDIA

Dr. Joshy Joseph
Principal Scientist & Associate Professor
Chemical Sciences and Technology Division

Tel: +91-471-2515 476
Fax: +91-471-2491 712
E-mail: joshyja@gmail.com, joshy@niist.res.in

CERTIFICATE

This is to certify that the work incorporated in this Ph.D. thesis entitled, *"DNA Assisted Ordered Assembly of Small Amphiphilic Molecules via Non-covalent Interactions"*, submitted by **Ms. Anjali B. R.** to the Academy of Scientific and Innovative Research (AcSIR) in fulfilment of the requirements for the award of the Degree of **Doctor of Philosophy in Sciences**, embodies original research work carried-out by the student. We further certify that this work has not been submitted to any other University or Institution in part or full for the award of any degree or diploma. Research materials obtained from other sources and used in this research work have been duly acknowledged in the thesis. Images, illustrations, figures, tables etc., used in the thesis from other sources, have also been duly cited and acknowledged.

20/06/2022

Anjali B. R.

20.06.2022

Dr. Joshy Joseph
(Thesis Supervisor)

STATEMENTS OF ACADEMIC INTEGRITY

I, Anjali B. R., a Ph. D. student of the Academy of Scientific and Innovative Research (AcSIR) with Registration No. 10CC16A39005 hereby undertake that, the thesis entitled *"DNA Assisted Ordered Assembly of Small Amphiphilic Molecules via Non-covalent Interactions"* has been prepared by me and that the document reports original work carried out by me and is free of any plagiarism in compliance with the UGC Regulations on *"Promotion of Academic Integrity and Prevention of Plagiarism in Higher Educational Institutions (2018)"* and the CSIR Guidelines for *"Ethics in Research and in Governance (2020)".*
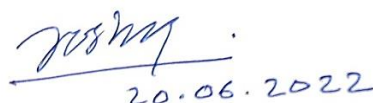
Anjali B. R.

June 20, 2022

Thiruvananthapuram

It is hereby certified that the work done by the student, under my supervision, is plagiarism-free in accordance with the UGC Regulations on *"Promotion of Academic Integrity and Prevention of Plagiarism in Higher Educational Institutions (2018)"* and the CSIR Guidelines for *"Ethics in Research and in Governance (2020)".*

Dr. Joshy Joseph

June 20, 2022

Thiruvananthapuram

DECLARATION

I, Anjali B. R., bearing AcSIR Registration No. 10CC16A39005 declare that my thesis entitled, *"DNA Assisted Ordered Assembly of Small Amphiphilic Molecules via Non-covalent Interactions"* is plagiarism free in accordance with the UGC Regulations on *"Promotion of Academic Integrity and Prevention of Plagiarism in Higher Educational Institutions (2018)"* and the CSIR Guidelines for *"Ethics in Research and in Governance (2020)".*

I would be solely held responsible if any plagiarised content in my thesis is detected, which is violative of the UGC regulations 2018.

20/06/2022

Anjali B.R.

June 20, 2022

Thiruvananthapuram

ACKNOWLEDGEMENTS

TABLE OF CONTENTS

CHAPTER 2 : PART B — **Anionic Polymer Assisted Ordered Assembly of Amphiphilic Fullerenes with Enhanced Electron Transport Properties** — **97-117**

CHAPTER 3 — **Hierarchical Assembly And DNA Assisted Reassembly of Tetraphenylethylene Amphiphiles** — **119-169**

LIST OF ABBREVIATIONS

Å	Angstrom
Ag	Silver
AgNPs	Silver nanoparticles
Al	Aluminium
AFM	Atomic Force Microscopy
AIE	Aggregation Induced Emission
a.u.	Arbitrary unit
CTDNA	Calf Thymus DNA
$CDCl_3$	Chloroform
CD_3CN	Acetonitrile
CD	Circular Dichroism
cm	Centimeter
Cy3	Cyanine-3
DLS	Dynamic Light Scattering
DMSO	Dimethyl Sulfoxide
DNA	Deoxyribo Nuceic Acid
DOX	Doxorubicin
DX	Double crossover
dsDNA	Double strand DNA
dA_n	Deoxyadenine
dT_n	Deoxythymidine
EtBr	Ethidium Bromide
EtOH	Ethanol
EDAX	Energy dispersive X-ray spectroscopy

ESI	Electrospray ionization
FFT	Fast Fourier Transform
G	Gram
H-bond	Hydrogen bond
HBC	Hexabenzocoronene
Hrs	Hours
HOMO	Highest occupied molecular orbital
HRMS	High resolution mass spectrometry
I_h	Icosahedron
K	Kelvin
K	Kilo
KBr	Potassium bromide
kV	Kilo volt
keV	Kilo electron volt
LLIP	Liquid–liquid interfacial precipitation
LCST	Lower critical solution temperature
LUMO	Lowest unoccupied molecular orbital
M	Molar
mm	Millimeter
MHz	Mega heartz
Min.	Minute
mL	Millilitre
mM	Millimolar
mol	Mole
nm	Nanometer
nM	Nanomolar

NMR	Nuclear magnetic resonance
ns	Nanosecond
OPM	Optical polarizing microscopy
OPV	oligo(p-phenylenevinylene)
PBS	Phosphate Buffered Saline
PCBM	Methyl [6, 6]-phenyl-C61-butyrate
pH	Hydrogen ion concentration at logarithmic scale
FCC	Face centred cubic
Fl.	Fluorescence
PCBM	[6,6]-phenyl-C_{61}-butyric acid methyl ester
ppm	Parts per million
PSS	Poly(sodium-4-styrene)sulfonate
RIR	Restriction of Intramolecular rotation
RNA	Ribonucleic acid
s	Second
SAED	Selected area electron diffraction
SCLC	Space charge limited current
ssDNA	Single stranded DNA
SEM	Scanning electron microscopy
T	Temperature
T_m	Melting temperature
Tyr	Tyrosine
TCSPC	Time correlated single photon counting
TEM	Transmission electron microscopy
TEG	Triethylene glycol

TPE	Tetraphenylethylene
THF	Tetrahydrofuran
TLC	Thin layer chromatography
TX	Triple crossover
UV-vis	Ultraviolet-visible
WAXS	Wide angle X-ray scattering
XRD	X-ray diffraction
ε	Molar extinction coefficient
%	Percentage
λ	Wavelength
λem	Wavelength of emission
λex	Wavelength of excitation
λmax	Maxima of wavelength
λ-DNA	Lambda DNA
μg	Microgram
μm	Micrometer
μM	Micromolar
μL	Microliter
°C	Degree Celsius
1D	One-dimensional
2D	Two-dimensional
3D	Three-dimensional
3WJ	Three-way junction

PREFACE

DNA nanotechnology makes use of the sequence complementarity of nucleic acids in building the long-range ordered, programmable DNA nanostructures, and prevails in engineering functional nanostructures through DNA origami, DNA tile assembly, and assembly of DNA amphiphiles. These current technologies rely on the synthesis and self-assembly of synthetic and modified oligonucleotides and their complex designs, which make it highly expensive and limits the large-scale production of DNA nanostructures.[1] In this context, developing long-range ordered, functional DNA nanostructures from random, unmodified oligonucleotides is still an unresolved challenge.[2] The present thesis addresses this challenge by proposing alternative strategies to attain DNA assisted assembly of small organic molecules by employing different non-covalent interactions.

The thesis is organized into four chapters including an introduction chapter, which gives an overview of the different supramolecular DNA nanostructures and general strategies involved in the assembly process. The chapter also discusses the major challenges in classical DNA nanotechnology and the current strategies adopted to resolve the problems in DNA based assemblies.

Second chapter discusses the ordered assembly of an amphiphilic pyridinium appended fullerene derivative (**FPy**) through electrostatic interactions with various oligonucleotides involving charge neutralization, DNA condensation and formation of ultrathin crystalline nanosheets (Chapter 2A). The differential interaction of **FPy** with long/short dsDNA and ssDNA were identified through spectroscopic and morphological analysis. Longer double strand DNAs such as linear λ-DNA and circular pBR322 plasmid DNA readily condense in presence of **FPy** to form few layer nanosheets with sub-micrometer lateral dimensions. The assembly in this case is guided by initial DNA condensation and subsequent fullerene-fullerene interactions. On the other hand, **FPy** binds efficiently to shorter DNA strands such as 20-mer dsDNA and ssDNA primarily through electrostatic interactions and subsequent charge neutralization lead to significantly crystalline nanosheets with lateral dimensions in the micrometer range. Further, the addressability of the **DNA/FPy** nanostructures were demonstrated using a Cy3-modified ssDNA (DNA2-Cy3), which also forms highly crystalline nanosheets in presence of **FPy** and exhibit strong quenching of Cy3 fluorescence through possible electron transfer interactions with fullerenes in the **DNA2-Cy3/FPy** assembly (*J. Photochem. Photobiol. B* **2022**, 226, 112352).

The strategy has been generalised for anionic polymers by demonstrating the ordered assembly of fullerene through interaction with polystyrene sulfonate (PSS). Chapter 2B discusses the formation of **PSS/FPy** hybrid and the ordered assembly of fullerenes in these

hybrid nanostructures. The fullerene/polymer assembly is investigated through spectroscopic and morphological analysis and the reorganisation of fullerene to an FCC lattice structure in presence of PSS is observed through XRD analysis. The enhanced electron transporting property of **PSS/FPy** hybrid compared to bare **FPy** by virtue of the FCC lattice structure is confirmed through SCLC method.

Chapter 3 discusses the design, synthesis and assembly/re-assembly process of three aniline appended amphiphilic TPE derivatives (**TPE1**, **TPE2** & **TPE3**) in the presence of CTDNA and short dsDNA. Hierarchical assembly process of TPE amphiphiles from fibrillar to nanoribbons/nanosheets structures has been discussed in detail. The disassembly and reassembly of TPE amphiphiles in presence of DNA leading to more ordered nanostructures is probed through different spectroscopic and morphological techniques. The initial fibril formation might be originated from the slipped stacking of TPE cores along with the van der Waals interaction between triethylene glycol chains. The difference in the number of triethylene chains attached to the TPE amphiphiles significantly contribute to the distinct assemblies of **TPE1**, **TPE2** and **TPE3**. Lateral association of fibrillar structures and formation of nanoribbons/nanosheets rely on the van-der Waals interaction between the triethylene glycol chains which in turn stabilise the TPE assemblies in water. DNA plays a key role in the reassembly process as it alters the hydrophilic-hydrophobic balance of the system and provide specific binding possibility to achieve a directional assembly without compromising the ultimate morphology of the respective assemblies. The crystalline assembly of TPE can be observed in all the three TPE/DNA hybrids and the reassembly process of **TPE2** in presence of CTDNA is studied in detail. Short dsDNA act as more rigid template for the assembly of TPE amphiphiles and is found to form more ordered structures compared to the crystalline assemblies formed by lengthy, flexible CTDNA.

Chapter 4 demonstrates the formation of hierarchical flower-like assembly from diaminotriazine appended TPE derivative (**TPE4**) through amphiphilic self-assembly and H-bonding interaction with polydeoxythymidine strands (dT_n). **TPE4** forms flower-like assemblies through the hierarchical organization of nanosheets, which is formed through the winding of ribbon like structures. Presence of dT_n prevents the initial lateral association of **TPE4** by triggering H-bond directed assembly of **TPE4.** Assembly with dT_n units result in the 1D-organization of TPE molecules on the oligonucleotide strands, which eventually transforms to 2D-network structures of **TPE4**/dT_n. The lateral association of more TPE amphiphiles on these network structures result in nanosheets which further stack to form flower-like assemblies with more ordered amphiphilic self-assembly than the initial assembly of **TPE4** alone. The morphological transformation of **TPE4** is thoroughly investigated through AFM analysis.

In conclusion, we have put forward simple strategies to make DNA nanostructures by the mutually assisted assembly of DNA and small amphiphiles via non-covalent approaches. These strategies make use of the inherent tendency of the amphiphiles to assemble in aqueous medium, directed by the unique structural characteristics of DNA. Ordered assemblies of fullerenes and TPE derivatives studied in this thesis are highly desirable in the context of their promising optoelectronic applications and the incorporation of DNA to the assembly further improve the potential of these nanostructures. These simple strategies to organise suitably designed small amphiphilic molecules in a more ordered fashion with the assistance of DNA can significantly contribute to the emerging field of DNA nanotechnology.

REFERENCES

1.   Pinheiro, A. V.; Han, D.; Shih, W. M.; Yan, H., Challenges and opportunities for structural DNA nanotechnology. *Nat. Nanotechnol.*, **2011**, 6 (12), 763-772.
2.   Vittala, S. K.; Saraswathi, S. K.; Joseph, J., Fullerene Cluster Assisted Self-Assembly of Short DNA Strands into Semiconducting Nanowires. *Chem. Eur. J.*, **2017**, 23 (62), 15759-15765.

Note: *The abbreviations of various compounds used here correspond to those given under respective chapters.*

AN INTRODUCTION TO DNA BASED SUPRAMOLECULAR ASSEMBLIES

1.1. ABSTRACT

The complex functional systems in nature rely on the principle of precise organization of simple basic units in a unique fashion to provide effective communication within the system and achieve desired functional properties. As a consequence, the function of each such supramolecular system in nature has been evolved from the intelligent design of its multi-component units, and the unique organization within them based on specific interactions. Following this nature's approach of precise organization, ordered assembly of functional entities like chromophores, biomolecules, nanoparticles, quantum dots, etc., with excellent physicochemical, optical, morphological and multiple stimuli-responsive properties were developed, which attracts the attention of research community from various fields. For example, generally, inorganic materials like metal oxides, nanoparticles, quantum dots, etc., have been engaged in nanodevice fabrication due to its outstanding performance originating from the appropriate structural characteristics, and crystalline ordering in the respective structures. However, most of these inorganic materials are associated with severe toxicity and can be replaced with the labile and comparatively safe small organic molecules by following the supramolecular assembly principles to achieve the required organization of the

molecules suitable for nanodevices and other nanotechnology-based applications, without compromising the safety aspects.

The precise organization of functional materials can be achieved through templated assemblies, often involving more ordered scaffolds like polymers, proteins or oligonucleotides to bind the moieties and to direct the desired assembly. Among these various templates, DNA as such and its engineered nanostructures are promising candidates in organizing small molecules, polymers, nanoparticles and biomolecules for various applications, because of their unique double-helical structure which allows molecular recognition/interactions through intercalation, electrostatic interactions and groove binding. Hybridization based DNA tile assembly, DNA origami and 3D lattice structures based on DNA-metal/semiconductor/nanoparticle building blocks are examples for different strategies adopted in the classical DNA nanotechnology. Apart from these classical approaches of utilizing long or complex scaffolds of DNA and its hybridization possibilities, there are plenty of other opportunities to accommodate specific functional moieties in the unique structure of DNA. This includes the phosphodiester recognition through electrostatic binding of cationic species, nucleobase recognition, intercalation, and major and minor groove binding interactions. This introductory chapter highlights the role of DNA to generate the ordered assembly of small amphiphilic molecules in aqueous media.

1.2. INTRODUCTION

The complex, functional living systems amaze the scientific community to inquire more into the secret of life and its endurance. The system become more and more complex as we unravel each stage and rely on precise organization of simple

basic units in a unique fashion to provide effective communication within them. These systems engage with the surroundings to grow, function and respond to the external stimuli to create an equilibrium condition. Function of each supramolecular system has been evolved from the intelligent design of its multicomponent units and the unique organization within them based on specific interactions. For example, the well-defined antenna network comprised of suitable pigments in light harvesting system, channel the energy to the respective reaction centers through efficient, spatially oriented energy transfer cascade.[1] Likewise, organization of lipids and proteins in biological membranes decide the transport of materials in and out of the living systems.[2] Actin filaments and microtubules are other examples to portray the excellent supramolecular architectural designs in living systems.[3] Supramolecular chemists always get fascinated about the dynamic assembly processes involved in actin filaments and microtubules and the cross-talk within them.[4-6] There are numerous other examples in the living system to inspire supramolecular researchers to develop novel systems with higher order organization in nanoscale to impart excellent functional properties.

Apart from biological systems, material world also looks into the supramolecular assemblies since the highly ordered arrangement often found to enhance the physicochemical, mechanical and optoelectronic properties of nanomaterials and devices. [7-9] So the precise nanoscale arrangement of molecules is highly desirable and well challenging to achieve excellent functional properties. Generally, inorganic materials like metal oxides, nanoparticles, quantum dots etc. have been engaged in nanodevice fabrication due to its outstanding performance originated from appropriate structural characteristics and crystalline ordering in the

respective structures.[10-12] These inorganic materials can be replaced with labile and comparatively safe organic molecules by adopting supramolecular chemistry to organize the molecules and thereby to enhance the material properties.[13-15]

1.3. Supramolecular assembly strategies

Supramolecular assemblies rely on various non-covalent interactions such as ionic (300–800 kJ/mol), ion-dipole (50–200 kJ/mol), hydrogen (H) bond (4–120 kJ/mol), dipole-dipole (4–40 kJ/mol), π–π stacking (1–20 kJ/mol), and van der Waals (1–10 kJ/mol) interaction (Figure 1.1). Synergistic combinations of some of these non-covalent forces suitably arrange the molecules to a desired construct in order to attain most favorable energy state. Apart from these forces, supramolecular assemblies in water are generally guided by the hydrophobic effects which try to reduce the contact of hydrophobic part with aqueous medium. This effect significantly contribute to the protein folding, formation of lipid-bilayer membrane, DNA structure etc.
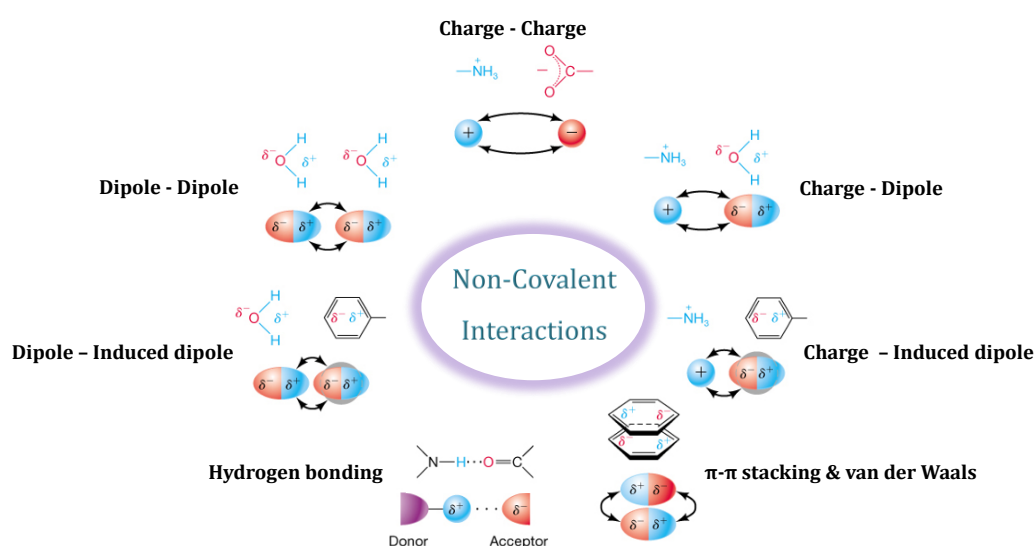
Figure 1.1. Schematic representation of different non-covalent interactions. (Modified from *https://www.chem.uwec.edu/Chem352_Resources/pages/lecture_materials/unit_I/lecture-2/overheads/Chem352-Lecture_2-print.pdf).*

1.3.1. π –π stacking and van der Waals interactions

π-systems are incredible candidates in supramolecular chemistry that hold great potential in self-assembly through the non-directional, dispersive π- π interactions. Stimuli responsive changes in the π- chromophore stacking are widely employed in various optoelectronics and biomedical applications. Thus, certain interesting π-chromophores based supramolecular systems are in demand due to its major functional applications in diverse fields. Moreover, suitable chemical modification can alter the stacking behaviour of the chromophore and is in turn reflected in the overall functional performance of the supramolecular system. So, the physicochemical properties of supramolecular systems can be modified considerably by the fine structural tuning of the π-system. The researchers have made great efforts to modulate the self-assembly of highly demanded π-systems like fullerenes, pyrene, OPV, perylene etc. by the incorporation of suitable entities.[16] Long alkyl chains and hydrophilic glycol chains are integrated in the molecular design in order to strengthen the supramolecular system through additional van der Waals interaction. Several literature reports convince the major role of these van der Waals interactions to decide the fate of the supramolecular system. [17]

1.3.2. Electrostatic interactions

Electrostatic interactions are stronger compared to van der Waals or π- π interactions and are non-directional since it is highly affected by the solvent system and other counter ions in the system. As the assembly of molecules majorly rely on the attraction and repulsion between the individual molecules, the electrostatic charges on the entities are highly important and the electrostatic balance play a major role in the formation of different supramolecular systems.   The ionic

interaction based supramolecular systems are well-explored in the field of drug delivery systems and sensing applications that utilizes the pH responsive charge switching in the molecular system.[18, 19]

1.3.3. Hydrogen bonding interactions

Highly directional hydrogen bonding interactions have great significance in the molecular recognition based supramolecular assemblies due to its highly specific nature. It offers versatile supramolecular structures with high stability and the strength and reversibility can be modulated through the suitable modifications in the H-bonding motifs. Apart from the dispersive interactions, H-bond interactions offer highly ordered supramolecular systems with excellent functional properties. Moreover, it offers control over the size and dimensionality of the system by proper choice of solvent systems, temperature etc.

1.4. Amphiphilic self-assembly

Amphiphiles are the most suitable candidates for supramolecular assembly process due to the inherent tendency of the amphiphilic design to associate each other in a less favorable environment and achieve minimum energy through self-organization. Amphiphiles, consist of solvophobic and solvophilic part, prefer to orient in the solvent system appropriately by reducing the exposure of solvophobic part to the outer surface and attain its stability by engaging the solvophilic interactions.[20] For example, the double helical structure of DNA is achieved by providing a hydrophobic space for the suitable encapsulation of the hydrophobic nucleobases in the interior of the phosphate backbone cage by expelling water molecules to the outside.[21] Thus, the spontaneous organization into ordered self-

assembled structures satisfies the entropy requirement by increasing the disordered configuration in the surroundings.

Most of the supramolecular designs in the biological system rely on amphiphilic self-assembly that contribute to the function and control of the entire vital tasks in living organisms. The structural design of DNA, protein folding, lipid-bilayer membrane designs etc. primarily rely on amphiphilic self-assembly by incorporating suitable supramolecular interactions like H-bonding, electrostatic interactions, hydrophobic effects, van der Waals interactions etc.[22-24] As a bioinspired strategy, amphiphilic self-assembly pave way to the development of advanced functional systems for various applications. A library of nanomaterials, spanning from zero dimension to three dimensions, can be achieved through amphiphilic self-assembly that include nanospheres, nanofibers, nanotubes, nanorods, nanoribbons, nanosheets, micelles, nanovesicles etc.[20, 25-27] A general understanding of the design strategies and self-assembly processes bring out novel materials with excellent functional properties. The formation of spherical micelle is considered as the classic example for the amphiphilic self-assembly that orient the solvophobic part to the interior in order to reduce the exposure to solvent molecules and the solvophilic part to the exterior, majorly guided by the solvophobic effect.[28]

The shape and size of the amphiphilic assembly are greatly depending upon the amphiphilic design, solvent system, pH, temperature etc. Thus, it's interesting to modulate the assembly through the suitable choice of these specific parameters. At present, the thorough knowledge developed by the supramolecular chemists is high to predict the shape of the amphiphilic assembly with more precision.[20] The design of an amphiphile with a hydrophilic head and two hydrophobic tails can form bilayer vesicles in the case of phospholipid membranes.[20] Besides the conventional bilayer

vesicles, there is multi-layered vesicles look–like onion structure. These various vesicle structures can carry both hydrophilic/hydrophobic drug molecule and this realization further pave way to the design of numerous drug delivery vehicles.[29] Pei and co-workers have introduced a novel redox-responsive cationic vesicular system for drug/SiRNA co-delivery based on amphiphilic pillar[5]arene capped with ferrocenium. Here, the structurally rigid pillar structures can encapsulate the drug molecules and the cationic ferrocenium units can hold the SiRNA effectively. The amphiphilic nature of this pillar[5]arene derivative made possible the formation of vesicular structures and the GSH responsive ferrocenium part take charge of the stimuli responsive assembly and disassembly as shown in Figure 1.2A.[25] Likewise, Wang and co-workers have developed a dual photo- and pH-responsive drug delivery system based on vesicular structures of pillar[6]arenes (Figure 1.2B).[30]
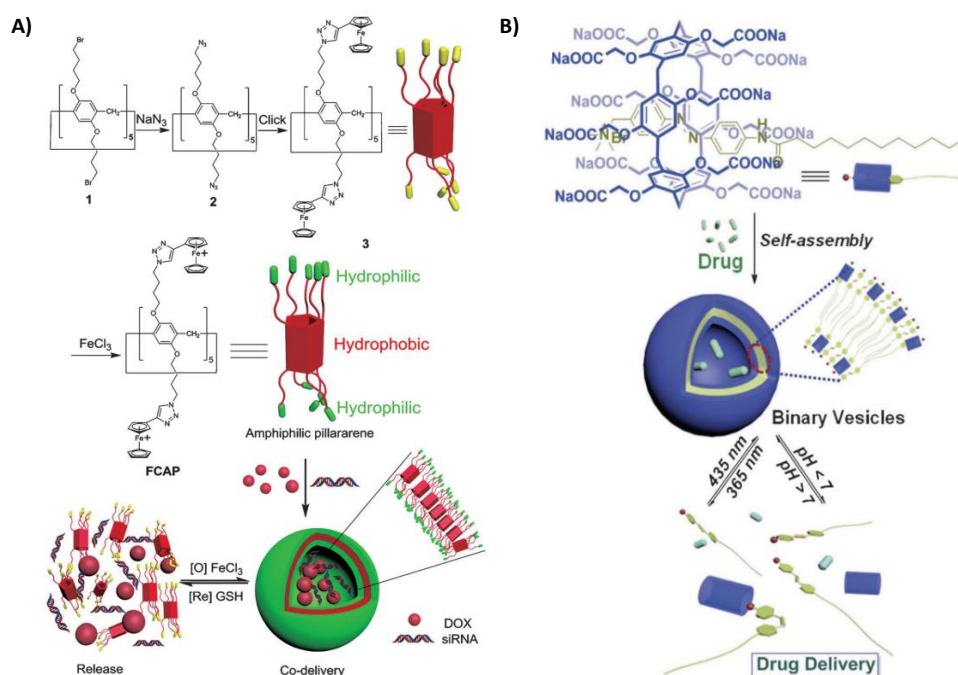
Figure 1.2. Chemical structure and schematic representation of A) amphiphilic pillar[5]arene derivative, formation of redox responsive drug/SiRNA delivery system and B) amphiphilic pillar[6]arene derivative, formation of dual photo and pH-responsive drug delivery system. (Adapted from reference 25 and 30).
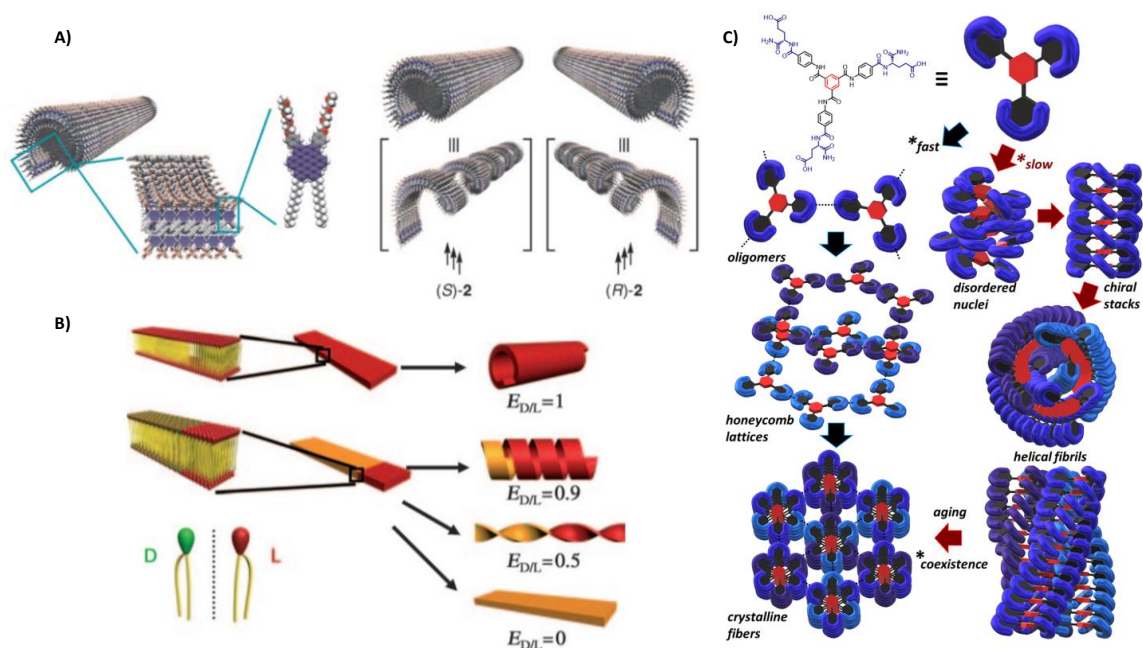
Figure 1.3. Schematic representations of A) formation of helical nanotubes from gemini-shaped chiral hexabenzocoronene derivative; B) formation of lipid nanotubes from D and L enantiomers under different ratios and C) Chemical structure and proposed self-assembly mechanism of benzene tricarboxamide monomer under different kinetic regimes (Adapted from reference 32, 33 and 34).

However, a bolaamphiphile with two hydrophilic heads connected through a hydrophobic part usually form a tubular structure with single wall thickness.[31] Amphiphilic molecules with a chiral centre generally make nano-twist in the assembly to form helical and twisted structures as shown in Figure 1.3A. A helical structure has a cylindrical curvature that can act as a precursor for tubular structures. In 2005, Aida and co-workers have reported the formation of right and left-handed helical graphitic nanotubes from the enantiomers of gemini shaped chiral hexabenzocoronene.[32] Later, Liu and co-workers have demonstrated the tunable chirality of the lipid nanotube by mixing the two enantiomers in different ratios as shown in Figure 1.3B.[33] The molecules with C_3-symmetry also form tubular structures, but generally formed through columnar stacking. Recently, Webber and

co-workers have investigated the hierarchical assembly and hydrogelation of benzene tricarboxamide, a C_3-symmetric discotic molecule. In this report, they have explored different self-assembly pathways by pH stimulus under kinetic control and is shown in Figure 1.3C.[34]

Apart from 1D nanostructures, the fabrication of 2D nanomaterials is also highly important and remain as a challenging task. The large surface area provided by the 2D nanosheet make it a suitable candidate for sensing, catalysis, optoelectronic applications etc. Several approaches have been developed for the synthesis of 2D nanomaterials that include Langmuir-Blodgett films,[35] self-assembled monolayers,[36] 2D covalent polymers,[37] co-ordination polymers,[38] metal-organic frameworks[39] etc.

The genre of supramolecular 2D-nanomaterials is expanding widely by the contribution from various research groups and is considered as an intelligent approach for the development of highly ordered nanostructures with controllable size and tunable properties. For example, Haner and co-workers have demonstrated the assembly of pyrene trimers in aqueous media to form 2D-nanosheets with controllable size. The well-ordered pyrene nanosheets with high-aspect ratio can be prepared by applying a slow temperature gradient (0.1 °C/min) and large number of smaller nanosheets by larger temperature gradient (20 °C/min).[40] Later, Takuechi and co-workers have achieved control over the surface area and the corresponding aspect ratio of supramolecular nanosheets by modulating the intermolecular interactions through suitable molecular design.[41] The 2D nanosheet assembly in solution phase can also be achieved from distinct disc shaped molecules, aromatic macrocycles, C_3-symmetric molecules etc. Myongsoo Lee and co-workers have been extensively worked on the development of functional 2D-nanostructures from

aromatic macrocyclic molecules modified with oligoether dendron.[42-47] They have shown the static and dynamic nanosheets from anthracene based macrocyclic geometrical isomers. The dynamic nature of the trans-form is stimulated by a thermal trigger (Figure 1.4A).[44] Later, they have developed porous homochiral 2D-nanosheets capable of enantioselective sieving by the design of suitable aromatic macrocycles and is shown in Figure 1.4B.[47]
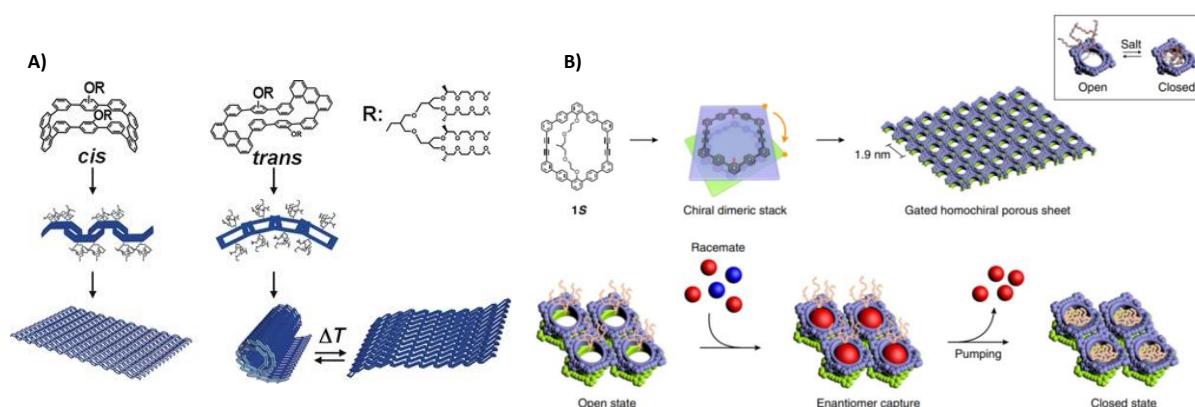
Figure 1.4. Chemical structure and schematic representation of A) anthracene based macrocycle and the formation of static and dynamic nanosheets from cis and trans forms; B) aromatic macrocycle and formation of homochiral porous nanosheets capable of enantioselective sorption. (Adapted from reference 44 and 47)

2D-nanosheets can also be formed through the lateral association of nanofibers by virtue of different non-covalent interactions like H-bonding, host-guest complexation, van der Waals interactions, hydrophobic interactions etc. The same group (Myongsoo Lee's group) has demonstrated the evolution of 2D nanosheet by the lateral association of the tubular structures formed from a see-saw shaped molecule in presence of *trans*-azobenzene. The 2D-nanosheets can accommodate a hydrophobic guest like *trans*-azobenzene and the *trans-cis* isomerization of azobenzene under UV irradiation trigger the disassembly of porous nanosheet structures to form initial tubular structures (Figure 1.5A).[46] Recently,

they have showed the length-wise division of the porous 2D-nanosheets, formed from aromatic macrocyclic amphiphiles with oligoether dendrons, to nanofibers with temperature control as shown in Figure 1.5B and is attributed to the subsequent change in environment of the oligoether chains on thermal dehydration.[45]
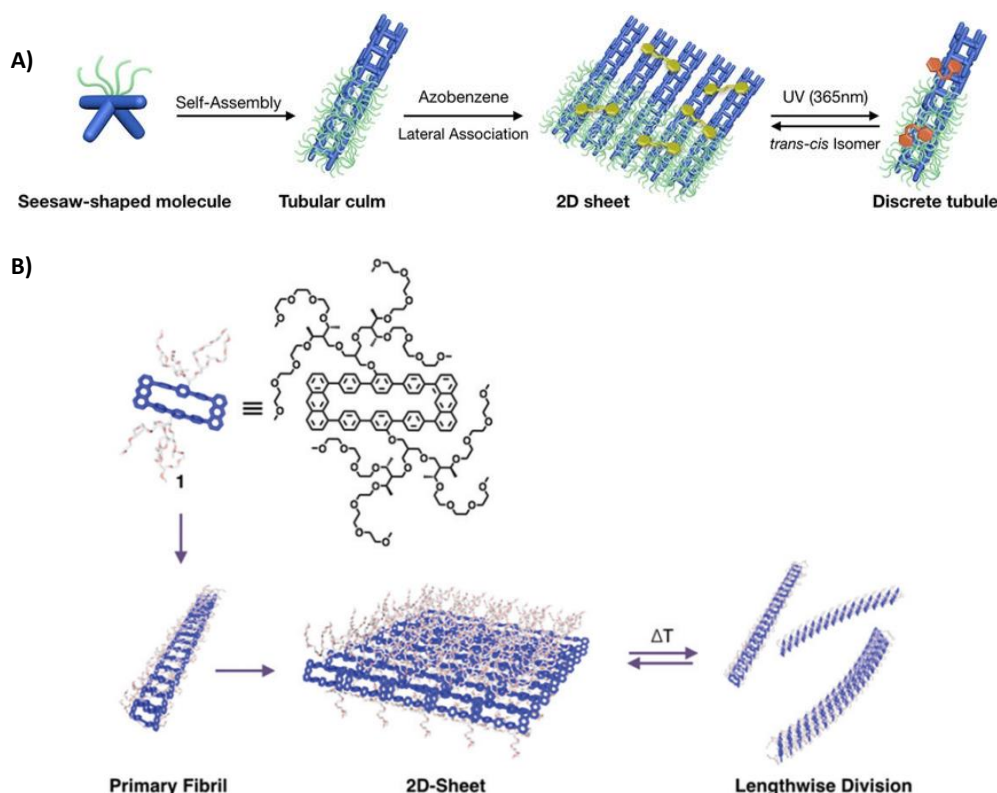
Figure 1.5. Molecular structure and schematic representations of A) See-saw shaped molecule and the formation of nanosheets through the lateral association of initial tubular assemblies in presence of azobenzene and its disassembly on trans-cis isomerisation under UV-irradiation; B) Aromatic macrocycle with oligoether dendrons and its self-assembly into 2D- nanosheets from initial fibrillar structure and its length-wise division under thermal trigger. (Adapted from reference 46 and 45).

In spite, the high aspect ratio 2D materials are generally achieved by the use of a 2D template, most often a protein array, DNA origami structure or tile assembly. [48-50] These finite, well-defined 2-D templates enable precision positioning of the

functional materials through effective binding.[51] For example, Abb and co-workers described the formation of 2D assemblies by controlling the amino acid sequences of oligopeptides.[52] In a different approach, Ringler and Shultz adopted a different approach to build proteins self-assembled networks on lipid monolayer, having l-rhamnulose-1-phosphate aldolase and streptavidin as building blocks.[53] Likewise, DNA also provides specific binding sites to organize functional moieties in an ordered manner. Thus, DNA is well-explored as a template for the development of ordered nanoscale assemblies.[54, 55] Detailed discussion on DNA structure, specific binding modes and the evolution of DNA nanotechnology has been provided in the subsequent sections.

1.5. DNA: structure and specific binding modes

DNA is a self-assembling biopolymer that forms double helices directed by canonical Watson-Crick base pairing and is stabilized by the hydrogen bonds, π-π stacking and hydrophobic interactions.[56] DNA is a nucleic acid that consists of two long chains of nucleotides twisted together into a double helix, where each strand is composed of a combination of four complementary bases such as adenine (A), thymine (T), guanine (G) and cytosine (C). These nucleotides are connected through phosphodiester linkages within a strand (deoxyribose sugars joined at both the 3'-hydroxyl and 5'-hydroxyl groups to phosphate groups in ester links is called phosphodiester linkage). The two strands are held together primarily through hydrogen bonds where adenine forms two hydrogen bonds with thymine and cytosine forms three hydrogen bonds with guanine. The region where the two strands are close to each other (deep–narrow) is called minor groove while the

region where they are away from each other (shallow–wide) is called major groove (Figure 1.6).
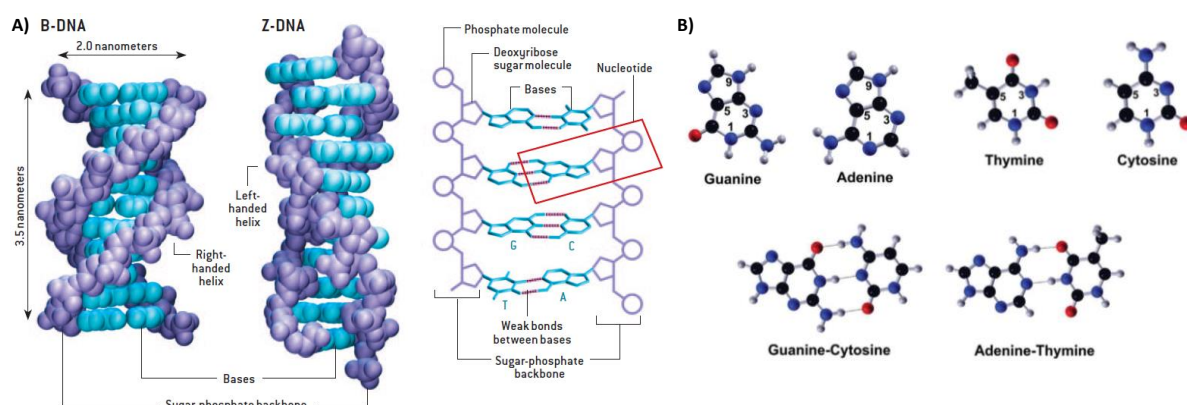
Figure 1.6. A) Structures of B-DNA and Z-DNA; B) Chemical structures of nucleobases and the representation of Watson-Crick base pairing (Adapted from reference 54).

The unique structure of DNA provide various binding sites through nucleobase recognition, phosphodiester recognition, major/minor groove binding, intercalation etc. as shown in Figures 1.7A and 1.7B.[57] Nucleobase recognition enables the specific binding of functional materials on templated DNA base through H-bonding interactions. Several research groups have employed molecules that are covalently linked with nucleobases to orient certain functional materials. The phosphodiester groups that are deprotonated at pH >2.5, can electrostatically interact with inorganic salts and organic cations and can be utilized for the generation of supramolecular DNA templated assemblies. Certain small molecules or nanoparticles can bind at the major/minor grooves of DNA by its shape complementarity either through phosphodiester recognition or nucleobase recognition. The suitable selection of functionalities with specificity towards A-T or G-C base pairs has been widely accepted in DNA based sensors and fluorescent markers. Small aromatic molecules can interact with the nucleobases through π-π

stacking and can be intercalated in between the nucleobase pairs. Ethidium bromide, SYBR green, Acridine orange, etc. are some of the examples for generally used DNA intercalators.
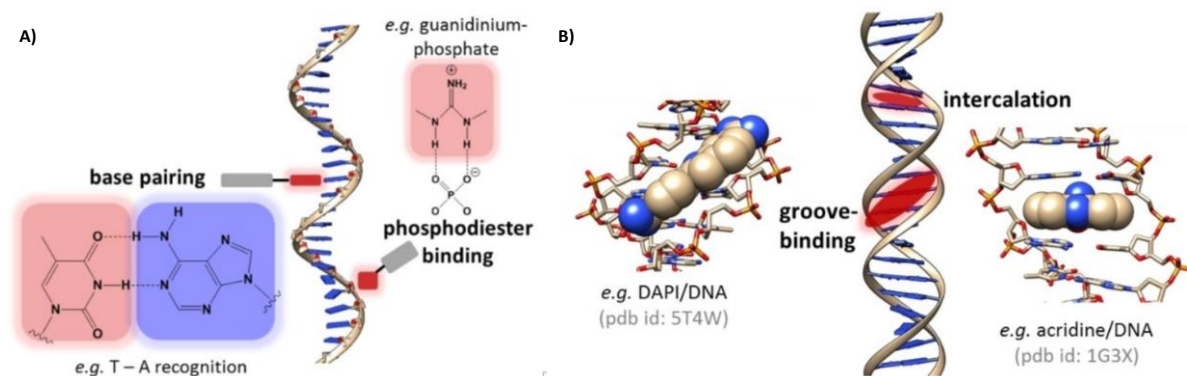
Figure 1.7. Possible DNA binding modes of functional materials to A) single stranded DNA, and B) double-stranded DNA (Adapted from reference 57).

These inherent structural features offer high programmability for DNA and the idea to use DNA as a structural material is emerged from the design of Holliday junctions formed as a recombinant intermediate in the cell. The Holliday junction, formed from four double stranded arms joined together as seen in Figure 1.8A, is more flexible to create rigid tiles through deliberate assembly process which in turn is capable to form larger arrays.[58, 59] G-quadruplexes are another special type of DNA structure formed from guanine rich nucleic acids in which four guanine bases are associated through Hoogsteen base pairing to form guanine tetrad and it further stack to form helical G-quadruplex (Figure 1.8B).[60, 61] Likewise, the special tetraplex i-motifs structures are formed from two cytosine rich duplexes intercalated with each other in an antiparallel orientation through non-Watson-Crick base pairing (Figure 1.8C) and serve as good candidate in biosensing, drug delivery, molecular switching etc. due to its ligand binding capacity and pH responsive nature.[62, 63]
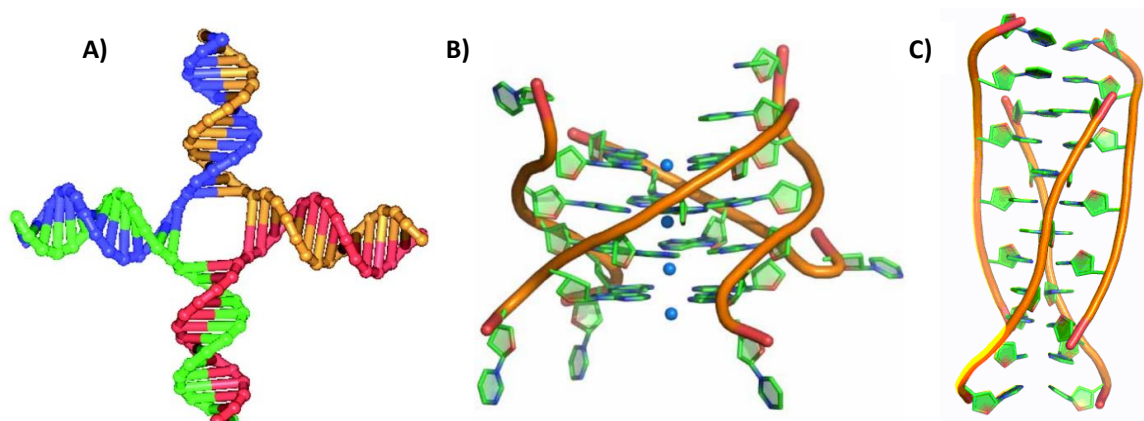
Figure 1.8. A) Schematic representation of Holliday junctions; B) G-quadruplex and C) Tetraplex i-motif structures. (Adapted from references 59, 61 and 63)

Moreover, the first level of DNA organization, a linear array of nucleosome core particles (NCP) is later become a model for novel DNA nanostructures. In the eukaryotic cell nucleus, DNA exists as chromatin, a compact but dynamic complex with histone proteins which uses various non-covalent interactions involving histone-histone and histone-DNA interactions to make stable, rigid and compact chromosomal structures as shown in Figure 1.9.[64] The way in which the centimeter-long DNA wrap around the histone protein to form compact micrometer sized nucleosome core particles is known as DNA condensation.

This fascinating process of DNA condensation remains as a great inspiration for the construction of different DNA nanoarchitectures. The multivalent cations can readily interact with the anionic phosphate backbone of DNA and charge neutralization leads to DNA condensation. Cationic polymers, dendrimers, nanoparticles etc. are employed for DNA condensation to form DNA condensates with different size and shape. Also, an effective DNA condensing agent with sufficient gene protection can be used for gene delivery applications. Furthermore, the spatially aligned DNA assemblies can be achieved by the control over DNA

condensation. Bar-Ziv and co-workers investigated the conformational changes of DNA brushes on spermine induced DNA condensation and achieved precise control over the DNA condensation mechanism to guide the assembly to desired dendritic patterns.[65] Further, they have employed similar strategy to achieve the precisely guided one dimensional assembly of DNA polymers on a patterned biochip.[66]
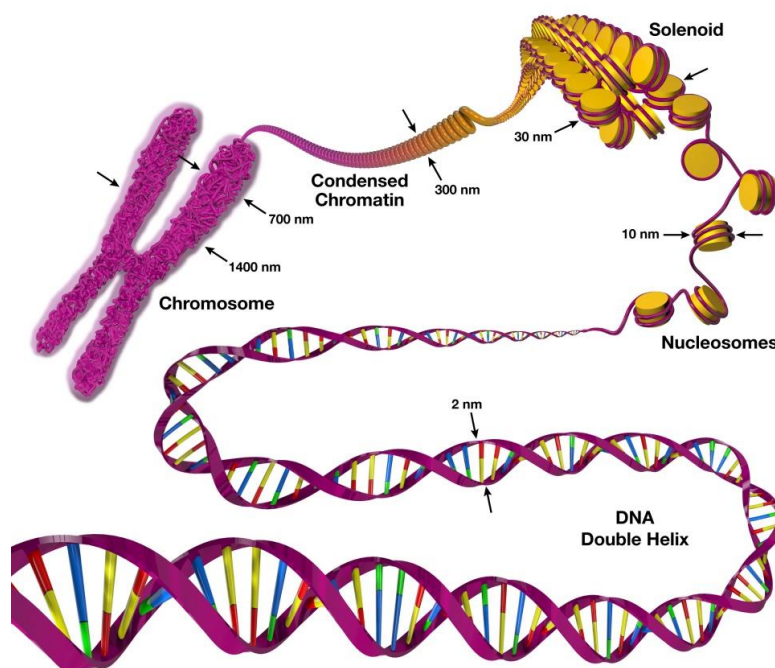
Figure 1.9. Schematic representation of hierarchical organization of DNA into chromosomes involving DNA condensation. (Adapted from http://brassica.plants.umanitoba.ca/~brienn/cyto/ l09/l09.html)

1.6. DNA based assembly strategies

The unique structure of DNA makes it a versatile template for the organization of materials through specific recognition sites in DNA. DNA nanotechnology is a well emerging field which contributes enormously to the field of structural and functional materials in a short span of time. DNA nanoarchitectures turn out to be a good choice for structural and functional materials in diverse fields and attributed to its high programmability and precise modulation ability. As part of

the DNA nanotechnology, different approaches have been developed to achieve the goal of making structural and functional nanomaterials. DNA can be used as a tile to form two dimensional architectures,[67] or long strands can be folded to make origami structures which also provide space for further functionalisation.[68, 69] DNA architectures functionalized with organic molecules can be made by incorporation of DNA intercalators or groove binders in the molecular design.[70-72] Covalent modification of DNA strands with suitable self-assembly partners provide great opportunities in the field of DNA architectures.[73] Non-covalent interactions can also be utilized to form DNA architectures,[74] which makes an easy way compared to DNA tile assembly or DNA origami, but the way has to be explored widely in the future.

1.6.1. Structural DNA nanotechnology

The evolution of DNA nanotechnology starts from the idea of Nadrian. C. Seeman, basically a crystallographer, to organize proteins and other biomolecules on immobile DNA junctions.[75, 76] The pioneering works of Seeman bring about the DNA tile-based assemblies. Later, Paul Rothemund has introduced the idea of DNA origami that involves the folding of long scaffold strands with the help of short staple strands. A brief description of these two unique methods in structural DNA nanotechnology has been provided in the following section.

1.6.1.1. DNA tile assembly

Tile-based DNA structures have been emerged to assemble higher order periodic and aperiodic lattices with greater rigidity through DNA sticky ends as shown in Figure 1.10A. The first DNA tile assembly, immobile four-way junction, has been formed from four DNA single strands, designed by Seeman and co-workers.[77] The core of a DNA tile can be designed by DNA double crossover (DX) motifs or

triple crossover (TX) motifs. A DX motif consists of two parallel double helices held together by two crossovers.[78] Further rigidity can be attained by more complex structures derived from the basic DX design.[79] Instead, a TX motif contains three parallel helices with four crossover junction and possesses greater rigidity compared to the DX motifs.[80] Rational assembly of these tile motifs can generate various DNA assemblies through the suitable modifications of sticky ends and hairpin loops.[81] The groups of Ya and LaBean have designed a 2D-nanogrid (Figure 1.10B) by a DNA tile based assembly of four interconnected four-armed junctions incorporated with biotin units and have shown the periodic arrangement of protein streptavidin on the designed 2D-nanogrid.[49]
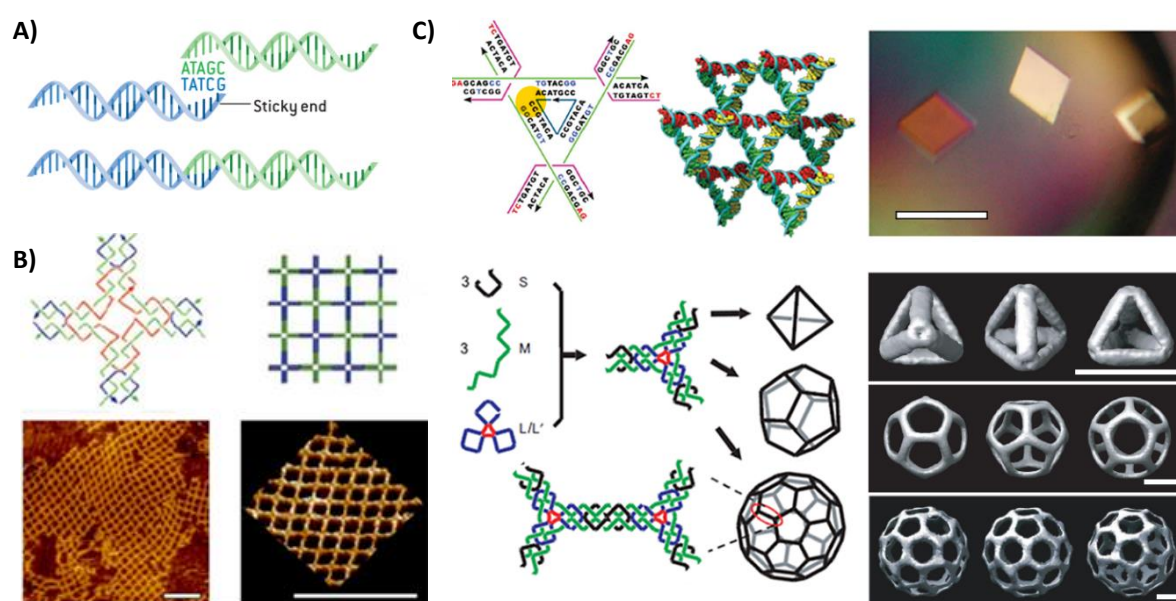
Figure 1.10. Schematic reperesentation of A) DNA sticky end; B) Four-arm junction and corresponding 2D assembly with the the AFM images of resulting 2D array on mica surface; C) Tensegrity triangle and the assembled with the optical image of the 3D crystals formed through the assembly of tensegrity traingles and the three star motifs joined to form different polyhedral structures. (Adapted from references 49 and 77).

During the same period, Mao and co-workers have designed tensegrity triangles in which three four-arm junctions associate to form DNA triangles with rigid vertices and flexible interhelical angles. In the later years, more complex 3D structures have been developed based on the design of tensegrity triangles.[82] In 2009, Seeman and co-workers achieved the formation of 3D-DNA crystals based on the precise, long-range ordered assembly of tensegrity triangles (Figure 1.10C).[83] Further, the tile based approach has been advanced by the construction of 3D wireframe polyhedral structures.[84] Even though, the tile based assembly strategy often fail to meet the requirement of highly periodical structures with large structural complexity.

1.6.1.2. DNA origami

In DNA origami based approach, a very long single stand DNA scaffold staple together with hundreds of short DNA strands complementary to different regions of scaffold DNA to form desired DNA nanostructures. Besides DNA tile based assembly, DNA origami approach can be employed to produce highly complex structures with desired shape and controlled dimension in good yield. The method of DNA origami is first proposed by Paul Rothemund in 2006 and demonstrated the assembly of single layered planar structures like rectangular, triangular and five point star shapes from single stranded viral DNA. They have also demonstrated the formation of complex smiley face since it offers the desired formation of aperiodic structures through the specific choice of staple strands (Figures 1.11A and 1.11B).[85] Successively, DNA origami approach has been adopted to make three dimensional structures with high precision and programmability. In 2009, Shih and co-workers first described the folding of DNA helices in honey comb-like lattices through DNA

origami method as shown in Figure 1.11C.[86] Later, Gothelf and co-workers have designed a 3D-DNA box with an openable lid responsive to the external supply of specific DNA keys. Furthermore, these vast library of DNA origami structures can be used for the precision positioning of desired functional moieties in a controlled dimension by suitable modification of staple DNA strands.[87]
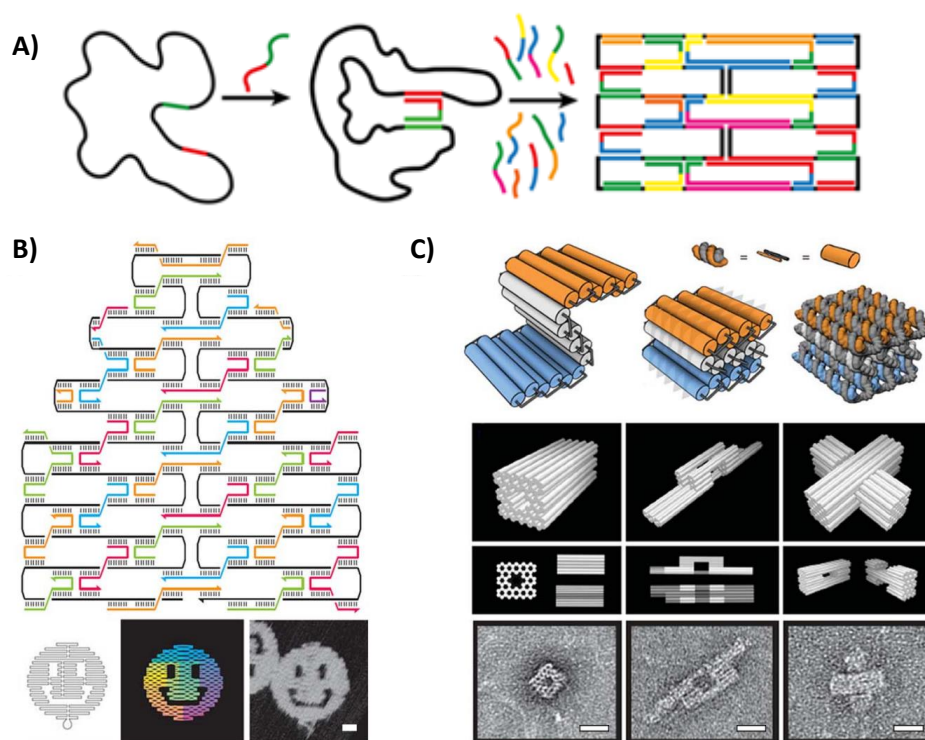
Figure 1.11. Schematic reperesentation of A) DNA origami based assembly process; B) Rasterlike pattern of the DNA origami structures to make arbitrary 2D structures; C) 3D-honey comb lattice structures formed by DNA origami approach. (Adapted from references 85 and 86)

1.6.2. Supramolecular DNA assembly

An entirely different approach has been emerged in DNA nanotechnology by taking advantage of supramolecular chemistry in the recent years. Within short span of time, the new strategy has revealed its potential to achieve the main objective of DNA nanotechnology, precision positioning of heteroelements with good

programmability, in a more feasible way compared to classical DNA nanotechnology approaches. In the novel approach, DNA building blocks are allowed to assemble with synthetic organic/inorganic materials as well as suitable polymeric materials to attain precisely aligned DNA incorporated supramolecular assemblies. This amazing association of supramolecular chemistry with DNA programmability is later termed as supramolecular DNA assembly.[88]

1.6.2.1. DNA assembly with synthetic insertions

The suitably inserted functional moieties can alter the hybridization pattern of DNA structures to provide specific geometries. The pioneering work in this field is delivered by Bergstrom and co-workers, who designed discrete DNA based macrocycle with rigid p-(2-hydroxyethyl)phenylethynylphenyl spacers.[89] Later, Sleiman and co-workers developed 2D-DNA hexagon with m-terphenyl based chemical insertion by the careful design of linker sequences to avoid multiple products. Further they have shown the precise organization of gold nanoparticles on each hexagonal vertex by the hybridization on extended arms on the vertices (Figure1.12A).[90] Single stranded DNA polygons were synthesized further through templated ligation and the gold nanoparticles were incorporated in the precise positions by the hybridization of ssDNA arms (Figure 1.12B).[91] The strategy has been advanced further to create 3D-DNA polyhedra by making connections through additional linkers on the top and bottom portions of DNA polygons and achieve the formation of DNA-based triangular prisms, cubes, pentagonal and hexagonal prisms, heteroprisms and biprisms as shown in Figure 1.12C.[92] Moreover, Sleiman and co-workers demonstrated the longitudinal assembly of DNA polygons to construct DNA

nanotubes that can accommodate different functional entities and selectively release the cargo (Figure 1.12D). [93]
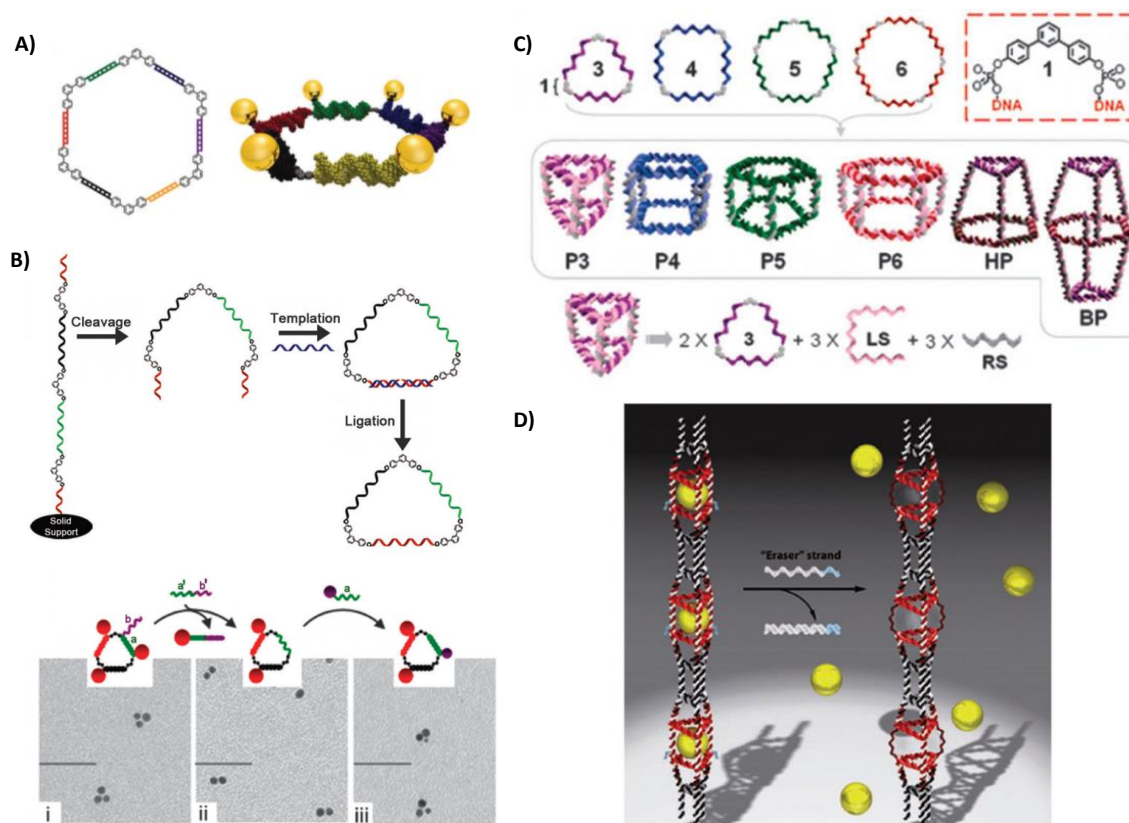
Figure 1.12. Schematic representation of A) 2D-DNA hexagon with m-terphenyl based chemical insertion; B) Formation of 2D- polygons through templated ligation and the corresponding TEM image after incorporation of AuNPs; C) Different 3-D DNA-polyhedra formed from corresponding 2D-polygons; D)1D-DNA nanotube that can encapsulate and release cargo selectively. (Adapted from references 90, 91, 92 and 93)

Furthermore, the intelligent incorporation of transition metal complexes in DNA structures provides a versatile library of DNA–metal constructs.[94] Sleiman's group has designed a DNA two-way junction with the insertion of $[Ru(bpy)_3]^{2+}$ and is shown in Figure 1.13A.[95] A different strategy has been adopted by Han and co-workers that rely on the design of metal binding artificial nucleobases in the DNA construct. This allows the desired assembly of DNA building blocks upon

introduction of suitable metal to the system.[96] The strategy was later employed to make a metal-DNA cage with precisely positioned metals on the vertices (Figure 1.13B).[97]
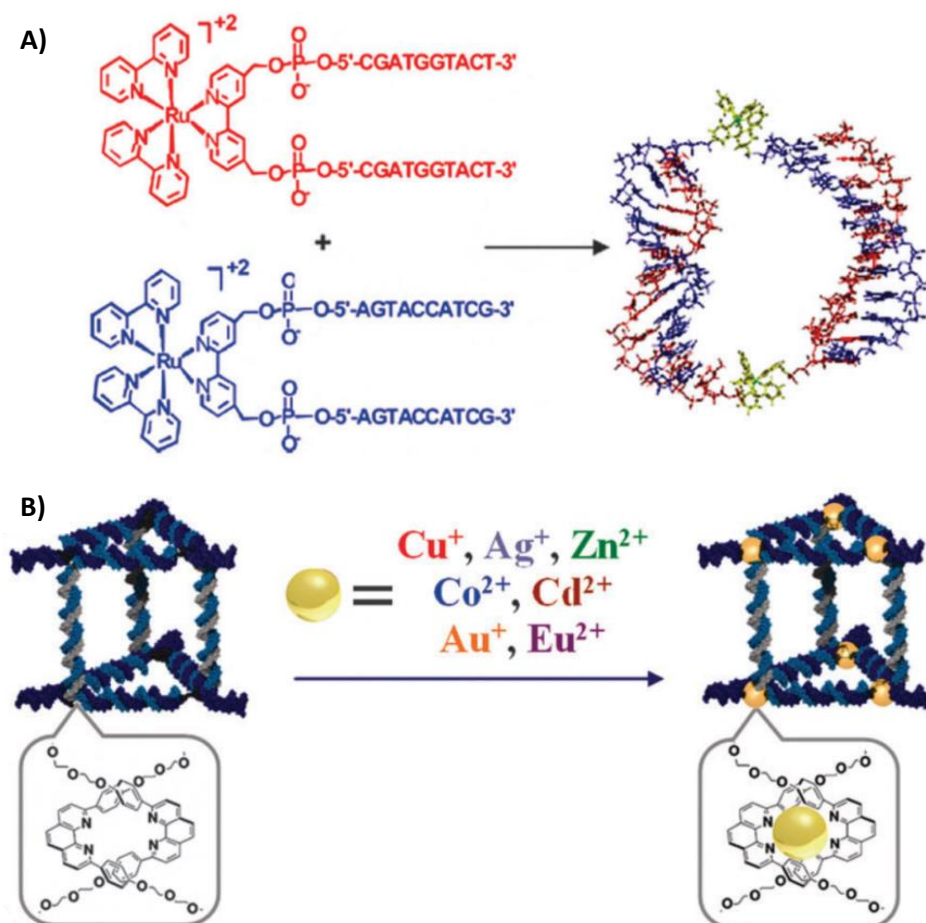
Figure 1.13. Formation of A) metal incorporated two-way junction DNA; B) 3D-Metal-DNA cages. (Adapted from references 95 and 97)

1.6.2.2. Assembly of chemically modified DNA

Another important strategy to build DNA nanostructures involve suitable chemical modification of DNA that leads to the supramolecular assembly of DNA conjugates. Thus, besides the above mentioned strategies, the assembly of chemically modified DNA is generally driven by the non-DNA part rather than Watson-Crick base pairing. There are various reports based on different DNA

conjugates like DNA-lipid, DNA–dendron, DNA-polymer, DNA-π chromophores etc., synthesized through solid phase synthesis and its self-assembly to provide large varieties of novel DNA nanostructures.

The amphiphilic nature of DNA conjugates often prefers micelle-like structures with a hydrophobic core and a hydrophilic DNA corona and can carry various cargo materials to the cellular environment. The DNA-lipid conjugates are generally preferred for gene/drug delivery applications since it provides biocompatibility, sufficient binding with different cargos and effective cellular internalization.[98] Tan and co-workers have designed a DNA-lipid conjugate with a PEG spacer to form a DNA-aptamer micelle useful for target specific delivery of antisense oligonucleotide and drug molecules.[99] Later, they have developed a molecular beacon micelle flares through the self-assembly of suitably designed diacyllipid-molecular beacon conjugates capable of intracellular mRNA imaging and gene delivery applications.[100] Moreover, the dynamic nature of DNA-lipid conjugate assemblies can be custom modulated by employing other suitable approaches. The same group has further reported the engineering of stability tunable DNA micelles by controlling the G-quadruplex formation as shown in Figure 1.14A.[101] Besides, Liu and co-workers have designed a DNA vesicle based on frame-guided assembly process involving gold nanoparticles modified with 20-mer and 6-mer ssDNAs and cholesterol attached complementary DNA strands and further assembly with sodium dodecyl sulfate. This strategy that provides vesicles with controllable dimensionality can be used to understand the formation mechanism of cellular membrane (Figure 1.14B).[102]
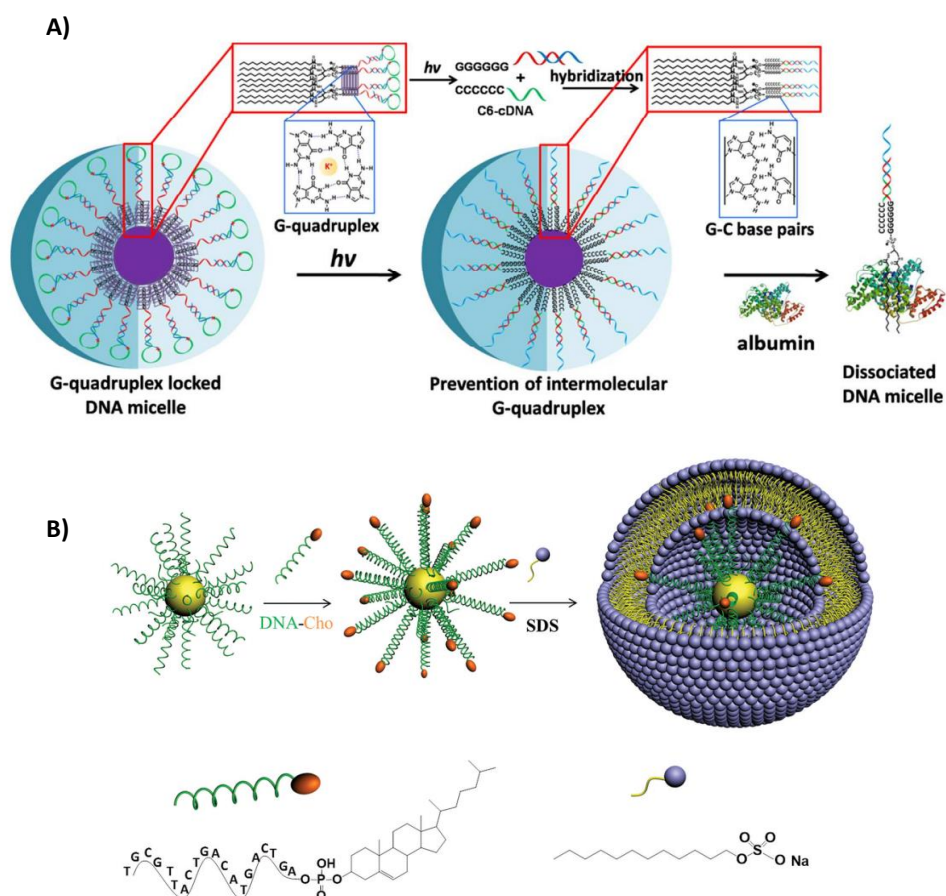
Figure 1.14. Schematic representation of A) DNA micelles stabilized by the formation of G-quadruplex and its dissociation upon UV-light exposure and binding with albumin; B) frame guided assembly process involving AuNps modified with 20-mer and 6-mer ssDNA, DNA modified with cholesterol and sodium dodecyl sulphate. (Adapted from references 101 and 102).

On the other hand, the conjugation of DNA with dendrimers provides the advantage of incorporation of multifunctionalities in the nanostructures, thereby the system can be applied for a variety of applications. Jean and co-workers have first reported the synthesis and self-assembly of a three component DNA–polyester dendrimer. Further, Sleiman and co-workers have achieved the formation of long range ordered 1D DNA nanofibers from the assembly of dendritic oligoethylene glycol modified DNA in an organic solvent and is shown in Figure 1.15A.[103] Later, Liu
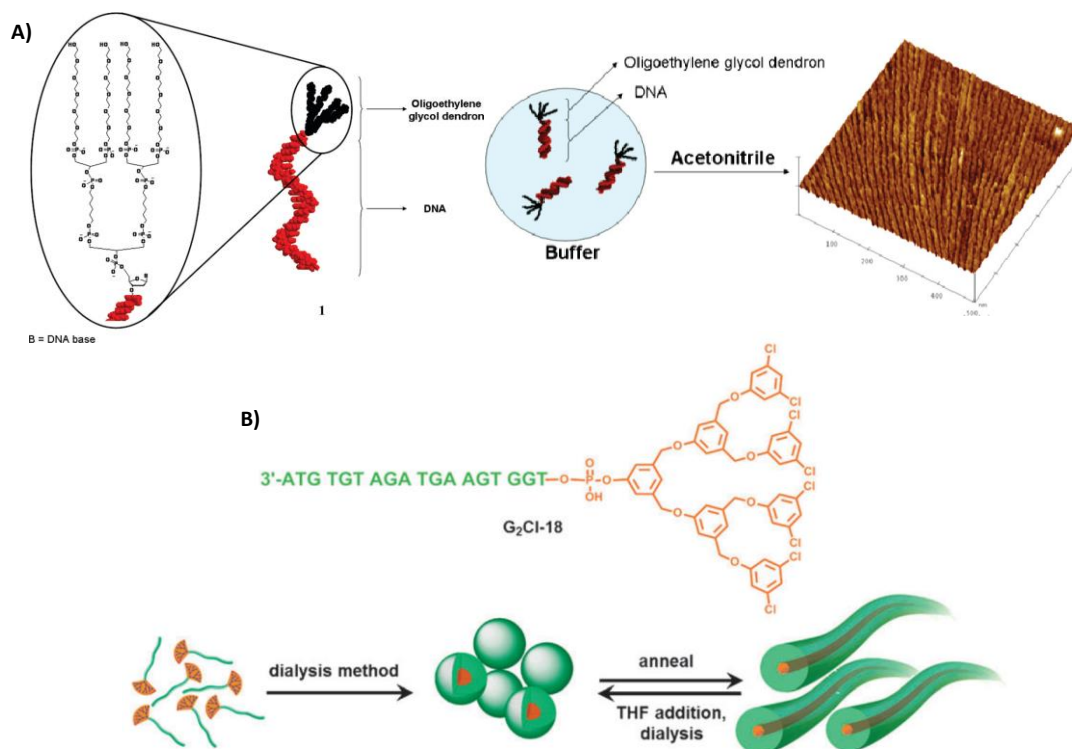
Figure 1.15. Schematic representation of A) dendritic oligoethylene glycol modified DNA and the AFM image of nanofibres formed during self-assembly in acetonitrile; B) DNA–dendron hybrid G2Cl-18 and the self-assembled spherical micelle and nanofibres that can be reversibly transformed. (Adapted from reference 103 and 105).

and co-workers have extensively worked on DNA-dendrimer conjugates and reported the formation of a series of novel DNA based assemblies.[104-106] In 2012, they have shown the formation of spherical DNA–dendron hybrid G2Cl-18 micelle and its reversible transformation to long nanofiber structures in aqueous solution (Figure 1.15B).[105] Later, Reji and co-workers explored the assembly of DNA-tetraphenylethylene based dendron to 2D-nanosheets and demonstrated its further surface functionalization with gold nanoparticles to enhance the catalytic activity of through precision positioning.[107]

Similarly, DNA diblock copolymers consist of DNA modified with hydrophobic polymer have gained great attention in the supramolecular DNA assembly and also can be employed for gene delivery applications. Park *et al.* has first reported the design of Poly(D,L-lactic-co-glycolic acid) (PLGA) attached antisense oligonucleotide for its delivery and they thoroughly investigated the cellular uptake behavior.[108] Subsequently, Mirkin and co-workers have designed DNA block-copolymer amphiphiles and further demonstrated its reversible and chemically programmable assembly behavior. Later, Liu and co-workers have developed morphology-changing DNA-b-PPO assemblies due to the *in situ* transition from diblock to triblock with pH change from 8 to 5. Further, they have utilized DNA-b-PPO to build DNA triblock polymer, PPO-dsDNA-PPO, through DNA hybridization and investigated the formation mechanism of spherical assemblies. In 2016, Park *et al.* utilized a thermos-responsive polymer, poly(N-isopropylacrylamide (PNIPAM) for the design of a dual responsive DNA diblock polymer (Figure 1.16A). The dual responsive multidimensional shape changing is due to hydrophilic nature of PNIPAM below lower critical solution temperature and the hydrophobic behaviour above lower critical solution temperature. Thus, DNA-b-PNIPAM-b-PMA is likely to form spherical assembly below LCST and cylindrical assembly above LCST. Moreover, the spherical shape can be retained even above LCST through hybridization with a complementary strand.[109] Recently, Sleiman and co-workers have demonstrated the formation of spherical DNA construct through the assembly of a DNA-polymer conjugate and its morphological transformation to DNA nanofibers on incorporation of cyanine dye to the conjugate (Figure 1.16B). The cyanine mediated assembly enables the controlled growth of nanofibers

through seeded-growth mechanism.[110] They have also demonstrated the use of the spherical nucleic acid for delivery of an anticancer drug, BKM120.[111]
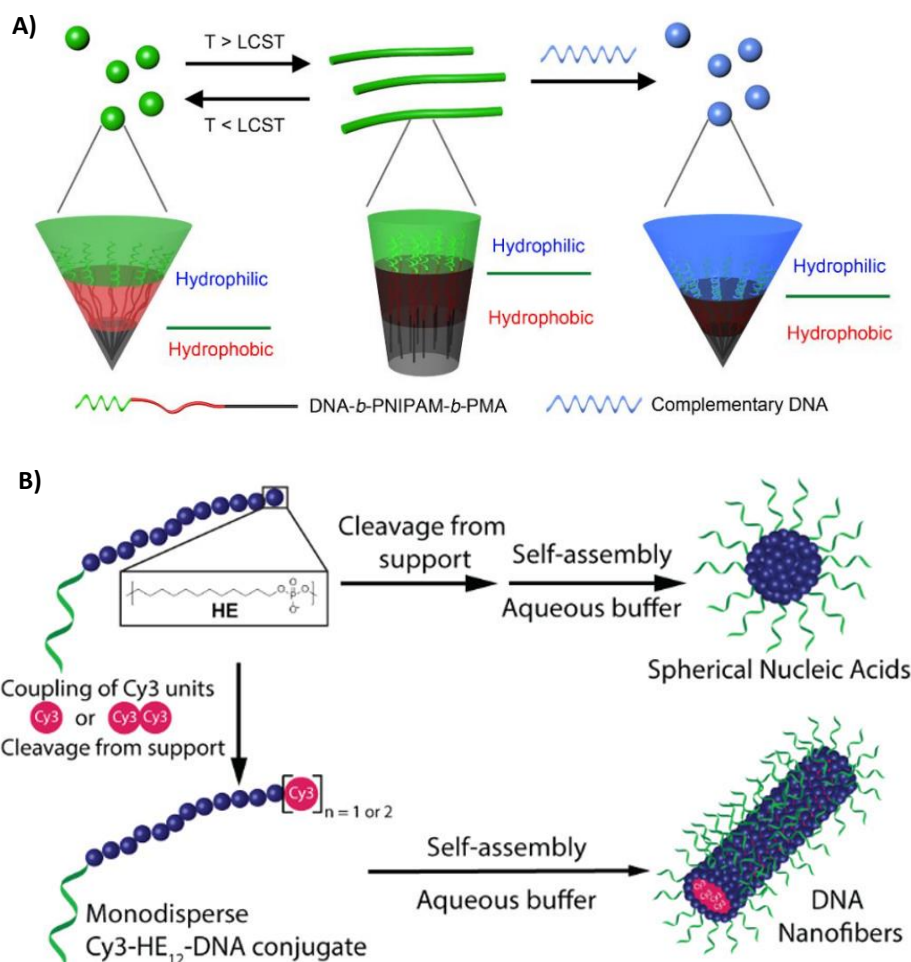
Figure 1.16. Schematic representation of A) dual responsive multidimensional shape changing of DNA diblock polymer; B) self-assembly of DNA –polymer conjugate and its morphological transformation with the covalent incorporation of cyanine dye (Adapted from references 109 and 110).

Covalently modified DNA with small molecules, capable of forming supramolecular polymers are greatly explored by several research groups and come up with lot of functional DNA nanostructures. The incorporation of chromophores in DNA structure can be either through the linkage with sugar unit or nucleobase, and is called nucleosidic chromophores. On the other hand, non-nucleocidic

chromophores are attached to the growing DNA strand through phosphoramidite chemistry. The nucleosidic chromophores can influence the Watson-Crick base pairing either through strong π-π stacking or by forming new H-bonds with the nuceobases. Major/minor groove binding aromatic nucleosidic chromophores often undergo further π-π stacking within them to form a supramolecular structure templated on DNA double helix. A simple modification to nucleobase structure is enough for making appropriate alterations in the DNA structure. Nucleobase analogues, simple aromatic hydrocarbons and heterocycles are highly recommended for the design of various DNA nanostructures. But, the non-nucleosidic chromophores generally assemble through the π-π stacking between themselves and with nucleobases and often lack the H-bonding possibility with the nucleobases. The occupancy of non- nucleosidic chromophore in the abasic sites of DNA is also reported. Moreover, the incorporation of fluorophores on DNA sequences through covalent linkages have made great impact in the biological research as well as in fluorescent material development.

Aromatic π-chromophores like pyrene, perylene, tetraphenylethylene etc. are generally employed for the design of DNA supramolecular polymers and this amphiphilic analogues self-assemble to form multidimensional structures with incredible functional properties. In 2006, Wagenknecht and co-workers have demonstrated the helical assembly of pyrene on duplex DNA through the incorporation of pyrene functionalised deoxyuridine to the sequence specific DNA strands.[112] Later, they have reported the white-light emitting DNA by arranging the donor and acceptor dyes on DNA backbone through covalent linkages.[113] They have further investigated the significant difference in the optical properties of Nile-red

assembly formed under non-covalent approach and covalent attachment on DNA by the design of a Nile red modified 2'-deoxyuridine.[114]

Later, Haner and co-workers, who have worked in the formation of DNA assisted π-stacked arrays of phenanthrene and pyrene, have achieved the a DNA-based light harvesting antenna by means of a DNA organised multichromophoric array of phenanthrene and pyrene.[115] Gradually, the idea of organising chromophores on DNA take a slight deviation to chromophore-guided assembly of DNA by prominently enhancing chromophore interactions, where the supramolecular assembly of chromophores take the charge of the assembly. Haner's group has achieved the formation of DNA grafted supramolecular polymers by the design of an oligopyrenotide strand on the 5'-end of an oligodeoxynucleotide.[116] Further, the group has demonstrated the heirarchical assembly of DNA grafted helical nanoribbon structures to extended nanoribbon-like structures in presence of complementary DNA strands through hybridisation (Figure 1.17A).[117] Later, the strategy has been extended to generate 2D-nanosheets, vesicles, nanotubes, nanowires etc. by utilising oligomers of various other π-chromophores like phenanthrene, anthracene, squaraine etc.[118-122] Likewise, they have designed a DNA conjugate with TPE sticky ends and demonstrated the formation of two different vesicles based on the different DNA arrangement under different conditions as shown in Figure 1.17B.[123]
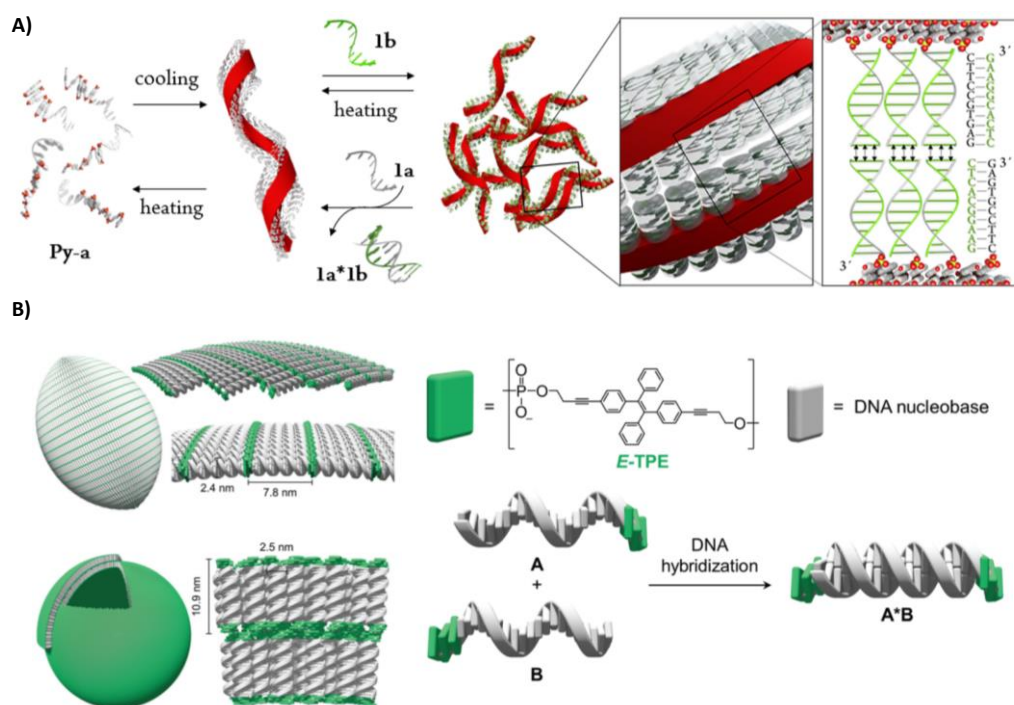
Figure 1.17. Schematic representation of A) heirarchical assembly of DNA grafted helical nanoribbon structures to extended nanoribbon-like structures; B) assembly of DNA conjugate with TPE sticky ends to form two different types of vesicles (Adapted from references 117 and 123).

Reji and co-workers have contributed majorly in the supramolecular DNA assembly by engineering DNA decorated lamellar structures with the design of various DNA amphiphiles using different π-chromophores including oligo(p-phenylene ethynylene), hexabenzocoronene, tetraphenylethylene, hexaphenyl benzene etc. A versatile library of DNA nanostructures like unilamellar vesicles, two-dimensional (2D) nanosheets, helical nanoribbons etc. can be provided by the variety of DNA amphiphiles and it also enable the organisation of other functional materials on this DNA nanostructures.

In aqueous environment, the amphiphilic nature of DNA-π chromophore hybrids tend it to orient the hydrophilic DNA part outside by protecting the

hydrophobic core in the interior. The dense population of DNA on the nanostructure surface provide opportunity for further functionalisation through hybridisation.
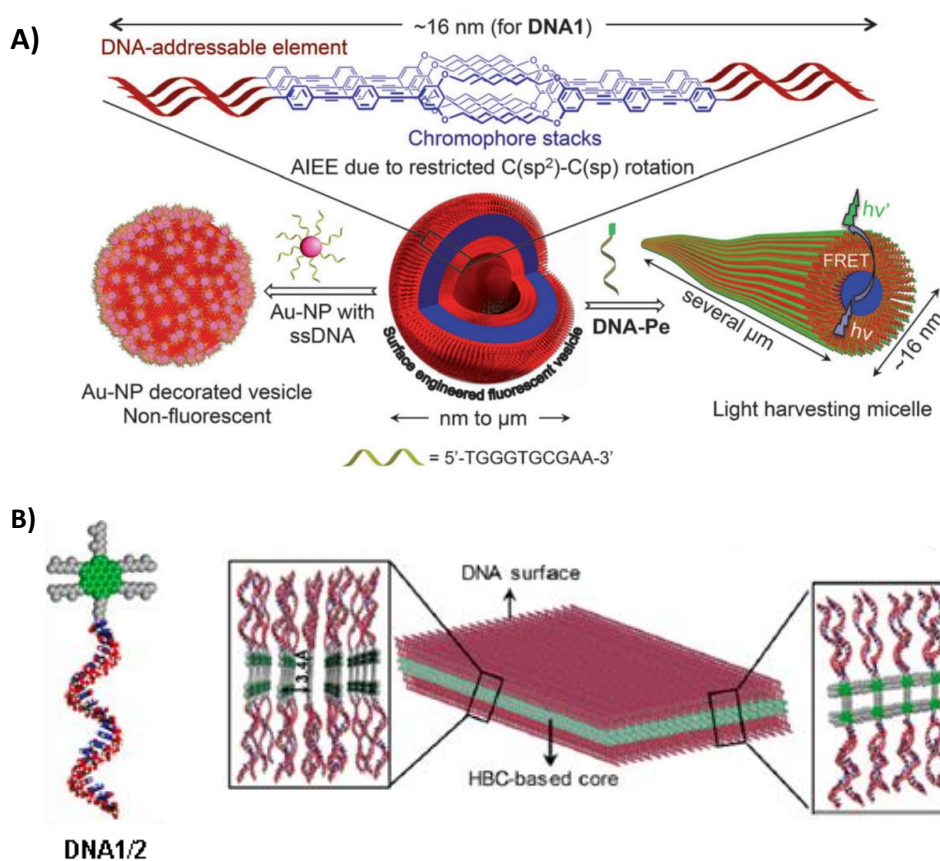
Figure 1.18. Schematic representation of A) assembly of DNA-OPE hybrid amphiphiles to surface engineered fluorescent vesicles and its surface decoration with gold nanoparticles and fluorophores; B) formation of 2-D crystalline nanosheets from HBC based DNA amphiphiles. (Adapted from references 124 and 125).

In 2014, Reji and co-workers demonstrated the reversible self-assembly of DNA-OPE hybrid amphiphiles to nanovesicles and the incorporation of gold nanoparticles to the surface of the vesicular assembly through DNA hybridisation. They have also shown the utility of these assemblies for generating a supramolecular antenna with the integration of suitable donor/acceptor chromophores (Figure 1.18A).[124] Later, they have achieved the formation of DNA decorated 2D-crystalline nanosheets by

the design of an hexabenzocoronene (HBC) based DNA amphiphile, by virtue of the large surface area imparted by the HBC core (Figure 1.18B).[125] In the following years, they have demonstrated the assembly of hexaphenylbenzene (HPB) attached DNA to helically twisted nanoribbons and established the utility as a scaffold for the generation of one-dimensional, chiral, plasmonic nanostructures.[126] They have also developed a pH responsive DNA vesicle based on amphiphilic C-rich DNA sequence attached with phenyleneethynylene as a nanocarrier.[127]

1.6.2.3. DNA templated assembly of small molecules via non-covalent approach

The non-covalent approach for the templated assembly of functional materials on DNA is highly desirable since it avoid the covalent modification of DNA, which require more sophisticated method and expertise for modified-DNA synthesis. The inherent structural characteristics of DNA provide various binding possibilities for different functional entities like small molecules, nanoparticles etc. through electrostatic interaction, intercalation, groove binding, H-bonding etc. The specific non-covalent interactions of suitably designed small molecules and DNA oligonucleotides lead to the helical arrangement of organic chromophores on DNA structure. In 2004, Armitage and co-workers have reported the helical assembly of cyanine dyes on specific DNA sequences through minor groove binding and discuss the excellent optical properties of the helical dye aggregates achieved via DNA templated supramolecular polymerization.[128] Two years later, Meijer and co-workers have demonstrated the supramolecular assembly of a nucleotide appended oligo(p-phenylenevinylene) (OPV) on a complementary oligonucleotide strand through A-T base pairing. Further, they have shown the helical assembly of

diaminotriazine appended naphthalene and OPV chromophores by virtue of H-bonding interactions.[129]
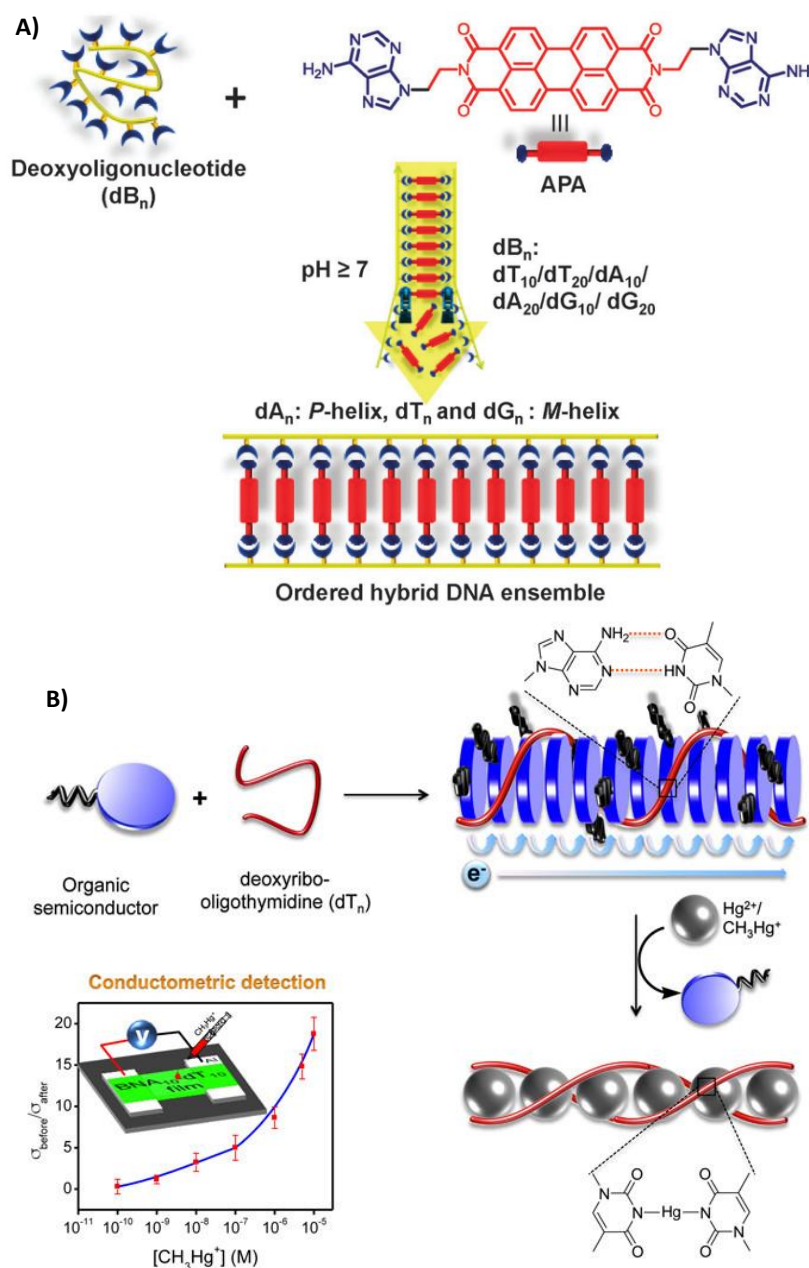
Figure 1.19. Schematic representation of A) double zipper assembly through the interaction of adenine functionalized perylene bisimide and deoxy-oligonucleotides; B) mercury sensing mechanism involving an organic semiconductor molecule and dTn based on strong interaction of mercury with thymine (Adapted from references 131 and 132).

Later, Wagenknecht and co-workers have investigated the non-covalent assembly of pyrene functionalized deoxyuridine on $(dA)_{17}$ and found that it possess similar optical properties as that of the assembly of pyrene functionalized deoxyuridine that are covalently attached to DNA. [130]

Further, the non-covalent approach has been adopted by Govindaraju and co-workers to design various functional DNA nanostructures. In 2015, they have demonstrated the mutual templating of an adenine functionalized perylene bisimide and deoxy-oligonucleotides to form a double zipper helical assembly as shown in Figure 1.19A.[131] Subsequently, they have designed a mercury sensing system by the mutually templated co-assembly of an organic semiconductor molecule, adenine conjugated naphthalene diimide, and deoxyribo-oligothymidine strands. The sensing mechanism rely on the strong interaction of mercury with the thymine units in the co-assembly, that eventually reflected in the chiroptical properties and electrical conductivity of 2D-sheets formed from templated assemblies of organic semiconductor and DNA due to the new assembly formation as shown in Figure 1.19B.[132]

Recently, our group has demonstrated the mutually assisted self-assembly of fullerene nanoclusters (FAn) and various oligonucleotides by the suitable design of an aniline appended amphiphilic fullerene derivative and achieved the formation of different DNA/fullerene conjugates with varying morphologies based on the type of oligonucleotide used for the assembly. The interaction of FAn with different DNA oligonucleotides primarily rely on groove binding favored by the presence of aniline moieties and the suitable nanocluster size (3-5 nm). Nanonetwork structures with chiral assembly of fullerene nanoclusters on DNA have been achieved on interaction with CTDNA and is shown in Figure 1.20A.[133] Meanwhile, the interaction with short

dsDNA results in the formation of semiconducting nanowires as shown in Figure 1.20B.[134]
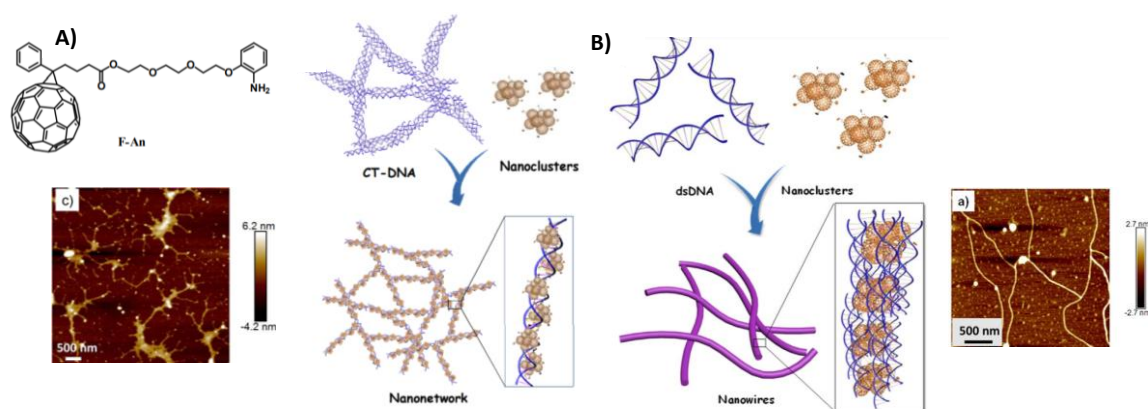
Figure 1.20. A) Molecular structure of FAn, schematic representations and corresponding AFM images of formation of nanonetwork on interaction with CT-DNA; B) formation of semiconducting nanowires on interaction with short dsDNA. (Adapted from references 133 and 134)

Further investigation on 3WJ-DNA/FAn hybrids shows the formation of 2D-nanosheets as in the Figure 1.21A. Correspondingly, the introduction of overhangs on 3WJ-DNA tends it to form entangled nanonetwork structures (Figure 1.21B).[135] Thus, the recent reports from our group collectively emphasis the simple non-covalent strategy, involving DNA groove binding of fullerene nanoclusters for the generation of versatile 1D and 2D DNA nanostructures beneficial for nanoelectronics applications. However, the potential of DNA to organize functional materials in a more ordered fashion through the use of simple non-covalent strategies by virtue of suitable amphiphilic design is yet to be investigated in detail.
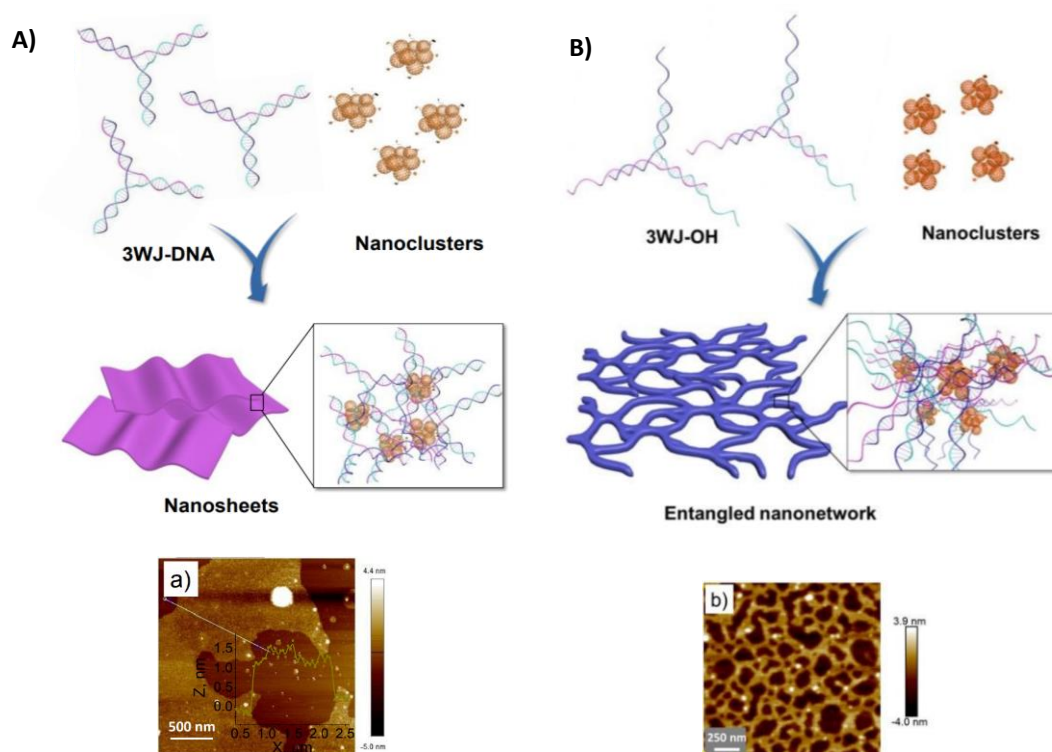
Figure 1.21. Schematic representations and corresponding AFM images of formation of A) nanosheets on interaction of FAn with 3WJ-DNA; B) Nanonetworks on interaction of FAn with 3WJ-DNA having overhangs. (Adapted from reference 135)

1.7. Objectives of the Present Investigation

DNA nanotechnology makes use of the sequence complementarity of nucleic acids in building long-range ordered, programmable DNA nanostructures, and prevails in engineering functional nanostructures through DNA origami, DNA tile assembly, and assembly of DNA amphiphiles etc. These current technologies rely on the synthesis and self-assembly of synthetic and modified oligonucleotides and the complex designs make it highly expensive and limit the large-scale production of DNA nanostructures. In this context, developing long-range ordered, functional DNA nanostructures from random, unmodified oligonucleotides is still an unresolved challenge. The present thesis addresses this challenge by proposing alternative strategies to attain DNA assisted assembly of small amphiphilic molecules by

employing different non-covalent interactions like electrostatic interaction, π-π stacking and H-bonding interactions.

The major objectives of the thesis include the DNA assisted ordered arrangement of amphiphilic small molecules by employing DNA condensation through charge neutralization (**Chapter 2A**), DNA intercalation through π-π stacking (**Chapter 3**) and nucleobase recognition through H-bonding interactions (**Chapter 4**). In order to investigate the present objective, we have employed fullerene/TPE based amphiphilic molecules with suitable pendant groups like pyridinium, aniline and diaminotriazine entities that can readily interact with various DNA oligonucleotides through different DNA binding modes. We have thoroughly investigated the differential interactions of these amphiphilic molecules with different DNA oligonucleotide strands in order to understand the role of DNA as a template for the ordered arrangement of functional moieties. As inspired from the DNA based assembly of fullerenes through electrostatic interactions, we have further demonstrated the ordered assembly of fullerenes by employing an anionic polymeric analogue, polystyrene sulfonate (**Chapter 2B**), and investigated the electron transport properties of the fullerene/polymer hybrid.

1.8. REFERENCES

1.   Qin, X.; Suga, M.; Kuang, T.; Shen, J. R., Photosynthesis. Structural basis for energy transfer pathways in the plant PSI-LHCI supercomplex. *Science* **2015,** *348* (6238), 989-95.

2.   Stillwell, W., Chapter 19 - Membrane Transport. In *An Introduction to Biological Membranes (Second Edition)*, Stillwell, W., Ed. Elsevier: **2016**; pp 423-451.

3.   Popp, D.; Robinson, R. C., Supramolecular cellular filament systems: How and why do they form? *Cytoskeleton* **2012,** *69* (2), 71-87.

4.   Pollard, T. D.; Borisy, G. G., Cellular motility driven by assembly and disassembly of actin filaments. *Cell* **2003,** *112* (4), 453-65.

5.   Wittmann, T.; Hyman, A.; Desai, A., The spindle: a dynamic assembly of microtubules and motors. *Nat. Cell Biol.* **2001,** *3* (1), E28-E34.

6.   Oberhofer, A.; Reithmann, E.; Spieler, P.; Stepp Willi, L.; Zimmermann, D.; Schmid, B.; Frey, E.; Ökten, Z., Molecular underpinnings of cytoskeletal cross-talk. *Proc. Natl. Acad. Sci.* **2020,** *117* (8), 3944-3952.

7.   Zhang, D.; Ren, W.; Zhu, Z.; Zhang, H.; Liu, B.; Shi, W.; Qin, X.; Cheng, C., Highly-ordered silicon inverted nanocone arrays with broadband light antireflectance. *Nanoscale Res. Lett.* **2015,** *10* (1), 9.

8.   Wu, Y.; Zhang, K.; Yang, B., Ordered Hybrid Micro/Nanostructures and Their Optical Applications. *Adv. Opt. Mater.* **2019,** *7* (7), 1800980.

9.   Feng, J.; Qiu, Y.; Jiang, L.; Wu, Y., Long-Range-Ordered Assembly of Micro-/Nanostructures at Superwetting Interfaces. *Adv. Mater.* **2022,** *34* (9), 2106857.

10.   Bai, Y.; Mora-Seró, I.; De Angelis, F.; Bisquert, J.; Wang, P., Titanium Dioxide Nanomaterials for Photovoltaic Applications. *Chem. Rev.* **2014,** *114* (19), 10095-10130.

11.   Wei, W.; Bai, F.; Fan, H., Oriented Gold Nanorod Arrays: Self-Assembly and Optoelectronic Applications. *Angew. Chem. Int. Ed.* **2019,** *58* (35), 11956-11966.

12.   Choi, M. K.; Yang, J.; Kang, K.; Kim, D. C.; Choi, C.; Park, C.; Kim, S. J.; Chae, S. I.; Kim, T.-H.; Kim, J. H.; Hyeon, T.; Kim, D.-H., Wearable red–green–blue

quantum dot light-emitting diode array using high-resolution intaglio transfer printing. *Nat. Commun.* **2015,** *6* (1), 7149.

13. Wei, Y.; Geng, Y.; Wang, K.; Gao, H.; Wu, Y.; Jiang, L., Organic ultrathin nanostructure arrays: materials, methods and applications. *Nanoscale Adv.* **2022,** *4* (11), 2399-2411.

14. Shi, Y.-L.; Wang, X.-D., 1D Organic Micro/Nanostructures for Photonics. *Adv. Funct. Mater.* **2021,** *31* (7), 2008149.

15. Yao, Y.; Zhang, L.; Orgiu, E.; Samorì, P., Unconventional Nanofabrication for Supramolecular Electronics. *Adv. Mater.* **2019,** *31* (23), 1900599.

16. Hoeben, F. J. M.; Jonkheijm, P.; Meijer, E. W.; Schenning, A. P. H. J., About Supramolecular Assemblies of π-Conjugated Systems. *Chem. Rev.* **2005,** *105* (4), 1491-1546.

17. Mahadevi, A. S.; Sastry, G. N., Cooperativity in Noncovalent Interactions. *Chem. Rev.* **2016,** *116* (5), 2775-2825.

18. Chen, S.; Cheng, S.-X.; Zhuo, R.-X., Self-Assembly Strategy for the Preparation of Polymer-Based Nanoparticles for Drug and Gene Delivery. *Macromol. Biosci.* **2011,** *11* (5), 576-589.

19. Liu, K.; Zheng, D.; Zhao, J.; Tao, Y.; Wang, Y.; He, J.; Lei, J.; Xi, X., pH-Sensitive nanogels based on the electrostatic self-assembly of radionuclide 131I labeled albumin and carboxymethyl cellulose for synergistic combined chemo-radioisotope therapy of cancer. *J. Mater. Chem. B* **2018,** *6* (29), 4738-4746.

20. Lombardo, D.; Kiselev, M. A.; Magazù, S.; Calandra, P., Amphiphiles Self-Assembly: Basic Concepts and Future Perspectives of Supramolecular Approaches. *Adv. Condens. Matter Phys.* **2015,** *2015*, 151683.

21.   Lindman, B.; Medronho, B.; Alves, L.; Norgren, M.; Nordenskiöld, L., Hydrophobic interactions control the self-assembly of DNA and cellulose. *Q. Rev. Biophys.* **2021,** *54*, e3.

22.   Camilloni, C.; Bonetti, D.; Morrone, A.; Giri, R.; Dobson, C. M.; Brunori, M.; Gianni, S.; Vendruscolo, M., Towards a structural biology of the hydrophobic effect in protein folding. *Sci. Rep.* **2016,** *6* (1), 28285.

23.   Lindman, B.; Medronho, B.; Alves, L.; Norgren, M.; Nordenskiöld, L., Hydrophobic interactions control the self-assembly of DNA and cellulose. *Q. Rev. Biophys.* **2021,** *54*.

24.   Zhang, J., Amphiphilic Membrane. In *Encyclopedia of Membranes*, Drioli, E.; Giorno, L., Eds. Springer Berlin Heidelberg: Berlin, Heidelberg, **2016**; pp 69-72.

25.   Chang, Y.; Yang, K.; Wei, P.; Huang, S.; Pei, Y.; Zhao, W.; Pei, Z., Cationic Vesicles Based on Amphiphilic Pillar[5]arene Capped with Ferrocenium: A Redox-Responsive System for Drug/siRNA Co-Delivery. **2014,** *53* (48), 13126-13130.

26.   Ishiwari, F.; Shoji, Y.; Fukushima, T., Supramolecular scaffolds enabling the controlled assembly of functional molecular units. *Chem. Sci.* **2018,** *9* (8), 2028-2041.

27.   Yashima, E.; Ousaka, N.; Taura, D.; Shimomura, K.; Ikai, T.; Maeda, K., Supramolecular Helical Systems: Helical Assemblies of Small Molecules, Foldamers, and Polymers with Chiral Amplification and Their Functions. *Chem. Rev.* **2016,** *116* (22), 13752-13990.

28.   Maibaum, L.; Dinner, A. R.; Chandler, D., Micelle Formation and the Hydrophobic Effect. *J. Phys. Chem. B* **2004,** *108* (21), 6778-6781.

29.   Xing, P.; Zhao, Y., Supramolecular Vesicles for Stimulus-Responsive Drug Delivery. *Small Methods* **2018,** *2* (4), 1700364.

30.   Hu, X.-Y.; Jia, K.; Cao, Y.; Li, Y.; Qin, S.; Zhou, F.; Lin, C.; Zhang, D.; Wang, L., Dual Photo- and pH-Responsive Supramolecular Nanocarriers Based on Water-Soluble Pillar[6]arene and Different Azobenzene Derivatives for Intracellular Anticancer Drug Delivery. *Chem. Eur. J.* **2015,** *21* (3), 1208-1220.

31.   da Silva, E. R.; Alves, W. A.; Castelletto, V.; Reza, M.; Ruokolainen, J.; Hussain, R.; Hamley, I. W., Self-assembly pathway of peptide nanotubes formed by a glutamatic acid-based bolaamphiphile. *Chem. Commun.* **2015,** *51* (58), 11634-11637.

32.   Jin, W.; Fukushima, T.; Niki, M.; Kosaka, A.; Ishii, N.; Aida, T., Self-assembled graphitic nanotubes with one-handed helical arrays of a chiral amphiphilic molecular graphene. *Proc. Natl. Acad. Sci. U S A.* **2005,** *102* (31), 10801-10806.

33.   Zhu, X.; Li, Y.; Duan, P.; Liu, M., Self-Assembled Ultralong Chiral Nanotubes and Tuning of Their Chirality Through the Mixing of Enantiomeric Components. *Chem. Eur. J.* **2010,** *16* (27), 8034-8040.

34.   VandenBerg, M. A.; Sahoo, J. K.; Zou, L.; McCarthy, W.; Webber, M. J., Divergent Self-Assembly Pathways to Hierarchically Organized Networks of Isopeptide-Modified Discotics under Kinetic Control. *ACS Nano* **2020,** *14* (5), 5491-5505.

35.   Gyepi-Garbrah, S. H.; Šilerová, R., The first direct comparison of self-assembly and Langmuir–Blodgett deposition techniques: Two routes to highly organized monolayers. *Phys. Chem. Chem. Phys.* **2002,** *4* (14), 3436-3442.

36. Ulman, A., Formation and Structure of Self-Assembled Monolayers. *Chem. Rev.* **1996,** *96* (4), 1533-1554.

37. Bi, S.; Yang, C.; Zhang, W.; Xu, J.; Liu, L.; Wu, D.; Wang, X.; Han, Y.; Liang, Q.; Zhang, F., Two-dimensional semiconducting covalent organic frameworks via condensation at arylmethyl carbon atoms. *Nat. Commun.* **2019,** *10* (1), 2467.

38. Tang, L.-P.; Yang, S.; Liu, D.; Wang, C.; Ge, Y.; Tang, L.-M.; Zhou, R.-L.; Zhang, H., Two-dimensional porous coordination polymers and nano-composites for electrocatalysis and electrically conductive applications. *J. Mater. Chem. A* **2020,** *8* (29), 14356-14383.

39. Chakraborty, G.; Park, I.-H.; Medishetty, R.; Vittal, J. J., Two-Dimensional Metal-Organic Framework Materials: Synthesis, Structures, Properties and Applications. *Chem. Rev.* **2021,** *121* (7), 3751-3891.

40. Vybornyi, M.; Rudnev, A.; Häner, R., Assembly of Extra-Large Nanosheets by Supramolecular Polymerization of Amphiphilic Pyrene Oligomers in Aqueous Solution. *Chem. Mater.* **2015,** *27* (4), 1426-1431.

41. Sasaki, N.; Yuan, J.; Fukui, T.; Takeuchi, M.; Sugiyasu, K., Control over the Aspect Ratio of Supramolecular Nanosheets by Molecular Design. *Chem. Eur. J.* **2020,** *26* (35), 7840-7846.

42. Sun, B.; Shen, B.; Urushima, A.; Liu, X.; Feng, X.; Yashima, E.; Lee, M., Asymmetric Transformation Driven by Confinement and Self-Release in Single-Layered Porous Nanosheets. *Angew. Chem. Int. Ed. Engl.* **2020,** *59* (50), 22690-22696.

43. Liu, X.; Zhou, X.; Shen, B.; Kim, Y.; Wang, H.; Pan, W.; Kim, J.; Lee, M., Porous Nanosheet Assembly for Macrocyclization and Self-Release. *J. Am. Chem. Soc.* **2020,** *142* (4), 1904-1910.

44.   Wang, Y.; Kim, Y.; Lee, M., Static and Dynamic Nanosheets from Selective Assembly of Geometric Macrocycle Isomers. *Angew. Chem. Int. Ed. Engl.* **2016,** *55* (42), 13122-13126.

45.   Wang, Y.; Feng, X.; Lee, M., Self-division of 2-D sheets in aromatic macrocycle assembly. *Org. Chem. Front.* **2021,** *8* (14), 3681-3685.

46.   Sun, H.; Dong, L.; Kim, Y.; Lee, M., Supramolecular Tubule from Seesaw Shaped Amphiphile and Its Hierarchical Evolution into Sheet. *Chem. Asian J.* **2020,** *15* (16), 2470-2474.

47.   Sun, B.; Kim, Y.; Wang, Y.; Wang, H.; Kim, J.; Liu, X.; Lee, M., Homochiral porous nanosheets for enantiomer sieving. *Nat. Mater.* **2018,** *17* (7), 599-604.

48.   Thomas, A.; Matthaei, J. F.; Baneyx, F., A Self-Assembling Two-Dimensional Protein Array is a Versatile Platform for the Assembly of Multicomponent Nanostructures. *Biotechnol. J.* **2018,** *13* (12), 1800141.

49.   Yan, H.; Park Sung, H.; Finkelstein, G.; Reif John, H.; LaBean Thomas, H., DNA-Templated Self-Assembly of Protein Arrays and Highly Conductive Nanowires. *Science* **2003,** *301* (5641), 1882-1884.

50.   Wang, P.; Gaitanaros, S.; Lee, S.; Bathe, M.; Shih, W. M.; Ke, Y., Programming Self-Assembly of DNA Origami Honeycomb Two-Dimensional Lattices and Plasmonic Metamaterials. *J. Am. Chem. Soc.* **2016,** *138* (24), 7733-7740.

51.   Carloni, L.-E.; Bezzu, C. G.; Bonifazi, D., Patterning Porous Networks through Self-Assembly of Programmed Biomacromolecules. *Chem. Eur. J.* **2019,** *25* (71), 16179-16200.

52.   Abb, S.; Harnau, L.; Gutzler, R.; Rauschenbach, S.; Kern, K., Two-dimensional honeycomb network through sequence-controlled self-assembly of oligopeptides. *Nat. Commun* **2016,** *7* (1), 10335.

53.   Ringler, P.; Schulz, G. E., Self-assembly of proteins into designed networks. *Science* **2003,** *302* (5642), 106-9.

54.   Espinosa Leal, L. A.; Lopez-Acevedo, O., On the interaction between gold and silver metal atoms and DNA/RNA nucleobases – a comprehensive computational study of ground state properties. *Nanotechnol. Rev.* **2015,** *4* (2), 173-191.

55.   Schultz, D.; Gardner, K.; Oemrawsingh, S. S. R.; Markešević, N.; Olsson, K.; Debord, M.; Bouwmeester, D.; Gwinn, E., Evidence for Rod-Shaped DNA-Stabilized Silver Nanocluster Emitters. *Adv. Mater.* **2013,** *25* (20), 2797-2803.

56.   Krueger, A. T.; Kool, E. T., Model systems for understanding DNA base pairing. *Curr. Opin. Chem. Biol.* **2007,** *11* (6), 588-594.

57.   Surin, M.; Ulrich, S., From Interaction to Function in DNA-Templated Supramolecular Self-Assemblies. *ChemistryOpen* **2020,** *9* (4), 480-498.

58.   Seeman, N. C., Nanotechnology and the double helix. *Sci. Am.* **2004,** *290* (6), 64-9, 72-5.

59.   Eichman, B. F.; Vargason, J. M.; Mooers, B. H. M.; Ho, P. S., The Holliday junction in an inverted repeat DNA sequence: Sequence effects on the structure of four-way junctions. *Proc. Natl. Acad. Sci. U S A.* **2000,** *97* (8), 3971-3976.

60.   Bochman, M. L.; Paeschke, K.; Zakian, V. A., DNA secondary structures: stability and function of G-quadruplex structures. *Nat. Rev. Genet* **2012,** *13* (11), 770-780.

61.   Weldon, C.; Eperon, I.; Dominguez, C., Do we know whether potential G-quadruplexes actually form in long functional RNA molecules? *Biochem. Soc. Trans.* **2016,** *44*, 1761-1768.

62. Dong, Y.; Yang, Z.; Liu, D., DNA Nanotechnology Based on i-Motif Structures. *Acc. Chem. Res.* **2014,** *47* (6), 1853-1860.

63. Snoussi, K.; Nonin-Lecomte, S.; Leroy, J. L., The RNA i-motif. *J. Mol. Biol.* **2001,** *309* (1), 139-53.

64. Richmond, T. J.; Davey, C. A., The structure of DNA in the nucleosome core. *Nature* **2003,** *423* (6936), 145-150.

65. Bracha, D.; Bar-Ziv, R. H., Dendritic and Nanowire Assemblies of Condensed DNA Polymer Brushes. *J. Am. Chem. Soc.* **2014,** *136* (13), 4945-4953.

66. Pardatscher, G.; Bracha, D.; Daube, S. S.; Vonshak, O.; Simmel, F. C.; Bar-Ziv, R. H., DNA condensation in one dimension. *Nat. Nanotechnol* **2016,** *11* (12), 1076-1081.

67. Yan, H.; LaBean, T. H.; Feng, L. P.; Reif, J. H., Directed nucleation assembly of DNA tile complexes for barcode-patterned lattices. *P. Natl. Acad. Sci. USA* **2003,** *100* (14), 8103-8108.

68. Yan, H.; Park, S. H.; Finkelstein, G.; Reif, J. H.; LaBean, T. H., DNA-templated self-assembly of protein arrays and highly conductive nanowires. *Science* **2003,** *301* (5641), 1882-1884.

69. Le, J. D.; Pinto, Y.; Seeman, N. C.; Musier-Forsyth, K.; Taton, T. A.; Kiehl, R. A., DNA-templated self-assembly of metallic nanocomponent arrays on a surface. *Nano Lett.* **2004,** *4* (12), 2343-2347.

70. Seifert, J. L.; Connor, R. E.; Kushon, S. A.; Wang, M.; Armitage, B. A., Spontaneous assembly of helical cyanine dye aggregates on DNA nanotemplates. *J. Am. Chem. Soc.* **1999,** *121* (13), 2987-2995.

71. Wang, M. M.; Silva, G. L.; Armitage, B. A., DNA-templated formation of a helical cyanine dye J-aggregate. *J. Am. Chem. Soc.* **2000,** *122* (41), 9977-9986.

72. Hannah, K. C.; Armitage, B. A., DNA-templated assembly of helical cyanine dye aggregates: A supramolecular chain polymerization. *Accounts Chem. Res.* **2004,** *37* (11), 845-853.

73. Datta, B.; Schuster, G. B.; McCook, A.; Harvey, S. C.; Zakrzewska, K., DNA-directed assembly of polyanilines: Modified cytosine nucleotides transfer sequence programmability to a conjoined polymer. *J. Am. Chem. Soc.* **2006,** *128* (45), 14428-14429.

74. Vittala, S. K.; Saraswathi, S. K.; Joseph, J., Fullerene Cluster Assisted Self-Assembly of Short DNA Strands into Semiconducting Nanowires. *Chem. Eur. J.* **2017**, 23, 15759.

75. Seeman, N. C., Nucleic-Acid Junctions and Lattices. *J. Theor. Biol.* **1982,** *99* (2), 237-247.

76. Kallenbach, N. R.; Ma, R. I.; Seeman, N. C., An Immobile Nucleic-Acid Junction Constructed from Oligonucleotides. *Nature* **1983,** *305* (5937), 829-831.

77. Seeman, N. C., Nucleic acid junctions and lattices. *J. Theor. Biol.* **1982,** *99* (2), 237-247.

78. Fu, T. J.; Seeman, N. C., DNA double-crossover molecules. *Biochemistry* **1993,** *32* (13), 3211-3220.

79. Tintoré, M.; Eritja, R.; Fábrega, C., DNA nanoarchitectures: steps towards biological applications. *Chembiochem* **2014,** *15* (10), 1374-90.

80. LaBean, T. H.; Yan, H.; Kopatsch, J.; Liu, F.; Winfree, E.; Reif, J. H.; Seeman, N. C., Construction, Analysis, Ligation, and Self-Assembly of DNA Triple Crossover Complexes. *J. Am. Chem. Soc.* **2000,** *122* (9), 1848-1860.

81. Jones Matthew, R.; Seeman Nadrian, C.; Mirkin Chad, A., Programmable materials and the nature of the DNA bond. *Science* **2015,** *347* (6224), 1260901.

82. Liu, D.; Wang, M.; Deng, Z.; Walulu, R.; Mao, C., Tensegrity: Construction of Rigid DNA Triangles with Flexible Four-Arm DNA Junctions. *J. Am. Chem. Soc.* **2004,** *126* (8), 2324-2325.

83. Zheng, J.; Birktoft, J. J.; Chen, Y.; Wang, T.; Sha, R.; Constantinou, P. E.; Ginell, S. L.; Mao, C.; Seeman, N. C., From molecular to macroscopic via the rational design of a self-assembled 3D DNA crystal. *Nature* **2009,** *461* (7260), 74-77.

84. He, Y.; Ye, T.; Su, M.; Zhang, C.; Ribbe, A. E.; Jiang, W.; Mao, C., Hierarchical self-assembly of DNA into symmetric supramolecular polyhedra. *Nature* **2008,** *452* (7184), 198-201.

85. Rothemund, P. W. K., Folding DNA to create nanoscale shapes and patterns. *Nature* **2006,** *440* (7082), 297-302.

86. Douglas, S. M.; Dietz, H.; Liedl, T.; Högberg, B.; Graf, F.; Shih, W. M., Self-assembly of DNA into nanoscale three-dimensional shapes. *Nature* **2009,** *459* (7245), 414-418.

87. Fu, J.; Liu, M.; Liu, Y.; Yan, H., Spatially-Interactive Biomolecular Networks Organized by Nucleic Acid Nanostructures. *Acc. Chem. Res.* **2012,** *45* (8), 1215-1226.

88. McLaughlin, C. K.; Hamblin, G. D.; Sleiman, H. F., Supramolecular DNA assembly. *Chem. Soc. Rev* **2011,** *40* (12), 5647-5656.

89. Shi, J.; Bergstrom, D. E., Assembly of Novel DNA Cycles with Rigid Tetrahedral Linkers. *Angew. Chem. Int. Ed. Engl.* **1997,** *36* (1-2), 111-113.

90.   Aldaye, F. A.; Sleiman, H. F., Sequential self-assembly of a DNA hexagon as a template for the organization of gold nanoparticles. *Angew. Chem. Int. Ed. Engl.* **2006,** *45* (14), 2204-9.

91.   Aldaye, F. A.; Sleiman, H. F., Guest-Mediated Access to a Single DNA Nanostructure from a Library of Multiple Assemblies. *J. Am. Chem. Soc.* **2007,** *129* (33), 10070-10071.

92.   Aldaye, F. A.; Sleiman, H. F., Modular Access to Structurally Switchable 3D Discrete DNA Assemblies. *J. Am. Chem. Soc.* **2007,** *129* (44), 13376-13377.

93.   Aldaye, F. A.; Lo, P. K.; Karam, P.; McLaughlin, C. K.; Cosa, G.; Sleiman, H. F., Modular construction of DNA nanotubes of tunable geometry and single- or double-stranded character. *Nat Nanotechnol* **2009,** *4* (6), 349-52.

94.   Yang, H.; Altvater, F.; de Bruijn, A. D.; McLaughlin, C. K.; Lo, P. K.; Sleiman, H. F., Chiral Metal–DNA Four-Arm Junctions and Metalated Nanotubular Structures. *Angew. Chem. Int. Ed.* **2011,** *50* (20), 4620-4623.

95.   Mitra, D.; Di Cesare, N.; Sleiman, H. F., Self-assembly of cyclic metal-DNA nanostructures using ruthenium tris(bipyridine)-branched oligonucleotides. *Angew. Chem. Int. Ed. Engl.* **2004,** *43* (43), 5804-8.

96.   Choi, J. S.; Kang, C. W.; Jung, K.; Yang, J. W.; Kim, Y.-G.; Han, H., Synthesis of DNA Triangles with Vertexes of Bis(terpyridine)iron(II) Complexes. *J. Am. Chem. Soc.* **2004,** *126* (28), 8606-8607.

97.   Yang, H.; McLaughlin, C. K.; Aldaye, F. A.; Hamblin, G. D.; Rys, A. Z.; Rouiller, I.; Sleiman, H. F., Metal–nucleic acid cages. *Nat. Chem* **2009,** *1* (5), 390-396.

98.   Raouane, M.; Desmaële, D.; Urbinati, G.; Massaad-Massade, L.; Couvreur, P., Lipid Conjugated Oligonucleotides: A Useful Strategy for Delivery. *Bioconjug. Chem.* **2012,** *23* (6), 1091-1104.

99.   Wu, Y.; Sefah, K.; Liu, H.; Wang, R.; Tan, W., DNA aptamer–micelle as an efficient detection/delivery vehicle toward cancer cells. *Proc. Natl. Acad. Sci.* **2010,** *107* (1), 5-10.

100.   Chen, T.; Wu, C. S.; Jimenez, E.; Zhu, Z.; Dajac, J. G.; You, M.; Han, D.; Zhang, X.; Tan, W., DNA Micelle Flares for Intracellular mRNA Imaging and Gene Therapy. *Angew. Chem. Int. Ed.* **2013,** *52* (7), 2012-2016.

101.   Jin, C.; Liu, X.; Bai, H.; Wang, R.; Tan, J.; Peng, X.; Tan, W., Engineering Stability-Tunable DNA Micelles Using Photocontrollable Dissociation of an Intermolecular G-Quadruplex. *ACS Nano* **2017,** *11* (12), 12087-12093.

102.   Dong, Y.; Yang, Z.; Liu, D., Using Small Molecules to Prepare Vesicles with Designable Shapes and Sizes via Frame-Guided Assembly Strategy. *Small* **2015,** *11* (31), 3768-3771.

103.   Carneiro, K. M. M.; Aldaye, F. A.; Sleiman, H. F., Long-Range Assembly of DNA into Nanofibers and Highly Ordered Networks Using a Block Copolymer Approach. *J. Am. Chem. Soc.* **2010,** *132* (2), 679-685.

104.   Wang, L.; Feng, Y.; Sun, Y.; Li, Z.; Yang, Z.; He, Y.-M.; Fan, Q.-H.; Liu, D., Amphiphilic DNA-dendron hybrid: a new building block for functional assemblies. *Soft Matter* **2011,** *7* (16), 7187-7190.

105.   Wang, L.; Feng, Y.; Yang, Z.; He, Y.-M.; Fan, Q.-H.; Liu, D., Reversibly controlled morphology transformation of an amphiphilic DNA–dendron hybrid. *Chem. Commun.* **2012,** *48* (31), 3715-3717.

106.   Goh, S. L.; Francis, M. B.; Fréchet, J. M. J., Self-assembled oligonucleotide-polyester dendrimers. *Chem. Commun.* **2002,** (24), 2954-2955.

107.   Krishnan, N.; Golla, M.; Thelu, H. V. P.; Albert, S. K.; Atchimnaidu, S.; Perumal, D.; Varghese, R., Self-assembly of DNA-tetraphenylethylene

amphiphiles into DNA-grafted nanosheets as a support for the immobilization of gold nanoparticles: a recyclable catalyst with enhanced activity. *Nanoscale* **2018,** *10* (36), 17174-17181.

108. Jeong, J. H.; Park, T. G., Novel Polymer−DNA Hybrid Polymeric Micelles Composed of Hydrophobic Poly(d,l-lactic-co-glycolic Acid) and Hydrophilic Oligonucleotides. *Bioconjug. Chem.* **2001,** *12* (6), 917-923.

109. Kim, C.-J.; Hu, X.; Park, S.-J., Multimodal Shape Transformation of Dual-Responsive DNA Block Copolymers. *J. Am. Chem. Soc.* **2016,** *138* (45), 14941-14947.

110. Bousmail, D.; Chidchob, P.; Sleiman, H. F., Cyanine-Mediated DNA Nanofiber Growth with Controlled Dimensionality. *J. Am. Chem. Soc.* **2018,** *140* (30), 9518-9530.

111. Bousmail, D.; Amrein, L.; Fakhoury, J. J.; Fakih, H. H.; Hsu, J. C. C.; Panasci, L.; Sleiman, H. F., Precision spherical nucleic acids for delivery of anticancer drugs. *Chem. Sci.* **2017,** *8* (9), 6218-6229.

112. Mayer-Enthart, E.; Wagenknecht, H.-A., Structure-Sensitive and Self-Assembled Helical Pyrene Array Based on DNA Architecture. *Angew. Chem. Int. Ed.* **2006,** *45* (20), 3372-3375.

113. Varghese, R.; Wagenknecht, H.-A., White-Light-Emitting DNA (WED). *Chem. Eur. J.* **2009**, 15 (37), 9307-9310.

114. Varghese, R.; Wagenknecht, H.-A., Non-covalent Versus Covalent Control of Self-Assembly and Chirality of Nile Red-modified Nucleoside and DNA. *Chem. Eur. J.* **2010,** *16* (30), 9040-9046.

115. Garo, F.; Häner, R., A DNA-Based Light-Harvesting Antenna. *Angew. Chem. Int. Ed.* **2012,** *51* (4), 916-919.

116. Vyborna, Y.; Vybornyi, M.; Rudnev, A. V.; Häner, R., DNA-Grafted Supramolecular Polymers: Helical Ribbon Structures Formed by Self-Assembly of Pyrene–DNA Chimeric Oligomers. *Angew. Chem. Int. Ed.* **2015,** *54* (27), 7934-7938.

117. Vyborna, Y.; Vybornyi, M.; Häner, R., From Ribbons to Networks: Hierarchical Organization of DNA-Grafted Supramolecular Polymers. *J. Am. Chem. Soc.* **2015,** *137* (44), 14051-14054.

118. Yu, H.; Alexander, D. T. L.; Aschauer, U.; Häner, R., Synthesis of Responsive Two-Dimensional Polymers via Self-Assembled DNA Networks. *Angew. Chem. Int. Ed.* **2017,** *56* (18), 5040-5044.

119. Bösch, C. D.; Jevric, J.; Bürki, N.; Probst, M.; Langenegger, S. M.; Häner, R., Supramolecular Assembly of DNA-Phenanthrene Conjugates into Vesicles with Light-Harvesting Properties. *Bioconjug. Chem.* **2018,** *29* (5), 1505-1509.

120. Yu, H.; Sabetti, M.; Häner, R., Formation of Supramolecular Nanotubes by Self-assembly of a Phosphate-linked Dimeric Anthracene in Water. *Chem. Asian J.* **2018,** *13* (8), 968-971.

121. Kownacki, M.; Langenegger, S. M.; Liu, S.-X.; Häner, R., Integrating DNA Photonic Wires into Light-Harvesting Supramolecular Polymers. *Angew. Chem. Int. Ed.* **2019,** *58* (3), 751-755.

122. Markova, L.; Probst, M.; Häner, R., Assembly and functionalization of supramolecular polymers from DNA-conjugated squaraine oligomers. *RSC Adv.* **2020,** *10* (73), 44841-44845.

123. Rothenbühler, S.; Iacovache, I.; Langenegger, S. M.; Zuber, B.; Häner, R., Supramolecular assembly of DNA-constructed vesicles. *Nanoscale* **2020,** *12* (41), 21118-21123.

124. Albert, S. K.; Thelu, H. V. P.; Golla, M.; Krishnan, N.; Chaudhary, S.; Varghese, R., Self-Assembly of DNA–Oligo(p-phenylene-ethynylene) Hybrid Amphiphiles into Surface-Engineered Vesicles with Enhanced Emission. *Angew. Chem. Int. Ed.* **2014,** *53* (32), 8352-8357.

125. Albert, S. K.; Sivakumar, I.; Golla, M.; Thelu, H. V. P.; Krishnan, N.; K. L, J. L.; Ashish; Varghese, R., DNA-Decorated Two-Dimensional Crystalline Nanosheets. *J. Am. Chem. Soc.* **2017,** *139* (49), 17799-17802.

126. Golla, M.; Albert, S. K.; Atchimnaidu, S.; Perumal, D.; Krishnan, N.; Varghese, R., DNA-Decorated, Helically Twisted Nanoribbons: A Scaffold for the Fabrication of One-Dimensional, Chiral, Plasmonic Nanostructures. *Angew. Chem. Int. Ed.* **2019,** *58* (12), 3865-3869.

127. Albert, S. K.; Golla, M.; Thelu, H. V. P.; Krishnan, N.; Varghese, R., A pH-Responsive DNAsome from the Self-Assembly of DNA–Phenyleneethynylene Hybrid Amphiphile. *Chem. Eur. J.* **2017,** *23* (35), 8348-8352.

128. Hannah, K. C.; Armitage, B. A., DNA-Templated Assembly of Helical Cyanine Dye Aggregates: A Supramolecular Chain Polymerization. *Acc. Chem. Res.* **2004,** *37* (11), 845-853.

129. Iwaura, R.; Hoeben, F. J. M.; Masuda, M.; Schenning, A. P. H. J.; Meijer, E. W.; Shimizu, T., Molecular-Level Helical Stack of a Nucleotide-Appended Oligo(p-phenylenevinylene) Directed by Supramolecular Self-Assembly with a Complementary Oligonucleotide as a Template. *J. Am. Chem. Soc.* **2006,** *128* (40), 13298-13304.

130. Sezi, S.; Wagenknecht, H.-A., DNA-templated formation of fluorescent self-assembly of ethynyl pyrenes. *Chem. Commun.* **2013,** *49* (81), 9257-9259.

131. Govindaraju, T.; Narayanaswamy, N.; Gorle, S.; Priyakumar, U., Double zipper helical assembly of deoxyoligonucleotides: Mutual templating and chiral imprinting to form hybrid DNA ensembles. *Chem. Commun.* **2014,** *51*.

132. Pandeeswar, M.; Senanayak, S. P.; Govindaraju, T., Nanoarchitectonics of Small Molecule and DNA for Ultrasensitive Detection of Mercury. *ACS Appl. Mater. Interfaces* **2016,** *8* (44), 30362-30371.

133. Vittala, S. K.; Joseph, J., Chiral self-assembly of fullerene clusters on CT-DNA templates. *Faraday Discuss.* **2018,** *207*, 459-469.

134. Vittala, S. K.; Saraswathi, S. K.; Joseph, J., Fullerene Cluster Assisted Self-Assembly of Short DNA Strands into Semiconducting Nanowires. *Chem. Eur. J.* **2017,** *23* (62), 15759-15765.

135. Vittala, S. K.; Saraswathi, S. K.; Ramesan, A. B.; Joseph, J., Nanosheets and 2D-nanonetworks by mutually assisted self-assembly of fullerene clusters and DNA three-way junctions. *Nanoscale Adv.* **2019,** *1* (10), 4158-4165.

DNA ASSISTED ASSEMBLY OF AN AMPHIPHILIC FULLERENE DERIVATIVE AND FORMATION OF ULTRATHIN CRYSTALLINE NANOSHEETS VIA DNA CONDENSATION
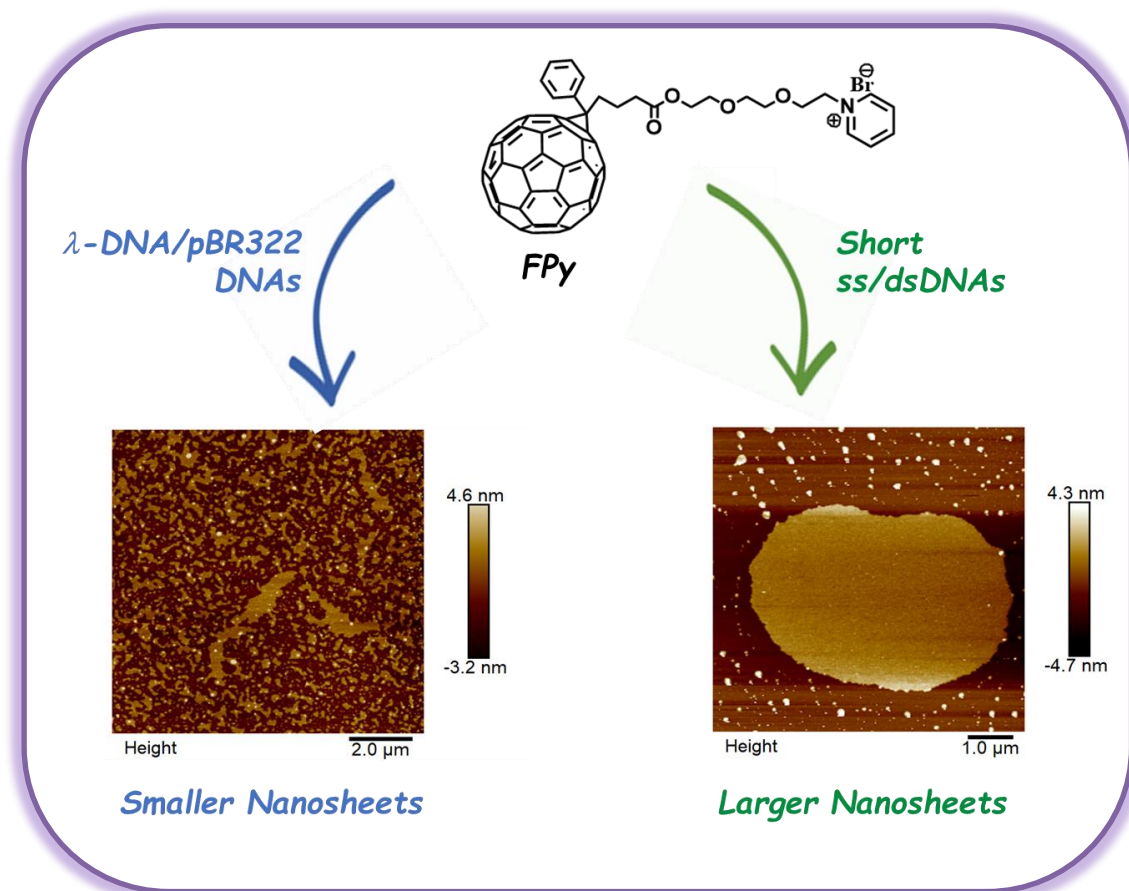
2A.1. ABSTRACT

*This chapter describes the mutually assisted assembly of an amphiphilic fullerene derivative and various DNA structures through non-covalent interactions, which leads to initial charge neutralisation and subsequent formation of ultrathin DNA-fullerene nanosheets with ordered fullerene assembly. The molecular design of cationic, amphiphilic fullerene derivative (**FPy**) ensures molecular solubility in 10%*

*DMSO-PBS buffer system and facile interactions with DNA through groove binding and electrostatic interactions of fullerene moiety and positively charged pyridinium moiety, respectively. The formation of **DNA/FPy** nanostructures were investigated in the presence of λ-DNA, pBR322 plasmid DNA, and single and double stranded 20-mer oligonucleotides using UV-visible spectroscopy, AFM and TEM analysis. λ-DNA and pBR322 plasmid DNA readily condense in presence of **FPy** leading to micrometer sized few layer nanosheets with significant crystallinity due to ordered arrangement of fullerenes. Similarly, single and double stranded 20-mer oligonucleotides also interact efficiently with **FPy** and form highly crystalline nanosheets, signifying the role of electrostatic interaction and subsequent charge neutralization in the condensation triggered assembly. However, there are significant differences in the crystallinity and ordered arrangements of fullerenes between these two cases, where longer DNA form condensed structures and less ordered nanosheets while short oligonucleotides lead to more ordered and highly crystalline nanosheets, which could be attributed to the differential DNA condensation. Finally, we have demonstrated the addressability of the assembly using a cyanine modified single strand DNA, which also forms highly crystalline nanosheets and exhibit efficient quenching of the cyanine fluorescence upon self-assembly.*

2A.2. INTRODUCTION

Fullerene, 'the beautiful molecule' described by Harold Kroto, is a truncated icosahedron (Ih) with 20 hexagons and 12 pentagons consist of sp^2 hybridized carbon atoms having a diameter of 7.1 Å.[1] As it resembles the geodesmic dome designed by the American architect R. Buckminster Fuller, fullerenes attained the name Buckminster Fullerene or simply 'Bucky Balls'. Fullerene was discovered in

1985 by Robert F. Curl, Harold W. Kroto and Richard E. Smalley and they have honored by the Nobel Prize in Chemistry in 1996.[2] Fullerenes, with the versatile physicochemical properties have created tremendous interest in science community and significantly contributed to the progress of different research areas. Fullerenes are still a matter of attraction for researchers and are considered as one of the most extensively studied carbon nanomaterial in recent years due to its excellent redox, optical and optoelectronic properties[3,4] along with its significant biological impacts.[5-7] Even though the fascinating structure imparts several advantages on its physical and chemical properties, highly hydrophobic cage raise challenge over its biomedical applications. The solubility issue of bare fullerene has been sensibly addressed by the synthesis of water soluble fullerene derivatives through proper chemical modifications.[8,9] Fullerenes find a stable platform at the fine edge of photovoltaic technological developments through extensive research on supramolecular assembly of pristine fullerenes and its derivatives.[10,11]

Fullerene molecules can be organized into various lattices through self/templated assembly to generate new properties by design. Self-organization of fullerenes has gathered much attention in developing various functional nanostructures with controlled dimensions and tailored properties.[12,13] As far as pristine fullerene is considered, solution-based processes are engaged since the solvent alone play role in their assembly. Different sample preparation procedures like vapor-driven crystallization[14] and solution-driven self-assemblies such as liquid–liquid interfacial precipitation (LLIP) (Figure 2A.1A)[15], template assisted dip drying[16] and drop drying[17] processes have been adapted to the assembly of C_{60}.
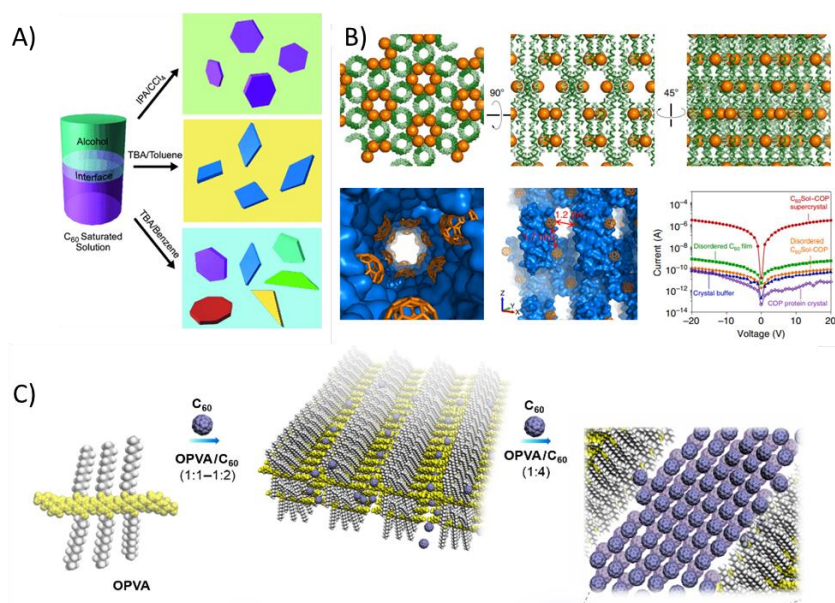
Figure 2A.1. Schematic representation of fullerene assemblies through: A) liquid–liquid interfacial precipitation (LLIP) method; B) Protein templated assembly & C) Gel-mediated assembly (Adapted from reference 15, 18 and 19).

Apart from the solvent mediated assembly process, templated assembly of pristine fullerenes has gained great attention due to the precision positioning and tailored properties. In 2015, Kim *et al.* reported the self-assembly of C_{60} into ordered superstructures through protein templated assembly. Here, the precisely engineered tetrameric helical bundle binds with C_{60} in solution, rendering it water soluble and the fullerene groups sandwiched between 2 Tyr residues from adjacent tetramers leads to the ordered assembly of fullerenes (Figure 2A.1B) with high charge conductance.[18] A recent study, by Ajayaghosh and co-workers, about the interaction of C_{60} with the π-gelator OPVA in toluene, reveals that the hybrid gel with different composition of OPVA/C_{60} make way for the formation of C_{60} clusters which gradually spread out to nucleate the growth of fullerene rods at the low molar ratio of C_{60} (1:1 to1:2) as shown in Figure 2A.1C. These C_{60} supramolecular rods in the π-gel medium exhibited high photocurrent in comparison to C_{60} loaded in a non π gel

medium. This study demonstrated the preparation of micrometer sized photoconducting rods of fullerenes for device application.[19]

Design and self-assembly of amphiphilic fullerenes is a diverse approach for the nanoscale fullerene organization for various potential applications.[20] Amphiphilic self-assembly can be achieved either through solvent mediated technics like liquid-liquid interfacial precipitation and Langmuir-Blodgett method (Figure 2A.2A)[21] or through supramolecular assembly process (Figure 2A.2B).[22] The supramolecular assemblies of amphiphilic fullerene derivatives with suitable functional moieties often provide better functional combinations in both optoelectronic and biological applications. For example, Prato and co-workers have reported the self-organization of a zinc phthalocyanine and C_{60} moieties in amphiphilic phthalocyanine-fullerene salt that provide a better electron transport between this donor-acceptor dyad.[23] Aida and co-workers also have used a similar concept to generate a photoconductive ambipolar coaxial nanotube through the
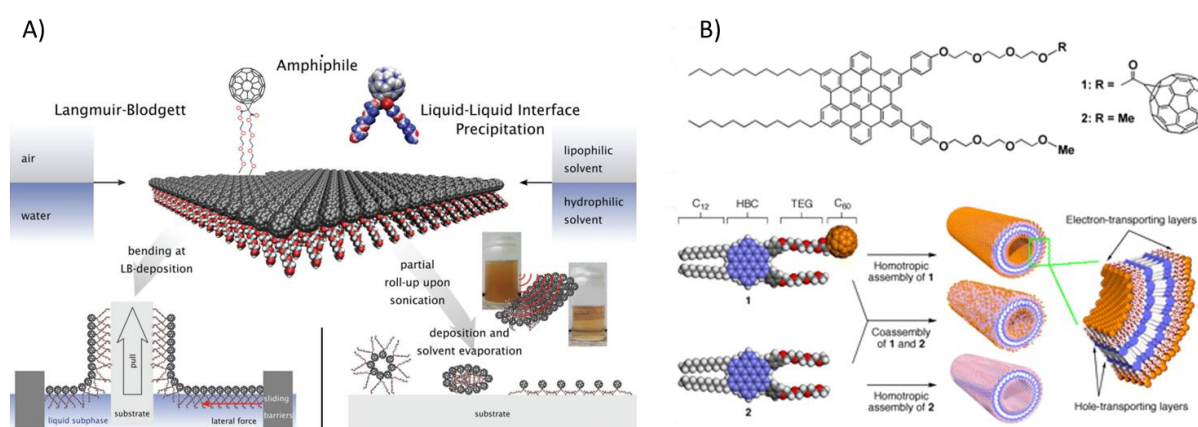
Figure 2A.2. Schematic representation of amphiphilic fullerene assemblies through A) solvent mediated methods and B) supramolecular assembly process (Adapted from reference 21 and 22).

amphiphilic self-assembly of a hexabenzocoronene-fullerene conjugate.[22] Likewise, Wagenknecht and co-workers demonstrated the templated supramolecular chromophore assemblies by the design of a DNA-fullerene conjugate.[24]

The fullerene/DNA interactions are investigated in early days by considering its biological implications such as DNA photocleavage[25], DNA condensation[26] etc. as shown in Figure 2A.3A & B and is further widely studied for the development of drug/gene delivery systems.[27,28] Suitable chemical modification of fullerenes with DNA interacting moieties further enhance the affinity of fullerenes with DNA and also helps to solubilize fullerene in water. Nakamura and co-workers extensively investigated the interaction of cationic fullerene derivative with DNA and its DNA condensation ability. The pioneering work from the group of Nakamura provides a library of amino-fullerenes for gene delivery applications.[29] Apart from the biological context, DNA/fullerene interactions are also engaged in optoelectronic fields to generate ordered nanoscale assembly of fullerenes through DNA templated
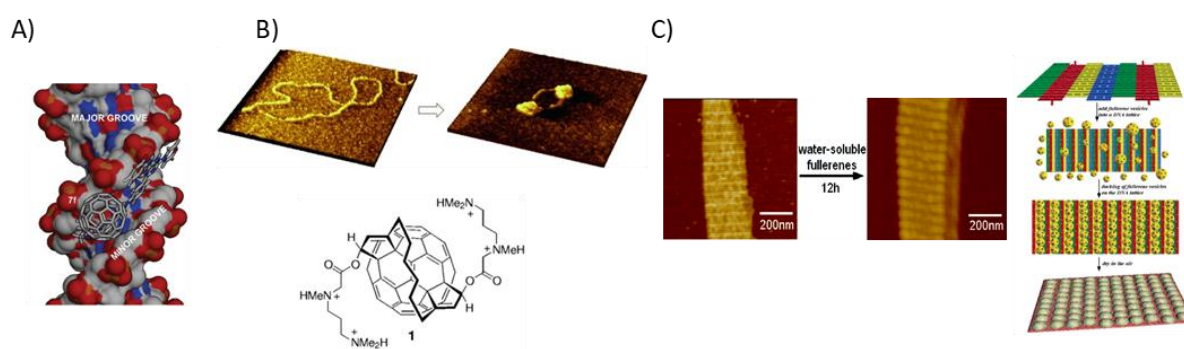
Figure 2A.3. A) Docked conformation of triazine appended fullerene derivative in DNA minor groove; B) AFM images showing condensation of plasmid DNA with cationic aminofullerenes; C) AFM images of template assembly of fullerene arrays on 2D DNA scaffolds and the schematic representation of self-assembly procedure of fullerene vesicles on the 2D DNA scaffolds (Adapted from reference 25, 29 and 30).

assembly strategies. Cheng *et al.* has employed 2D-DNA lattices, designed *via* DNA tile assembly, for the formation of fullerene arrays in aqueous media by means of groove binding and electrostatic interaction with the phosphate backbone(Figur 2A.3C).[30] However, this strategy involves the primary design of a DNA scaffold, which is a challenging task.[31]

Recently, our group has introduced a facile, non-covalent strategy for the formation of fullerene/DNA nanostructures through the design of an aniline appended fullerene derivative (**FAn**) and its interaction with various DNA structures (Figure 2A.4). The mutually assisted assemblies of **FAn** nanoclusters with different DNA structures like CT-DNA, dsDNA and 3WJ-DNA have achieved the formation of nanonetwork[32], nanowire[33] and nanosheet-like[34] DNA/fullerene nanostructures as shown in Figure 2A.4.
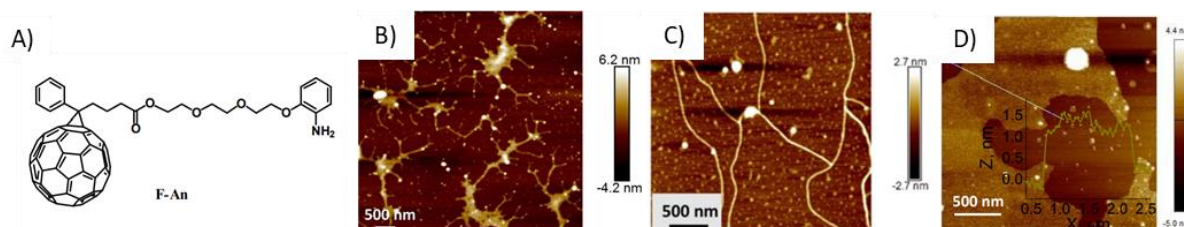
Figure 2A.4. A) Molecular structure of aniline appended fullerene derivative Fan. AFM images of: B) Nanonetwork formation from CT-DNA/FAn hybrid; C) Nanowires formation from dsDNA/FAn hybrid and D) Nanosheets from 3WJ-DNA/FAn hybrid. (Adapted from reference 32, 33 and 34).

In this Chapter, we have demonstrated the DNA assisted, long range, ordered assembly of fullerenes through a facile non-covalent approach using a cationic fullerene amphiphile (**FPy**) and various DNA structures leading to the formation of micrometer sized ultrathin nanosheets. Longer duplex DNAs such as linear λ-DNA and circular pBR322 plasmid DNA readily condense in presence of **FPy** to form

nanosheet structures with sub-micrometer lateral dimensions. On the other hand, short single strand and double strand DNAs form extended nanosheets with significantly higher crystallinity. Here, the **DNA/FPy** nanosheet formation is encouraged by electrostatic interaction of DNA with the cationic **FPy**, subsequent charge neutralization and possible fullerene-fullerene and fullerene-nucleobase π-π stacking interactions. Subtle changes in the hydrophilic-hydrophobic balance of the amphiphilic fullerene derivative upon interactions with DNA also contribute to the formation of nanosheets with ordered assembly of fullerenes. Finally, we have demonstrated the addressability of the nanosheet assembly using a cyanine modified single strand DNA, which exhibit efficient quenching of cyanine fluorescence through possible electron transfer from cyanine to fullerene by means of **DNA/FPy** assembly.

2A.3. RESULTS AND DISCUSSION

2A.3.1. SYNTHESIS AND CHARACTERISATION OF FULLERENE AMPHIPHILE

The fullerene amphiphile (**FPy**) is carefully designed to integrate a DNA binding moiety like cationic pyridinium group, which will enhance the solubility in aqueous media, enhance the hydrophilicity of the molecule and efficiently interact with DNA through electrostatic interactions.[35,36] This molecular design will further assist the self-assembly of fullerene moiety via charge neutralization upon electrostatic interaction of pyridinium group with anionic DNA structures. Cationic pyridinium group is linked with fullerene through a triethylene glycol chain, which imparts more hydrophilicity to the molecule and the synthesis of **FPy** was carried out by a previously reported muti-step synthesis procedure[33] as shown in Scheme 2A.1.
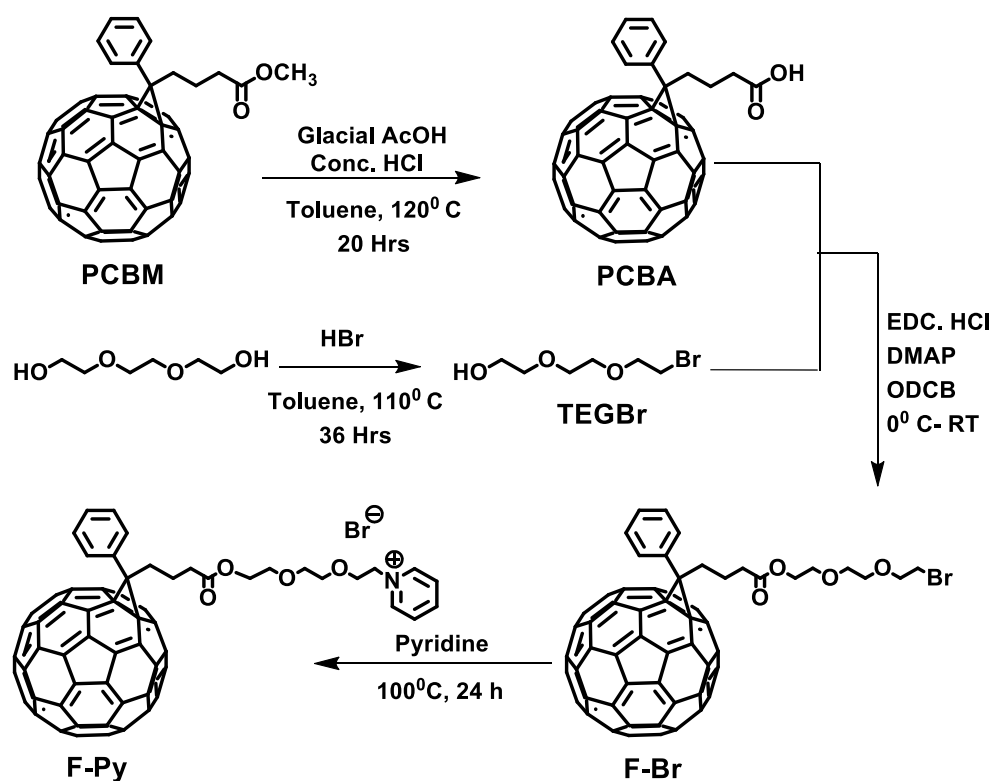
Scheme 2A.1. Synthesis of pyridinium appended fullerene amphiphile, **FPy.**

Methyl [6, 6]-phenyl-C61-butyrate (**PCBM**) is used as the fullerene precursor, which on acid hydrolysis yielded [6, 6]-Phenyl-C61-butyric acid (**PCBA**). EDC coupling of **PCBA** with 2-(2-(2-bromoethoxy)ethoxy)ethanol (**TEGBr**) gave bromo-substituted fullerene derivative (**F-Br**). Quaternization reaction of **FBr** with pyridine provided cationic **FPy**. Synthesized molecules were characterized through ^{1}H and ^{13}C NMR spectroscopy and mass spectrometry, which is detailed in experimental section. Solubility of **FPy** was checked in highly polar solvent, DMSO and 10% DMSO-PBS mixture for the purpose of DNA interaction studies and found that **FPy** is readily soluble in both solvent systems. UV-visible absorption spectra of **FPy** in DMSO and DMSO-PBS mixture showed similar peaks with λ_{max} around 260 nm and

334 nm as shown in Figure 2A.5A. TEM and AFM analysis of **FPy** ensures the molecular solubility in 10% DMSO-PBS mixture (Figures 2A.5B & 2A.5C).
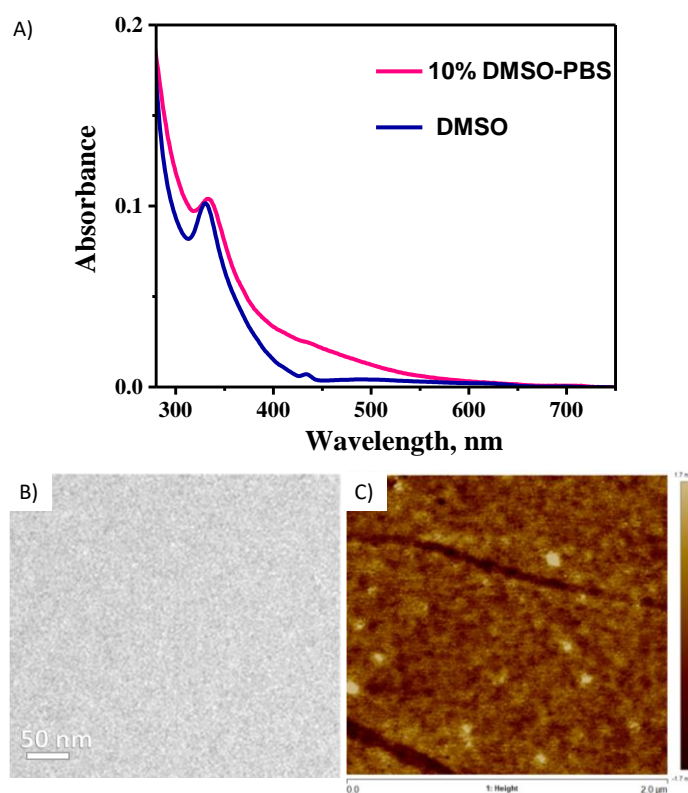
Figure 2A.5. A) Absorption spectra of **FPy** in DMSO & 10% DMSO-PBS; B & C) TEM & AFM analysis of **FPy** in 10% DMSO-PBS.

2A.3.2. DNA INTERACTION STUDIES OF FPy WITH LONG dsDNAS

The interactions of **FPy** with long dsDNAs become important since the previous studies of **FPy** with CT-DNA reveal its DNA condensing ability.[32] To investigate further on **DNA/FPy** interactions, we have selected long dsDNAs like long linear λ–DNA and circular plasmid DNA, specifically pBR322 DNA.

2A.3.2.1. DNA titration experiments

UV-visible absorption studies were carried out to monitor the condensation of long dsDNAs in presence of cationic **FPy**. In a typical titration experiment, small aliquots of DNA were titrated against 3 μM solution of **FPy** in 10% DMSO-PBS with a

maximum 5% dilution. The UV-Visible absorption changes during the titration of **FPy** against λ-DNA and pBR322 DNA are shown in Figure 2A.6A & B. Since DNA bases strongly absorb around 260 nm, a gradual enhancement in absorption around 260 nm was expected. On the other hand, both the chromophore/DNA interactions and DNA condensation are known to cause significant hypochromism at the chromophore absorption band and the DNA absorption band at 260 nm due to the enhanced masking of the chromophores.[37]
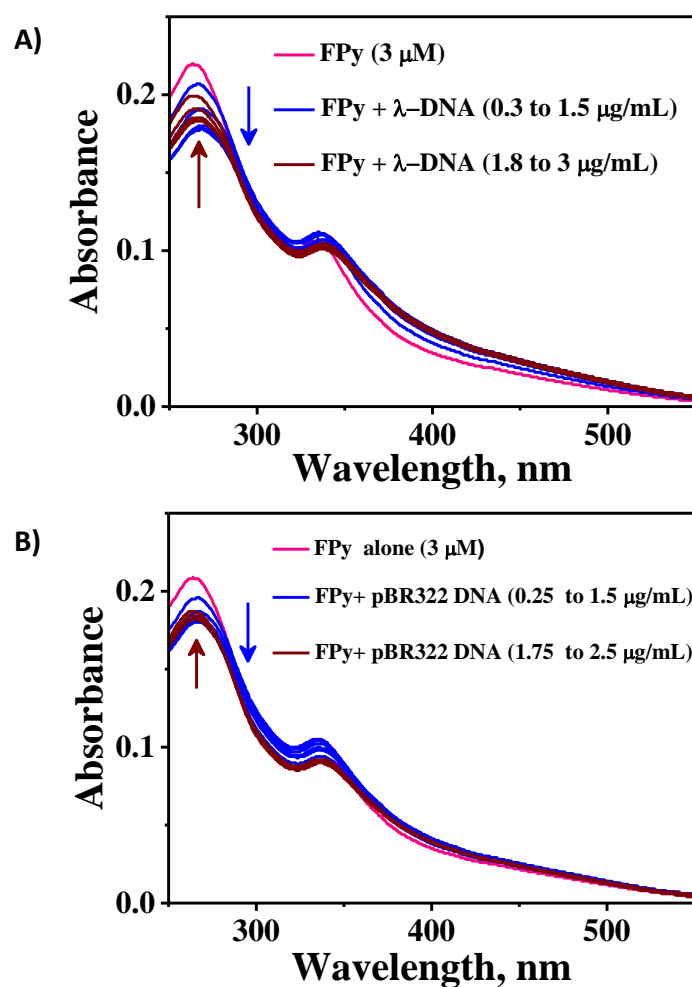
Figure 2A.6. Changes in the absorption spectra of **FPy** with the addition of: A) λ-DNA and B) pBR322 DNA.
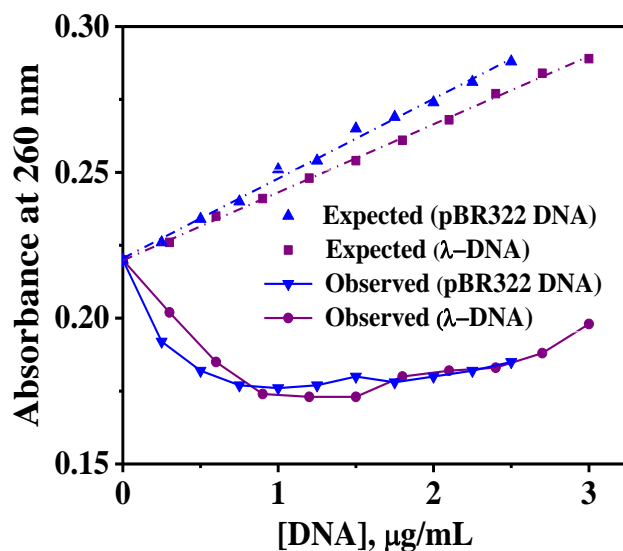
Figure 2A.7. Absorption changes at 260 nm in the presence and absence of **FPy** with increasing concentration of λ-DNA and pBR322 DNA. (Expected values are sum of absorbance values corresponding to **FPy** and added DNA).

The hypochromicity around 260 nm in these cases are affected by the increasing λ-DNA/pBR322 plasmid DNA concentrations and hence a secondary plot of absorbance at 260 nm was used for further analysis which provide a clear picture of the changes in 260 nm absorption band under the titration conditions (Figure 2A.7). From the secondary plots, we have obtained significant hypochromism values of 34% and 36% around 260 nm upon addition of λ-DNA and pBR322 DNA, respectively to **FPy** solutions. The observed large hypochromicity and changes in the DNA absorption around 260 nm could be attributed to the efficient condensation of these DNA structures in the presence of positively charged **FPy** via charge neutralization.[38,39] The gradual increase in absorption around 260 nm after certain concentration of DNA is due to the presence of excess DNA added to the system. Absorption around 334 nm also showed gradual changes during DNA addition as a result of aggregation of **FPy**. Here, the condensation of λ–DNA and pBR322 DNA is made possible through the electrostatic interaction between cationic pyridinium

moiety and phosphate backbone of DNA, leading to charge neutralization, which in turn results in aggregation of amphiphilic fullerene.[40,41]

2A.3.2.2. Ethidium bromide displacement assay

Apart from the possible electrostatic interactions between **FPy** and DNA, several literature reports suggest the possibility of DNA groove binding of fullerene and DNA intercalation of pyridinium moiety. We have conducted the ethidium bromide displacement assay to understand the intercalation of **FPy** on λ–DNA and pBR322 DNA. Ethidium bromide (EtBr) is a known DNA intercalator and forms a highly fluorescent DNA/EtBr complex in water. Ethidium bromide displacement assay is based on the aggregation induced quenching of ethidium bromide fluorescence when it gets replaced from the intercalative site by any other strong DNA intercalator.[42] The complexes of λ–DNA/EtBr and pBR322DNA/EtBr were
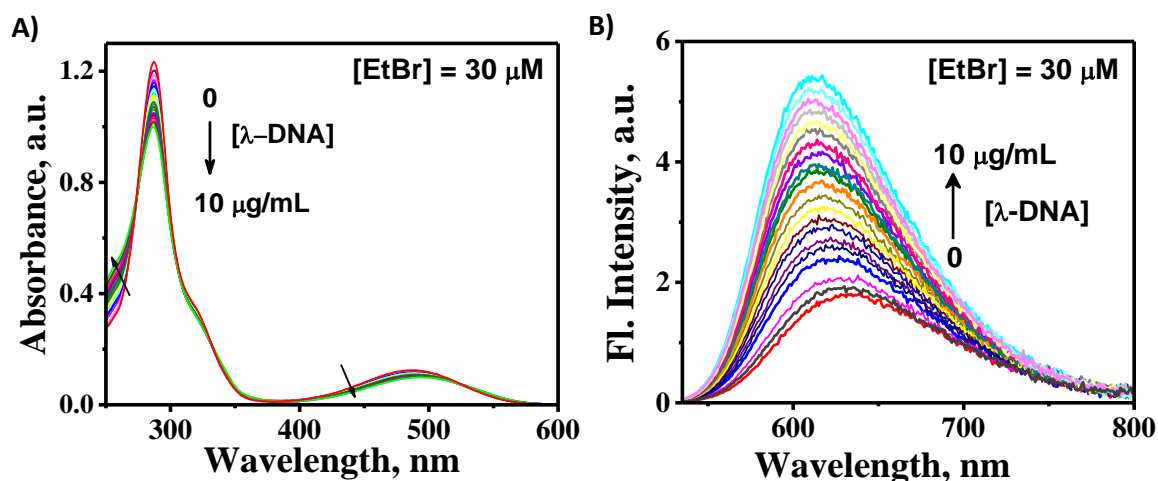
Figure 2A.8. Changes in the A) absorption spectra and B) emission spectra of ethidium bromide with addition of λ-DNA.
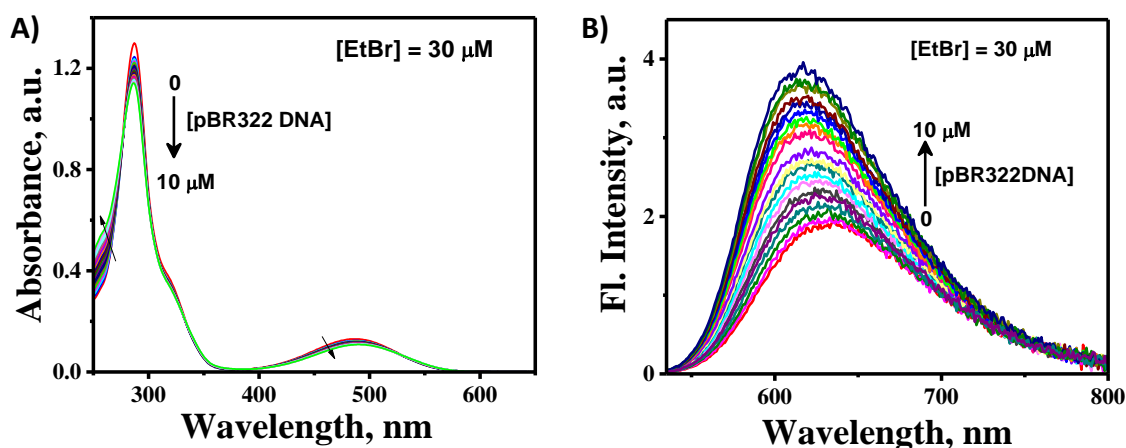
Figure 2A.9. Changes in the A) absorption spectra and B) emission spectra of ethidium bromide with addition of pBR322 DNA.

made separately through titration and the changes in absorption and emission of EtBr are shown in Figure 2A.8 and Figure 2A.9. The gradual increase in emission is due to the intercalation of EtBr in between the DNA nucleobases. The addition of **FPy** to both DNA/EtBr complexes result in intercalation of **FPy** and subsequent release of bound EtBr which resulted in a reduction in fluorescence due to EtBr aggregation as shown in Figures 2A.10 & 2A.11.
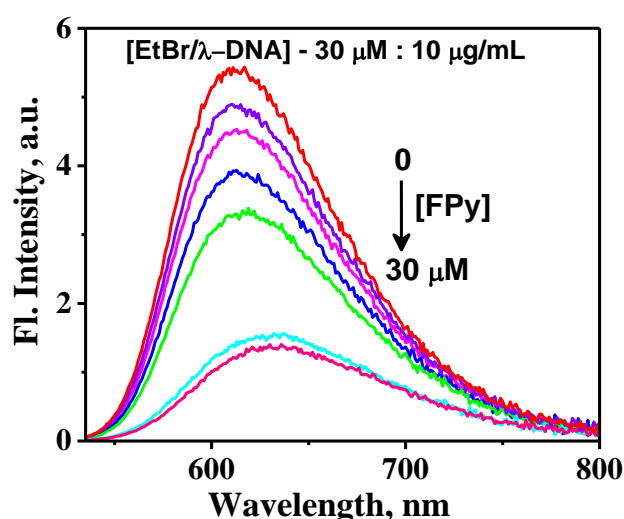
Figure 2A.10. Changes in the emission spectra of ethidium bromide/λ-DNA complex (30 μM : 10 μg/mL) with addition of **FPy**.
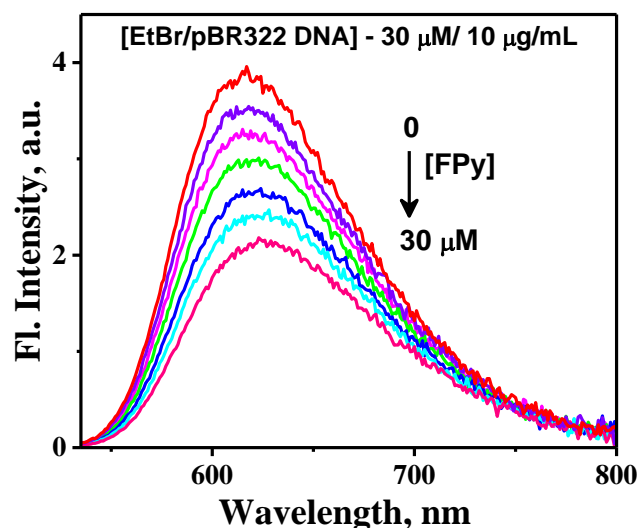
Figure 2A.11. Changes in the emission spectra of ethidium bromide/pBR322 DNA complex (30 μM : 10 μg/mL) with addition of **FPy**.

2A.3.2.3. Morphological analysis

Morphological analysis of λ**-DNA/FPy** hybrids using Transmission Electron Microscopy (TEM) and Atomic Force Microscopy (AFM) revealed the formation of nanosheets having thickness around 10 nm and sub-micrometer lateral dimensions. The well-defined edges of λ**-DNA/FPy** nanosheet indicates the ordered arrangement of fullerenes in the nanosheet and is confirmed with the crystalline SAED pattern (Figures 2A.12A & 2A.12B). On the other hand, **pBR322 DNA/FPy** hybrid forms aggregated structures of smaller nanosheets having thickness around 6 nm as shown in Figures 2A.12C & 2A.12D. In both cases, the initial condensation of the longer DNA by **FPy**, further assist the organization of fullerenes through π-π interactions leading to nanosheet structures composed of DNA and fullerenes.
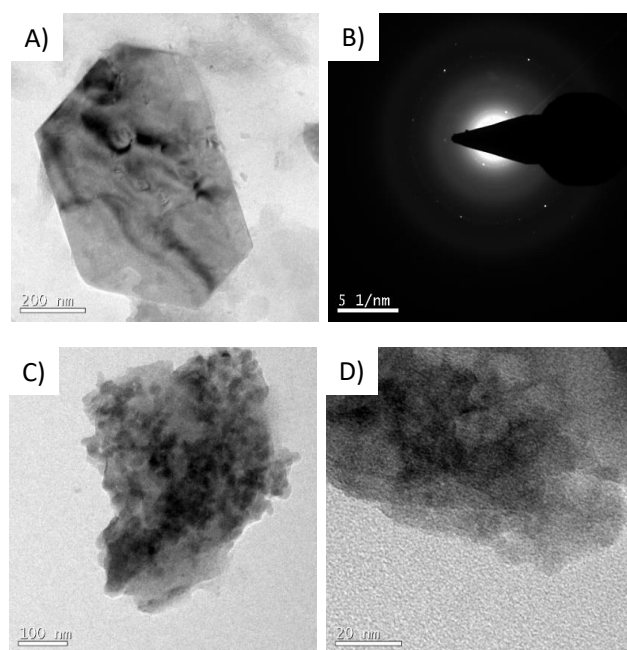
Figure 2A.12. A) TEM image and B) SAED pattern of **λ-DNA/FPy** hybrid C) TEM image and D) magnified TEM image of **pBR322 DNA/FPy** hybrid.

2A.3.3. CONDENSATION AND MUTUALLY ASSISTED ASSEMBLY OF LONG dsDNA WITH FPy

The process of condensation and subsequent formation of nanosheet assembly were thoroughly investigated through concentration dependent studies using Atomic Force Microscopy (AFM) and Dynamic Light Scattering (DLS) analysis. Concentration dependent growth of nanosheet structures was monitored through AFM analyses by varying the concentration of **FPy** from 1 μM to 6 μM with fixed concentrations of different DNAs. λ-DNA alone displays supercoiled thick strands of DNA which readily condense into spherical condensates in presence of 1 μM of **FPy** as shown in Figures 2A.13A & 2A.13B. Formation of micrometer sized nanosheets were observed under 3 μM concentration of **FPy** and further increase in **FPy** concentration up to 6 μM resulted in the formation of nanosheets with sub-micrometer lateral dimension (Figure 2A.13C & D). Similarly, AFM analyses of

72

pBR322 DNA/FPy hybrids (Figure 2A.13E, F & G) showed considerable increase in the amount of sub-micrometer sized nanosheets and formation of larger nanosheets through minor association of smaller sheets on increase in **FPy** concentration.
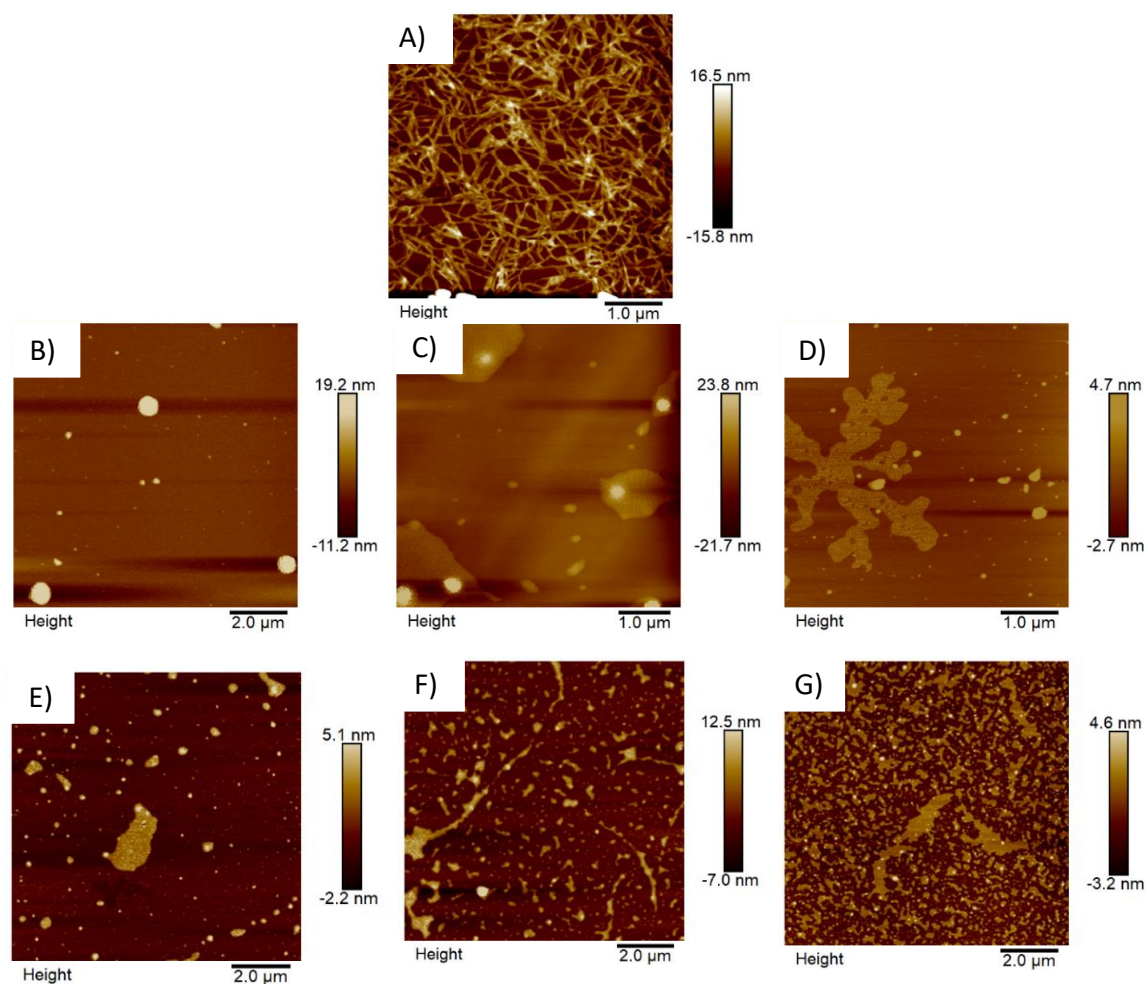
Figure 2A.13. AFM images of: A) λ-DNA alone; B), C) & D) **λ-DNA** (0.1 nM)/**FPy** hybrid at **FPy** concentrations of 1 μM, 3 μM & 6 μM respectively; E), F) & G) AFM images of **pBR322 DNA** (1 nM)/**FPy** hybrids at **FPy** concentrations of 1 μM, 3 μM & 6 μM, respectively.

DLS analysis was carried out in very low concentration (nM level) of **FPy** in order to validate the initial condensation process effectively and is shown in Figure 2A.14. Initially, λ-DNA alone showed larger size, around 600 nm, with a broader size distribution. Eventually, the λ-DNA condense to form smaller aggregates with

narrow size distribution on subsequent addition of **FPy**. After the addition of 20 nM concentration of **FPy**, size of DNA hybrid began to increase successively due to the lateral growth of nanosheet through fullerene assembly (Figure 2A.14A). Similarly, **pBR322 DNA/FPy** hybrids also showed initial DNA condensation and subsequent formation of nanosheet as shown in Figure 2A.14B.
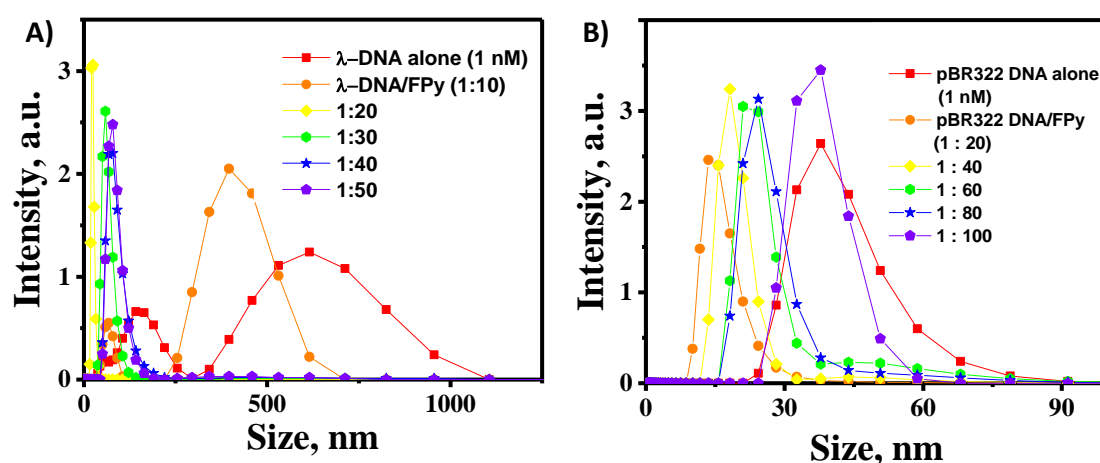
Figure 2A.14. Changes in the size of: A) λ-**DNA/FPy** hybrid and B) **pBR322 DNA/FPy** hybrid with the increase in **FPy** concentration.

2A.3.4. DNA INTERACTION STUDIES OF FPy WITH SHORT ds/ssDNAs

In order to understand the role of DNA condensation in generating hierarchical nanostructures, we have investigated the interaction of **FPy** with 20-mer DNA oligonucleotide single and double strands. In principle, due to the short length of the 20-mer single strands and duplex, effective condensation of DNA may not be possible and hence we can differentiate the role of DNA condensation while using these single and double stranded DNA oligonucleotides.[43]

2A.3.4.1. DNA titration experiments

Initial DNA interaction studies were carried out through DNA titration experiments with 20-mer dsDNA and ssDNA strands using UV-visible spectroscopy as shown in Figure 2A.15A & B. Absorption around 260 nm was found to be

increasing with increase in dsDNA concentration. In order to understand the hypochromic changes in the case of dsDNA and ssDNA, we have compared the changes around 260 nm with control experiments where similar amounts of dsDNA and ssDNA were added to blank solutions. Analyses using secondary plots (Figure 2A.15C) revealed the difference in absorption around 260 nm in both cases (with **FPy** and blank), which clearly showed a maximum hypochromicity of 13% for dsDNA and 20% for ssDNA.

The changes in the absorption around 260 nm for λ-DNA/pBR322 DNA and short 20-mer dsDNA are significantly different where we observed large hypochromicity (~36%) due to effective DNA condensation in the former case, whereas only moderate hypochromicity (10-20%) was observed in the latter due to DNA binding interactions of **FPy**. Moreover, the interaction is highly pronounced in case of ssDNA compared to dsDNA as shown in Figure 2A.15C. Absorption around 334 nm showed a successive reduction with addition of ds/ssDNA due to the self-assembly/aggregation[44] of **FPy** and observed a maximum hypochromicity of 26% and 34%, for dsDNA and ssDNA, respectively. The observed UV-Visible absorption changes of **FPy** in presence of dsDNA and ssDNA indicate efficient interactions with both single stranded and double stranded DNA suggestive of the major contribution of electrostatic interactions compared to the groove binding or intercalation in fullerene aggregation.
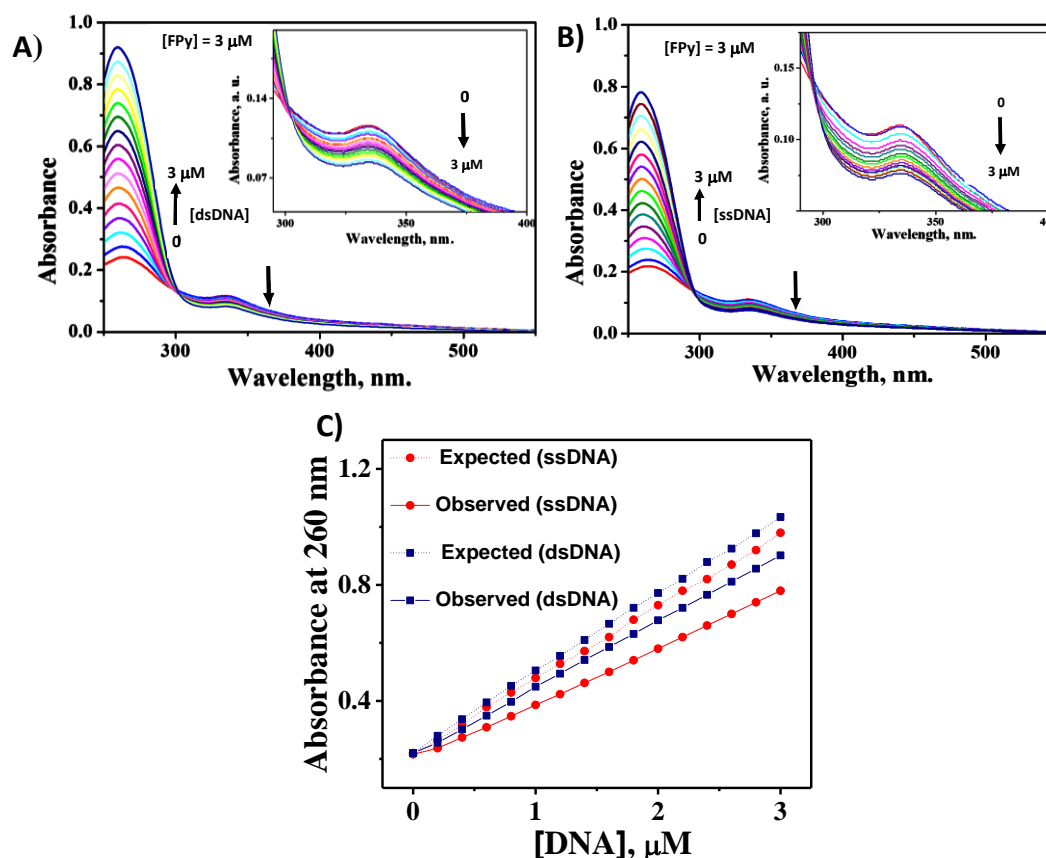
Figure 2A.15. Changes in the absorption spectra of **FPy** with the addition of: A) dsDNA and B) ssDNA in 10% DMSO-PBS. (Insets show the zoomed portion between 290 nm & 400 nm); C) Absorption changes at 260 nm in the presence and absence of **FPy** with increasing concentration of dsDNA and ssDNA. (Expected values are sum of absorbance values corresponding to **FPy** and added dsDNA/ssDNA).

2A.3.4.2. Ethidium bromide displacement assay, Thermal denaturation and Circular dichroism studies

In order to confirm the intercalation of **FPy** on dsDNA, ethidium bromide displacement assay has been carried out. The successive addition of **FPy** to dsDNA/EtBr complex (30 μM : 1.5 μM) decreased the fluorescence emission intensity of EtBr (Figure 2A.16) due to the replacement of EtBr by **FPy**. Thermal denaturation studies of **dsDNA/FPy** hybrid showed a very small change ($\Delta T_m \sim 1°C$) compared to the melting temperature of dsDNA as shown in Figure 2A.17A. The

circular dichroism studies also showed negligible changes in the CD signals for **ssDNA/FPy** hybrid and the small reduction in CD signal at higher **FPy** concentration indicates the minor perturbation in DNA helicity on interaction with **FPy** at higher concentrations of **FPy** (Figure 2A.17B).
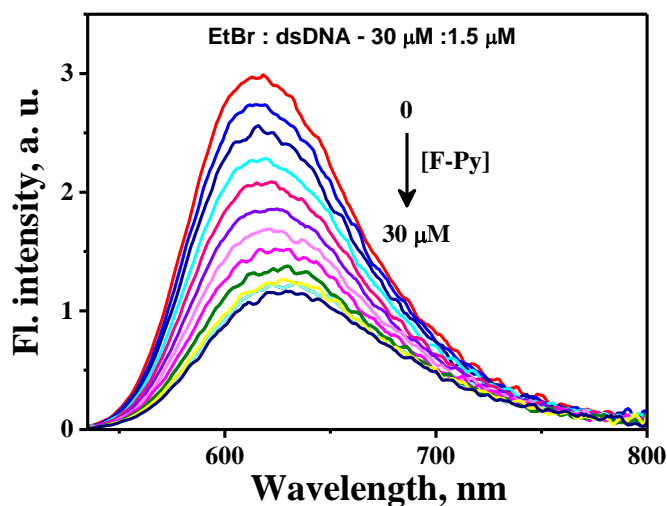
Figure 2A.16. Changes in the emission spectra of ethidium bromide/dsDNA complex (30 μM : 1.5 μM) with addition of **FPy**.
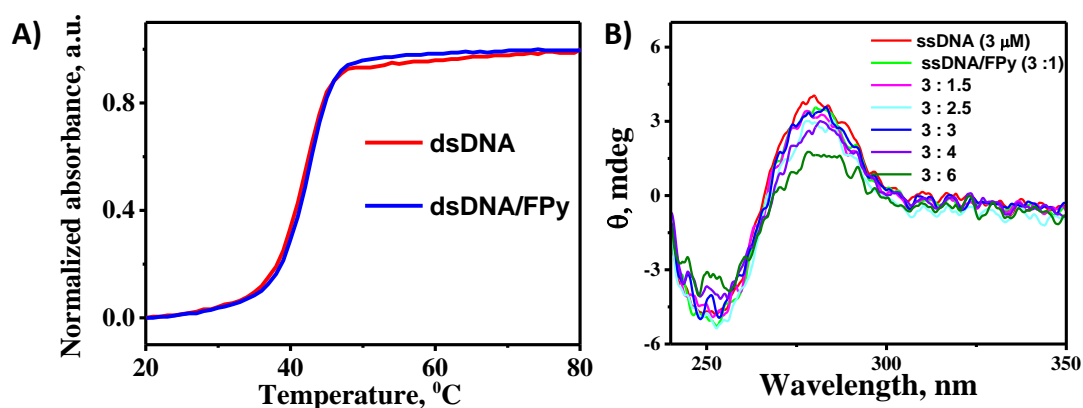
Figure 2A.17. A) Thermal denaturation curves for dsDNA (T_m = 42°C) and **dsDNA/FPy** (3 μM : 3 μM) (T_m = 43 °C) in 10 % DMSO-PBS, B) Changes in circular dichroism (CD) spectra of ssDNA with different concentrations of **FPy**.

2A.3.4.3. Morphological analysis

AFM and TEM images of the nanosheet structures resulting from the interaction of **FPy** with short dsDNA and ssDNA are shown in Figures 2A.18A & 2A.18B and Figures 2A.19A & 2A.19B. Interaction of **FPy** with dsDNA lead to the formation of extended nanosheets with lateral dimensions of several micrometers, in contrast to the more condensed, sub-micrometer structures in the case of longer DNAs. Similarly, **FPy** and ssDNA interact efficiently to form larger and more crystalline nanosheets as evidenced by the AFM, TEM images and SAED pattern (Figures 2A.19A, 2A.19B & 2A.19C). As discussed earlier, due to the shorter length of the DNA strands, the contribution of DNA condensation can be omitted, while the charge neutralization via electrostatic interaction between **FPy** and dsDNA/ssDNA play a major role in the organization of fullerenes and DNA in these nanostructures. Here, the nanostructures are majorly guided by the fullerene-fullerene interactions and hence ssDNA with more structural flexibility could lead to more crystalline and extended nanosheets. Further, the exposed hydrophobic nucleobases in ssDNA also may be contributing via π-π interactions with fullerenes. These results are in agreement with the UV-Vis titration experiments which predict the efficient interactions of **FPy** with ssDNA leading to extended fullerene/ssDNA assemblies and the presence of ssDNA across these nanostructures was confirmed via EDAX analysis of **ssDNA/FPy** hybrid nanosheets (Figure 2A.19 D).
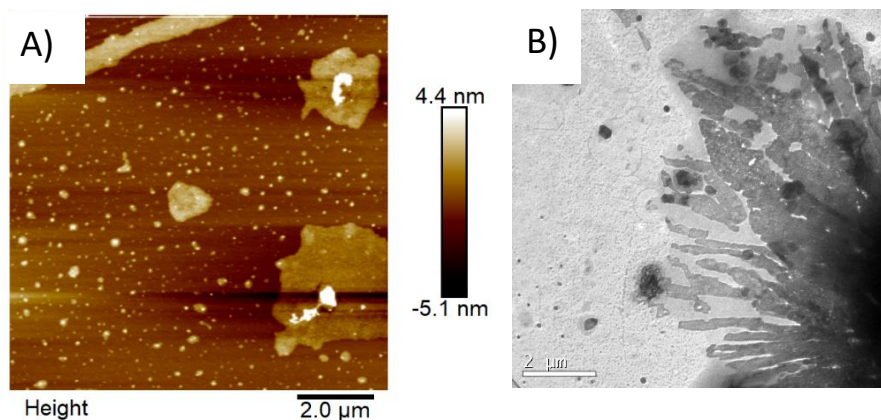
Figure 2A.18. A) AFM and B) TEM images of **dsDNA/FPy** hybrid (3 μM : 3 μM)
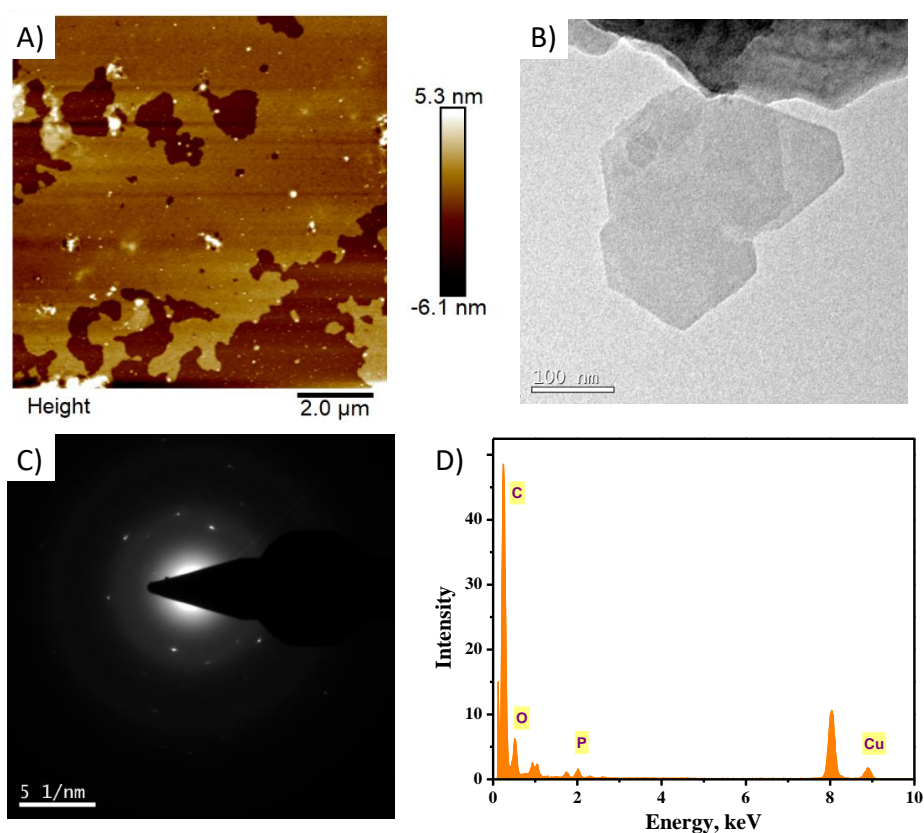
Figure 2A.19. A) AFM and B) TEM images of **ssDNA/FPy** hybrid (3 μM : 3 μM); C) Corresponding SAED pattern and D) EDAX analysis data.

2A.3.5. MUTUALLY ASSISTED ASSEMBLY OF SHORT ssDNA AND FPy

In order to understand the role of **FPy** in the nanostructure formation, we have monitored the concentration dependent growth of nanosheet structures through AFM analyses by varying the concentration of **FPy** from 1 μM to 6 μM with

fixed concentrations of different DNAs. Successive development of nanosheets with increase in concentration of **FPy** can be monitored through AFM analysis (Figure 2A.20) and it clearly showed the growth of nanosheet in lateral dimension by varying the **FPy** concentration from 1 µM to 6 µM. However, the thickness of the nanosheet remains same, around 3-4 nm, under different **FPy** concentration ruling out extended aggregate formation in this case. These results demonstrate that formation of ultrathin nanosheets is markedly facilitated by the increase in **FPy** concentrations.
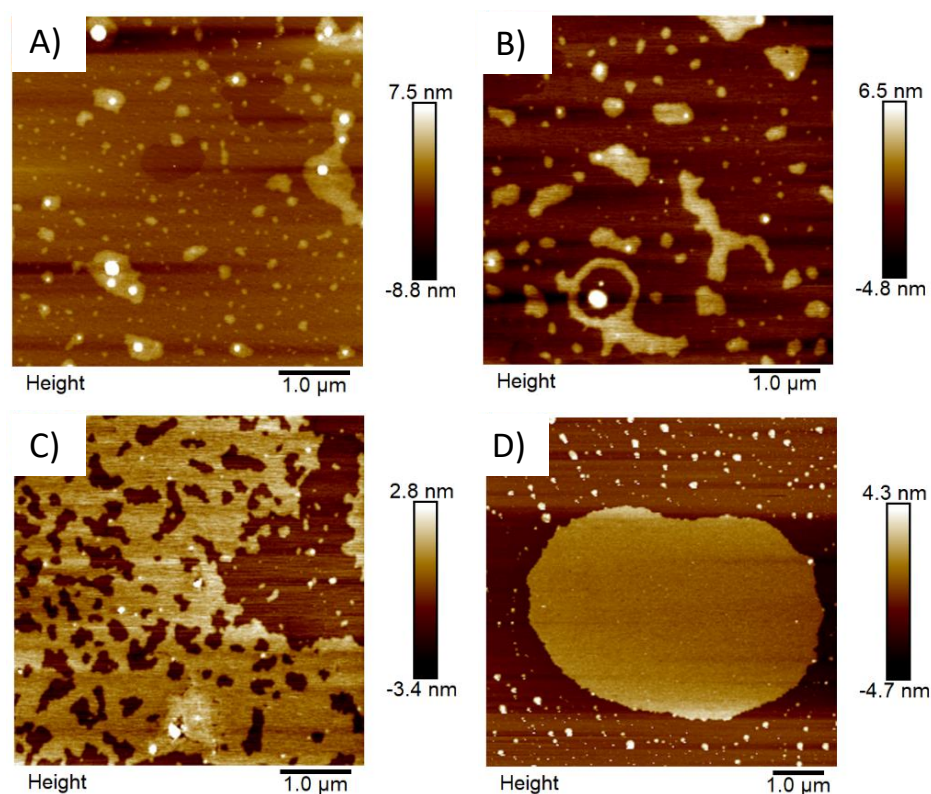
Figure 2A.20. AFM images of **ssDNA/FPy** hybrid at different **FPy** concentrations of A) 1 µM; B) 2 µM; C) 3 µM & D) 6 µM with fixed ssDNA concentration (3 µM).

The morphological analyses of **ssDNA/FPy** hybrid under different time intervals portrayed the successive growth of nanosheet with time as shown in Figure 2A.21. Initially, it forms small spherical particles around which smaller

nanosheets begin to form within 5 minutes. Micrometer sized nanosheets were formed within 30 minutes and the nanosheet thickness remained same even after two days due to repulsive interaction between the nanosheets having excess DNA on the surface.
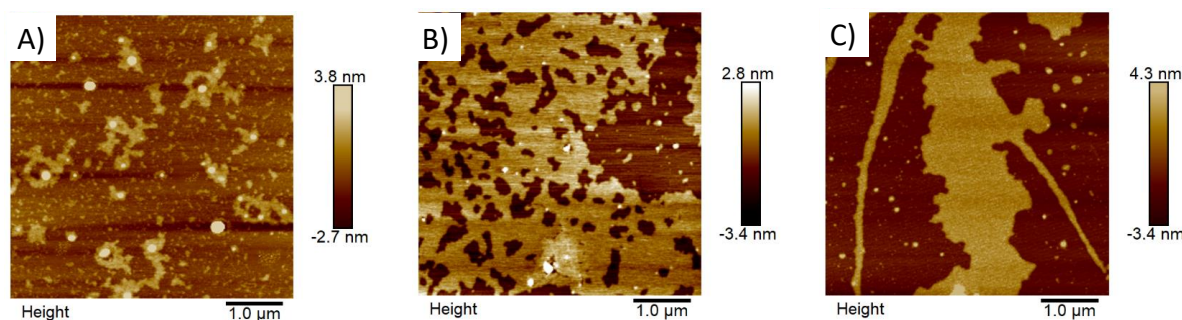
Figure 2A.21. AFM images of **ssDNA/FPy** (3:3) hybrids under different incubation time of A) 5 minutes; B) 30 minutes and C) 2 days.

The nanosheet formation can be described as the mutually assisted assembly of DNA and **FPy** through electrostatic interaction and fullerene π- π stacking. Initially, the charge neutralization brings the short DNAs together and it brings the fullerenes in close proximity to have π- π stacking between fullerenes, which in turn lead to the formation of micrometer sized nanosheets. Thus, we can propose a general mechanism for the interaction of **FPy** with both long and short ds/ssDNAs as shown in Figure 2A.22, that involves initial charge neutralization/DNA condensation and further fullerene assembly through π-π stacking. However, the choice of long or short ds/ssDNAs has major influence in the nanosheet assembly.
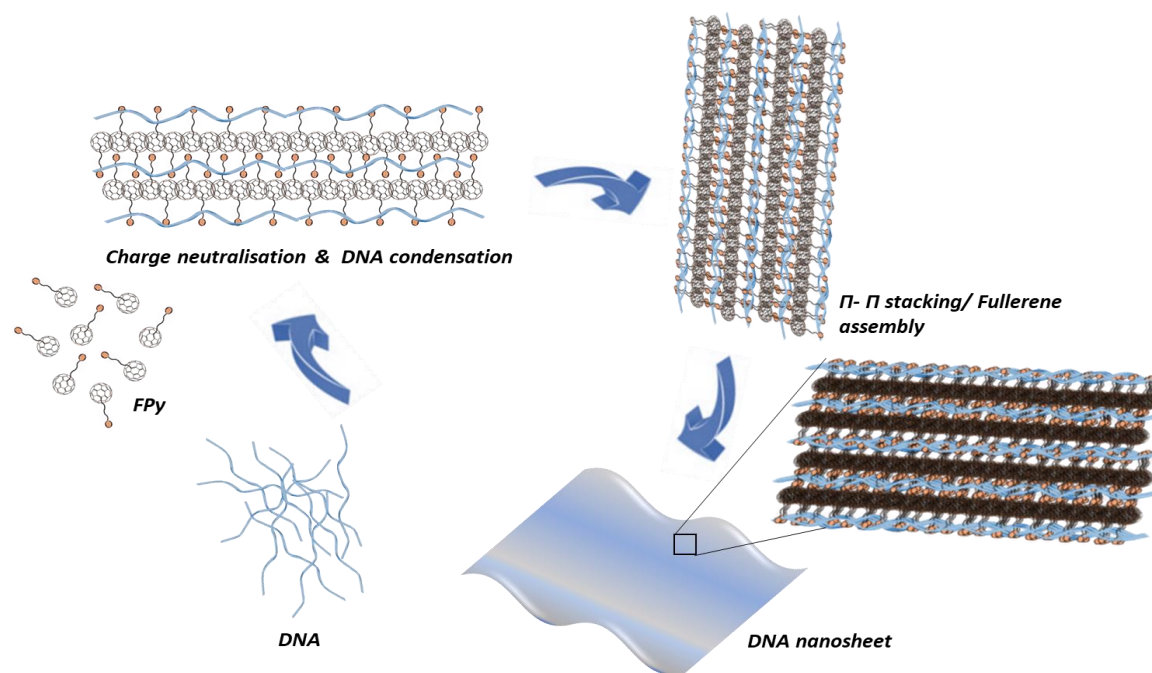
Figure 2A.22. Cartoonic representation of proposed mechanism involved in ultrathin nanosheet formation achieved through the initial charge neutraisation, DNA condensation and fullerene assembly.

2A.3.6. ADDRESSABILITY OF FPy/DNA HYBRID NANOSTRUCTURES

The mutually assisted assembly of **FPy** and various DNA structures to form significantly crystalline, ordered nanosheets open up the possibility of engineering functional nanostructures with these building blocks. The addressability of these DNA nanostructures via functionalization of the short oligonucleotide strand was demonstrated using a fluorescent probe (Cyanine-3) modified single strand DNA (DNA2-Cy3). The formation of nanosheet structures by the interactions of **FPy** with DNA2-Cy3 was established using UV-Vis spectroscopy, AFM and TEM analyses. Further, we have probed the fluorescence of Cy3 to understand the assembly properties using fluorescence spectroscopy and imaging techniques. Figure 2A.23A
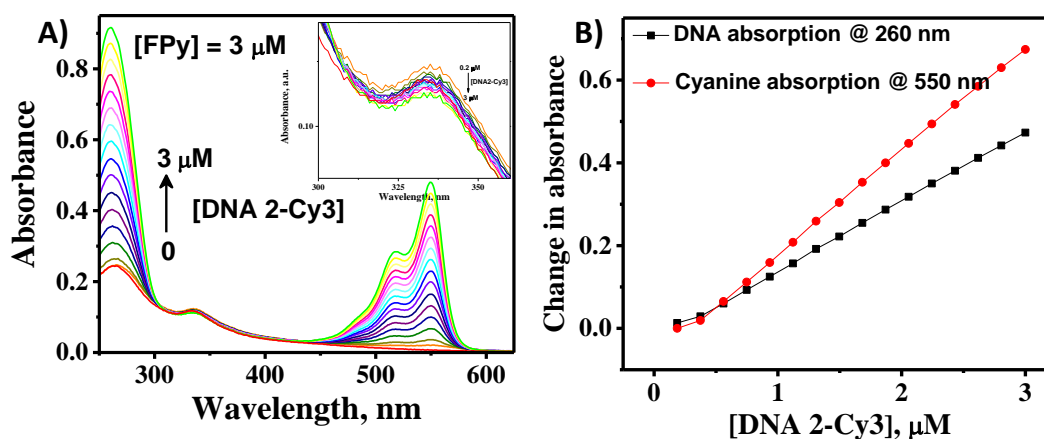
Figure 2A.23. A) Change in absorption spectra of **FPy** (3 μM) in phosphate buffer (10 mM; pH 7.4) with subsequent addition of DNA2-Cy3 (Inset: Zoomed portion indicating the absorption changes around 334 nm); B) Absorption changes at 260 nm (corresponds to DNA) and 550 nm (corresponds to Cyanine) with subsequent addition of DNA2-Cy3 to a fixed concentration of **FPy** (3 μM).

shows the changes in absorption spectra of **FPy** (3 μM) with increasing concentration of DNA2-Cy3. The changes in absorption at 260 nm corresponding to the combined absorption of **FPy** and DNA and at 550 nm corresponding to the Cy3 absorption are plotted against the concentration of DNA2-Cy3 (Figure 2A.23B). The decreased slope for the 260 nm band is indicative of the hypochromicity at 260 nm, as observed in the case of **FPy** binding with ssDNA.

Morphological analyses of **DNA2-Cy3/FPy** nanostructures using AFM and TEM techniques showed the formation of nanosheets with lateral dimensions in the micrometer range (Figures 2A.24A), very similar to the earlier observed **ssDNA/FPy** nanosheet structures, but with significantly higher crystallinity as evident from the lattice fringes and corresponding Fast Fourier Transform (FFT) patterns as shown in Figures 2A.24B & 2A.24C. The interaction of hydrophobic Cy3 with fullerene through possible π-π interactions also could be contributing to the ordered

arrangement and higher crystallinity of the **DNA2-Cy3/FPy** nanosheets. Figure 2A.25 schematically represents the possible ordered assembly of fullerenes and DNA2-Cy3 in these nanosheet structures.
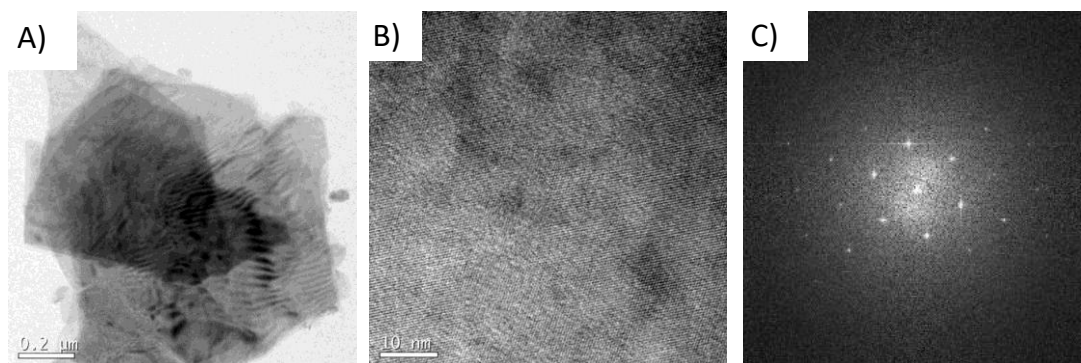
Figure 2A.24. A) TEM image of nanosheet formed through **DNA2-Cy3/FPy** interaction; B) High resolution TEM image of **DNA2-Cy3/FPy** hybrid (3 μM : 3 μM); C) Corresponding FFT pattern.
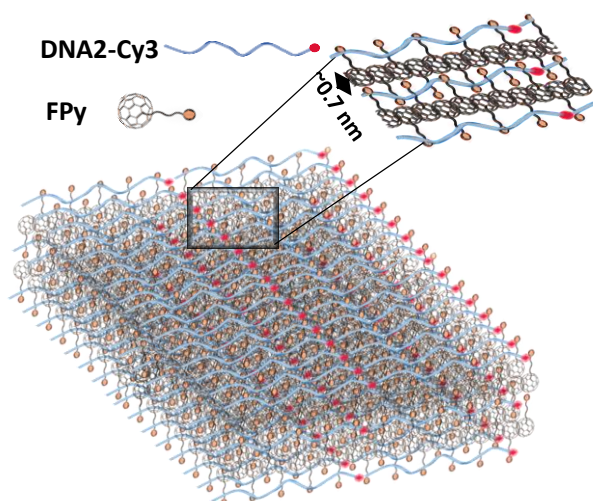
Figure 2A.25. Schematic representation of nanosheets formed through **DNA2-Cy3/FPy** interaction.

The fluorescence emission properties of DNA2-Cy3 in presence of different concentrations of **FPy** are given in Figure 2A.26A. Even at very low concentration (1.5 μM) of **FPy**, the fluorescence of DNA2-Cy3 strand showed significant quenching, which could be attributed to possible electron transfer from Cy3 to fullerene

facilitated by the ordered assembly of fullerene and Cy3-modified ssDNA. At **FPy**
concentrations of ~30 μM, corresponding to total charge neutralization (1 : 20 ratio
of DNA2-Cy3 to **FPy**), we observed complete quenching of fluorescence from DNA2-
Cy3, which confirmed the **ssDNA/FPy** assembly. Further, the confocal fluorescence
images of the assembled **DNA2-Cy3/FPy** nanosheets (Figure 2A.26B) showed
fluorescence from the edges of the nanosheets corresponding to free fluorophores
on the edges, whereas the cyanine fluorophores incorporated in the assembly got
strongly quenched. Thus, these fluorescence experiments support the hypothesis
that the short-oligonucleotides could be functionalized to demonstrate the
addressability of **DNA/FPy** nanostructures.
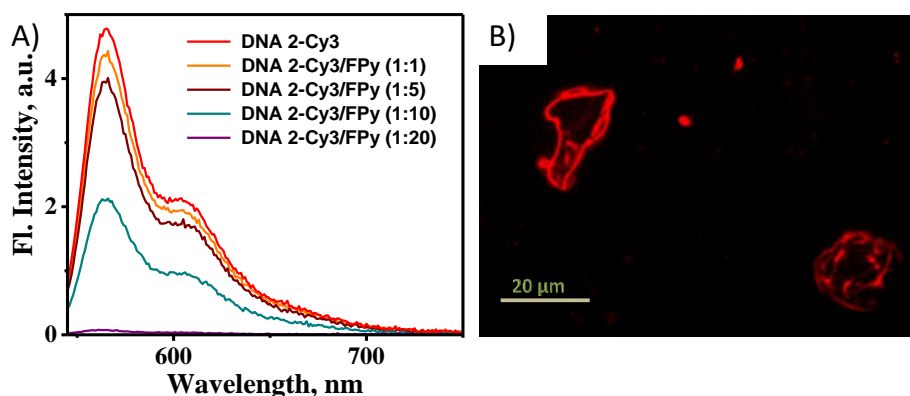
Figure 2A.26. A) Fluorescence spectra showing the quenching of DNA2-Cy3 (1.5
μM) emission with gradual addition of **FPy**; B) Confocal microscopic images of
DNA2-Cy3/FPy hybrid (3 μM : 3 μM).

2A.4. CONCLUSIONS

In conclusion, we have demonstrated the ordered assembly of an amphiphilic
pyridinium appended fullerene derivative (**FPy)** through electrostatic interactions
with various oligonucleotides involving charge neutralization, DNA condensation
and formation of ultrathin crystalline nanosheets. The differential interaction of **FPy**
with various DNA structures such as long linear λ-DNA, circular pBR322 plasmid

DNA, short 20-mer ds and ssDNA were investigated and the resulting **DNA/FPy** hybrid nanostructures were characterized using AFM and TEM imaging techniques. Longer double strand DNAs such as linear λ-DNA and circular pBR322 plasmid DNA readily condense in presence of **FPy** to form few layer nanosheets with sub-micrometer lateral dimensions. The assembly in this case is guided by initial DNA condensation and subsequent fullerene-fullerene interactions. On the other hand, **FPy** binds efficiently to shorter DNA strands such as 20-mer dsDNA and ssDNA primarily through electrostatic interactions and subsequent charge neutralization lead to significantly crystalline nanosheets with lateral dimensions in the micrometer range. Since DNA condensation is not facile in this case, binding interactions of amphiphilic **FPy**, subsequent charge neutralization and fullerene-fullerene interactions guide this assembly. In both cases, subtle changes in the hydrophilic-hydrophobic balance of the amphiphilic fullerene derivative upon interactions with DNA play a major role in the self-assembly process. Further, the addressability of the **DNA/FPy** nanostructures were demonstrated using a Cy3-modified ssDNA (DNA2-Cy3), which also forms highly crystalline nanosheets in presence of **FPy** and exhibit strong quenching of Cy3 fluorescence through possible electron transfer from Cy3 to fullerene facilitated by the ordered assembly of fullerene and Cy3-modified ssDNA.[45,46] These results open up new prospects in the development of functional DNA nanostructures through non-covalent interactions and hence have potential applications in the context of DNA nanotechnology.

2A.5. EXPERIMENTAL SECTION

2A.5.1. MATERIALS AND METHODS

The synthesis and purification of amphiphilic, pyridinium appended fullerene derivative, **FPy** was carried out by following modified literature procedures[33], and was characterized thoroughly using various spectroscopic and analytical techniques (^{1}H NMR, ^{13}C NMR, HRMS) before subjected to further photophysical and DNA interaction studies. ^{1}H-NMR spectra were recorded using DPX 500 MHz spectrometer using tetramethylsilane (TMS) as the internal standard and deuterated solvents were used for the measurements. JEOL JM AX 505 HA electron spray HRMS was used to record mass spectra. MALDI-TOF mass spectra were obtained on an AXIMA-CFR PLUS (KRATOS SHIMADZU) MALDI-TOF mass spectrometer. All reagents and materials for synthesis were purchased from Sigma-Aldrich, Alfa Aesar and Spectrochem chemical suppliers. All the oligonucleotides used in this chapter (Linear λ-DNA, circular plasmid DNA (pBR322 DNA) and short ssDNAs) were purchased from Sigma Aldrich. The 20-mer DNA sequences used in the present studies are DNA1: 5'-CGT CAC GTA AAT CGG TTA AC-3', DNA2: 5'-GTT AAC CGA TTT ACG TGA CG-3' and DNA2-Cy3 : 5'-Cy3-GTT AAC CGA TTT ACG TGA CG-3'. DNA1/DNA2 forms the duplex DNA (dsDNA) upon annealing while DNA2 and DNA2-Cy3 were used as single strands.

2A.5.2. DNA INTERACTION STUDIES OF FPy

For DNA interaction studies of **FPy**, all the experiments were performed in 10% DMSO-PBS mixture (10 mM PBS, 2 mM NaCl). The fullerene derivative was initially dissolved in DMSO and then diluted to obtain appropriate concentrations in 10% DMSO-PBS mixture. DNA interaction studies of **FPy** solutions (3μM) were carried out in quartz cuvette with a path length of 1 cm. Small aliquots of DNA were

added and monitored the absorbance using Shimadzu UV-2600 PC UV-Vis spectrophotometer. The fluorescence emission spectra were recorded on a SPEX FLUOROLOG-3 (FL3-221) spectrofluorometer. Ethidium bromide displacement assay were carried out by the measurement of fluorescence emission with subsequent addition of **FPy** to DNA/EtBr complex at an excitation wavelength of 515 nm. Circular dichroism measurements were performed on a Jasco J-810 spectropolarimeter with a quartz cuvette having 1 mm path length. Fluorescence quenching experiments were done by recording the emission spectra of DNA2-Cy3 (1.5 μM) by adding different equivalence of **FPy** (λ_{exc} = 530 nm). DLS analyses were carried out with DLS-Zetasizer (Malvern Nano ZS) operating with a He-Ne laser at a wavelength of 633 nm. Each analysis was triplicated and the mean value is reported. In each run, 10-15 measurements were made.

2A.5.3. MORPHOLOGICAL ANALYSIS OF DNA/FPy HYBRIDS

TEM samples were prepared by mixing DNA and **FPy** in 10% DMSO-PBS mixture with an incubation time of 30 minutes and dropped on carbon coated Cu grid. HRTEM measurements were carried out by using FEI-Tecnai T 30, with EDAX at accelerating voltage of 300 kV. Samples were imaged with a Hamamatsu ORCA CCD camera. AFM samples were prepared by mixing DNA and **FPy** in 10% DMSO-PBS mixture with an incubation time of 30 minutes, dropped on mica surface and dried in air. AFM analyses were carried out with BRUKER MULTIMODE AFM operating with a tapping mode regime and a micro fabricated TiN cantilever tips (NT-MDT-NSG series) with a resonance frequency of 299 kHz and a spring constant of 20 to 80 Nm^{-1}. Confocal imaging was done by dropping the solution as such on a cleaned glass plate using a NIKON A1R Si spectral confocal microscope (Nikon, Tokyo, Japan) at a wavelength of 561 nm to view the red fluorescence.

2A.5.4. SYNTHESIS AND CHARACTERIZATION OF FPy

2A.5.4.1. Synthesis of [6, 6]-Phenyl-C61-butyric acid, PCBA

To a solution of **PCBM** (200 mg, 0.22 mmol) in toluene (100 mL), glacial acetic acid (30 mL) and concentrated hydrochloric acid (15 mL) was added. The mixture was refluxed for 20 hours. The reaction was monitored by TLC (silica/toluene : PCBM, R_f : 0.6; PCBA, R_f : 0.0). Aqueous layer in the reaction mixture was discarded and the volatile components in the organic layer was removed under reduced pressure. The product was precipitated by methanol, dried to obtain black solid with quantitative yield (189 mg, 0.20 mmol). Mass (HRMS); calculated for $C_{71}H_{12}O_2$, 896.09; found, 897.09 (M+H).

2A.5.4.2. Synthesis of 2-(2-(2-bromoethoxy)ethoxy) ethanol , TEGBr

To a solution of 2,2'-(ethane-1,2-diylbis(oxy)diethanol (10 g, 0.066 mmol) in toluene (150 mL), HBr (15 mL of 48% aqueous solution) was added. The reaction was refluxed at 110 °C for 36 hours. The organic layer was separated using ethyl acetate (2 × 100mL). The solvent was reduced by rotary evaporation and the crude product was purified by column chromatography using 30% ethyl acetate-hexane mixture (Rf : 0.5) to a yellow liquid in 11.3% yield (0.75g). ^{1}H NMR (500 MHz, CDCl3), δ (ppm): 3.84 (t, J =6 Hz, 2H), 3.76 (t, J =4 Hz, 2H), 3.66 (s, 4H), 3.63 (t, J =4.5 Hz, 2H), 3.50 (t, J =6 Hz, 2H); ^{13}C NMR (125 MHz, CDCl$_3$), δ (ppm): 72.56, 71.15, 70.50, 61.70, 30.56; HRMS (m/z): [M]+ calculated for $C_6H_{13}BrO_3$, 212.00; found, 213.01 (M+H).

2A.5.4.3. Synthesis of 2-(2-(2-bromoethoxy)ethoxy) ethyl [6,6]-phenyl-C61-butyrate, F-Br

To a solution of **PCBA** (100mg, 0.0558 mmol) in 1,2-dichlorobenzene (6mL), 4-dimethylaminopyridine (12 mg, 0.0558 mmol), EDC-HCl (64 mg, 0.1674 mmol) were added and stirred for 10 min at 0 °C. To the reaction mixture 2-(2-(2-

bromoethoxy) ethoxy)ethanol (32 μL, 0.1116 mmol) was added directly and stirred overnight at room temperature. The crude mixture was separated by column chromatography using chloroform (R$_f$: 0.7) to give the pure product as brown colour solid in 31% yield (38.6 mg). ^{1}H NMR (500 MHz, CDCl$_3$), δ (ppm): 7.93 (d, J =7.5Hz, 2H), 7.56 (t, J =7Hz, 2H), 7.48 (t, J =6.5Hz, 1H), 4.24 (t, J= 4.5Hz, 2H), 3.82 (t, J =6.5Hz, 2H), 3.7(m, 6H), 3.5(t, J =6Hz, 2H), 2.93(t, J =8Hz, 2H), 2.57(t, J =7.5Hz, 2H), 2.19 (m, J=7.5Hz, 2H). ^{13}C NMR (125 MHz, CDCl$_3$), δ (ppm): 174.23, 148.29, 147.80, 145.85, 145.70, 145.26, 145.01, 144.88, 144.69, 144.58, 144.43, 144.32, 144.17, 144.03, 143.61, 143.05, 142.73, 142.08, 142.12, 141.19, 141.06, 139.04, 138.57, 135.79, 133.61, 128.04, 127.26, 121.72, 78.97, 70.06, 69.43, 68.20, 67.93, 62.9, 32.91, 27.42, 22.3; MALDI (m/z): [M]+ calculated for C$_{77}$H$_{23}$BrO$_4^+$, 1090.07; found, 1113.06 (M+Na).

2A.5.2.3. Synthesis of 1-(2-(2-(2-(((([6,6]-phenyl-C61-butyroyl)oxy)-ethoxy)ethoxy) ethyl)pyridine-1-ium bromide, FPy

(2-(2-(2-bromoethoxy)ethoxy)ethyl [6,6]-phenyl-C61-butyrate (20 mg, 0.018 mmol) was added in 2 mL of pyridine. The reaction mixture was refluxed at 100 °C for 24 h. Pyridine was evaporated and the residue was washed with methanol. Black colour solid thus obtained is the product, **FPy**. ^{1}H NMR (500 MHz, DMSO-d$_6$), δ (ppm): 9.03 (d, J = 5.5 Hz, 2H), 8.18 (t, J = 7 Hz, 2H), 8.06 (d, J = 7.5 Hz, 2H), 7.60 (t, J = 7.5 Hz, 2H), 7.49 (s, 1H), 4.8 (t, J = 4.5 Hz, 2H), 4.08 (t, J = 4.5 Hz, 2H), 3.91 (t, J = 4.75 Hz, 2H), 3.47 (t, J = 4.25 Hz, 4H), 2.93 (t, J = 8 Hz, 2H), 2.56 (t, J = 7 Hz, 2H), 2.07 (m, J = 7.66 Hz, 2H); ^{13}C NMR (125 MHz, CDCl$_3$), δ (ppm): 173.09, 146.06, 145.21, 145.12, 145.07, 144.71, 144.57, 144.52, 144.42, 144.22, 143.37, 143.13, 143.05, 142.98, 142.95, 142.91, 142.69, 142.15, 142.10, 141.98, 141.76, 139.02, 138.47, 136.71, 133.10, 128.34, 125.27, 122.55, 100.81, 79.46, 71.31, 70.20, 69.18, 68.10, 64.29,

50.15, 32.66, 22.19; MALDI (m/z): [M]+ calculated for $C_{82}H_{28}NO_4^+$, 1090.20; found, 1090.20.

2A.6. REFERENCES

(1)   Kroto, H. W.; Heath, J. R.; O'Brien, S. C.; Curl, R. F.; Smalley, R. E. C60: Buckminsterfullerene. *Nature* **1985**, *318*, 162-163.

(2)   Kroto, H. Symmetry, Space, Stars, and C60 (Nobel Lecture). *Angew. Chem. Int. Ed. Engl.* **1997**, *36*, 1578-1593.

(3)   Prato, M. [60]Fullerene chemistry for materials science applications. *J. Mater. Chem.* **1997**, *7*, 1097-1109.

(4)   Guldi, D. M.; Illescas, B. M.; Atienza, C. M.; Wielopolski, M.; Martín, N. Fullerene for organic electronics. *Chem. Soc. Rev* **2009**, *38*, 1587-1597.

(5)   Friedman, S. H.; DeCamp, D. L.; Sijbesma, R. P.; Srdanov, G.; Wudl, F.; Kenyon, G. L. Inhibition of the HIV-1 protease by fullerene derivatives: model building studies and experimental verification. *J. Am. Chem. Soc.* **1993**, *115*, 6506-6509.

(6)   Schinazi, R. F.; Sijbesma, R.; Srdanov, G.; Hill, C. L.; Wudl, F. Synthesis and virucidal activity of a water-soluble, configurationally stable, derivatized C60 fullerene. *Antimicrob. Agents Chemother.* **1993**, *37*, 1707-1710.

(7)   Bernstein, R.; Prat, F.; Foote, C. S. On the Mechanism of DNA Cleavage by Fullerenes Investigated in Model Systems: Electron Transfer from Guanosine and 8-Oxo-Guanosine Derivatives to C60. *J. Am. Chem. Soc.* **1999**, *121*, 464-465.

(8)   Eiichi, N.; Hidetoshi, T.; Shigeru, Y.; Takashi, S.; Yukio, S. Biological Activity of Water-Soluble Fullerenes. Structural Dependence of DNA Cleavage,

Cytotoxicity, and Enzyme Inhibitory Activities Including HIV-Protease Inhibition. *Bull. Chem. Soc. Jpn.* **1996**, *69*, 2143-2151.

(9)   Brettreich, M.; Hirsch, A. A highly water-soluble dendro[60]fullerene. *Tetrahedron Lett.* **1998**, *39*, 2731-2734.

(10)   Miyazawa, K. i. Synthesis and Properties of Fullerene Nanowhiskers and Fullerene Nanotubes. *J. Nanosci. Nanotechnol.* **2009**, *9*, 41-50.

(11)   Babu, S. S.; Möhwald, H.; Nakanishi, T. Recent progress in morphology control of supramolecular fullerene assemblies and its applications. *Chem. Soc. Rev* **2010**, *39*, 4021-4035.

(12)   Zhang, X.; Hsu, C.-H.; Ren, X.; Gu, Y.; Song, B.; Sun, H.-J.; Yang, S.; Chen, E.; Tu, Y.; Li, X.; Yang, X.; Li, Y.; Zhu, X. Supramolecular [60]Fullerene Liquid Crystals Formed By Self-Organized Two-Dimensional Crystals. *Angew. Chem. Int. Ed.* **2015**, *54*, 114-117.

(13)   Ariga, K.; Shrestha, L. K. Zero-to-one (or more) nanoarchitectonics: how to produce functional materials from zero-dimensional single-element unit, fullerene. *Materials Advances* **2021**, *2*, 582-597.

(14)   Lei, Y.; Wang, S.; Lai, Z.; Yao, X.; Zhao, Y.; Zhang, H.; Chen, H. Two-dimensional C60 nano-meshes via crystal transformation. *Nanoscale* **2019**, *11*, 8692-8698.

(15)   Shrestha, L. K.; Ji, Q.; Mori, T.; Miyazawa, K. i.; Yamauchi, Y.; Hill, J. P.; Ariga, K. Fullerene Nanoarchitectonics: From Zero to Higher Dimensions. **2013**, *8*, 1662-1679.

(16)   Liu, H.; Li, Y.; Jiang, L.; Luo, H.; Xiao, S.; Fang, H.; Li, H.; Zhu, D.; Yu, D.; Xu, J.; Xiang, B. Imaging As-Grown [60]Fullerene Nanotubes by Template Technique. *J. Am. Chem. Soc.* **2002**, *124*, 13370-13371.

(17)   Wang, L.; Liu, B.; Yu, S.; Yao, M.; Liu, D.; Hou, Y.; Cui, T.; Zou, G.; Sundqvist, B.; You, H.; Zhang, D.; Ma, D. Highly Enhanced Luminescence from Single-Crystalline C60·1m-xylene Nanorods. *Chem Mater* **2006**, *18*, 4190-4194.

(18)   Kim, K.-H.; Ko, D.-K.; Kim, Y.-T.; Kim, N. H.; Paul, J.; Zhang, S.-Q.; Murray, C. B.; Acharya, R.; DeGrado, W. F.; Kim, Y. H.; Grigoryan, G. Protein-directed self-assembly of a fullerene crystal. *Nat. Commun* **2016**, *7*, 11429.

(19)   Nair, V. S.; Mukhopadhyay, R. D.; Saeki, A.; Seki, S.; Ajayaghosh, A. A π-gel scaffold for assembling fullerene to photoconducting supramolecular rods. *Sci Adv* **2016**, *2*, e1600142-e1600142.

(20)   Das, S.; Herrmann-Westendorf, F.; Schacher, F. H.; Täuscher, E.; Ritter, U.; Dietzek, B.; Presselt, M. Controlling Electronic Transitions in Fullerene van der Waals Aggregates via Supramolecular Assembly. *ACS Applied Materials & Interfaces* **2016**, *8*, 21512-21521.

(21)   Das, S.; Preiß, J.; Plentz, J.; Brückner, U.; von der Lühe, M.; Eckardt, O.; Dathe, A.; Schacher, F. H.; Täuscher, E.; Ritter, U.; Csáki, A.; Andrä, G.; Dietzek, B.; Presselt, M. Controlling Intermolecular Interactions at Interfaces: Case of Supramolecular Tuning of Fullerene's Electronic Structure. *Adv. Energy Mater.* **2018**, *8*, 1801737.

(22)   Yamamoto, Y.; Zhang, G.; Jin, W.; Fukushima, T.; Ishii, N.; Saeki, A.; Seki, S.; Tagawa, S.; Minari, T.; Tsukagoshi, K.; Aida, T. Ambipolar-transporting coaxial nanotubes with a tailored molecular graphene-fullerene heterojunction. *Proc Natl Acad Sci U S A.* **2009**, *106*, 21051-21056.

(23)   Guldi, D. M.; Gouloumis, A.; Vázquez, P.; Torres, T.; Georgakilas, V.; Prato, M. Nanoscale Organization of a Phthalocyanine–Fullerene System: Remarkable

Stabilization of Charges in Photoactive 1-D Nanotubules. *J. Am. Chem. Soc.* **2005**, *127*, 5811-5813.

(24)   Ensslen, P.; Gärtner, S.; Glaser, K.; Colsmann, A.; Wagenknecht, H.-A. A DNA–Fullerene Conjugate as a Template for Supramolecular Chromophore Assemblies: Towards DNA-Based Solar Cells. *Angew Chem Int Ed Engl.* **2016**, *55*, 1904-1908.

(25)   Patel, M.; Harikrishnan, U.; Valand, N.; Mehta, D.; Joshi, K.; Kumar, P.; Chikhalia, K.; George, L.-B.; Jasrai, Y.; Menon, S. Novel cationic fullerene derivatized s-triazine scaffolds as photoinduced DNA cleavage agents: Design, synthesis, biological evaluation and computational investigation. *RSC Adv.* **2013**, *3,* 8734-8746.

(26)   Isobe, H.; Sugiyama, S.; Fukui, K.-i.; Iwasawa, Y.; Nakamura, E. Atomic Force Microscope Studies on Condensation of Plasmid DNA with Functionalized Fullerenes. *Angew. Chem. Int. Ed.* **2001**, *40*, 3364-3367.

(27)   Nakamura, E.; Isobe, H.; Tomita, N.; Sawamura, M.; Jinno, S.; Okayama, H. Functionalized Fullerene as an Artificial Vector for Transfection. *Angew. Chem. Int. Ed.* **2000**, *39*, 4254-4257.

(28)   Montellano, A.; Da Ros, T.; Bianco, A.; Prato, M. Fullerene C60 as a multifunctional system for drug and gene delivery. *Nanoscale* **2011**, *3*, 4035-4041.

(29)   Nakamura, E.; Isobe, H. In vitro and in vivo gene delivery with tailor-designed aminofullerenes. *Chem Rec.* **2010**, *10*, 260-270.

(30)   Song, C.; Chen, Y.-Q.; Xiao, S.-J.; Ba, L.; Gu, Z.-Z.; Pan, Y.; You, X.-Z. Assembly of Fullerene Arrays Templated by DNA Scaffolds. *Chem. Mater* **2005**, *17*, 6521-6524.

(31)   Pinheiro, A. V.; Han, D.; Shih, W. M.; Yan, H. Challenges and opportunities for structural DNA nanotechnology. *Nat. Nanotechnol* **2011**, *6*, 763-772.

(32)   Kulala Vittala, S.; Joseph, J. Chiral self-assembly of fullerene clusters on CT-DNA templates. *Faraday Discuss.* **2018**, *207*, 459-469.

(33)   Vittala, S. K.; Saraswathi, S. K.; Joseph, J. Fullerene Cluster Assisted Self-Assembly of Short DNA Strands into Semiconducting Nanowires. *Chem. Eur. J.* **2017**, *23*, 15759-15765.

(34)   Vittala, S. K.; Saraswathi, S. K.; Ramesan, A. B.; Joseph, J. Nanosheets and 2D-nanonetworks by mutually assisted self-assembly of fullerene clusters and DNA three-way junctions. *Nanoscale Adv.* **2019**, *1*, 4158-4165.

(35)   Chang, Y.; Jin, L.; Duan, J.; Zhang, Q.; Wang, J.; Lu, Y. New conjugated poly(pyridinium salt) derivative: AIE characteristics, the interaction with DNA and selective fluorescence enhancement induced by dsDNA. *RSC Adv.* **2015**, *5*, 103358-103364.

(36)   Wang, Z.; Gu, Y.; Liu, J.; Cheng, X.; Sun, J. Z.; Qin, A.; Tang, B. Z. A novel pyridinium modified tetraphenylethene: AIE-activity, mechanochromism, DNA detection and mitochondrial imaging. *J. Mater. Chem B* **2018**, *6*, 1279-1285.

(37)   Lu, Y.; Lv, J.; Zhang, G.; Wang, G.; Liu, Q. Interaction of an anthracycline disaccharide with ctDNA: Investigation by spectroscopic technique and modeling studies. *Spectrochim. Acta A Mol. Biomol. Spectrosc.* **2010**, *75*, 1511-1515.

(38)   Besteman, K.; Van Eijk, K.; Lemay, S. G. Charge inversion accompanies DNA condensation by multivalent ions. *Nat. Phy.* **2007**, *3*, 641-644.

(39)   Bloomfield, V. A. J. B. Condensation of DNA by multivalent cations: Considerations on mechanism. *Biopolymers* **1991**, 31, 1471-1481.

(40)   Fan, Y.; Wang, H.; He, C.; Qiao, F.; Wang, S.; Wang, Y. DNA Condensation Induced by a Star-Shaped Hexameric Cationic Surfactant. *ACS Appl. Mater. Interfaces* **2017**, *9*, 23333-23341.

(41)   Pi-Boleda, B.; Ramisetty, S.; Illa, O.; Branchadell, V.; Dias, R. S.; Ortuño, R. M. Efficient DNA Condensation Induced by Chiral β-Amino Acid-Based Cationic Surfactants. *ACS Appl. Bio Mater.* **2021**, *4*, 7034-7043.

(42)   Banerjee, A.; Singh, J.; Dasgupta, D. Fluorescence spectroscopic and calorimetry based approaches to characterize the mode of interaction of small molecules with DNA. *J. fluoresc.* **2013**, *23*, 745-752.

(43)   Bloomfield, V. A. Condensation of DNA by multivalent cations: Considerations on mechanism. *Biopolymers* **1991**, *31*, 1471-1481.

(44)   Guldi, D. M.; Hungerbuehler, H.; Asmus, K.-D. Unusual redox behavior of a water soluble malonic acid derivative of C60: evidence for possible cluster formation. *J. Phys. Chem.* **1995**, *99*, 13487-13493.

(45)   Meng, F.; Hua, J.; Chen, K.; Tian, H.; Zuppiroli, L.; Nüesch, F. Synthesis of novel cyanine–fullerene dyads for photovoltaic devices. *J. Mater. Chem.* **2005**, *15*, 979-986.

(46)   De Jonghe-Risse, J.; Heier, J.; Nüesch, F.; Moser, J.-E. Ultrafast charge transfer in solid-state films of pristine cyanine borate and blends with fullerene. *J. Mater. Chem A* **2015**, *3*, 10935-10941.

ANIONIC POLYMER ASSISTED ORDERED ASSEMBLY OF AMPHIPHILIC FULLERENES WITH ENHANCED ELECTRON TRANSPORT PROPERTIES
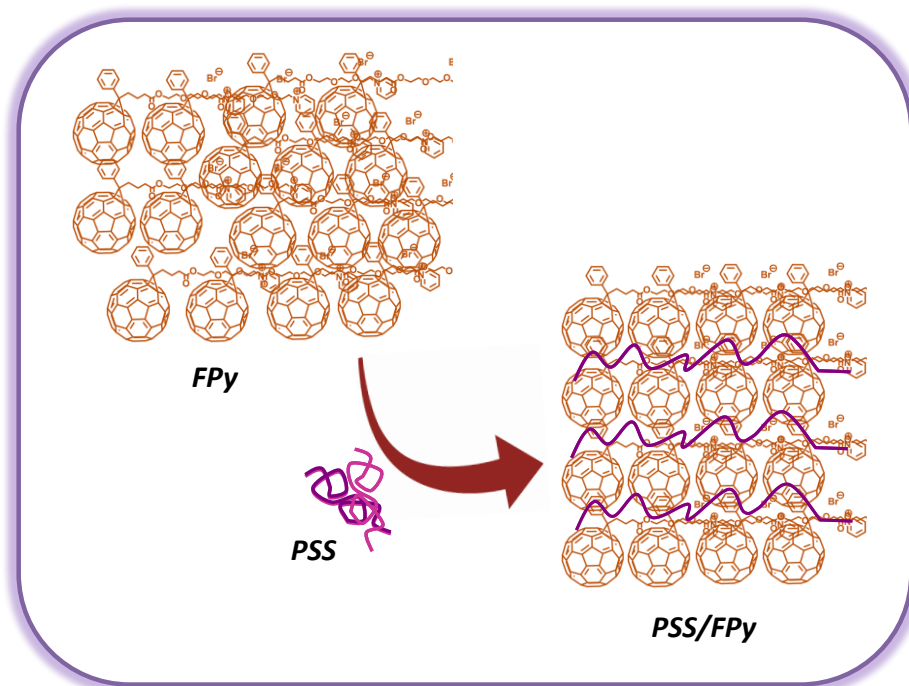
2B.1. ABSTRACT

*Ordered assembly of fullerenes via self-assembly or templated assembly have high significance in organic electronic applications, especially since the charge mobility across fullerenes is highly dependent on the structural order. In this work, we have employed polymer directed assembly of the pyridinium appended fullerene derivative, **FPy**, to enhance its charge carrier mobility by lowering the energy disorder. In the previous Chapter (Chapter 2A), we have demonstrated the mutually assisted assembly of the amphiphilic fullerene derivative, **FPy** with anionic biopolymer, DNA, through electrostatic and groove binding interactions leading to ordered fullerene/DNA nanostructures. In the present chapter, the ordered fullerene assembly*

*is achieved through the interaction with a commercially available anionic polymer, polystyrene sulfonate (**PSS**). Interaction of **FPy** with **PSS** was initially investigated using UV-visible absorption spectroscopy and the corresponding morphological changes were monitored through SEM, TEM and AFM analyses. Morphological analyses reveal the formation of ultrathin crystalline nanosheets with an ordered assembly of fullerenes. Crystallinity of nanosheets can be deduced from SAED pattern and is further confirmed by XRD analysis. Fullerenes in the **PSS/FPy** hybrid forms FCC lattice structure with the disappearance of peaks related to other lattice structures present in bare **FPy**. Electron mobility of fullerene nanosheets measured by SCLC method (0.92 x 10^{-3} cm^2V^{-1}S^{-1}) showed one order enhancement in **PSS/FPy** hybrid compared to **FPy** alone, which could be attributed to the reduced energy disorder in FCC lattice structure of the former. The results presented in this work suggest the potential use of the polymer assisted assembly of amphiphilic fullerenes in improving the electron transport properties of various optoelectronic devices.*

2B.2. INTRODUCTION

Fullerene, with its unique structure and electronic properties, has become an excellent choice in organic electronic applications as an electron acceptor and transport material. The extended use of fullerenes in organic electronic devices such as organic solar cells (OSCs) and organic field effect transistors (OFETs) is due to low reorganization energy, accelerated forward and backward electron transfer when compared to planar electron acceptors and also their excellent carrier mobility.[1, 2] The role of fullerenes and its derivatives in Organic Field Effect Transistors (OFETs) are very significant. Among the numerous members of fullerene family, fullerene-C_{60} is the most utilized one in OFETs and also the one with highest

reported mobility.[3] The high mobility of fullerene-C_{60} is due to the high symmetry and the deep-lying LUMO.[4]

Another reason for the wide utilization of Phenyl-C_{61}-butyric acid methyl ester (PCBM) in optoelectronics applications is its better solution processability. The combination of PCBM and the semiconducting polymer P3HT is a popular donor-acceptor system (Figure 2B.1) used in polymer bulk heterojunction solar cells and its charge carrier properties rely on the blend morphology and its heterogeneity.[5, 6] Several attempts have been made to improve the long range crystallinity of the active layer in order to enhance the charge carrier properties by utilizing various solution processes, deposition methods[7-10] and by incorporating suitable additives and compatibilizers.[11-13]
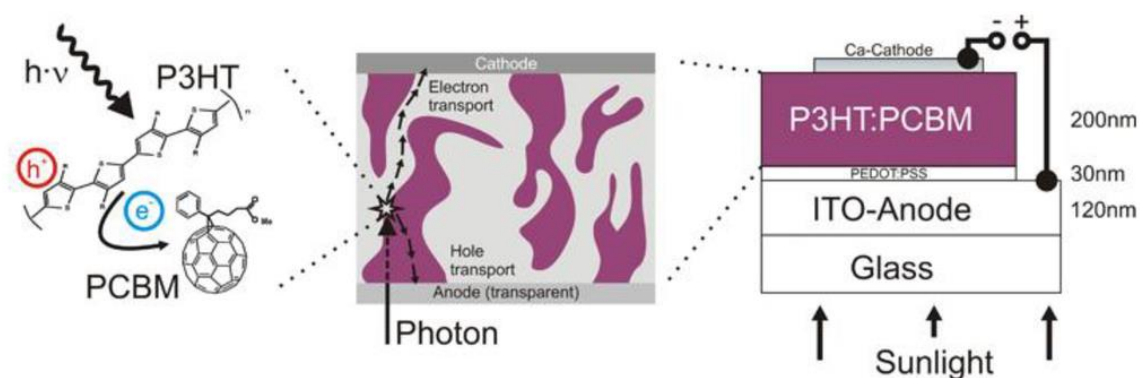
Figure 2B.1. A) Schematic representation of photo-induced electron transfer from p3HT to PCBM and the typical device structure of bulk- hetero junction solar cells (Adapted from reference 5).

P3HT block copolymer can act as a better compatibilizer in improving the morphology of p3HT/PCBM blend as discussed in several literature reports.[14-16] Sun *et al.* employed a diblock copolymer consisting of polystyrene and p3HT as a compatibilizer to improve the p3HT crystallinity and thereby to enhance the power conversion efficiency of polymer bulk heterojunction solar cells (Figure 2B.2A).[17]

Besides, Sofia *et al*. proposed a synthetic methodology to generate hybrid copolymers with covalently linked fullerene units, as shown in Figure 2B.2B, to use as a compatibilizer in order to improve the morphology of p3HT/PCBM blend.[18-20]
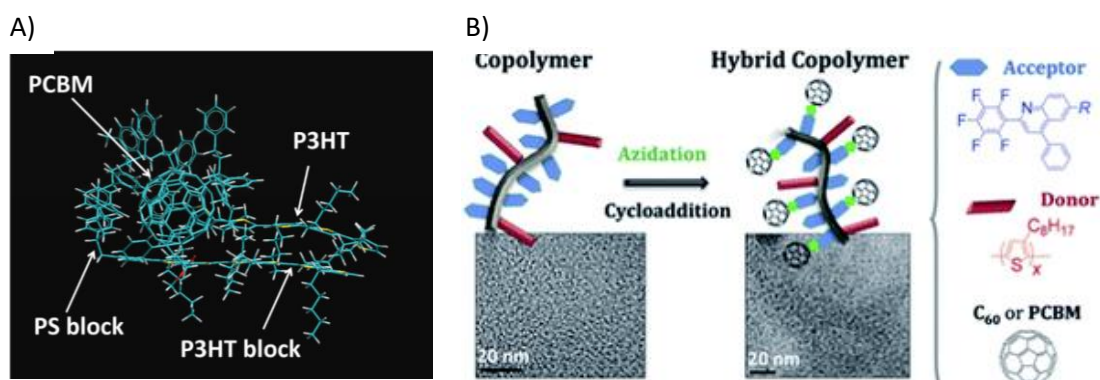
Figure 2B.2. A) Optimized structure of an oligomeric blend of P3HT/PCBM with a single copolymer chain of PS-b-P3HT; B) Schematic representation and corresponding TEM images of copolymer consists of rr-poly(3-alkyl-thiophene) and poly(perfluorophenyl-quinoline) blocks and hybrid copolymers attached with fullerenes (Adapted from reference 17 & 18).

The dependence of device performance on surface heterogeneity and morphology has been discussed in several literature reports which suggest the ordered molecular arrangement in the active layer for better photovoltaic performance.[21-23] Huang and co-workers have investigated the correlation between structural disorder and energy disorder (*ie.* broadening of energy levels) in fullerene electron transport layers and open–circuit voltage in perovskite solar cells.[22] The studies show that a simple solvent annealing method lower the structural disorder in PCBM assembly by forming an FCC lattice structure (Figure 2B.3A). This, in turn reduce the energy disorder in the system and thereby enhances the electron transport properties and open-circuit voltage of the device. Over the same period, the pioneering work of Lei and co-workers on fullerene ammonium iodide (PCBANI) established the n-doping mechanism and improved electron transport properties of

PCBANI through partial electron transfer from iodide to fullerene core.[23] Further, they have improved the electron transport properties by the formation of a more ordered lamellar assembly of PCBANI through a solvent dispersion method (Figure 2B.3B).[24]
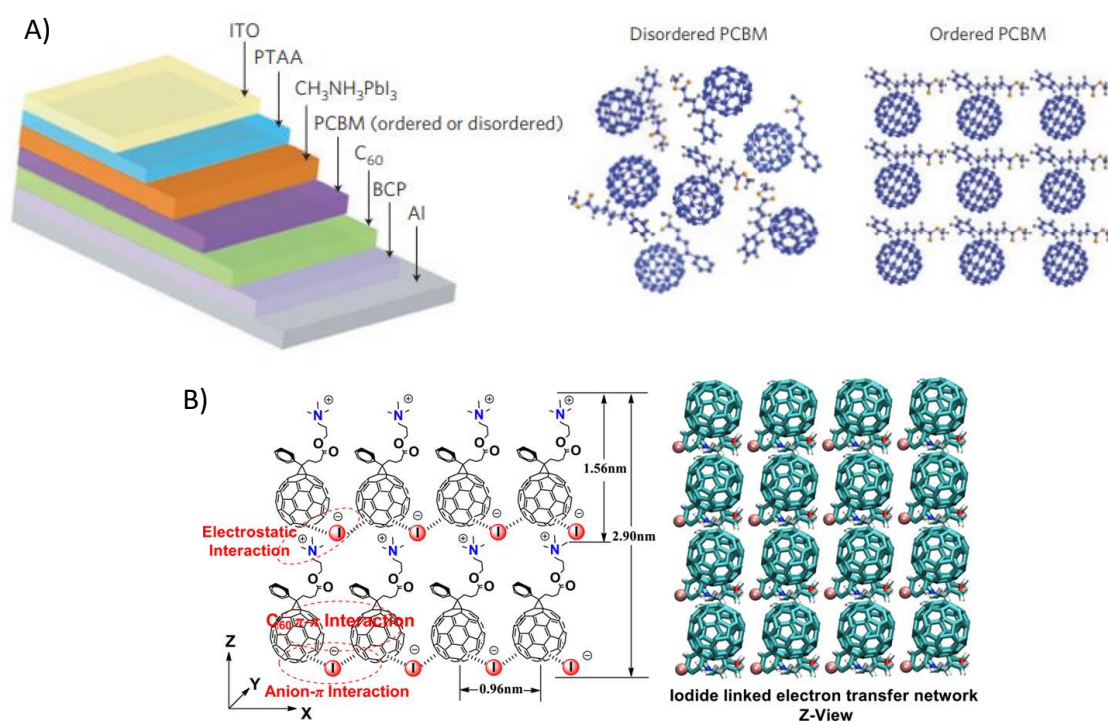
Figure 2B.3. A) Device structure of the perovskite solar cells and the schematic representation of disordered and ordered PCBM structures formed through various methods. B) Schematic representation of the structure of self-assembled PCBANI through solvent dispersion method and the corresponding optimized structures from computational modelling (Adapted from reference 22 and 24).

Various strategies have been developed to obtain an ordered fullerene assembly in charge carrier transport layer in order to enhance the charge conductance.[25-28] Nakanishi and co-workers have achieved the formation of closely packed fullerenes in lamellar mesophase structures by the design of alkyl substituted fullerene derivatives (Figure 2B.4) and investigated the charge carrier mobility of organized fullerenes in liquid crystalline states, that exhibit high charge

conductance.[25] The co-assembly of an amphiphilic fullerene derivative and insoluble fullerene derivatives has been adopted by Zhang *et al.*, which results in large crystalline domains with high conductance.[28]
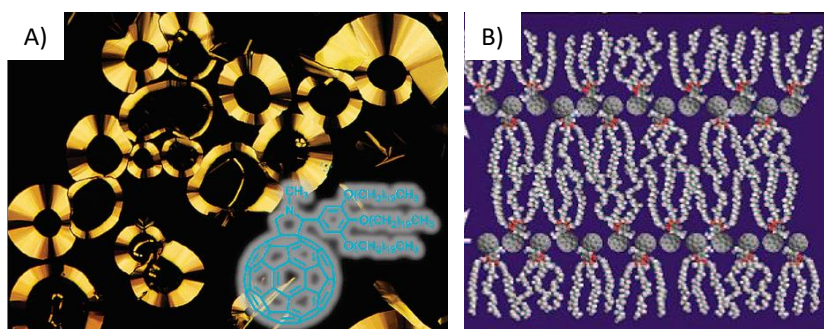
Figure 2B.4. A) Polarizing optical microscopic image of mesophase structures of fullerene derivative shown in the insight and B) the schematic representation of corresponding liquid crystalline assembly (Adapted from reference 25).

Covalent cross-linking is another well-accepted strategy adopted in bulk heterojunction solar cells that impart excellent structural durability for the device by preventing the high aggregation or crystallization tendency of fullerene molecules.[29] Hsu and co-workers have improved the power conversion efficiency of an inverted polymer solar cell by the thermal cross-linking of a fullerene derivative functionalized with a dendron containing two styryl groups.[30] Further, the same group utilized oxetane functionality for cross-linking, which also helps to make better adhesion with the TiO_2 surface.[31] Functionalities like epoxides[32], halides[33], azides[34] *etc.* are also utilized for cross-linking and contribute to the advances in fullerene based solar cells. Recently, our group has adapted the cross-linking approach to develop solvent resistive adhesive films through the design of a fullerene-benzoxazine derivative[35] for electron transport in inverted polymer solar cells (Figure 2B.5A) and put forward a rational design strategy for the development

of new polyfullerenes with aniline appended fullerene derivative by employing oxidative polymerization of aniline (Figure 2B.5B).[36]
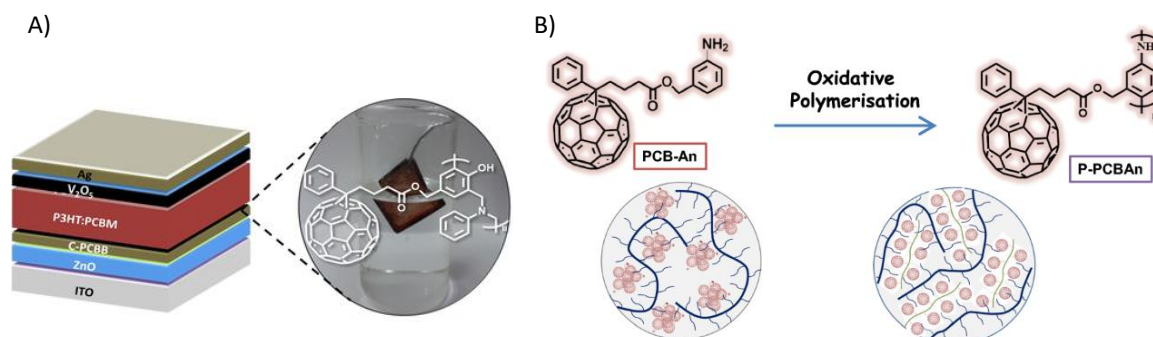
Figure 2B.5. A) Device structure and the cross-linked solvent-resistive adhescent film in the electron transport layer consist of fullerene-benzoxazine derivative and B) Schematic representation of polymer grafted fullerenes formed through oxidative polymerization of aniline appended fullerene derivative (Adapted from references 35 and 36).

Since all the aforementioned strategies require millimolar concentration of fullerenes to meet the desired electron mobility and most of these processes are laborious and energy consuming, the search for more facile methods is still continuing. Herein, we have adopted the electrostatic interaction between cationic pyridinium appended fullerene derivative (**FPy,** Figure 2B.6A) and an anionic polymer, polystyrene sulfonate (**PSS**, Figure 2B.6B, used in combination with PEDOT as a solubilizing agent in photovoltaic devices) to generate long-range ordered assembly of fullerenes for better charge transport properties using micromolar amounts of fullerenes. As in the case of **DNA/FPy** assemblies, the electrostatic interactions and π- π interactions guide the assembly of **FPy** and **PSS** to form ultrathin crystalline nanosheets. XRD analysis shows the FCC lattice structure of **PSS/FPy** hybrid and all other peaks in bare **FPy**, which corresponds to triclinic and octahedral lattices, get diminished on assembling with **PSS**. Consequently, we have

achieved enhanced electron mobility for **PSS/FPy** hybrid compared to bare **FPy** in response to the long-range crystalline order. Further, we have carried out a comparative study with **PCBM** and **PSS/PCBM** hybrid in order to understand the significance of amphiphilic design of **FPy** and the **PSS/FPy** assembly process in enhancing the electron transport properties.

2B.3. RESULTS AND DISCUSSION

2B.3.1. INTERACTION STUDIES OF FPy WITH PSS

As reported in the previous chapter, the absorption of **FPy** in 10% DMSO-water mixture shows two absorption peaks around 260 nm and 334 nm. Interaction of **FPy** with the anionic polymer, **PSS** was initially monitored through the changes in absorption spectrum of **FPy** (3 µM) with subsequent addition of **PSS** (Figure 2B.6C). A gradual reduction in absorption is observed at 334 nm, indicating the aggregation of fullerene molecules in presence of **PSS** due to the possible electrostatic interaction of cationic fullerene with the anionic polymer and π- π interactions between fullerene units. The sudden reduction in absorption around 260 nm with the first addition of **PSS** is also due to the fullerene aggregation via interaction with **PSS** and further increase in absorption around 260 nm is due to the absorption of **PSS** in this wavelength range. The strong electrostatic interaction between pyridinium moiety and the sulphate groups on **PSS** reduce the repulsion between cationic fullerene molecules and gradually bring **FPy** molecules together to form an assembly of fullerenes.
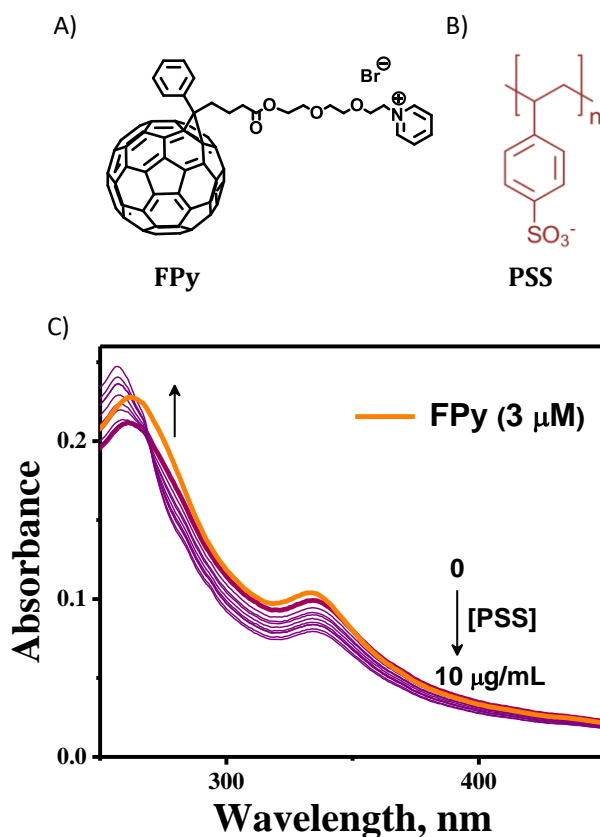
Figure 2B.6. Molecular structure of A) **FPy**, B) **PSS** and C) Changes in the absorption spectra of **FPy** with the addition of **PSS**.

2B.3.2. MORPHOLOGICAL ANALYSIS OF PSS/FPy HYBRID

The morphology of **PSS/FPy** hybrids were thoroughly characterised through SEM, TEM and AFM analysis and is compared with the sheet like structures of **PSS** alone in 10% DMSO-water mixture. SEM analysis shows the formation of micrometre sized sheet like morphology of **PSS/FPy** hybrid with fine edges, which can be visually distinguished from the sheet like morphology of amorphous **PSS** as seen in Figure 2B.7 A & B. TEM analysis of **PSS/FPy** hybrid reveals the crystallinity of the nanosheets originates from the ordered array of fullerenes and is further confirmed from the SAED pattern (Figure 2B.7C, D & E). **PSS/FPy** hybrid and **PSS** alone can also be distinguished from the AFM images as shown in Figure 2B.8, that show smaller nanosheets of **PSS/FPy** hybrid, with a lateral dimension of 100-500

nm and thickness around 3 nm, compared to larger amorphous sheets (~ 2 μm) of

PSS.
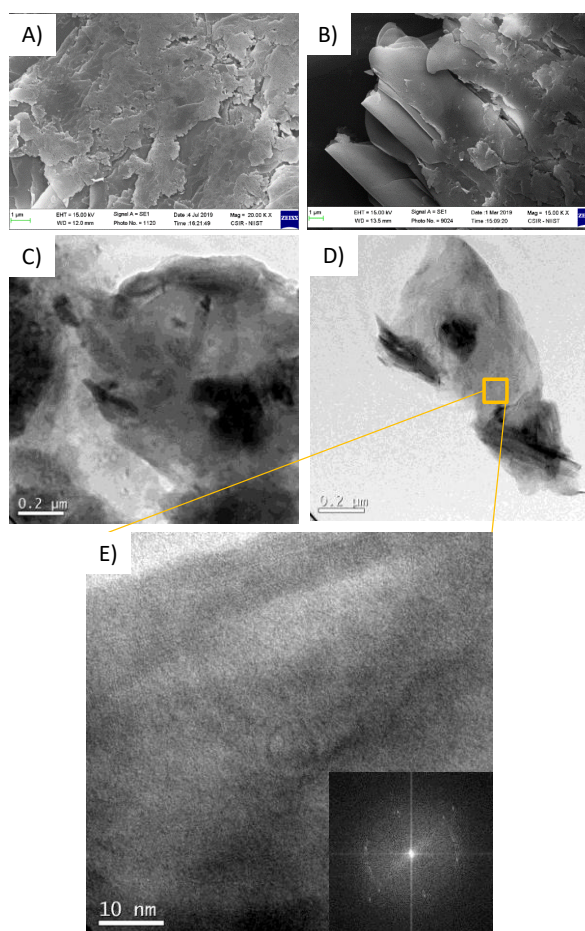
Figure 2B.7. SEM images of A) **PSS** alone; B) **PSS/FPy** hybrid; TEM images of C) **PSS** alone; D) **PSS/FPy** hybrid and E) Magnified TEM image of **PSS/FPy** hybrid (Inset : SAED pattern).
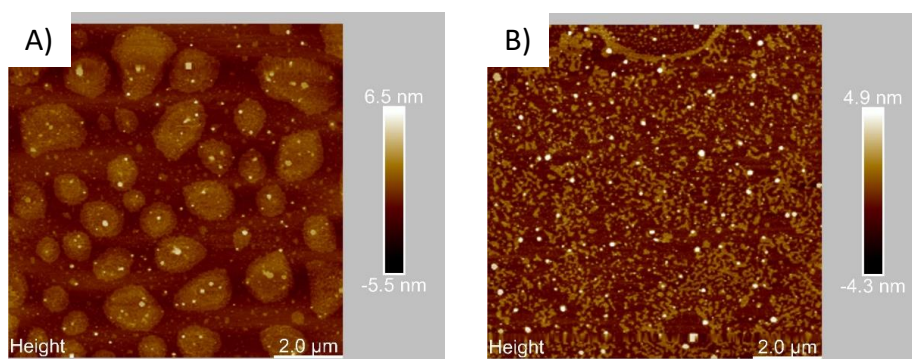
Figure 2B.8. AFM images of A) **PSS** alone and B) **PSS/FPy** in 10% DMSO-water mixture dropcasted on mica surface.

2B.3.3. XRD ANALYSIS

To get more insight into the ordered assembly of fullerenes on the nanosheet structures, we have carried out the XRD analysis of **PSS/FPy** hybrid and were compared with that of bare **FPy**, under similar conditions (Figure 2B.9). The XRD peaks of bare **FPy** can be assigned to various close packed structures of fullerene, including FCC, octahedral, triclinic *etc.*[37-40]. But the peaks corresponding to FCC alone is retained in the XRD pattern of **PSS/FPy** hybrid, which clearly support the ordered assembly of fullerenes in the nanosheet structures. Moreover, the peculiar FCC structure of fullerene is highly recommendable in electron transporting layers due to less energy disorder in the FCC close packed structure.[22]
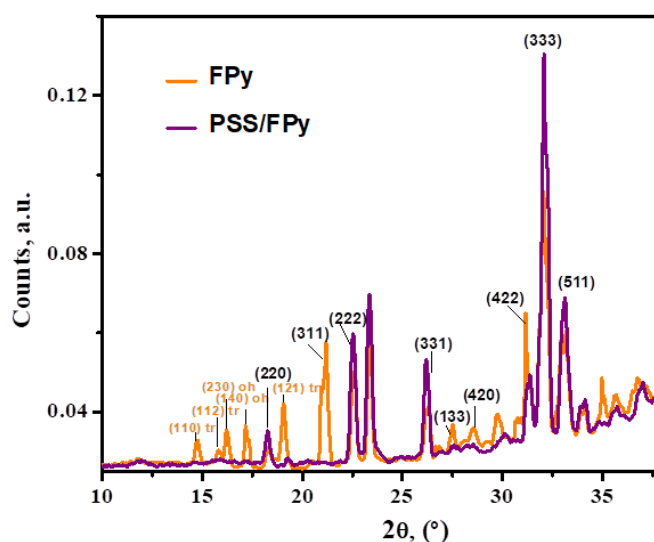
Figure 2B.9. XRD spectra of **FPy** alone & **PSS/FPy** hybrid.

2B.3.4. ELECTRON MOBILITY MEASUREMENTS BY SCLC METHOD

Since the FCC structure has significance in reducing energy disorder and thereby enhancing the electron transport properties in photovoltaic devices, we have carried out the electron mobility measurements of the **PSS/FPy** hybrid nanosheets via space charge limited current (SCLC) method. In comparison to bare

107

FPy, a significant enhancement in electron mobility can be seen while assembling **FPy** with **PSS** and it can be attributed to the FCC lattice structure of **FPy** in the hybrid nanosheets. Bare **FPy** shows an electron mobility of $(1.2 \pm 0.5) \times 10^{-4}$ cm^{2}V^{-1}S^{-1} and is ten times enhanced in **PSS/FPy** hybrid $((0.92 \pm 0.2) \times 10^{-3}$ cm^{2}V^{-1}S$^{-1})$ with comparable layer thickness as shown in Figure 2B.10.
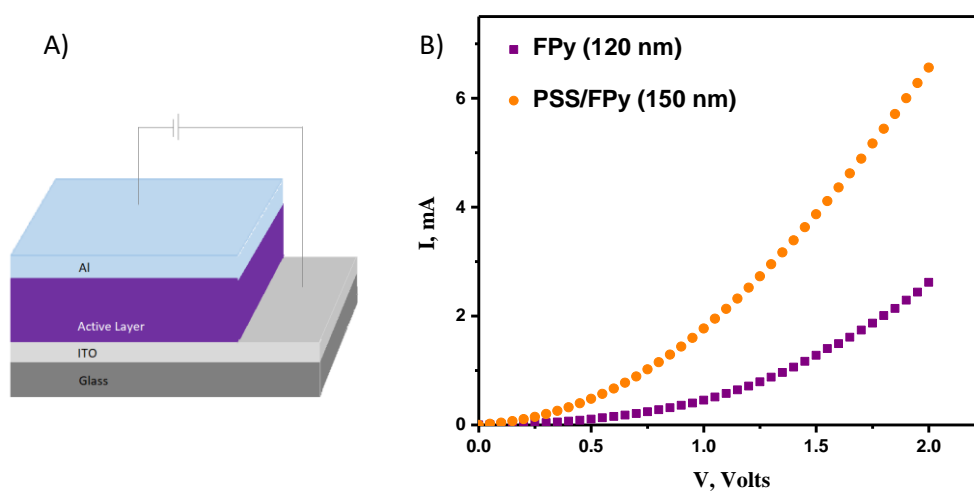
Figure 2B.10. A) Device structure for electron mobility measurements by SCLC method and B) Mobility measurements of **FPy** and **PSS/FPy**.

A control experiment has been carried out with **PCBM** to specify the importance of molecular design and highly ordered organization of **FPy** with anionic polymer, **PSS**. The experiments have been done in similar conditions to avoid the effects of solution processing. Bare **FPy** shows comparable electron mobility $((3.8 \pm 0.3) \times 10^{-4}$ cm^{2}V^{-1}S$^{-1})$ with the standard **PCBM** $((5 \pm 0.5) \times 10^{-4}$ cm^{2}V^{-1}S$^{-1})$ and the incorporation of **PSS** reduces the electron transporting ability of **PCBM** to $(1.6 \pm 0.04) \times 10^{-4}$ cm^{2}V^{-1}S^{-1}, since organisation of **PCBM** is altered in presence of **PSS**. Contrarily, **PSS** can enhance the electron mobility of **FPy** to $(1.8 \pm 0.6) \times 10^{-3}$ cm^{2}V^{-1}S^{-1} by organizing the fullerene moieties in an FCC lattice structure (Figure 2B.11).
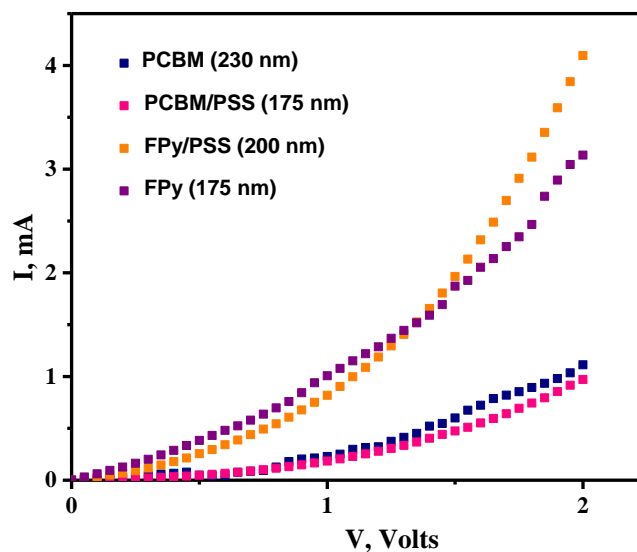
Figure 2B.11. Mobility measurements of **PCBM**, **PSS/PCBM**, **FPy** and **PSS/FPy**.

2B.4. CONCLUSIONS

In this chapter, we have employed the suitably designed cationic fullerene derivative, **FPy** and an anionic polymer, polystyrene sulfonate (**PSS**) to achieve an ordered fullerene assembly, mainly through electrostatic interactions. The formation of ultrathin crystalline nanosheets is observed through the morphological analysis of fullerene/polymer hybrid and the crystalline nature of the assembly is confirmed from SAED pattern. The XRD analyses revealed the reorganisation of fullerenes in presence of **PSS** to an FCC lattice structure, which is favourable for the enhanced electron transporting properties of fullerene layer. Subsequently, the electron mobility measurements of **FPy** and **PSS/FPy** hybrid by SCLC method showed one order enhancement in the electron transporting ability of **PSS/FPy** hybrid compared to bare **FPy**. Further, the comparative study of electron transporting properties of **FPy** and **PSS/FPy** hybrid with that of **PCBM** and **PSS/PCBM** hybrid signify the importance of amphiphilic design of cationic fullerene

and its ordered assembly within **PSS/FPy** hybrid in enhancing the electron transport property. In summary, this chapter put forward a facile method, utilising micromolar concentration of fullerenes, to improve the charge carrier transport of fullerene layers in optoelectronic devices by the suitable design of an amphiphilic fullerene derivative and its interaction with a commercially available anionic polymer.

2B.5. EXPERIMENTAL SECTION

2B.5.1. MATERIALS AND METHODS

All the reagents and solvents were purchased from Sigma-Aldrich, TCI chemicals and Spectrochem chemical suppliers. Poly(sodium-4-styrene)sulfonate (**PSS**) with an average molecular weight of 70,000 was used in the present study and is purchased from Sigma-Aldrich.

2B.5.2. INTERACTION STUDIES OF FPy WITH PSS

.   Interaction of **FPy** with **PSS** was initially monitored with Shimadzu UV-2600 PC UV-Vis spectrophotometer by the subsequent addition of PSS from a stock solution of 1 mg/mL to a fixed concentration of **FPy** (3 μM).

2B.5.3. MORPHOLOGICAL AND XRD ANALYSIS

All the samples were prepared with fixed concentrations of **FPy** (3 μM) and **PSS** (10 μg/mL). TEM samples were prepared by passing 20-30 μL of solutions through a carbon-coated Cu grid. HR-TEM analyses were carried out with FEI-Tecnai G2 30, with EDAX at accelerating voltage of 300 kV. Samples were imaged with a Hamamatsu ORCA CCD camera. SEM and AFM samples were prepared by drop-casting 20-30 μL of samples to freshly cleaved mica surface. The samples were dried in air overnight and kept in vacuum desiccator prior to analysis. The SEM images

were recorded after sputtering with gold using Zeiss EVO 18cryo SEM Special Edn., operating with an accelerating voltage of 20 kV. AFM analyses were carried out with a Bruker multimode AFM instrument operating with a tapping mode regime. Micro-fabricated TiN cantilever tips (NT-MDT-NSG series) with a resonance frequency of 299 kHz and a spring constant of 20–80 Nm^{-1} were used. AFM section analyses were performed offline using Nanoscope Analysis 1.5 software. XRD analyses were performed by XEUSS SAXS/WAXS system using a Genix microsource from Xenocs and the generator was operated at 0.6 mA and 50 kV. FOX2D mirror and two pairs of scatter-less slits from Xenocs were used to collimate the Cu Kα radiation with λ = 1.54 Å. A Mar345 image plate detector and Fit2D software were used to obtain the 2D- WAXS pattern.

2B.5.4. SCLC MEASUREMENTS

The fullerene solution (**FPy** or **PSS/FPy**) in 10% DMSO-water mixture was drop-casted on an ITO surface after depositing Al electrode through thermal evaporation. The drop-casted ITO plates were allowed to dry on a hot plate at 70°C to get an active layer on top of the surface. The devices were finished by glass encapsulation to avoid degradation of the active layer. Control devices (**PCBM** and **PSS/PCBM**) were fabricated through similar procedure using **PCBM** solutions in 10% THF-water mixture. Charge carrier mobility is measured in the SCLC regime as described by $J=9\varepsilon_0\varepsilon_r\mu V^2/8L^3$, where ε_0 is the permittivity of free space (8.854×10^{-12} F/m), ε_r is the dielectric constant of the active layer (~3), μ_e is the electron mobility, V is the voltage drop across the device and L is the active layer thickness.[41]

2B.6. REFERENCES

1.   Hasobe, T., Supramolecular nanoarchitectures for light energy conversion. *Phys. Chem. Chem. Phys.* **2010**, 12 (1), 44-57.

2.   Segura, J. L.; Martín, N.; Guldi, D. M., Materials for organic solar cells: the C60/π-conjugated oligomer approach. *Chem. Soc. Rev.* **2005**, 34 (1), 31-47.

3.   Zhang, Y. S.; Murtaza, I.; Meng, H., Development of fullerenes and their derivatives as semiconductors in field-effect transistors: exploring the molecular design. *J. Mater. Chem. C* **2018**, 6 (14), 3514-3537.

4.   Nielsen, C. B.; Holliday, S.; Chen, H.-Y.; Cryer, S. J.; McCulloch, I., Non-Fullerene Electron Acceptors for Use in Organic Solar Cells. *Acc. Chem. Res.* **2015**, 48 (11), 2803-2812.

5.   Eslamian, M., Spray-on Thin Film PV Solar Cells: Advances, Potentials and Challenges. *Coatings* **2014**, 4 (1), 60-84.

6.   Cook, S.; Katoh, R.; Furube, A., Ultrafast Studies of Charge Generation in PCBM:P3HT Blend Films following Excitation of the Fullerene PCBM. *J. Phys.Chem. C* **2009**, 113 (6), 2547-2552.

7.   Xu, J.; Buin, A.; Ip, A. H.; Li, W.; Voznyy, O.; Comin, R.; Yuan, M.; Jeon, S.; Ning, Z.; McDowell, J. J.; Kanjanaboos, P.; Sun, J.-P.; Lan, X.; Quan, L. N.; Kim, D. H.; Hill, I. G.; Maksymovych, P.; Sargent, E. H., Perovskite–fullerene hybrid materials suppress hysteresis in planar diodes. *Nat. Commun.* **2015**, 6 (1), 7081.

8.   Wang, Q.; Shao, Y.; Dong, Q.; Xiao, Z.; Yuan, Y.; Huang, J., Large fill-factor bilayer iodine perovskite solar cells fabricated by a low-temperature solution-process. *Energy Environ. Sci.* **2014**, 7 (7), 2359-2365.

9.   Jeon, N. J.;   Noh, J. H.;   Kim, Y. C.;   Yang, W. S.;   Ryu, S.;   Seok, S. I., Solvent engineering for high-performance inorganic–organic hybrid perovskite solar cells. *Nat. Mater.* **2014**, 13 (9), 897-903.

10.   Jeon, N. J.;   Noh, J. H.;   Yang, W. S.;   Kim, Y. C.;   Ryu, S.;   Seo, J.;   Seok, S. I., Compositional engineering of perovskite materials for high-performance solar cells. *Nature* **2015**, 517 (7535), 476-480.

11.   Krebs, F. C., Fabrication and processing of polymer solar cells: A review of printing and coating techniques. *Sol. Energy Mater. Sol. Cells* **2009**, 93 (4), 394-412.

12.   Søndergaard, R. R.;   Hösel, M.;   Krebs, F. C., Roll-to-Roll fabrication of large area functional organic materials. *J. Polym. Sci. B Polym. Phys.* **2013**, 51 (1), 16-34.

13.   Wengeler, L.;   Schmitt, M.;   Peters, K.;   Scharfer, P.;   Schabel, W., Comparison of large scale coating techniques for organic and hybrid films in polymer based solar cells. *Chem. Eng. Process.: Process Intensif.* **2013**, 68, 38-44.

14.   Galloway, J. A.;   Jeon, H. K.;   Bell, J. R.;   Macosko, C. W., Block copolymer compatibilization of cocontinuous polymer blends. *Polymer* **2005**, 46 (1), 183-191.

15.   Sommer, M.;   Hüttner, S.;   Steiner, U.;   Thelakkat, M., Influence of molecular weight on the solar cell performance of double-crystalline donor-acceptor block copolymers. *Appl. Phys. Lett.* **2009**, 95 (18), 183308.

16.   Sary, N.;   Richard, F.;   Brochon, C.;   Leclerc, N.;   Lévêque, P.;   Audinot, J.-N.;   Berson, S.;   Heiser, T.;   Hadziioannou, G.; Mezzenga, R., A New Supramolecular Route for Using Rod-Coil Block Copolymers in Photovoltaic Applications. *Adv. Mater.* **2010**, 22 (6), 763-768.

17. Sun, Z.; Xiao, K.; Keum, J. K.; Yu, X.; Hong, K.; Browning, J.; Ivanov, I. N.; Chen, J.; Alonzo, J.; Li, D.; Sumpter, B. G.; Payzant, E. A.; Rouleau, C. M.; Geohegan, D. B., PS-b-P3HT Copolymers as P3HT/PCBM Interfacial Compatibilizers for High Efficiency Photovoltaics. *Adv. Mater.* **2011**, 23 (46), 5529-5535.

18. Kakogianni, S.; Kourkouli, S. N.; Andreopoulou, A. K.; Kallitsis, J. K., A versatile approach for creating hybrid semiconducting polymer–fullerene architectures for organic electronics. *J. Mater.Chem. A* **2014**, 2 (21), 8110-8117.

19. Kakogianni, S.; Lebedeva, M. A.; Paloumbis, G.; Andreopoulou, A. K.; Porfyrakis, K.; Kallitsis, J. K., Semiconducting end-perfluorinated P3HT–fullerenic hybrids as potential additives for P3HT/IC70BA blends. *RSC Adv.* **2016**, 6 (100), 98306-98316.

20. Kakogianni, S.; Andreopoulou, A. K.; Kallitsis, J. K., Synthesis of Polythiophene–Fullerene Hybrid Additives as Potential Compatibilizers of BHJ Active Layers. *Polymers* **2016**, 8 (12), 440.

21. Ballantyne, A. M.; Ferenczi, T. A. M.; Campoy-Quiles, M.; Clarke, T. M.; Maurano, A.; Wong, K. H.; Zhang, W.; Stingelin-Stutzmann, N.; Kim, J.-S.; Bradley, D. D. C.; Durrant, J. R.; McCulloch, I.; Heeney, M.; Nelson, J.; Tierney, S.; Duffy, W.; Mueller, C.; Smith, P., Understanding the Influence of Morphology on Poly(3-hexylselenothiophene):PCBM Solar Cells. *Macromolecules* **2010**, 43 (3), 1169-1174.

22. Shao, Y.; Yuan, Y.; Huang, J., Correlation of energy disorder and open-circuit voltage in hybrid perovskite solar cells. *Nat. Energy* **2016**, 1 (1), 15001.

23. Wang, H. H.; Sun, X.; Lin, Z. C.; Pang, Z. F.; Kong, X. Q.; Lei, M.; Li, Y. F., Self-assembly of highly conductive self-n-doped fullerene ammonium halides and their application in the in situ solution-processable fabrication of working electrodes for alcohol electrooxidation. *RSC Adv.* **2018**, 8 (17), 9503-9511.

24. Sun, X.; Chen, W.; Liang, L.; Hu, W.; Wang, H.; Pang, Z.; Ye, Y.; Hu, X.; Wang, Q.; Kong, X.; Jin, Y.; Lei, M., Construction of Electron Transfer Network by Self-Assembly of Self-n-Doped Fullerene Ammonium Iodide. *Chem. Mater.* **2016**, 28 (23), 8726-8731.

25. Nakanishi, T.; Shen, Y.; Wang, J.; Yagai, S.; Funahashi, M.; Kato, T.; Fernandes, P.; Möhwald, H.; Kurth, D. G., Electron Transport and Electrochemistry of Mesomorphic Fullerenes with Long-Range Ordered Lamellae. *J. Am. Chem. Soc.* **2008**, 130 (29), 9236-9237.

26. Chu, C.-C.; Raffy, G.; Ray, D.; Guerzo, A. D.; Kauffmann, B.; Wantz, G.; Hirsch, L.; Bassani, D. M., Self-Assembly of Supramolecular Fullerene Ribbons via Hydrogen-Bonding Interactions and Their Impact on Fullerene Electronic Interactions and Charge Carrier Mobility. *J. Am. Chem. Soc.* **2010**, 132 (36), 12717-12723.

27. Ma, D.; Lv, M.; Lei, M.; Zhu, J.; Wang, H.; Chen, X., Self-Organization of Amine-Based Cathode Interfacial Materials in Inverted Polymer Solar Cells. *ACS Nano* **2014**, 8 (2), 1601-1608.

28. Zhang, J.; Li, C.-Z.; Williams, S. T.; Liu, S.; Zhao, T.; Jen, A. K. Y., Crystalline Co-Assemblies of Functional Fullerenes in Methanol with Enhanced Charge Transport. *J. Am. Chem. Soc.* **2015**, 137 (6), 2167-2170.

29. Lee, J. U.; Jung, J. W.; Jo, J. W.; Jo, W. H., Degradation and stability of polymer-based solar cells. *J. Mater. Chem.* **2012**, 22 (46), 24265-24283.

30. Hsieh, C.-H.; Cheng, Y.-J.; Li, P.-J.; Chen, C.-H.; Dubosc, M.; Liang, R.-M.; Hsu, C.-S., Highly Efficient and Stable Inverted Polymer Solar Cells Integrated with a Cross-Linked Fullerene Material as an Interlayer. *J. Am. Chem. Soc.* **2010**, 132 (13), 4887-4893.

31. Cheng, Y.-J.; Cao, F.-Y.; Lin, W.-C.; Chen, C.-H.; Hsieh, C.-H., Self-Assembled and Cross-Linked Fullerene Interlayer on Titanium Oxide for Highly Efficient Inverted Polymer Solar Cells. *Chem. Mater.* **2011**, 23 (6), 1512-1518.

32. Drees, M.; Hoppe, H.; Winder, C.; Neugebauer, H.; Sariciftci, N. S.; Schwinger, W.; Schäffler, F.; Topf, C.; Scharber, M. C.; Zhu, Z.; Gaudiana, R., Stabilization of the nanomorphology of polymer–fullerene "bulk heterojunction" blends using a novel polymerizable fullerene derivative. *J. Mater. Chem.* **2005**, 15 (48), 5158-5163.

33. Kim, B. J.; Miyamoto, Y.; Ma, B.; Fréchet, J. M. J., Photocrosslinkable Polythiophenes for Efficient, Thermally Stable, Organic Photovoltaics. *Adv. Funct. Mater.* **2009**, 19 (14), 2273-2281.

34. Nam, C.-Y.; Qin, Y.; Park, Y. S.; Hlaing, H.; Lu, X.; Ocko, B. M.; Black, C. T.; Grubbs, R. B., Photo-Cross-Linkable Azide-Functionalized Polythiophene for Thermally Stable Bulk Heterojunction Solar Cells. *Macromolecules* **2012**, 45 (5), 2338-2347.

35. Vittala, S. K.; Ravi, R.; Deb, B.; Joseph, J., A Cross-Linkable Electron-Transport Layer Based on a Fullerene-Benzoxazine Derivative for Inverted Polymer Solar Cells. *ChemPlusChem* **2020**, 85 (7), 1534-1541.

36. Vittala, S. K.; Ravi, R.; Deb, B.; Joseph, J., Rational synthesis of a polymerizable fullerene–aniline derivative: study of photophysical, morphological and photovoltaic properties *J. Chem. Sci.* **2018**, 130 (10), 135.

37. Sathish, M.; Miyazawa, K. i., Synthesis and Characterization of Fullerene Nanowhiskers by Liquid-Liquid Interfacial Precipitation: Influence of C60 Solubility. *Molecules* **2012**, 17 (4).

38. Gopiraman, M.; Saravanamoorthy, S.; Ullah, S.; Ilangovan, A.; Kim, I. S.; Chung, I. M., Reducing-agent-free facile preparation of Rh-nanoparticles uniformly anchored on onion-like fullerene for catalytic applications. *RSC Adv.* **2020**, 10 (5), 2545-2559.

39. Minato, J.-i.; Miyazawa, K. i., Solvated structure of C60 nanowhiskers. *Carbon* **2005**, 43 (14), 2837-2841.

40. Sathish, M.; Miyazawa, K., Synthesis and characterization of fullerene nanowhiskers by liquid-liquid interfacial precipitation: influence of C60 solubility. *Molecules* **2012**, 17 (4), 3858-65.

41. Jia, T.; Zhou, W.; Chen, Y.; Han, J.; Wang, L.; Li, F.; Wang, Y., Highly efficient polymer solar cells based on a universal cathode interlayer composed of metallophthalocyanine derivative with good film-forming property. *J. Mater. Chem. A* **2015**, 3 (8), 4547-4554.

HIERARCHICAL ASSEMBLY AND DNA ASSISTED REASSEMBLY OF TETRAPHENYLETHYLENE AMPHIPHILES
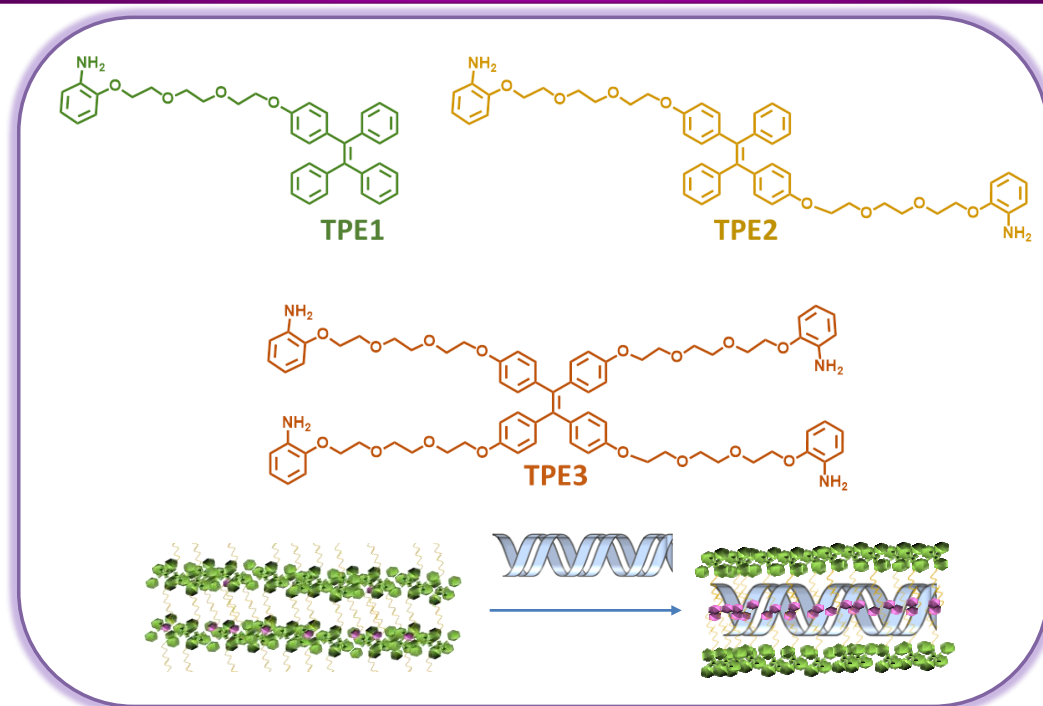
3.1. ABSTRACT

*This chapter discusses the design, synthesis and assembly/re-assembly process of three aniline appended amphiphilic TPE derivatives (**TPE1**, **TPE2** & **TPE3**) in the presence of CTDNA and short dsDNA. DNA plays a key role in the reassembly process as it alters the hydrophilic-hydrophobic balance of the system and provides specific binding possibility to achieve a directional assembly without compromising the ultimate morphology of the respective assemblies. TPE derivatives were synthesized by modified synthetic procedures and characterized using NMR and HRMS techniques. Hierarchical assembly process of these TPE amphiphiles from fibrillar to nanoribbons/nanosheets structures has been discussed in detail and the disassembly*

*and reassembly of TPE amphiphiles in presence of DNA, leading to more ordered nanostructures is probed through different spectroscopic and morphological techniques. The difference in the number of triethylene glycol chains attached to the TPE amphiphiles significantly contribute to the distinct assemblies of **TPE1**, **TPE2** and **TPE3**. The initial fibril formation might be originated from the slipped stacking of TPE cores along with the van der Waals interaction between triethylene glycol chains. Lateral association of fibrillar structures and formation of nanoribbons/nanosheets rely mostly on the van der Waals interaction between the triethylene glycol chains which in turn stabilize the TPE assemblies in water. The crystalline assembly of TPE can be observed in all the three TPE/DNA hybrids and the reassembly process of **TPE2** in presence of CTDNA is studied in detail. Short dsDNA act as more rigid template for the assembly of TPE amphiphiles and is found to form more ordered structures compared to the crystalline assemblies formed by lengthy, flexible CTDNA.*

3.2. INTRODUCTION

Tetraphenylethylene (TPE) is well-known for its AIE behavior that results from the restricted intramolecular rotation of phenyl rings upon molecular aggregation (Figure 3.1A).[1] This unique photophysical process of TPE attracts major interest in optoelectronics and bio/chemosensors.[2-7] Apart from the excellent optical properties, the AIE luminogens also have advantage of easy synthesis, functionalization and self-assembling properties.[8, 9] The stimuli-responsive molecular aggregation and AIE behavior of TPE are frequently applied in bio/chemical sensors,[2] fluorescence imaging,[10] optoelectronic devices etc. and is made possible through different non-covalent interactions like π-π stacking,[11] electrostatic[12] and van der Waals interactions,[13] metal co-ordination,[14] host-guest

interactions[15] etc. Based on electrostatic interaction, Li *et al.* have developed a glucose sensing probe consists of ammonium modified TPE derivative and an anionic polymer having a phenylboronic acid group. In presence of glucose and glucose oxidase, the electrostatically bound TPE/polyanion hybrid get disaggregated since the H_2O_2 produced during glucose oxidation can reduce the phenyl boronic acid to a weaker phenolic acid, thereby lessens the negative charges on the polyanion.[16] Later, Li *et al.* have developed an enzyme responsive fluorescent vesicle based on ionic complexation between a water-soluble TPE derivative and an enzyme substrate, myristoylcholine chloride, that may find applications in the treatment of Alzheimer's disease (Figure 3.1B).[17] Dinca and co-workers have employed metal co-ordination based enhanced emission of TPE for the first time, by anchoring luminogens within a rigid matrix (Figure 3.1C).[18] Later, Yin *et al.* have developed supramolecular rosettes with tunable emission properties through co-ordination driven self-assembly of terpyridine conjugated TPE ligands and have achieved pure white-light emission under wide range of water fractions.[19] Likewise, a covalent polymerization method has also been employed by Zhao and co-workers to restrict the rotation of TPE rotors and produce porous ultrathin 2D nanosheets sensitive to volatile organic compounds (VOCs) (Figure 3.1D). The vapor sensing is achieved by virtue of the enhanced emission on interaction with electron rich volatile organic molecules, which is similar to AIE behavior.[20] The host-guest interaction has also utilized in the design of AIE based luminescent materials, mainly to provide stimuli responsive properties. Huang and co-workers have reported the controllable self-assembly of a pillar[5]arene based amphiphilic supramolecular copolymers with TPE and viologen units to find application in self-imaging targeted drug-delivery (Figure 3.1E).[21]
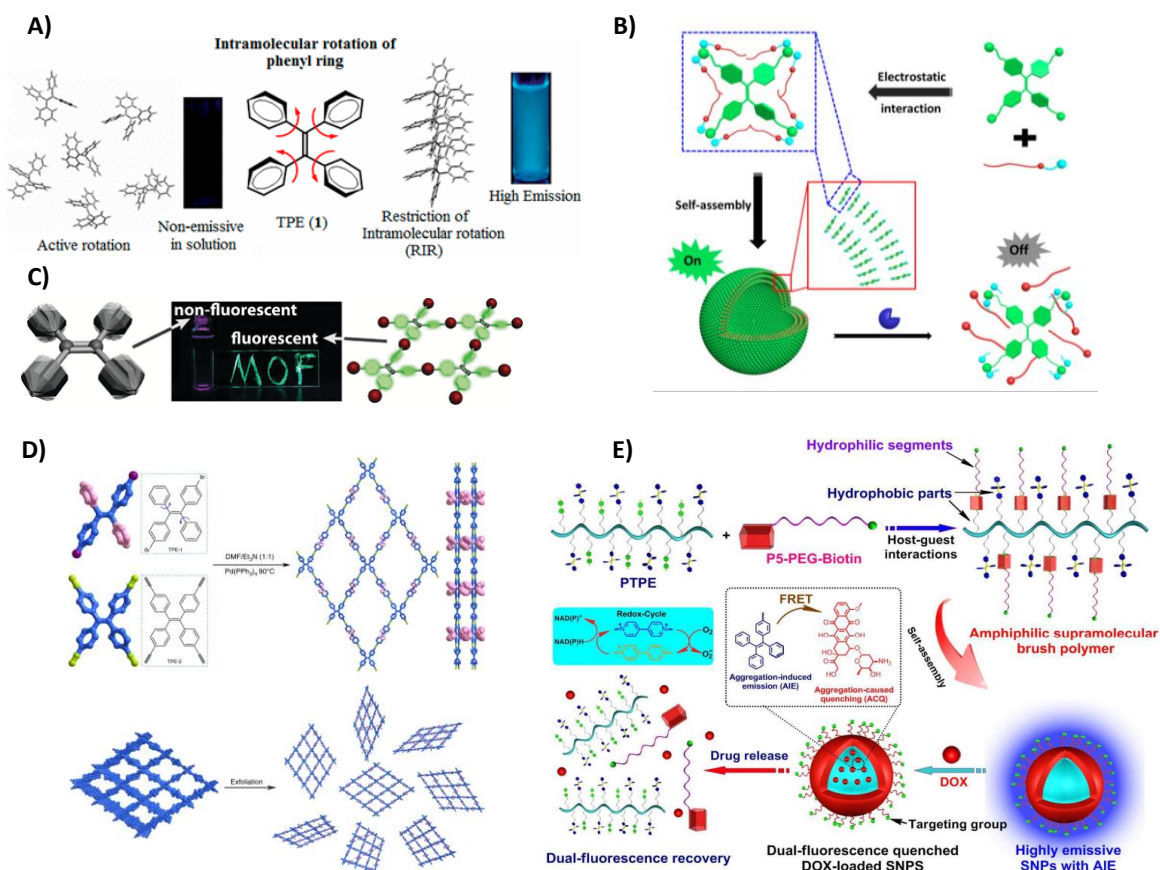
Figure 3.1. Schematic representation of A) AIE in TPE molecule caused by RIR; B) Self-assembly and enzyme responsive disassembly of TPE based fluorescent vesicle based on electrostatic interaction; C) AIE induced by metal co-ordination; D) Formation of ultrathin 2D nanosheets through covalent polymerization method and E) Self-assembly and stimuli-responsive drug release based on host-guest interactions. (Adapted from references 7, 17, 18, 20 and 21, respectively)

The interactions of TPE with biomolecules like proteins, DNA etc. have been investigated by several research groups in order to employ the AIE properties in sensing, bio-imaging and various other biological applications.[22-24] In early years, charged TPE derivatives are widely suggested for the fluorescence based biosensing applications as it produce significant changes in the fluorescence signal on interaction with bioanalytes.[16] Ben-Zhong Tang and co-workers, who first proposed the concept of AIE,[1] have utilized the AIE character of TPE to design a label-free

fluorescent probe for G-qudraplex formation and real-time monitoring of DNA folding.[25] Later, they have introduced a thymine functionalized TPE derivative for the selective detection of adenine rich ssDNA based on AIE characteristics (Figure 3.2A)[26]. A bimodal fluorogenic/magnetic resonance probe has been designed by Li *et al.* with a four-armed star shaped TPE based copolymer for bacterial detection, in response to the non-covalent interaction between copolymer and bacteria surface.[27] Similarly, Han and co-workers put forward the design of a sugar bearing TPE molecule to use as a 'turn-on' fluorescence sensor for carbohydrate binding protein, lectins and glycosidase based on differential interaction with these bioanalytes.[28]

Moreover, quite a few attempts have been made to control and modulate the AIE properties by the proper incorporation of AIEgens in different biomolecular scaffolds. Haner and co-workers have designed TPE modified complementary DNA strands and its molecular aggregation and emission properties have been controlled by DNA hybridization (Figure 3.2B).[29] Later, Lei *et al.* have employed a tetrapod G-quadruplex and i-motif to achieve controlled molecular assembly and modulate fluorescence intensity. Further they have demonstrated the utility of the probe as a sequence-specific DNA detection assay.[30]

The supramolecular systems based on TPE assemblies are highly recommended for drug/gene delivery applications as it provides an additional advantage of fluorescence-based delivery monitoring. Zhang *et al.* has developed a novel gene delivery strategy, based on effective plasmid DNA condensation by a cationic peptide functionalized TPE core that enables the tracking of gene delivery process (Figure 3.2C).[31] Recently, our group has investigated the DNA condensation and assembly process of a viologen appended TPE derivative (Figure 3.2D).[32] Wang

and co-workers have achieved the formation of fluorescent supramolecular nanoparticles for intracellular trafficking of protein delivery by the design of TPE involved metal-organic cages.[33] Likewise, Yang and co-workers have developed a self-imaging drug delivery vehicle by the hierarchical assembly of an amphiphilic peptide polymer conjugate and they found that the DOX-loaded tubisomes are efficient for inhibition of cancer cell proliferation.[34]
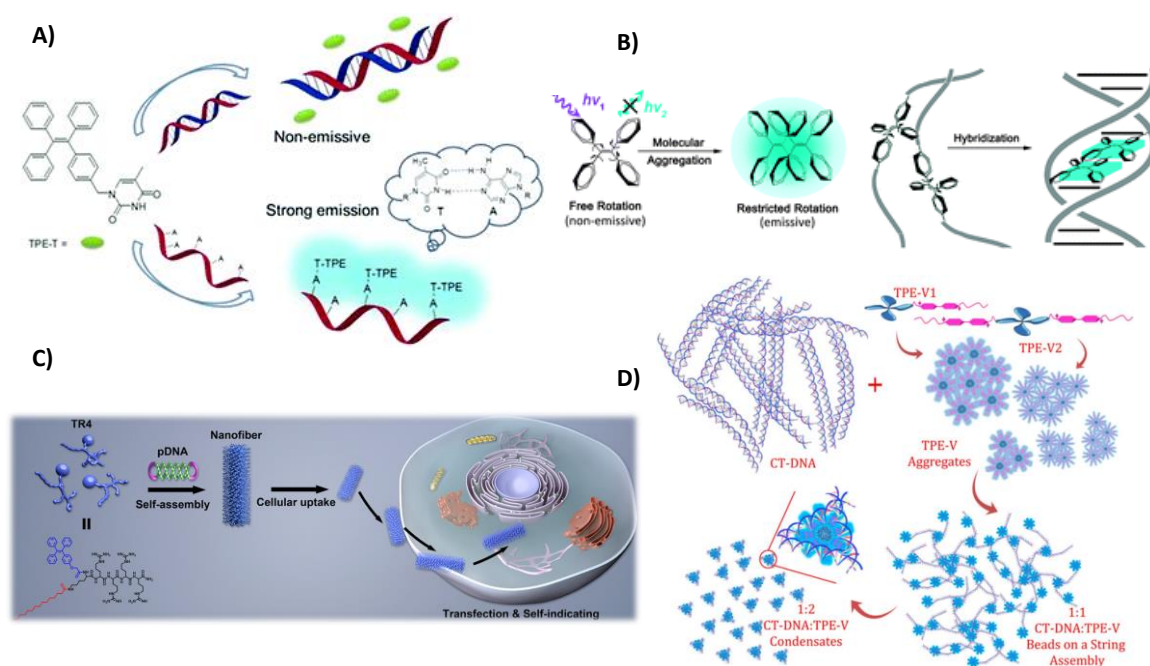
Figure 3.2. Schematic representation of A) Selective detection of adenine rich ssDNA based on AIE properties of thymine attached TPE derivative; B) DNA hybridization controlled AIE behavior of TPE/DNA conjugate; C) plasmid DNA condensation and gene delivery using peptide functionalized TPE derivative and D) CTDNA condensation and self-assembly of viologen appended TPE derivatives. (Adapted from references 26, 29, 31 and 32, respectively).

Apart from the benefits of AIE characteristics, the supramolecular aspects of TPE are less revealed due to the difficulty in achieving well-defined structures from these non-planar AIE luminogens. Nevertheless, the assembly of AIEgens are highly desirable as it provide well-ordered emissive nanoscale materials for advanced

applications in various fields. AIEgen based ordered supramolecular assemblies can only be achieved through the precise molecular design and suitable choice of supramolecular strategies.
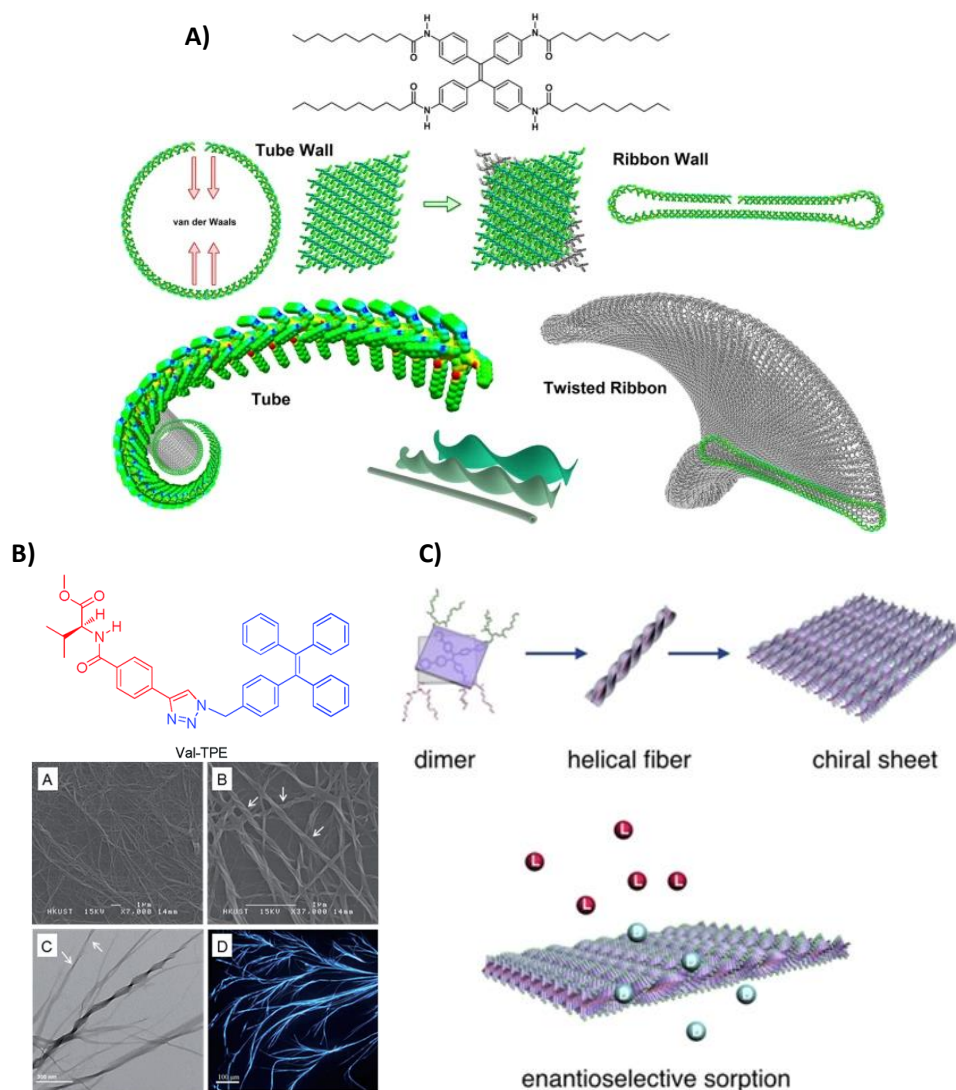
Figure 3.3. A) Schematic representation of possible pathway for the formation of chiral superstructures from achiral TPE derivative; B) Molecular structure of amino acid attached TPE derivative, Val-TPE and the SEM, TEM and fluorescent images of helical nanofibres formed on solid substrate through solvent evaporation and C) Schematic representation of formation of chiral sheet by the self-assembly of TPE amphiphile and enantioselective sorption. (Adapted from references 35, 36 and 37, respectively).

Bhosale and co-workers have designed a TPE derivative with four long alkyl chains attached through amide linkages and achieved the ordered right-handed chiral superstructure from achiral TPE (Figure 3.3A).[35] Likewise, Tang and co-workers have reported the formation of helical nanofibers from a chiral amino acid attached TPE derivative, which exhibit AIE characteristics along with aggregation-induced circular dichroism (AICD) and circularly polarized luminescence (CPL). The AICD and CPL indicates that the chirality of amino acid is transferred to TPE moiety (Figure 3.3B).[36] Later, Lee and co-workers have reported the self-assembly of amphiphilic TPE derivatives to chiral 2D-nanosheets capable of enantioselective sorption with fluorescence based sensing characteristics (Figure 3.3C).[37] Recently. our group has demonstrated the dynamic switching of self-assembled nanofibers formed from diaminotriazine appended TPE derivative by using molecular recognition strategy and achieved better control over the morphology of 1D assemblies of TPE AIEgens.[38]

Thus, the amphiphilic self-assembly of TPE is highly encouraged for the development of well-defined ordered nanostructures in recent years. However, there are fewer reports on reorganization and formation of ordered crystalline assembly of **TPE** amphiphiles via molecular recognition. Crystalline supramolecular assemblies are of great interest due to their exciting material properties that can be suitably modulated via external stimuli and modify the inherent molecular interactions within the system.[39-41] The stimuli responsive behaviour in supramolecular assemblies is often accompanied by morphological transformation[42-44] or switching between H and J assembly.[45] Certain external agents can also induce pathway dependent assembly process to yield entirely different

morphological structures. There are fewer reports suggesting the molecular reorganization that finally attain an indistinguishable morphology, since it is difficult to probe molecular reassembly process that doesn't leave much evidence after reorganization.

Herein, we have investigated the DNA assisted supramolecular reassembly of hierarchically assembled **TPE** amphiphiles through DNA intercalation. Stable, supramolecular nanoribbon assemblies have been achieved with micromolar concentrations of **TPE1** and **TPE2** amphiphiles, having single and double hydrophilic arms appended with an aniline moiety, in ethanol-water mixtures by adjusting the ethanol percentage in the aqueous media according to the structural organization requirement of the molecule. The hydrophobic–hydrophilic balance in the assembly gets altered by the addition of DNA to the initial assemblies, causing a spontaneous reorganization of **TPE1** molecules along with the intercalation of aniline moiety in between the nucleobase pairs. Even though, the process doesn't make any changes in the overall morphology after reassembly, DNA gets incorporated in the nanoribbon, which is confirmed through EDAX analysis. Moreover, XRD analysis and SAED patterns of **TPE1/CTDNA** hybrid suggest more ordered arrangement of amphiphiles in the DNA incorporated structures due to the directional assembly of **TPE1** through intercalative binding with DNA. The observation is further supported by fluorescence lifetime measurements. On the other hand, **TPE2**, having two hydrophilic arms reassemble gradually with time and the reassembly is well-probed through morphological and spectroscopic analysis. **TPE3** with four side arms form stable nanosheet structures in 10% DMSO-PBS mixture and is reassembled with dsDNA to get more crystalline nanosheets. DNA

incorporated assemblies of **TPE2** and **TPE3** were compared with the reassembled structures of respective molecules after heat-cool, which show significant difference in the crystallinity of both assemblies. Thus, herein, we have demonstrated the supramolecular reassembly of tetraphenylethylene amphiphiles through interaction with DNA to achieve crystalline supramolecular assembly, which is different from the less ordered initial assembly of all three TPE amphiphiles, without any morphological transformations.

3.3. RESULTS AND DISCUSSION

3.3.1. SYNTHESIS AND CHARACTERISATION OF TPE AMPHIPHILES
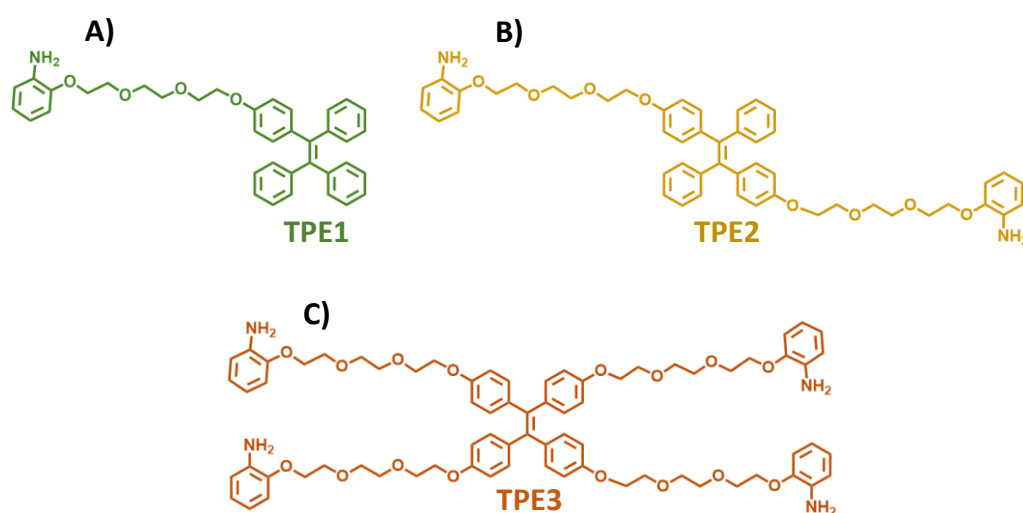
Figure 3.4. Molecular structures of A) **TPE1**, B) **TPE2**, and C) **TPE3**.

Design of tetraphenylethylene amphiphiles **TPE1**, **TPE2** and **TPE3** is envisioned to form DNA nanostructures in aqueous media through supramolecular assembly strategies. One, two and four aniline moieties are incorporated in the molecular design of **TPE1**, **TPE2** and **TPE3**, respectively to ensure the interaction with DNA through intercalation, and these aniline groups are attached to the TPE core through hydrophilic triethylene glycol chains to impart amphiphilicity to the TPE derivatives (Figure 3.4A, B & C).
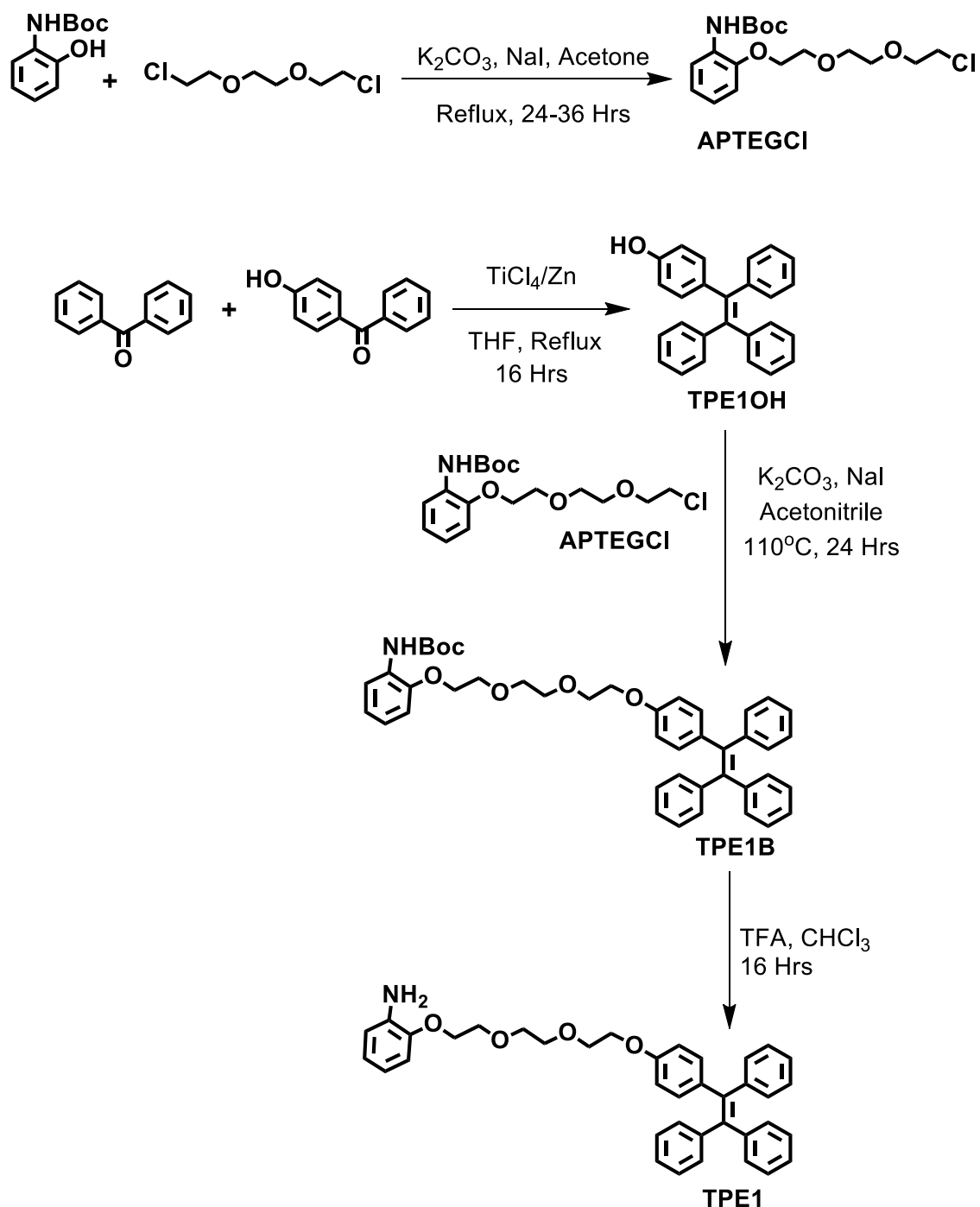
Scheme 3.1. Synthesis of aniline appended TPE amphiphile, **TPE1**.

The syntheses of TPE amphiphiles have been achieved through a multi-step synthesis procedure as shown in Scheme 3.1. TPE core is synthesised by following McMurry reaction by using different hydroxy-benzophenone derivatives. Aniline group is attached to the triethylene glycol chain through O-alkylation of 2-

aminophenol and the synthesised aniline appended triethylene glycol chain is attached to the hydroxyl derivatives of TPE through another O-alkylation step to get **TPE1B, 2B** & **3B**. Subsequent Boc-deprotection using Tetrafluoroacetic acid (TFA) yielded the respective final products **TPE1, 2** & **3** in quantitative yield. The Boc-deprotection is confirmed through NMR analysis by the disappearance of peak at 1.5. Detailed synthetic procedures and characterization data for all the intermediates and final molecules are given in the experimental section.
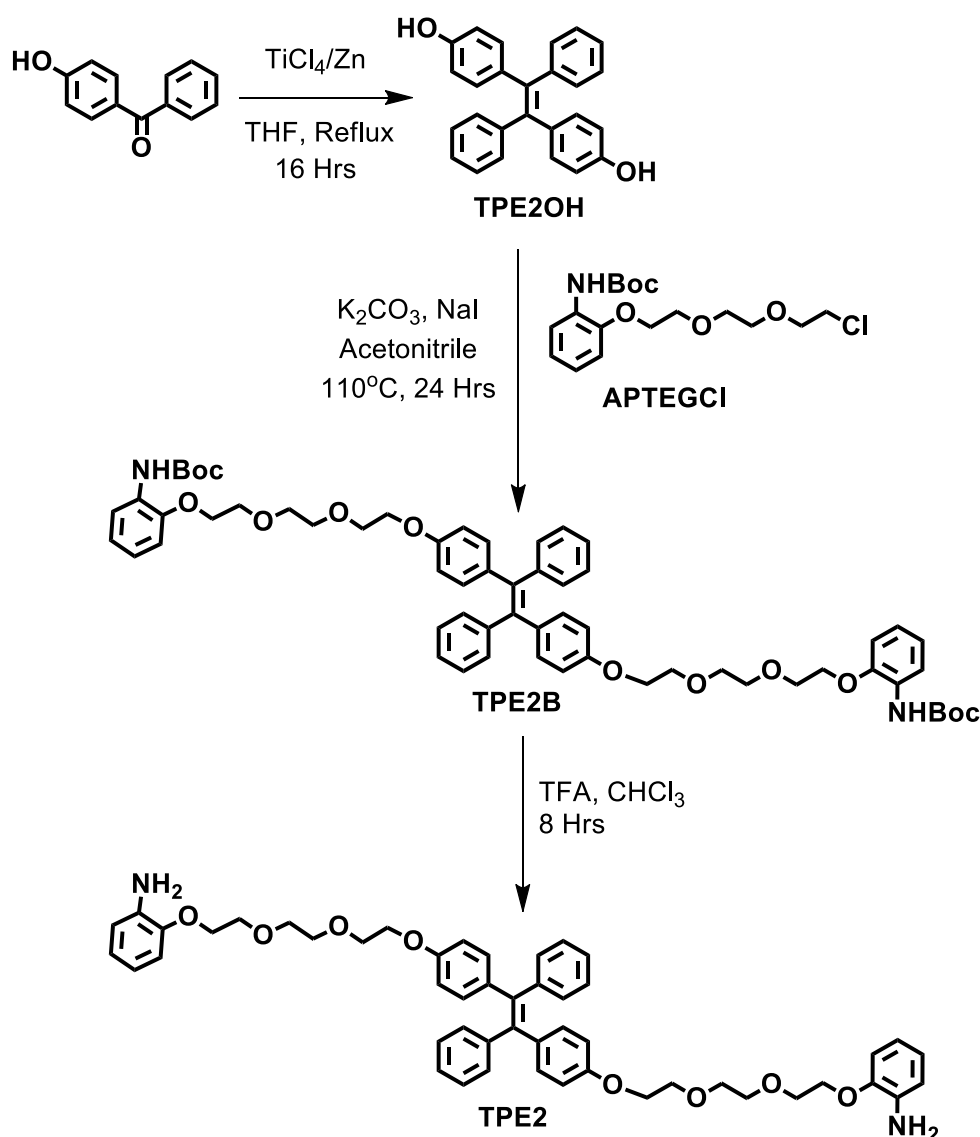
Scheme 3.2. Synthesis of aniline appended TPE amphiphile, **TPE2**.
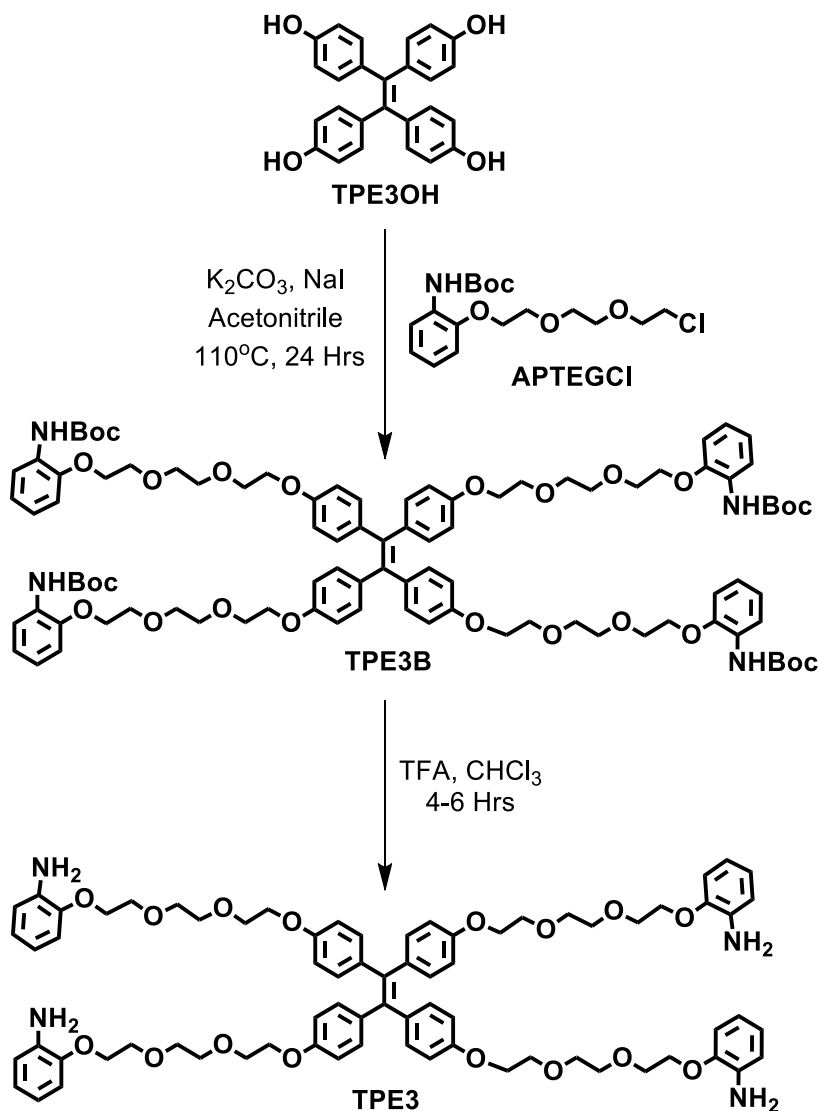
Scheme 3.3. Synthesis of aniline appended TPE amphiphile, **TPE3**.

3.3.2. PHOTOPHYSICAL STUDIES AND AGGREGATION BEHAVIOUR OF TPE AMPHIPHILES

TPE amphiphiles with predominant changes in their chemical structure show considerable difference in their solubility, and thereby show different aggregation tendency in different solvent systems. The aggregation tendencies are initially monitored through absorption studies and are further confirmed through AFM analysis before choosing the right solvent system for further studies.

131
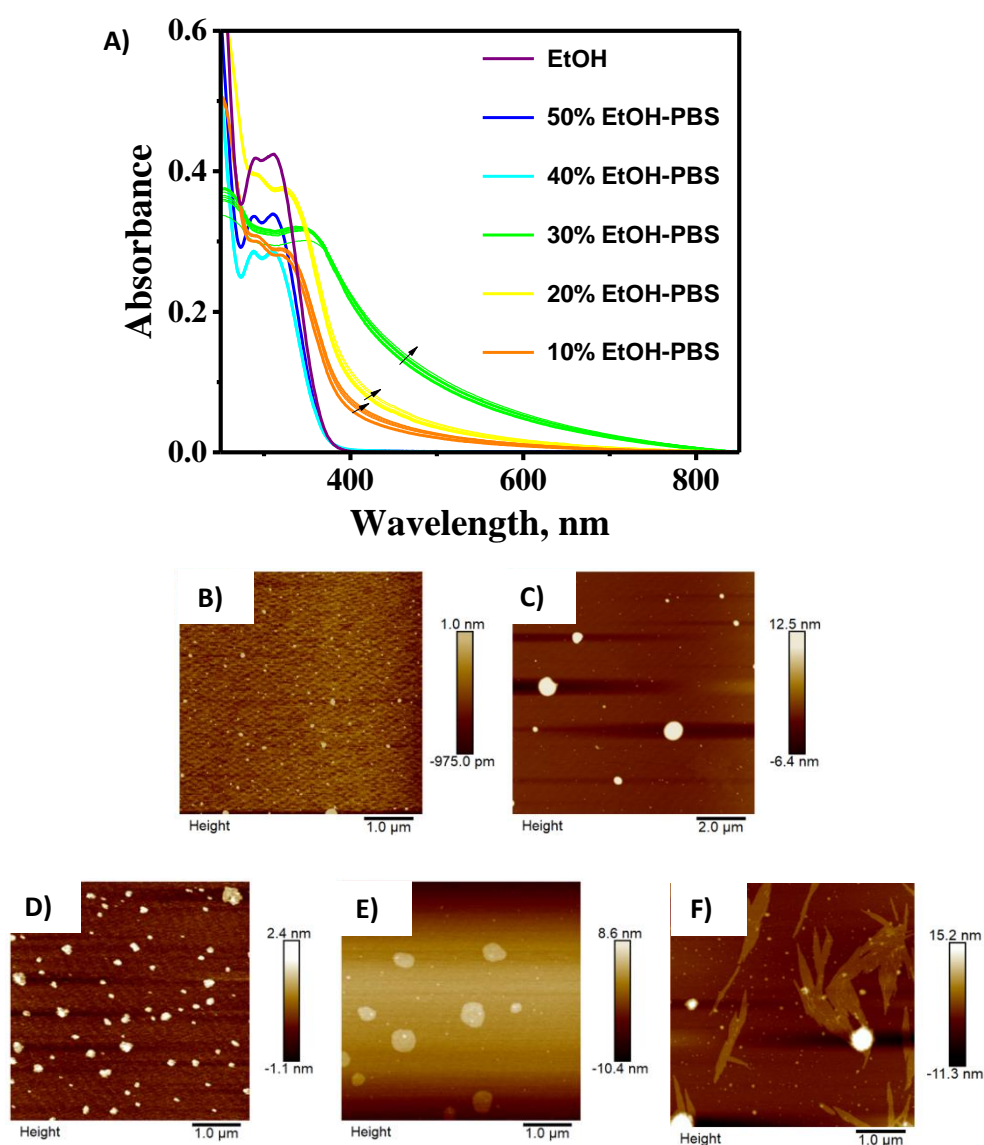
Figure 3.5. A) Absorption spectra showing the aggregation tendency of **TPE1** in various ethanol/PBS mixtures. AFM images of **TPE1** in B) 40% ethanol/PBS & C) 30% ethanol/PBS at a concentration of 16 μM; D, E & F) AFM images of **TPE1** in 10% ethanol/PBS mixture at concentrations of 0.3 μM, 3 μM & 25 μM, respectively.

TPE1 and **TPE2** are found to be readily soluble in ethanol and the absorption spectra show maximum at 290 nm with a shoulder band around 320 nm corresponding to the TPE absorption as shown in Figures 3.5A & 3.6A. The corresponding absorption spectra of **TPE1** and **TPE2** at different ethanol/PBS mixtures clearly indicate the aggregation tendency in these aqueous systems. In the

case of **TPE1**, there are no changes in the absorption spectra with time, up to 40%

ethanol/PBS and further decrease in ethanol percentage shows significant

aggregation of **TPE1**. Corresponding AFM image of **TPE1** in 40% ethanol/PBS also

didn't show formation of any aggregates (Figure 3.5B). But in 30% ethanol/PBS

mixture, it started to form larger aggregates as shown in Figure 3.5C. Moreover, AFM

images of **TPE1** in 10% ethanol/PBS show various aggregated structures like

nanoflakes, nanosheets at different concentrations of **TPE1** as shown in Figure 3.5D,

E & F. Meanwhile, **TPE2** forms elongated nanoribbon-like structures in 40%

ethanol/PBS through lateral association of initially formed nanofibrils and is shown

in Figures 3.6B, 3.6C & 3.6D.

Based on these aggregation studies, we have selected suitable aqueous media

for each TPE derivative for further experiments. We have also considered the use of

minimum ethanol percentage in the solvent system required for stable assembly

formation in order to avoid the condensation of CTDNA during DNA interaction

studies. For **TPE1** and **TPE2**, which are readily soluble in ethanol, the studies have

been carried out in 10% ethanol/PBS and 40% ethanol/PBS, respectively. The broad

absorption of both **TPE1** and **TPE2** in ethanol-PBS solutions indicates TPE

aggregation as shown in Figures 3.7A & 3.7B. **TPE3** tends to aggregate in 10%

DMSO-PBS mixture as observed from the broad absorption band shown in Figure

3.7C. Hydrophilic-hydrophobic balance imparted by the amphiphilic molecular

design of these TPE amphiphiles assist the molecular assembly in respective

aqueous environments to form characteristic nanoscale structures, which are

thoroughly investigated further by TEM and AFM analysis.
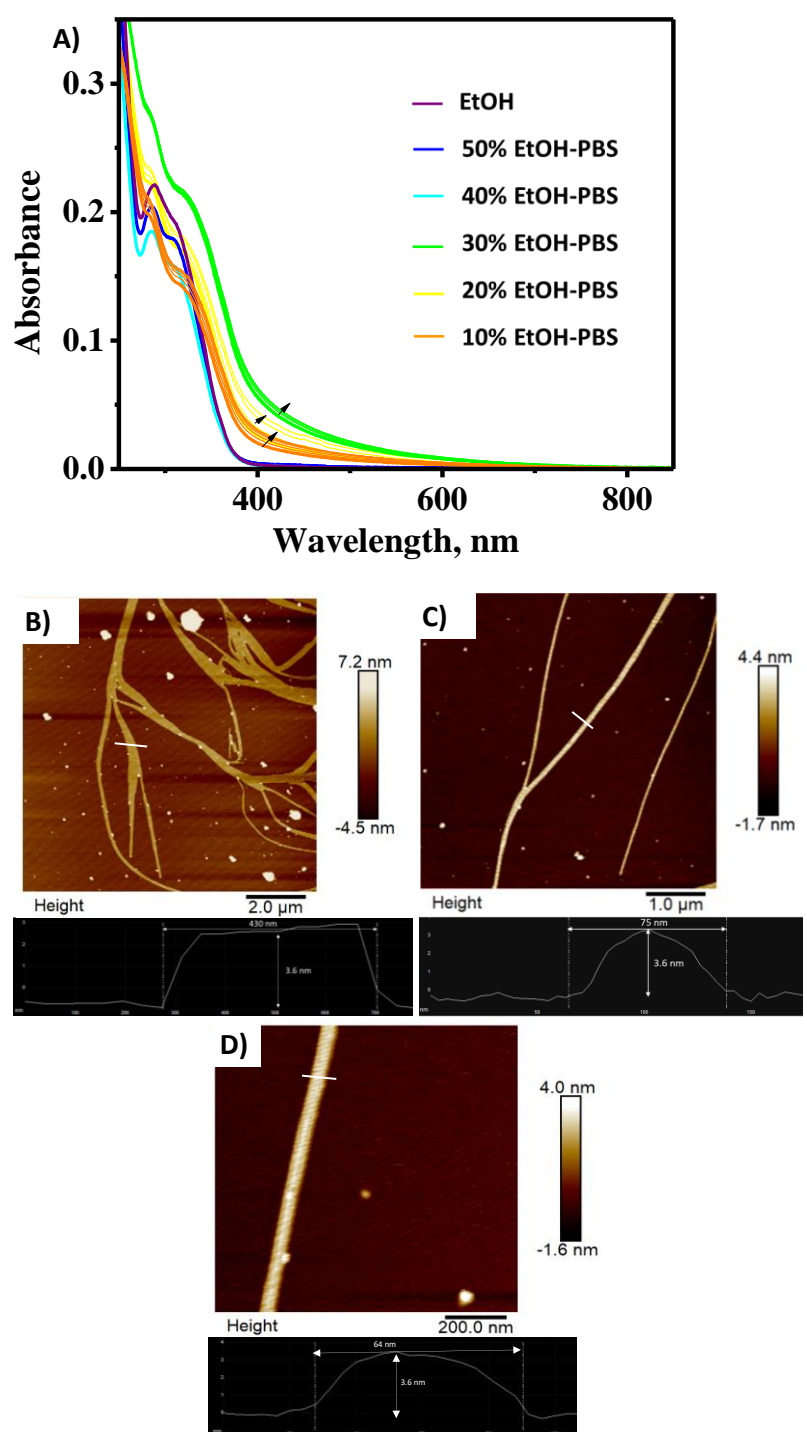
Figure 3.6. A) Absorption spectra showing the aggregation tendency of **TPE2** in various ethanol/PBS mixtures; B, C & D) AFM images and corresponding height images of **TPE2** in 40% ethanol/PBS mixture at a concentration of 7 µM, showing the formation of nanoribbon-like structures through possible lateral association of elongated fibrillar units.
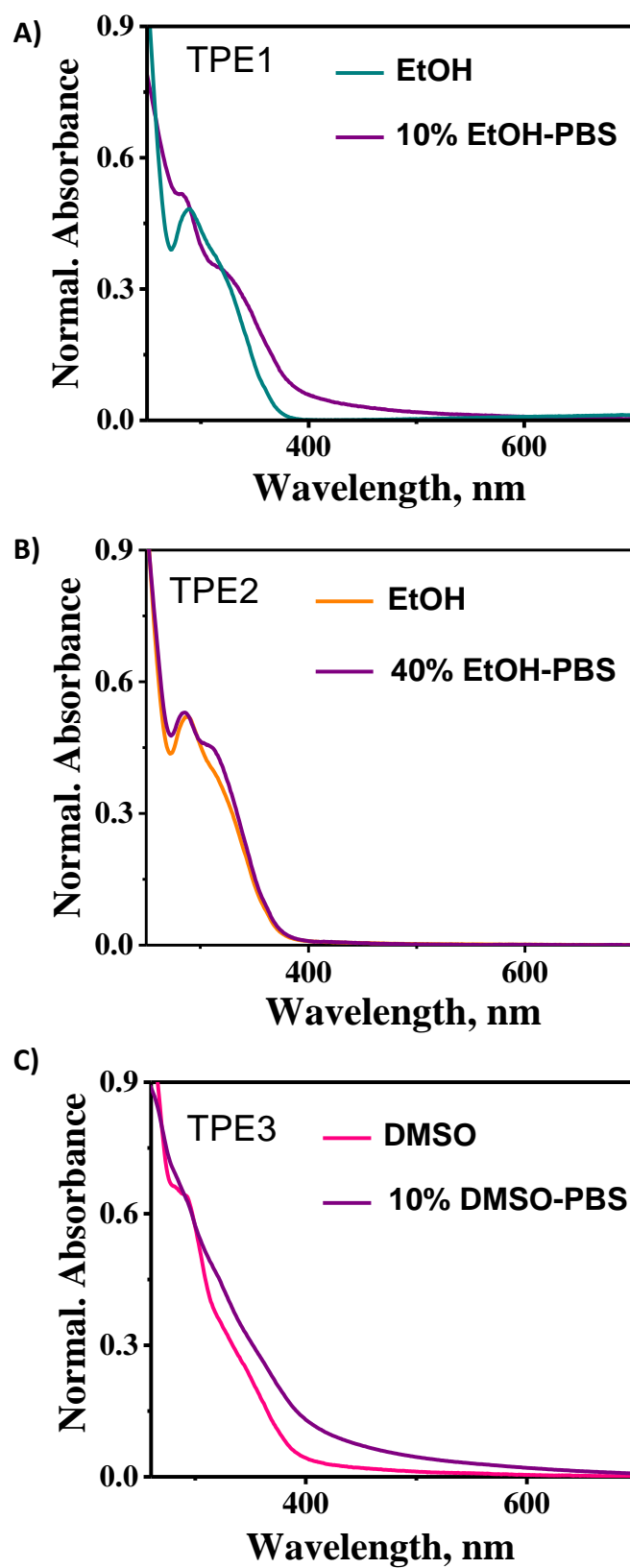
Figure 3.7. Change in absorption spectra of A) **TPE1**; B) **TPE2** and C) **TPE3** in suitable aqueous media selected for further studies.

3.3.3. SELF-ASSEMBLY OF TPE AMPHIPHILES

TPE1, **TPE2** and **TPE3** tend to assemble in aqueous media due to the synergistic effect of π-π stacking between the TPE core and aniline moieties and van der Waals interaction within the ethylene glycol chains.[46-48] AFM analysis of **TPE1** assembly shows the formation of nanosheet like structures with a thickness around 3 nm and the lateral dimension of the nanosheets get varied from 150 nm to 1 μm as shown in Figure 3.8A. **TPE2** forms nanoribbon like structures with few micrometres in length as shown in Figure 3.8B. On the other hand **TPE3**, with its four side arms, forms nanosheets in 10% DMSO-PBS and is shown in Figure 3.8C.
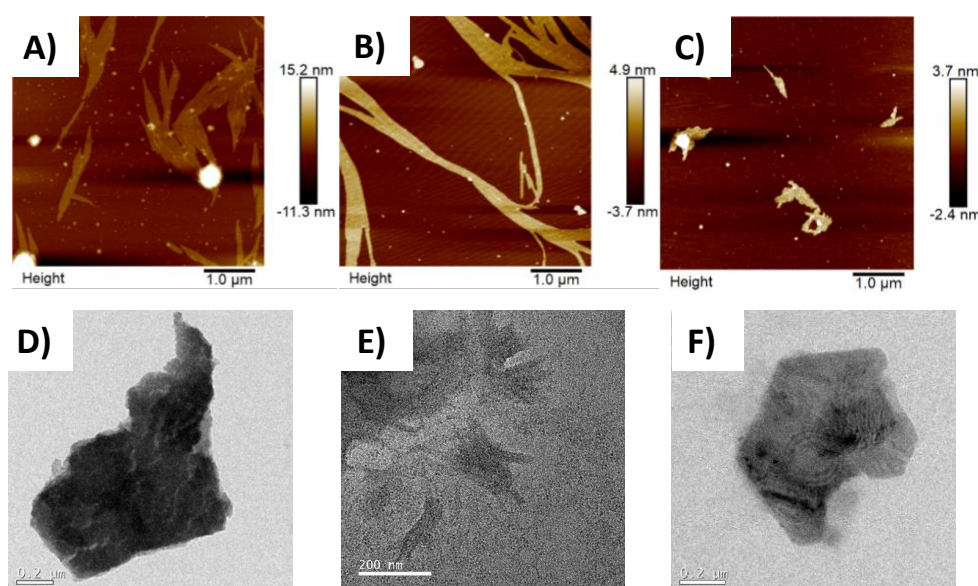
Figure 3.8. AFM images of A) **TPE1**; B) **TPE2** & C) **TPE3** drop casted from 10% ethanol-PBS, 40% ethanol- PBS and 10% DMSO-PBS mixture, respectively and the corresponding TEM images of D) **TPE1**; E) **TPE2** & F) **TPE3**.

Nanosheet formation is also encouraged by the comparatively lower polarity of the solvent mixture which tries to reduce the exposure of triethylene glycol chains on four sides to the outer surface, thereby facilitating more lateral associations. TEM

analysis of the respective assemblies further confirms the ribbon and sheet like morphologies (Figures 3.8D, 3.8E & 3.8F).

A close look at the **TPE1** nanosheet reveal the presence of repeating fibrillar units of width around 25 nm, which can accommodate around ten **TPE1** molecules and these fibrillar units are separated by a distance of ~4 nm (Figure 3.9A). Thus, we can assume that larger nanosheets are formed through the lateral association of pre-formed fibrils of stacked TPE cores, having hydrophilic, triethylene glycol arms at both ends as shown in Figures 3.9B, 3.9C & 3.9D. The initial fibril formation might be originated from the slipped stacking of TPE cores along with the van der Waals interaction between triethylene glycol chains. Better understanding of the lateral assembly process is obtained from **TPE2** assembly in 40% ethanol-PBS. The higher ethanol content in the solvent mixture helps to understand the assembly process better. Lateral association of fibrils can be clearly seen in **TPE2** assembly, which eventually form nanoribbon like structures with a thickness of ~3.6 nm, corresponding to three stacked layers of **TPE2** (Figures 3.9E, 3.9F, 3.9G & 3.9H). The increase in thickness might be due to the more slipped stacks of **TPE2** compared to **TPE1**, since the π- π stacking of TPE core in **TPE2** assembly in higher ethanol percentage is comparatively weaker than that of **TPE1**. Single fibrillar width within a nanoribbon is around 33 nm as shown in the height profile which can accommodate around ten units of **TPE2** while considering the molecular dimension. Formation of more elongated assemblies of **TPE2** nanoribbons might be due to the presence of hydrophilic arms on both sides of **TPE2**, which provide more stability to the assembled system in aqueous media, compared to the shorter assemblies of **TPE1** having single arm. This might also be the reason for stable nanofibrils we

could see in the AFM images of **TPE2** assembly with less lateral association as seen in Figure 3.6.
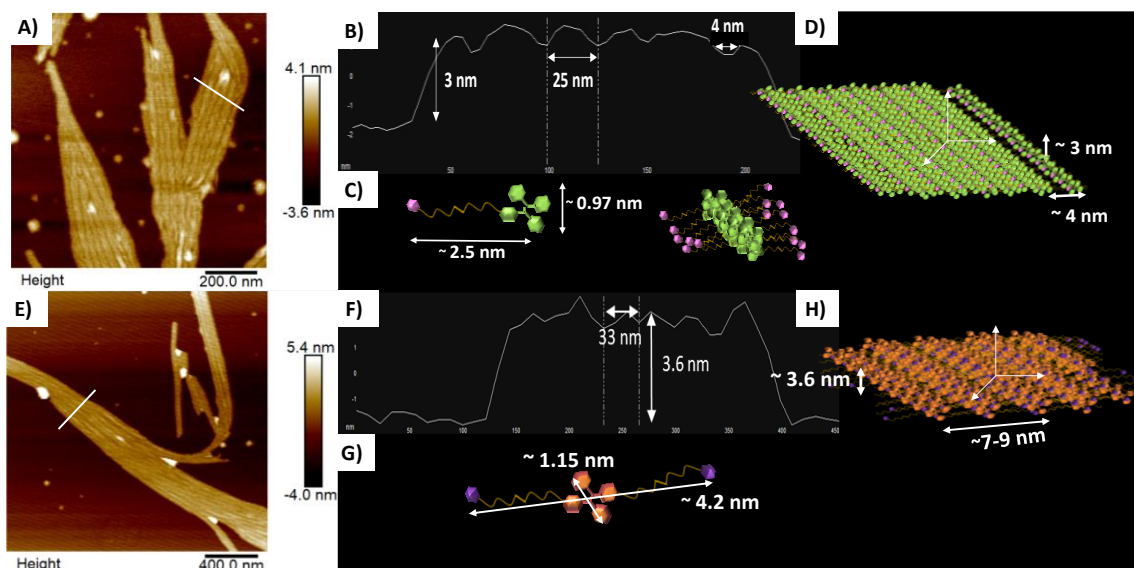
Figure 3.9. A) AFM image of **TPE1** in 10% ethanol-PBS; B) Corresponding height profile; C & D) Schematic representation of **TPE1** with corresponding molecular dimensions and the formation of nanosheets; E) AFM image o**f TPE2** in 40% ethanol-PBS; F) Corresponding height profile; G & H) Schematic representation of **TPE2** with corresponding molecular dimensions and the formation of nanoribbons.

3.3.4. DNA INTERACTION STUDIES AND REASSEMBLY OF TPE AMPHIPHILES

The addition of anionic DNA can alter the hydrophilic-hydrophobic balance in the systems by possible interactions with the amphiphilic TPE derivatives with appended anilines, which further make the assembly susceptible for reorganisation. Aniline moieties are known to interact with DNA through intercalation and the hydrophobic TPE core can promote further assembly process.[49, 50]
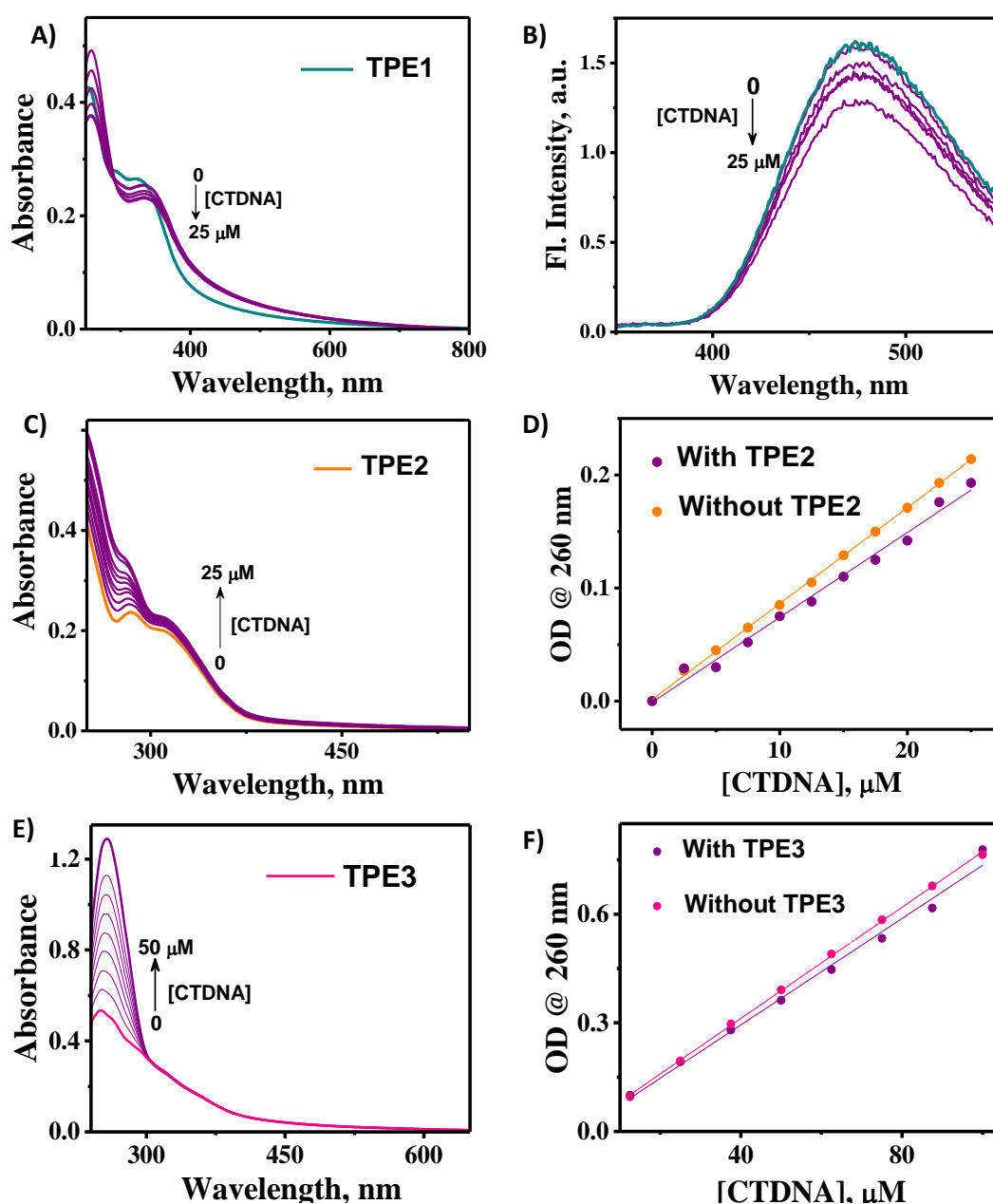
Figure 3.10. A) Changes in absorption spectra and B) Emission spectra of **TPE1** with addition of CTDNA in 10% Ethanol-PBS; C) Changes in absorption spectra of **TPE2** with addition of CTDNA in 40% Ethanol-PBS; D) Absorption changes at 260 nm in the presence and absence of **TPE2** with increasing concentration of CTDNA; E) Changes in absorption spectra of **TPE3** with addition of CTDNA in 10% DMSO-PBS and F) Absorption changes at 260 nm in the presence and absence of **TPE3** with increasing concentration of CTDNA.

Interaction of DNA with the hierarchical assembly of TPE amphiphiles were initially monitored through UV-vis absorption spectroscopy by observing the changes in the absorption spectra of preformed **TPE1**, **TPE2** and **TPE3** assemblies with the addition of Calf Thymus DNA (CTDNA). DNA interaction with **TPE1** assembly can be assessed by the changes in absorption bands at 290 nm and 320 nm. Absorption around 320 nm shows hypochromism along with a 13 nm red shift which indicates the interaction of **TPE1** assembly with CTDNA (Figure 3.10A). The absorption around 290 nm also reduced considerably in the first addition of DNA due to the disassembly of TPE and further increase in absorbance is attributed to the nucleobase absorption around 260 nm. Disassembly of **TPE1** can be further confirmed from the decrease in fluorescence intensity with addition of DNA (Figure 3.10B), since TPE is an AIEgen.

Addition of CTDNA to **TPE2** assembly shows an increase in overall absorption at 290 nm and 320 nm as shown in Figure 3.10C and the positive change in absorption might be due to the contribution from CTDNA alone if there is no interaction between **TPE2** and CTDNA. But, the interactions in **TPE2/CTDNA** can be confirmed by a control experiment by monitoring the absorption change at 260 nm with subsequent addition of CTDNA in the presence and absence of **TPE2** and the secondary plot (Figure 3.10D), which suggests comparatively less interaction of DNA with **TPE2** assembly. These significant differences in DNA interaction with **TPE1** and **TPE2** might be due to the higher molecular interactions within **TPE2** amphiphiles compared to **TPE1**, due to the van der Waals forces acting between two hydrophilic arms in **TPE2**. Accordingly, **TPE3**, with four hydrophilic arms, form much stronger assembly than **TPE1** and **TPE2** and show smaller changes in the absorption on interaction with CTDNA as evident from Figures 3.10E & 3.10F.

3.3.4.1. Reassembly of TPE1 with CTDNA

Prior to the reassembly studies, we have carried out the interaction studies of **TPE1** in 40% ethanol/PBS with CTDNA in order to understand the capability of DNA to trigger the self-assembly of **TPE1**, since there's no aggregate formation in 40% ethanol-PBS (Figure 3.5B) as observed in the previous studies. The absorption studies show a gradual enhancement in the overall absorption of **TPE1** and the secondary plot indicates comparatively less interaction of **TPE1** with CTDNA (Figures 3.11A & 3.11B).
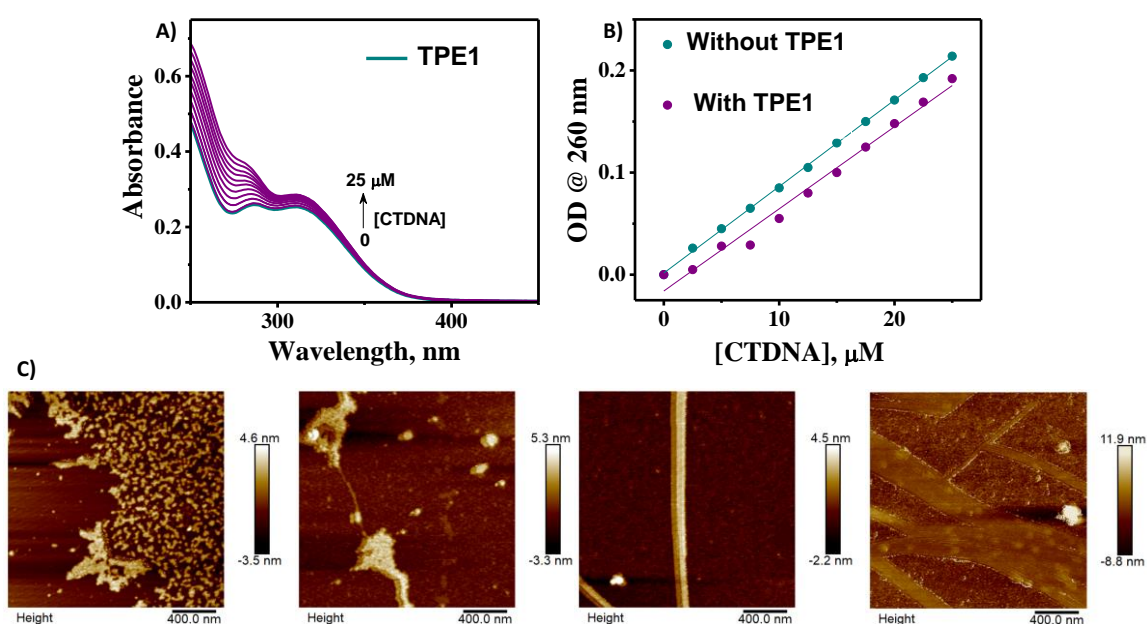
Figure 3.11. A) Changes in absorption spectra of **TPE1** in 40% ethanol/PBS with addition of CTDNA; B) Absorption changes at 260 nm in the presence and absence of **TPE1** with increasing concentration of CTDNA and C) AFM images of **TPE1/CTDNA** (16 μM : 25 μM) in 40% ethanol/PBS.

However, morphological analysis of **TPE1/CTDNA** after 30 minutes of incubation showed the formation of nanoribbon-like structures from nanofibrillar units as shown in the AFM images (Figure 3.11C), which could be resulted from the change in solvent polarity after addition of anionic DNA

Since AFM and TEM analysis provide more insight into the reassembly process of TPE amphiphiles in presence of CTDNA, we have mainly focused on the morphological analysis of the respective TPE/DNA hybrid assemblies in selected aqueous media. For example, Figures 3.12A & 3.12B show the AFM image and height profile of **TPE1** (25 μM) in presence of CTDNA (25 μM) in 10% Ethanol-PBS solvent mixture. Formation of comparatively stable assemblies of **TPE1** with CTDNA is evident from the AFM image which shows that the fibrillar assembly width in between two grooves is increased from 25 nm for **TPE1** alone to 45 nm for **TPE1/CTDNA** and there is a slight increase in the lateral dimension of ribbons from ~200 to ~300 nm (Figures 3.12A & 3.12B). This might be due to the incorporation of CTDNA in between the TPE assembly which can hold more **TPE1** molecules together in an assembly than individual assembly among **TPE1** amphiphiles. TEM analysis shows the highly crystalline assembly of **TPE1/CTDNA** as observed in the SAED pattern (Figures 3.12C & 3.12D), which is in agreement with the XRD analysis (Figure 3.13A) also. Lifetime measurements of **TPE1** and **TPE1/CTDNA** show three component decay profile, as shown in Figure 3.13B and Table 3.1, in which **TPE1/CTDNA** possess longer lifetime compared to **TPE1** and this might be due to the extended exciton migration in **TPE1/CTDNA** assemblies.[51] These morphological observations along with the spectroscopic studies collectively suggest the **TPE1** reassembly in presence of CTDNA. The proposed reassembly process involves possible intercalative interaction of aniline moieties between the DNA nucleobases, which aligns more TPE amphiphiles on both sides of DNA as schematically represented in Figure 3.12E.
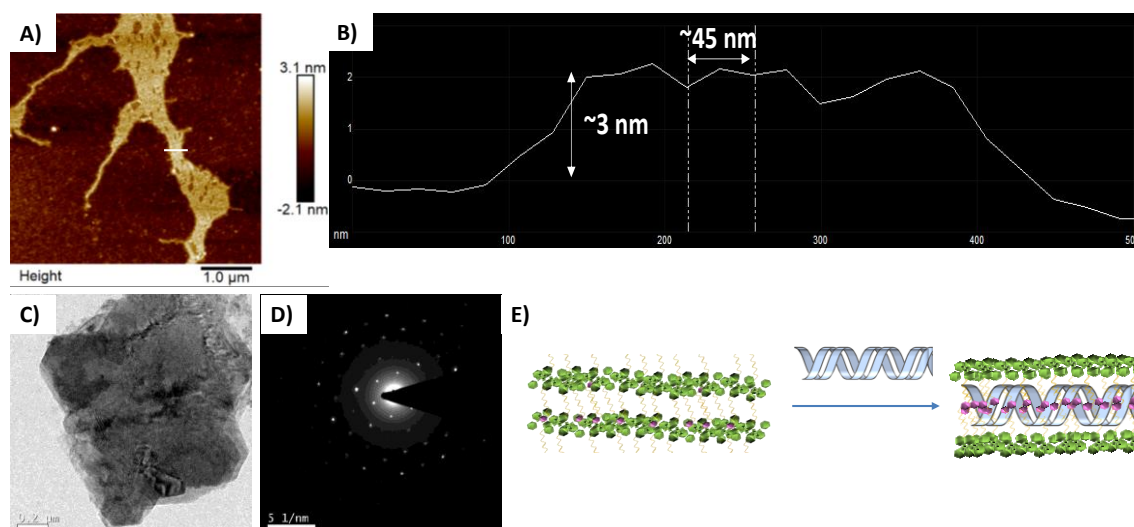
Figure 3.12. A) AFM image; B) Corresponding height profile; C) TEM image and D) Corresponding SAED pattern of **TPE1/CTDNA** (1:1) in 10% Ethanol-PBS mixture and E) Cartoonic representation of reassembly of **TPE1** in presence of CTDNA.
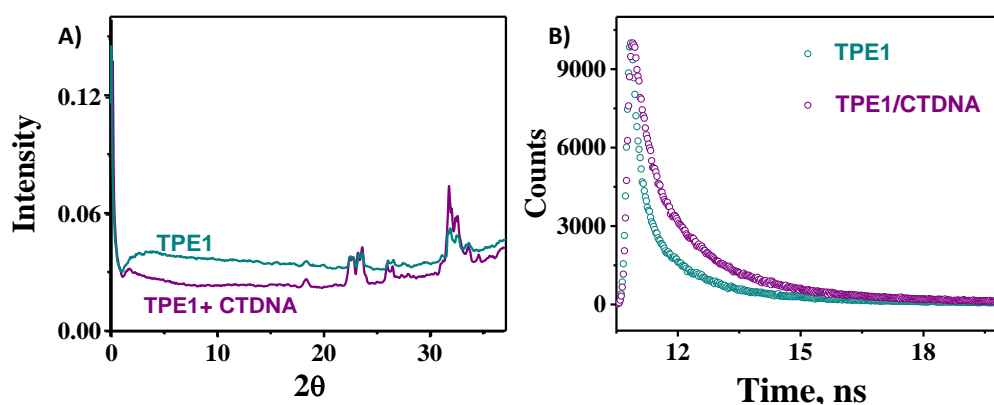
Figure 3.13. A) XRD spectra and B) Fluorescence lifetime measurements of **TPE1** and **TPE1/CTDNA**.

Table 3.1. Lifetime measurements of **TPE1** and **TPE1/CTDNA** with corresponding relative amplitudes.

	Life time (ns)	Relative Amplitude
TPE1	7.28 1.51 0.262	45 % 40 % 15 %
TPE1/CTDNA	7.81 1.89 0.435	52 % 13 % 35 %

3.3.4.2. Reassembly of TPE2 with CTDNA

The disassembly and reassembly of **TPE2** through CTDNA interactions is evident in AFM and TEM images in which the existence of smaller irregular aggregates, fibres and well-formed nanoribbon like structures are identified (Figures 3.14A-D). The crystalline nature of as-formed nanoribbons can be confirmed from the clear lattice fringes in the high-resolution TEM image as shown in Figure 3.14E. The presence of DNA in the well-formed nanoribbon is further confirmed through EDAX analysis (Figure 3.15A).
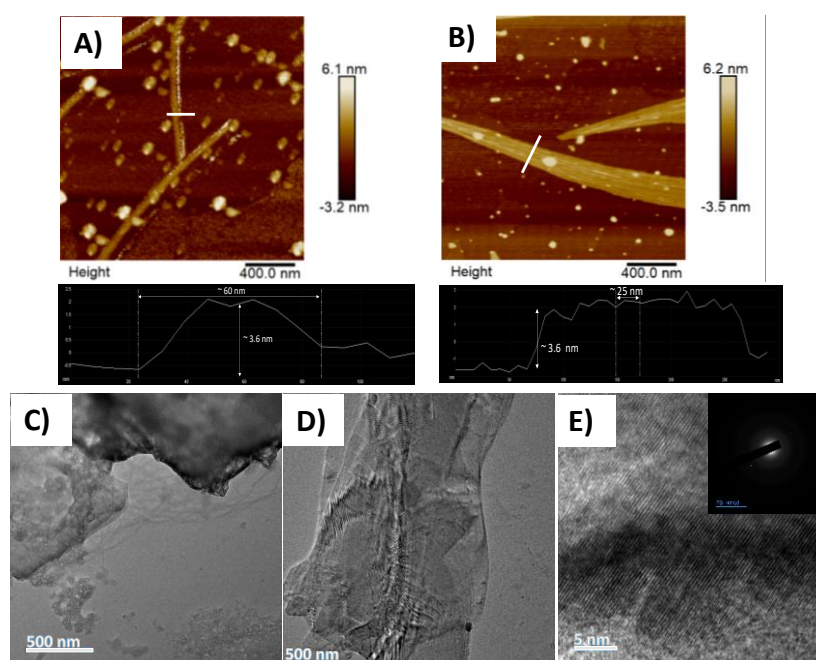
Figure 3.14. A & B) AFM images and C, D & E) TEM images of **TPE2/CTDNA** (1:3.5) in 40% ethanol/PBS, showing the reassembly of **TPE2** in presence of CTDNA.

The disassembly and reassembly of **TPE2** with CTDNA can be portrayed through time dependent DLS analysis which shows the disappearance of larger (~500 nm sized) assemblies and subsequent formation of smaller (~250 nm sized) assemblies within 2 hours. Further formation of larger (~750 nm sized) assemblies can be monitored within 3 hour and it retain the hydrodynamic size even after one day (Figure 3.15B). Further, we have monitored the time dependent changes in

TPE2 fluorescence (Figure 3.15C) that shows an initial reduction in emission intensity followed by a time dependent enhancement close to the initial value. Disassembly and reassembly of **TPE2** can be clearly observed by plotting the change in emission intensity at 340 nm as shown in Figure 3.15D. Addition of CTDNA causes an immediate reduction in fluorescence intensity and is further decreased to a minimum value within 1 hour, indicating the gradual disassembly of **TPE2** in presence of CTDNA. After 1 hour, **TPE2** amphiphiles reassemble with DNA to get a comparable fluorescence as that of the initial assembly.
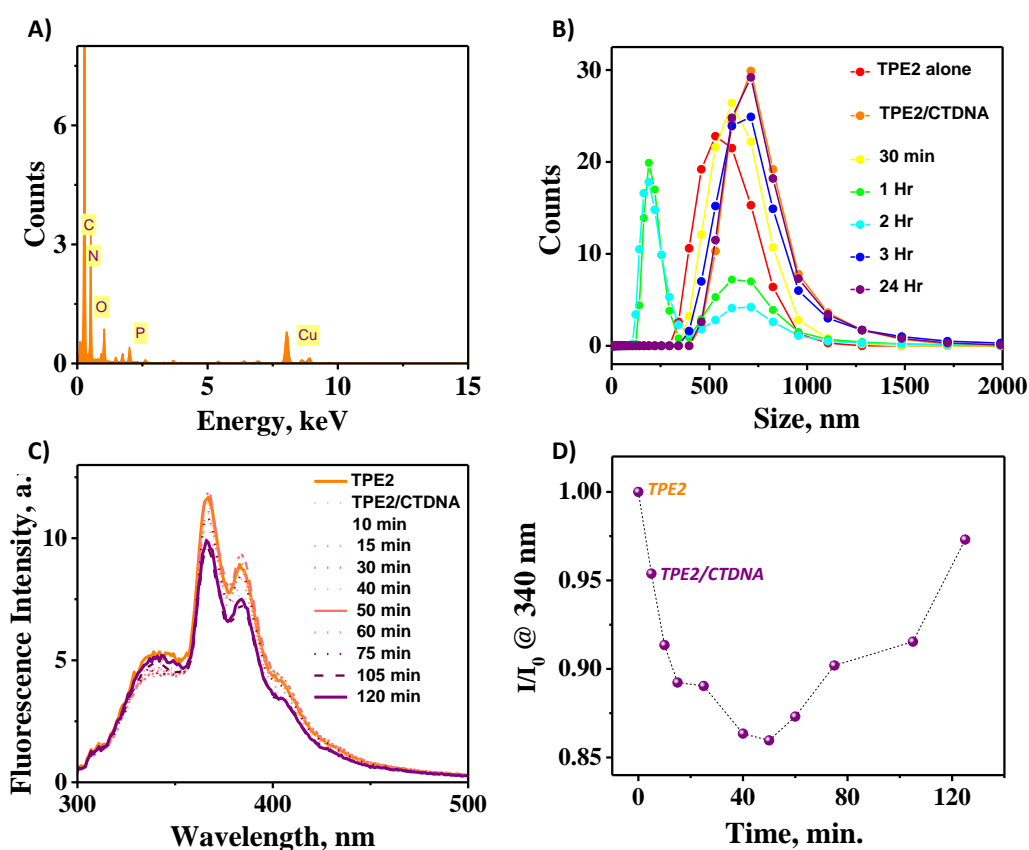
Figure 3.15. A) EDAX analysis of **TPE2/CTDNA**; B) Time dependent DLS analysis of **TPE2/CTDNA**; C) Time dependent fluorescence analysis of **TPE2/CTDNA** and D) Time dependent fluorescence changes at 340 nm for **TPE2/CTDNA**.

Moreover, temperature dependent fluorescence measurements of respective assemblies (Figures 3.16A & 3.16B) and the plot of temperature versus fluorescence

intensity of **TPE2** and **TPE2/CTDNA** at 367 nm show that **TPE2/CTDNA** assemblies begin to form even at 50 °C on cooling, while **TPE2** at 40 °C, indicating the more stable assembly of **TPE2/CTDNA** (Figure 3.16C).
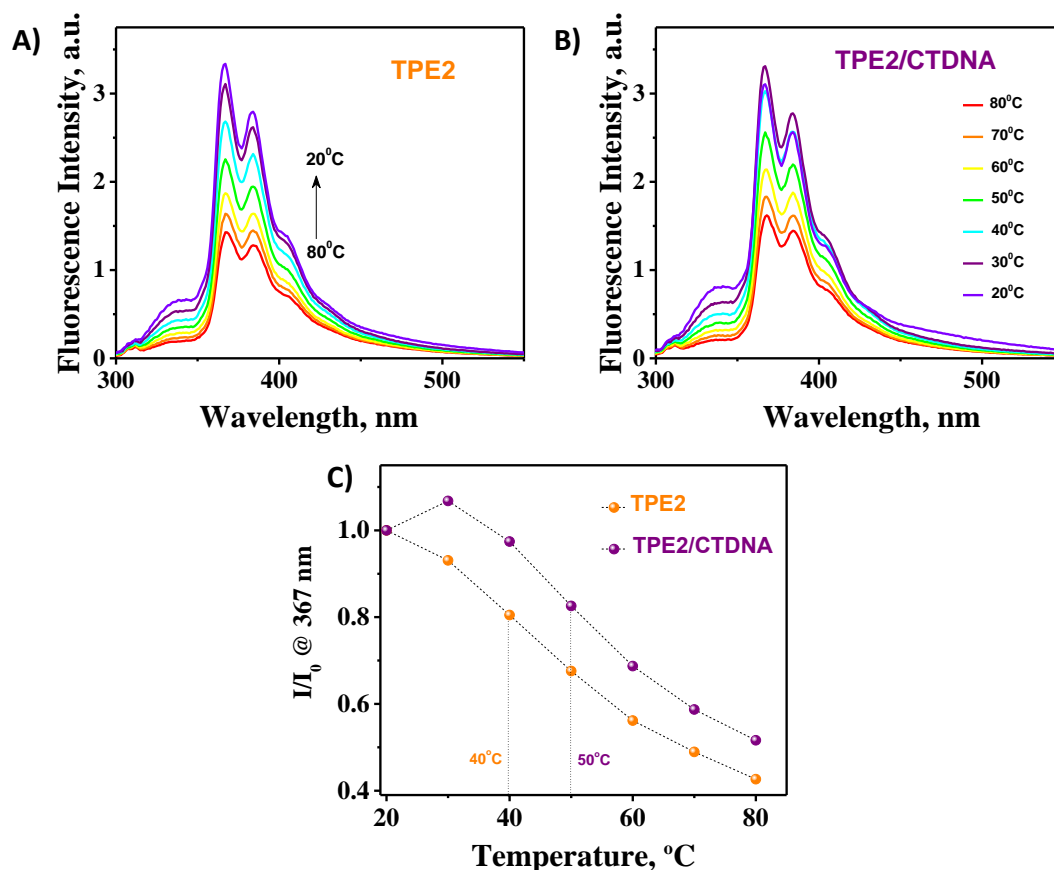
Figure 3.16. Temperature dependent fluorescence analysis of A) **TPE2** and B) **TPE2/CTDNA**; C) Fluorescence based melting curve for **TPE2** and **TPE2/CTDNA**.

Further, we have studied the assembly and reassembly of **TPE2** in 10% DMSO-PBS on interaction with CTDNA and also during heat-cool process. Absorption studies show the aggregation tendency of **TPE2** in 10% DMSO-PBS as evident from the broadened spectrum, shown in Figure 3.17A. The TEM image shows that **TPE2** forms nanosheets having a lateral dimension below 500 nm in 10% DMSO-PBS mixture (Figure 3.17B). Interaction of CTDNA is initially monitored through absorption studies that show considerable hypochromism and spectral broadening during CTDNA titration (Figure 3.17C). On the other hand, the heat-cool

process shows significantly different spectral changes as showed in Figure 3.17D. The broad absorption band of **TPE2** aggregate around 330 nm is gradually reduced and probably reached monomeric state during gradual heating to 80 °C. Further cooling doesn't bring back the initial assembly, instead forms a new assembly with a slight blue shift in the 285 nm peak (Figure 3.17D). These initial observations clearly indicate the formation of entirely different assemblies during interaction with CTDNA and heat-cool process of **TPE2**. But, the morphological analysis of **TPE2/CTDNA** hybrid shows that the addition of CTDNA doesn't significantly change the nanosheet morphology (Figure 3.18A). However, the nanosheets become more crystalline as evident from the SAED pattern (Figure 3.18C). This might be due to the reorganisation of **TPE2** molecules by the incorporation of CTDNA through intercalation of aniline moieties. Meanwhile, heating and subsequent cooling of **TPE2** alone form more extended, stable and well-ordered nanosheets with high crystalline nature, in response to the strong interaction among hydrophilic arms on both sides of **TPE2** during heat-cool process (Figures 3.18B & 3.18D). XRD analysis also confirms the high crystallinity of individual **TPE2** assembly after heat-cool compared to the **TPE2/CTDNA** assembly (Figure 3.18E). The less ordered assembly of **TPE2** with CTDNA might be due to the lengthy and flexible nature of CTDNA that controls the assembly process. Therefore, the use of a short and rigid dsDNA scaffold might provide more information and comparatively more ordered nanoscale structures.
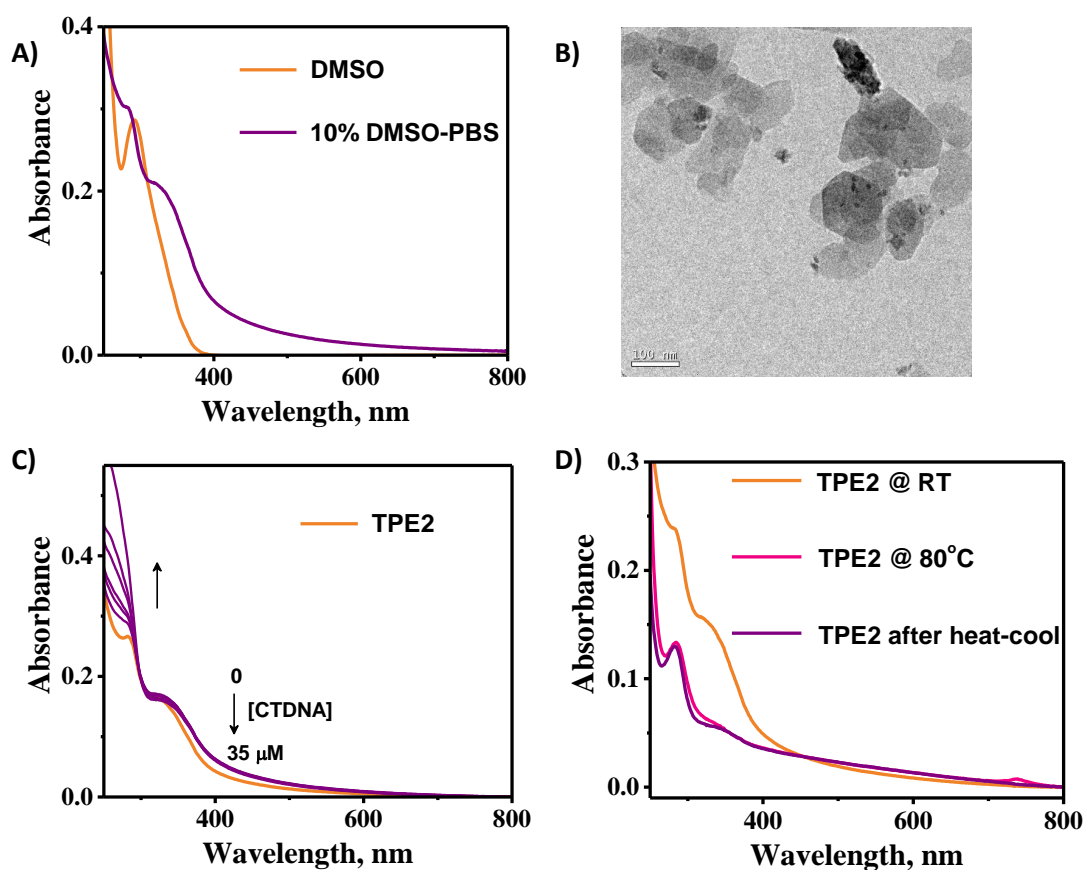
Figure 3.17. A) Absorption spectra of **TPE2** in DMSO and 10% DMSO-PBS; B) TEM image of TPE2 (15 μM) in 10% DMSO-PBS; Changes in absorption spectra of **TPE2** in 10% DMSO-PBS C) with addition of CTDNA, D) with heat-cool process.
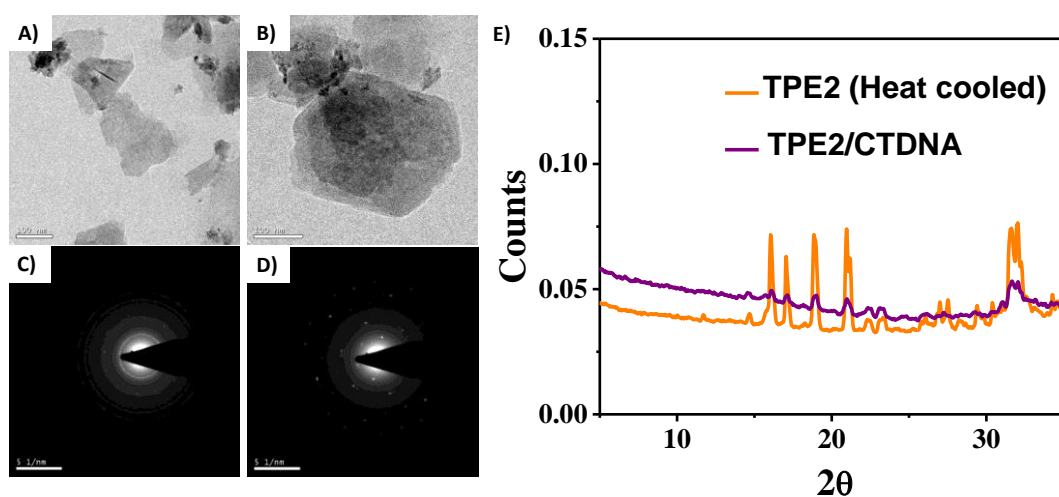
Figure 3.18. TEM images of A) **TPE2/CTDNA**; B) **TPE2** after heat-cool in 10% DMSO/PBS; C & D) Corresponding SAED patterns of **TPE2/CTDNA** and **TPE2** after heat-cool, respectively; E) XRD spectra of **TPE2** after heat–cool & **TPE2/CTDNA**.
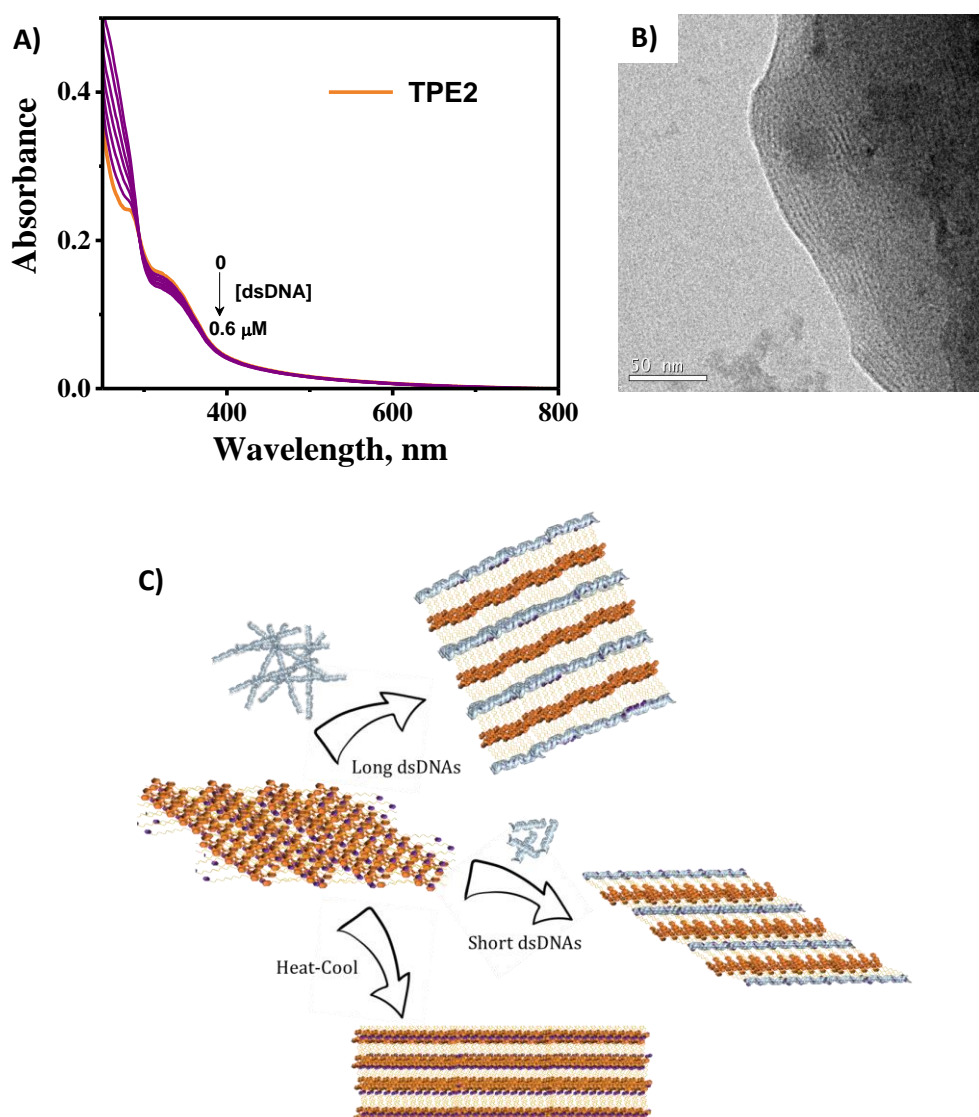
Figure 3.19. A) Changes in absorption spectra of **TPE2** in 10% DMSO-PBS with addition of short 20-mer dsDNA; B) TEM image of **TPE2/dsDNA** in 10% DMSO-PBS and C) Schematic representation of reassembly of **TPE2** with long dsDNA, short dsDNA and after heat-cool process.

The interaction of **TPE2** assembly in 10% DMSO/PBS with short 20-mer dsDNA is confirmed through absorption studies and shows significant hypochromism in **TPE2** absorption during titration experiment as shown in Figure 3.19A. As expected, the assembly of **TPE2** with short and rigid 20-mer dsDNA scaffold bring out more ordered crystalline assembly as evident from the clear

lattice fringes in **TPE2/dsDNA** nanosheet structures (Figure 3.19B). Thus, we can modulate the ordered crystalline assembly of **TPE2**, without significant morphological change, by the suitable choice of short/long dsDNA or by heat-cool process. Figure 3.19C shows the cartoonic representation of probable reassembly of **TPE2** with different stimuli.

3.3.4.3. Reassembly of TPE3 with dsDNA

TPE3, with four hydrophilic side arms form more stable and extended nanosheets in 10% DMSO-PBS due to strong hydrophobic interaction within **TPE3**. As we observed from the previous studies, the interaction of stable **TPE3** assembly with CTDNA is comparatively less. Thereby, we have studied the interaction with short 20-mer dsDNA and the small reduction in absorbance around 330 nm clearly indicates the interaction of **TPE3** assembly with short dsDNA (Figure 3.20A). Figure 3.20B shows the formation of extended nanosheets in **TPE3/dsDNA** hybrid and it shows clear lattice fringes in the nanosheets, depicting the high crystallinity. The SAED pattern, shown in Figure 3.20D, also confirms the high crystallinity of **TPE3/dsDNA** nanosheets. Thus, the introduction of dsDNA tends to realign the **TPE3** molecules by disturbing the initial arrangement, for the interaction with dsDNA through intercalation as shown in Figure 3.20C. Moreover, the heat-cool process of **TPE3** alone results in the formation of highly crystalline nanosheets, which is significantly different from that of **TPE3/dsDNA** (Figures 3.20E-G), as in the case of **TPE2.** Here also the van der Waals interaction between four hydrophilic triethylene glycol arms in **TPE3** play a major role in achieving the highly ordered nanosheets during the heat-cool process.
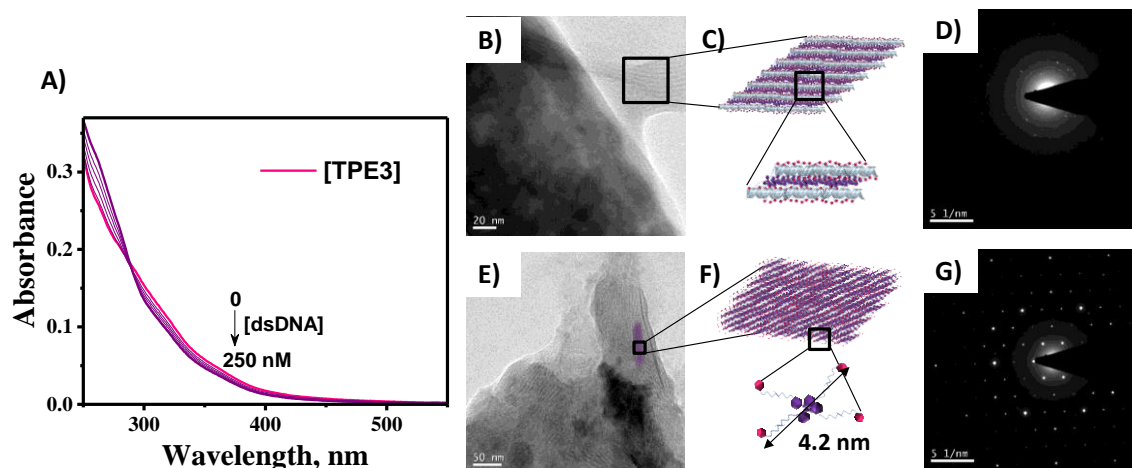
Figure 3.20. Changes in absorption spectra of **TPE3** in 10% DMSO-PBS with addition of 20-mer dsDNA; B) TEM image; C & D) corresponding schematic representation and SAED pattern of **TPE3/dsDNA** assembly in 10% DMSO-PBS; E) TEM image; F & G) corresponding schematic representation and SAED pattern of **TPE3**, after heat-cool in 10% DMSO-PBS.

3.4. CONCLUSIONS

Herein, we have demonstrated the hierarchical assembly and reassembly of suitably designed tetraphenylethylene amphiphiles in aqueous environment utilizing its DNA binding capability. Hierarchical assembly of TPE amphiphiles to nanoribbons/nanosheets through lateral association of initial fibrillar structures is well studied using TEM and AFM analysis. The disassembly and reassembly of TPE amphiphiles along with DNA is probed through different spectroscopic and morphological analysis. DNA plays a key role in the reassembly process as it alters the hydrophilic-hydrophobic balance of the system and provide specific binding possibility to achieve a directional assembly without compromising the ultimate morphology of the respective assemblies. Moreover, crystallinity of the assembly can be differentially modulated for these TPE amphiphiles, without involving any morphological transformations, through suitable choice of aqueous media, short or

long dsDNAs or by heat-cool process. This simple strategy to organize suitably designed small amphiphilic molecules with DNA can significantly contribute to the functional advances in these types of DNA nanostructures and emerging field of DNA nanotechnology.

3.5. EXPERIMENTAL SECTION

3.5.1. MATERIALS AND METHODS

All the reagents and solvents were purchased from sigma Aldrich, TCI and Spectrochem chemical suppliers. CTDNA and 20-mer ssDNAs were purchased from Sigma Aldrich. dsDNA used for the present study was prepared by the hybridization of complementary strands (DNA1: 5'-CGT CAC GTA AAT CGG TTA AC-3' and DNA2: 5'-GTT AAC CGA TTT ACG TGA CG-3') by annealing the two strands in 10 mM PBS with 2mM NaCl.

The TPE assemblies were prepared by the addition of molecularly dissolved **TPE1**, **TPE2** and **TPE3** in ethanol or DMSO to the respective solvent mixtures as specified in each experiment to get 25 μM, 15 μM and 30 μM concentrations of **TPE1**, **TPE2** and **TPE3** respectively and the TPE/nucleobase ratio for each hybrid is specified in the figure caption. All the experiments were carried out in this specified concentration of TPE amphiphiles, unless otherwise mentioned. Addition of micromolar concentration of CTDNA or dsDNA results in the TPE/DNA assembly. The heat-cooled samples were prepared by the gradual heating and cooling from 80 ℃ to 20 ℃ at a rate of 5 ℃/min.

3.5.2. SPECTROSCOPIC ANALYSIS

Absorption studies were carried out in a quartz cuvette having a path length of 1 cm using Shimadzu UV-2600 PC UV-Vis spectrophotometer. Emission spectra

were recorded using SPEX FLUOROLOG-3 (FL3-221) Spectrofluorometer with a slit width of 1.5 at an excitation wavelength of 380 nm and 290 nm for **TPE1** and **TPE2**, respectively. Lifetime measurements were carried out by picosecond Time Resolved Single Photon Counting system (TC-SPC, Horiba, Delta Flex) employing 270 nm laser as excitation source and picosecond photon detection module (PPD-850) as a detector. The life time decay profiles were deconvoluted using EzTime software and fitted with chi-square value 1 ± 0.1.

3.5.3. MORPHOLOGICAL ANALYSIS

AFM samples were prepared by dropping 20 μL solutions of respective assemblies to freshly cleaved mica sheets having a dimension of 1 cm × 1 cm. The samples were air dried for one day and vacuum dried prior to the analysis. AFM analyses were carried out with Bruker Multimode AFM operating with a tapping mode regime and micro fabricated antimony doped Si cantilever tips (Bruker-TESP series) with a resonance frequency of 320 kHz and a spring constant of 42 Nm^{-1}. TEM samples were prepared by passing 20 μL solutions through carbon coated Cu grid. The samples were air dried overnight and vacuum dried prior to analysis. HRTEM measurements were carried out by using JEOL JEM-F200 instrument with STEM, EDS and dual EELS at an accelerating voltage of 200 kV.

3.5.4. DLS AND XRD ANALYSIS

Dynamic Light Scattering experiments have been done by DLS-Zetasizer (Malvern Nano ZS) operating with a He-Ne laser at a wavelength of 633 nm. Each analysis was triplicate and the mean value is reported. In each run, 10-15 measurements were made. WAXS analyses were performed on XEUSS SAXS/WAXS system using a Genix microsource from Xenocs and the generator was operated at

0.6 mA and 50 kV. FOX2D mirror and two pairs of scatter-less slits from Xenocs were used to collimate the Cu Kα radiation with λ = 1.54 Å. A mar345 dtb image plate detector and Fit2D software were used to obtain the 2D-WAXS pattern.

3.5.5. SYNTHESIS AND CHARACTERISATION OF TPE AMPHIPHILES

3.5.5.1. Synthesis of 4-(1,2,2-triphenylvinyl)phenol, TPE1OH :
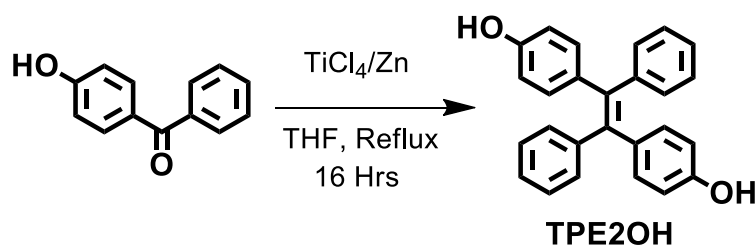
Scheme 3.4. Synthesis of **TPE2OH**.

Benzophenone (2 g, 11 mmol), 4-hydroxybenzophenone (2.18 g, 11 mmol) and zinc dust (6.47 g, 99 mmol) were taken in a 250 mL round bottom flask fitted with a reflux condenser. The flask was evacuated and purged with argon three times. 75 mL of dry THF was added under argon atmosphere and the mixture was cooled to 0-5°C. $TiCl_4$ (6.02 mL, 55 mmol) was slowly added to the cooled mixture and was warmed to room temperature, stirred for 30 minutes, and then refluxed overnight. The reaction was quenched with 10% aqueous potassium carbonate solution and a large amount of water was added until the solid turned grey or white. The mixture was extracted with ethyl acetate three times and the collected organic layer was washed twice with brine solution. The mixture was then dried over Na_2SO_4 anhydrous sodium sulphate. The solvent was evaporated and the crude product was purified through column chromatography on silica-gel using 2% hexane-ethyl acetate as eluent. White solid, yield = 36%. ^{1}H NMR (500 MHz, $CDCl_3$), δ (TMS, ppm): 7.08 (t, J = 5.5 Hz, 6 H), 7.07 (t, J = 3 Hz, 6H), 7.03 (t, J = 4.5 Hz, 3H), 6.88 (d, J = 10 Hz,

2H), 6.56 (d, J = 10 Hz, 2H), 4.76 (s, 1H); ^{13}C NMR (100 MHz, CDCl$_3$), δ (TMS, ppm):

154 .05, 144.02, 143.92, 143.91, 143.74, 140.97, 140.46, 140.19, 136.35, 132.75,

131.56, 131.39, 131.36, 131.35, 128.17, 127.73, 127.66, , 127.63, 126.42, 126.40,

126.28, 115.31, 114.62; HRMS (m/z): [M]$^+$ calculated for C$_{26}$H$_{20}$O, 348.15; found,

348.15.

3.5.5.2. Synthesis of tert-butyl (2-(2-(2-(2-chloroethoxy)ethoxy)ethoxy) phenyl)carbamate (APTEGCl)
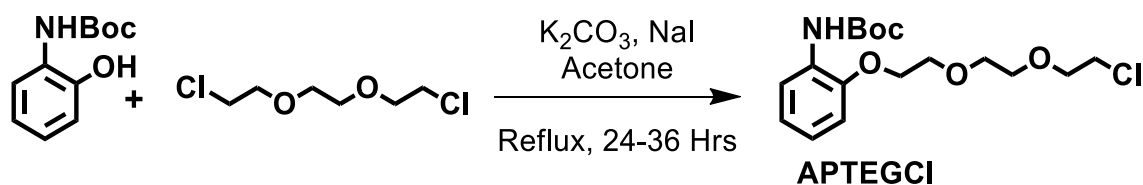
Scheme 3.5 Synthesis of **APTEGCl**.

To a solution of Boc protected aminophenol (500 mg, 2.39 mmol) in acetone

was added K$_2$CO$_3$ (825.74 mg, 5.97 mmol) and NaI (823.9 mg, 5.5 mmol) and

refluxed for 30 minutes. 1,2-bis(2-chloroethoxy)ethane (447.07 mg, 2.39 mmol) was

added to this mixture and was refluxed for 36 hours. The reaction mixture was

filtered and the crude product was purified through silica gel column

chromatography using 15 % hexane-ethyl acetate as eluent. Yellow viscous liquid,

yield = 70 %. ^{1}H NMR (500 MHz, CDCl$_3$), δ (TMS, ppm): 8.06 (s, 1H), 6.94 (m, 3H),

6.87 (d, J= 7.5 Hz, 1H), 4.18 (t, J= 5 Hz, 2H), 3.86 (t, J= 5 Hz, 2H), 3.76 (m, 7H), 3.72 (s,

1 H), 1.5 (s, 9 H); ^{13}C NMR (100 MHz, CDCl$_3$), δ (TMS, ppm): 153.05, 146.85, 129.02,

122.5, 118.9, 112.46, 77.03, 70.75, 70.42, 69.53, 68.68, 68.55, 42.45, 28.41; HRMS

(m/z): calculated for C$_{17}$H$_{26}$ClNO$_5$, 359.15; Found : 382.14 28 (M+23). Check the

correct format and modify. Delete this comment)

3.5.5.3. Synthesis of tert-butyl(2-(2-(2-(2-(4-(1,2,2-triphenylvinyl)phenoxy) ethoxy)ethoxy)ethoxy)phenyl) carbamate, TPE1B
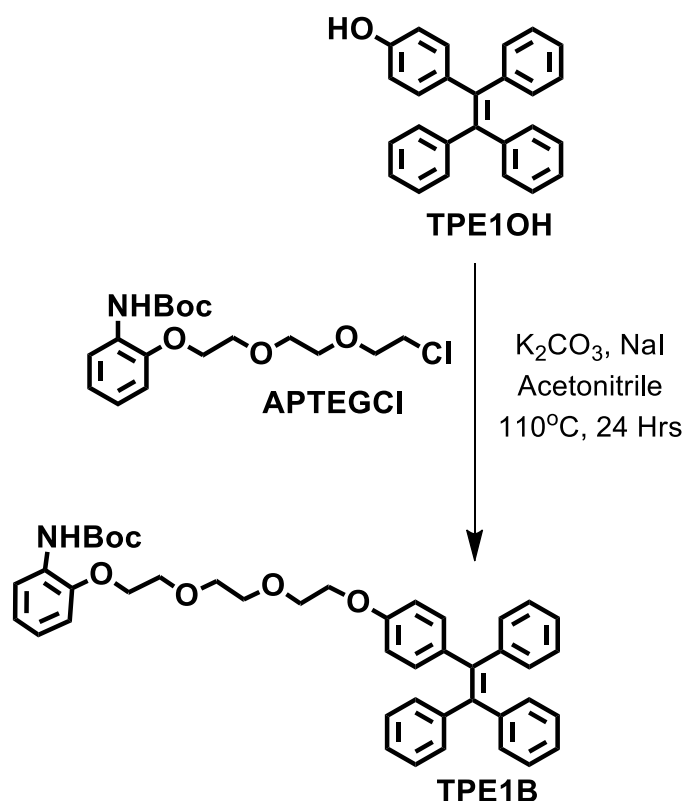
Scheme 3.6. Synthesis of **TPE1B**.

To a solution of **TPE1OH** (40 mg, 0.115 mmol) in acetonitrile was added K_2CO_3 (40 mg, 0.287 mmol) and NaI (4 mg, 0.026 mmol) and refluxed for 30 minutes. **APTEGCl** (50 mg, 0.138 mmol) was added to this mixture and was refluxed for 36 hours. The reaction mixture was filtered and the crude product was purified through silica gel column chromatography using 10% hexane-ethyl acetate as eluent. Yellow viscous liquid, yield = 40%. ^1H NMR (500 MHz, CDCl$_3$), δ (TMS, ppm): 8.02 (s, 1H) , 6.98 (m, 8H), 6.95 (d, J = 1, 2H), 6.94 (t, J= 2, 2H), 6.92 (m, 6H), 6.8 (m, 6H), 4.07 (t, J= 4 Hz, 2H), 3.95 (t, J= 5 Hz, 2H), 3.74 (m, 4H), 3.64 (s, 4H), 1.5 (s, 9 H); ^{13}C NMR (100 MHz, CDCl$_3$), δ (TMS, ppm): 156.20, 151.80, 145.67, 142.90, 139.43, 139.08, 135.27, 131.45, 130.30, 128.08, 126.66, 126.55, 125.31, 125.20, 121.27,

120.85, 117.40, 112.64, 111.77, 79.5, 69.84, 69.86, 68.78, 68.54, 67.86, 66.11, 27.37;

HRMS (m/z): [M]+ calculated for $C_{43}H_{45}NO_6$, 671.32; found, 694.32 (M+23).

3.5.5.4. Synthesis of 2-(2-(2-(2-(4-(1,2,2-triphenylvinyl)phenoxy)ethoxy)ethoxy)ethoxy)aniline, TPE1
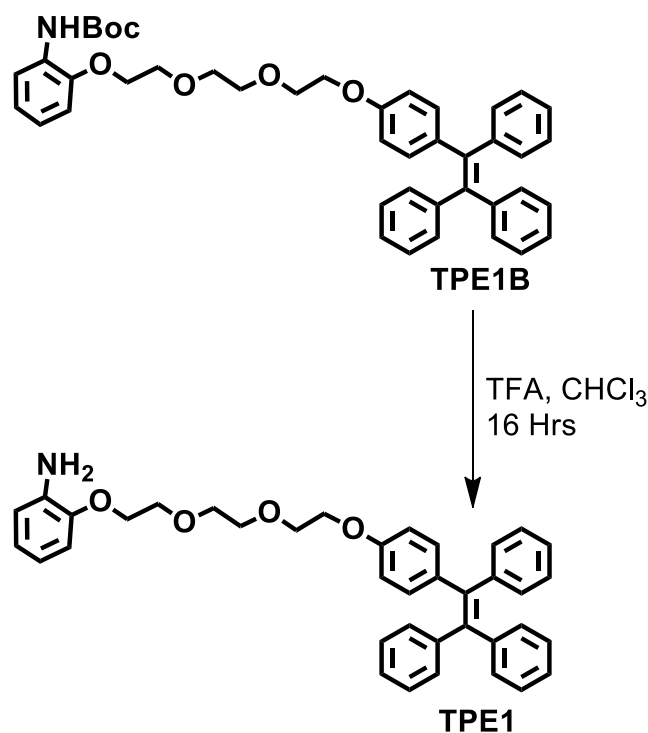
Scheme 3.7. Synthesis of **TPE1**.

TPE1B (420 mg, 0.625 mmol) in chloroform (3 ml) was added trifluoroacetic acid (765 µL) and stirred overnight at room temperature. The solvent was removed under reduced pressure and the reaction mixture was extracted with chloroform (10 mL). The organic layer was washed with water (2 x 10 mL) and neutralised with sodium bicarbonate (1 M). It was then separated, dried over Na_2SO_4 and evaporated under reduced pressure to give the product as brown viscous liquid in quantitative yield. ^{1}H NMR (500 MHz, CDCl3), δ (ppm): 7.08 (m, 8H), 7.01 (m,7H), 6.91 (d, J = 8.5, 2H), 6.78 (t, J= 1.5, 2H), 6.70 (m, 2H), 6.64 (d, J= 8.5, 2H), 4.15 (t, J= 4.5 Hz, 2H), 4.05

(t, J= 4.5 Hz, 2H), 3.83 (m, 4H), 3.73 (s, 4H); ^{13}C NMR (100 MHz, CDCl$_3$), δ (TMS, ppm): 157.20, 146.61, 143.98, 143.93, 140.46, 140.14, 136.38, 136.24, 132.51, 131.36, 131.34, 131.32, 127.71, 127.58, 126.35, 126.25, 126.22, 121.91, 118.93, 115.81, 113.69, 113.21, 70.80, 70.74, 69.80, 68.47, 67.21; HRMS (m/z): [M]$^+$ calculated for C$_{38}$H$_{37}$NO$_4$, 571.70; found, 572.28 (M+1).

3.5.5.5. Synthesis of 1,2-Bis(4-hydroxyphenyl)-1,2-diphenylethene, TPE2OH
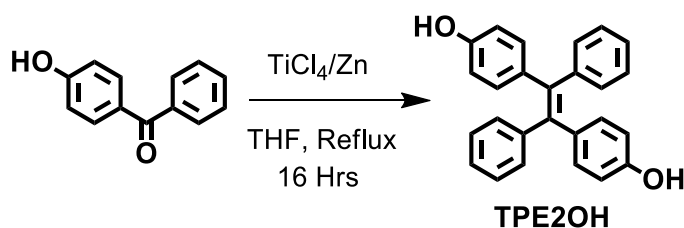
Scheme 3.8. Synthesis of **TPE2OH**.

4-hydroxybenzophenone (5 g, 25 mmol) and zinc dust (8.17 g, 125 mmol) were taken in a 250 mL round bottom flask fitted with a reflux condenser. The flask was evacuated and purged with argon three times. 75 mL of dry THF was added under argon atmosphere and the mixture was cooled to 0-5 °C. TiCl$_4$ (13.7 mL, 125 mmol) was slowly added to the cooled mixture and was slowly warmed to room temperature, stirred for 30 minutes, and then refluxed overnight. The reaction was quenched with 10% aqueous potassium carbonate solution and a large amount of water was added until the solid turned grey or white. The mixture was extracted with ethyl acetate three times and the collected organic layer was washed twice with brine solution. The mixture was dried over anhydrous sodium sulphate. The solvent was evaporated and the crude product was purified through column chromatography on silica- gel using 10% hexane-ethyl acetate as eluent. White solid, yield = 64%. ^{1}H NMR (500 MHz, CDCl$_3$), δ (TMS, ppm): 7.00-7.11 (m, 10H), 6.8 (t,

4H), 6.5 (d, 4H); ^{13}C NMR (100 MHz, CDCl$_3$), δ (TMS, ppm): 154.02, 144.12, 139.69, 136.54, 132.70, 131.37, 127.61, 126.22, 114.56; calculated for C$_{26}$H$_{20}$O$_2$, 364.15; found, 364.15.

3.5.5.6. Synthesis of (E)-di-tert-butyl((((((((((1,2-diphenylethene-1,2-diyl)bis(4,1-phenylene))bis(oxy))bis(ethane-2,1-diyl))bis(oxy))bis(ethane-2,1-diyl))bis(oxy))bis(ethane-2,1-diyl))bis(oxy))bis(2,1-phenylene))dicarbamate, TPE2B
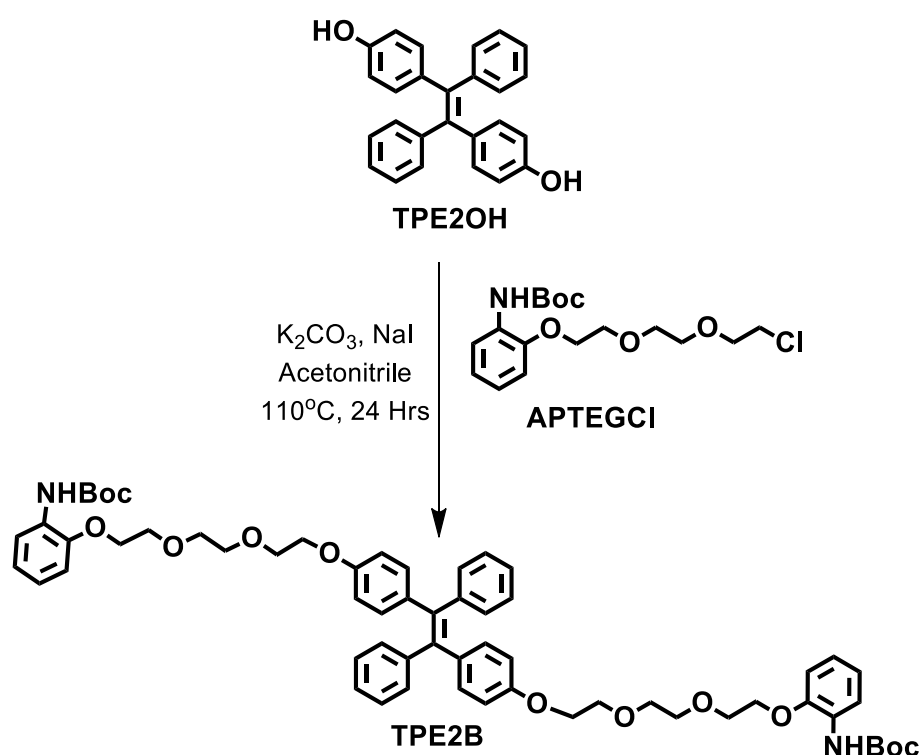
Scheme 3.9. Synthesis of **TPE2B**.

To a solution of **TPE2OH** (100 mg, 0.274 mmol) in acetonitrile was added K$_2$CO$_3$ (239.2 mg, 1.71 mmol) and NaI (234.8 mg, 1.57 mmol) and refluxed for 30 minutes. **APTEGCl** (297 mg, 0.824 mmol) was added to this mixture and was refluxed for 36 hours. The reaction mixture was filtered and the crude product was purified through silica gel column chromatography using 10% hexane-ethyl acetate as eluent. Yellow viscous liquid, yield = 40%; ^{1}H NMR (500 MHz, CDCl$_3$), δ (TMS,

ppm): 8.05 (s, 2H), 7.72 (d, 2H), 7.44 (d, J= 7.5 Hz, 2H), 7.32 (d, J= 7.5 Hz, 2H), 6.91 (m, 16 H), 6.56 (m, 2H), 4.13 (m, 6H), 3.82 (m, 5H), 3.70 (t, J = 10 Hz, 9H), 3.59 (d, J = 6 Hz, 2 H), 3.40 (m, 2H), 1.51 (s, 18 H); ^{13}C NMR (100 MHz, CDCl$_3$), δ (TMS, ppm): 171.24, 157.1, 152.8, 146.7, 139.6, 136.6, 132.5, 131.3,129.1, 127.6, 127.5, 121.8, 114.7, 112.8, 80.2, 72.3, 70.7, 69.6, 28.4; HRMS (m/z): [M]$^+$ calculated for C$_{60}$H$_{70}$N$_2$O$_{12}$, 1010.49; found, 1033.49 (M+23).

3.5.5.7. Synthesis of (E)-2,2'-(((((((((1,2-diphenylethene-1,2-diyl)bis(4,1-phenylene))bis(oxy))bis(ethane-2,1-diyl))bis(oxy))bis(ethane-2,1diyl))bis(oxy))bis(ethane-2,1-diyl))bis(oxy))di aniline, TPE2

Scheme 3.10. Synthesis of **TPE2**.

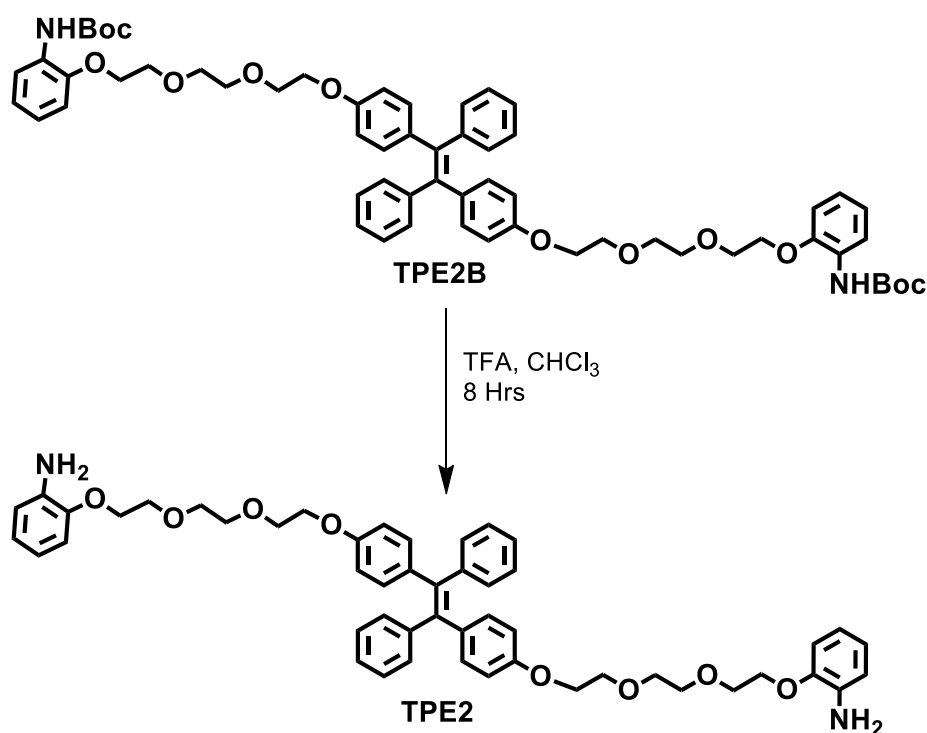To a solution of **TPE2B** (100 mg, 0.098 mmol) in chloroform (717 μL) was added trifluoroacetic acid (239 μL, 3.136 mmol) and stirred 8 hours at room temperature. The solvent was removed under reduced pressure and the reaction

mixture was extracted with chloroform (10 mL). The organic layer was washed with water (2 × 10 mL) and neutralised with sodium bicarbonate (1 M). It was then separated, dried over Na_2SO_4 and evaporated under reduced pressure to give the product as brown viscous liquid with 90 % yield. ^1H NMR (500 MHz, $CDCl_3$), δ (TMS, ppm): 6.99 (m, 8 H), 6.91 (m, 5H), 6.81 (t, J = 7 Hz, 2H), 6.72 (m, 6 H), 6.69 (m, 4 H), 6.64 (d, 1H), 4.16 (m, 6H), 4.04 (t, J = 4.5 Hz, 2H), 3.86 (t, J = 4.5 Hz, 8 H), 3.75 (m, 4H), 3.63 (m, 4H); ^{13}C NMR (100 MHz, $CDCl_3$), δ (TMS, ppm): 171.24, 157.1, 152.8, 146.7, 139.6, 136.6, 132.5, 131.3,129.1, 127.6, 127.5, 121.8, 114.7, 112.8, 80.2, 72.3, 70.7, 69.6, 28.4; HRMS (m/z): $[M]^+$ calculated for $C_{50}H_{54}N_2O_8$, 810.39; found, 810.39.

3.5.5.8. Synthesis of tert-butyl tetra-tert-butyl(((((((((ethene-1,1,2,2-tetrayltetrakis(benzene-4,1-diyl))tetrakis(oxy))tetrakis(ethane-2,1-diyl)) tetrakis(oxy))tetrakis(ethane-2,1-diyl))tetra kis(oxy)) tetrakis (ethane-2,1-diyl)) tetrakis(oxy))tetrakis(benzene-2,1diyl))tetra carbamate, TPE3B

To a solution of **TPE4OH** (22 mg, 0.055 mmol) in DMF was added K_2CO_3 (96 mg, 0.687 mmol) and NaI (95.4 mg, 0.64 mmol) and refluxed for 30 minutes. **APTEGCl** (100 mg, 0.277 mmol) was added to this mixture and was refluxed for 36 hours. The reaction mixture was filtered and the crude product was purified through silica gel column chromatography using 50 % hexane-ethyl acetate as eluent. Yellow viscous liquid, yield 40%.
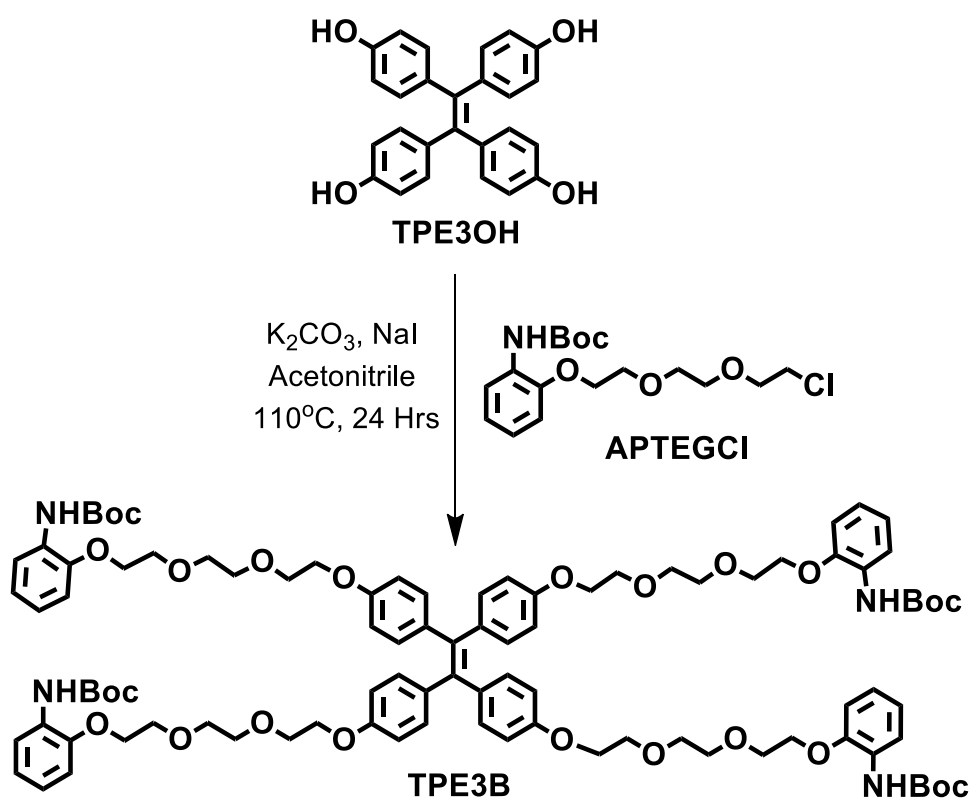
Scheme 3.11. Synthesis of **TPE3B**.

¹H NMR (500 MHz, CDCl₃), δ (TMS, ppm): 8.05 (s, 4H), 7.43 (d, 4H), 6.90 (m, 20H), 6.61 (d, J = 8.5, 8H), 4.16 (t, J= 4.5 Hz, 8H), 4.03 (t, J= 5 Hz, 8H), 3.83 (m, 16H), 3.73 (s, 16H), 1.51 (s, 36 H); ¹³C NMR (100 MHz, CDCl₃), δ (TMS, ppm): 156.97, 152.86, 146.72, 138.37, 137.02, 132.50, 129.12, 122.32, 121.90, 118.45, 113.66, 112.82, 80.26, 70.89, 70.74, 69.87, 69.60, 68.91, 67.15, 28.42; HRMS (m/z): [M]⁺ calculated for $C_{94}H_{120}N_4O_{24}$: 1688.83; found, 1711.83 (M+23).

3.5.5.9. Synthesis of 2,2',2'',2'''-((((((((ethene-1,1,2,2-tetrayltetrakis (benzene-4,1-diyl))tetrakis(oxy))tetrakis(ethane-2,1-diyl))tetrakis(oxy))tetrakis (ethane-2,1-diyl))tetrakis(oxy))tetrakis(ethane-2,1-diyl))tetrakis (oxy))tetraaniline, TPE3

TPE3B (67 mg, 0.039 mmol) in chloroform (582 μL) was added trifluoroacetic acid (194 μL, 2.537 mmol) and stirred overnight at room

temperature. The solvent was removed under reduced pressure and the reaction mixture was extracted with chloroform (10 mL). The organic layer was washed with water (2 × 10 mL) and neutralised with sodium bicarbonate (1 M). It was then separated, dried over Na_2SO_4 and evaporated under reduced pressure to give the product. Brown viscous liquid, yield = 70%.
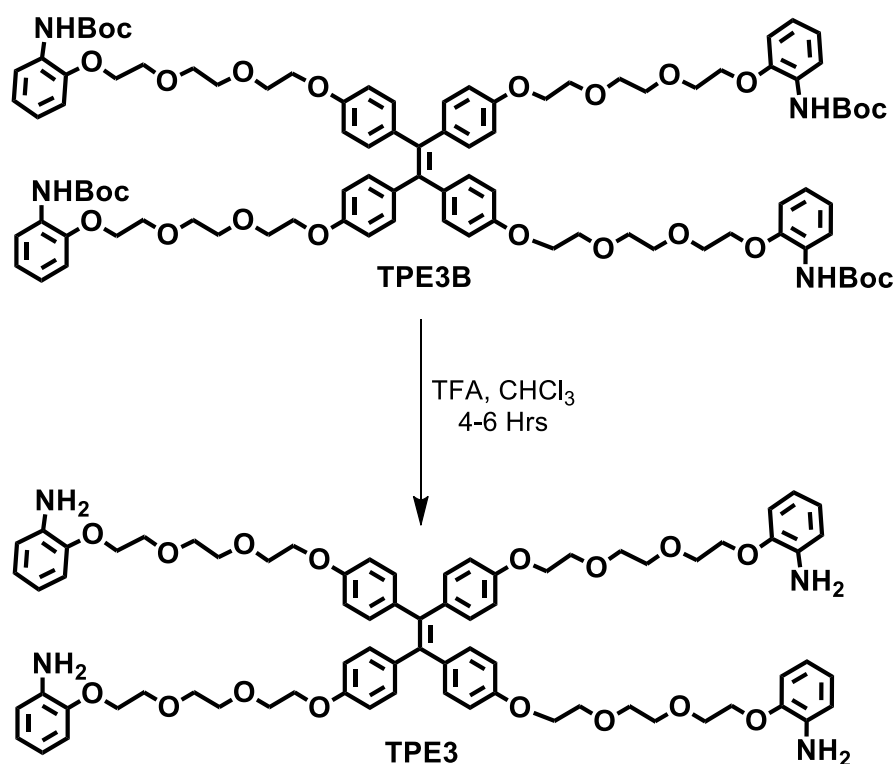
Scheme 3.12. Synthesis of **TPE3**.

^{1}H NMR (500 MHz, CDCl$_3$), δ (TMS, ppm): 6.89 (d, J = 8.5 Hz, 8H), 6.78 (t, J = 7 Hz, 8H), 6.67 (d, J = 7.5 Hz, 8H), 6.63 (t, J =10.5 Hz, 8 H), 4.12 (m, 8 H), 4.03 (d, J= 4.5 Hz, 8H), 3.83 (m, 16H), 3.73 (m, 16H); ^{13}C NMR (100 MHz, CDCl$_3$), δ (TMS, ppm):156.9, 146.3, 132.5, 121.8, 118.3, 115.4, 113.7, 113.1, 70.7, 69.6, 68.4, 67.2, 60.38; HRMS (m/z): [M]$^+$ calculated for $C_{74}H_{88}N_4O_{16}$, 1288.62; found, 1311.69.

3.6. REFERENCES

1. Hong, Y.; Lam, J. W. Y.; Tang, B. Z., Aggregation-induced emission: phenomenon, mechanism and applications. *Chem. Commun.* **2009,** (29), 4332-4353.

2. Wang, M.; Zhang, G.; Zhang, D.; Zhu, D.; Tang, B. Z., Fluorescent bio/chemosensors based on silole and tetraphenylethene luminogens with aggregation-induced emission feature. *J. Mater. Chem.* **2010,** *20* (10), 1858-1867.

3. Hong, Y.; Lam, J. W.; Tang, B. Z., Aggregation-induced emission: phenomenon, mechanism and applications. *Chem. Commun.* **2009,** (29), 4332-53.

4. Hong, Y.; Lam, J. W.; Tang, B. Z., Aggregation-induced emission. *Chem. Soc. Rev.* **2011,** *40* (11), 5361-88.

5. Zhao, Z.; Lam, J. W. Y.; Tang, B. Z., Tetraphenylethene: a versatile AIE building block for the construction of efficient luminescent materials for organic light-emitting diodes. *J. Mater. Chem* **2012,** *22* (45), 23726-23740.

6. Ding, D.; Li, K.; Liu, B.; Tang, B. Z., Bioprobes based on AIE fluorogens. *Acc. Chem. Res.* **2013,** *46* (11), 2441-53.

7. La, D. D.; Bhosale, S. V.; Jones, L. A.; Bhosale, S. V., Tetraphenylethylene-Based AIE-Active Probes for Sensing Applications. *ACS Appl. Mater. Interfaces* **2018,** *10* (15), 12189-12216.

8. Hu, R.; Leung, N. L.; Tang, B. Z., AIE macromolecules: syntheses, structures and functionalities. *Chem. Soc. Rev.* **2014,** *43* (13), 4494-562.

9. Wu, T.; Huang, J.; Yan, Y., Self-Assembly of Aggregation-Induced-Emission Molecules. *Chem. Asian J.* **2019,** *14* (6), 730-750.

10. Yu, K.; Pan, J.; Husamelden, E.; Zhang, H.; He, Q.; Wei, Y.; Tian, M., Aggregation-induced Emission Based Fluorogens for Mitochondria-targeted Tumor Imaging and Theranostics. *Chem. Asian J.* **2020,** *15* (23), 3942-3960.

11. Li, Y.; Xu, L.; Su, B., Aggregation induced emission for the recognition of latent fingerprints. *Chem. Commun.* **2012,** *48* (34), 4109-11.

12. La, D. D.; Malegaonkar, J. N.; Kobaisi, M. A.; Bhosale, R. S.; Bhosale, S. V.; Bhosale, S. V., Spermine-directed supramolecular self-assembly of water-soluble AIE-active tetraphenylethylene: nanobelt, nanosheet, globular and nanotubular structures. *New J. Chem.* **2018,** *42* (18), 15379-15386.

13. Salimimarand, M.; La, D. D.; Kobaisi, M. A.; Bhosale, S. V., Flower-like superstructures of AIE-active tetraphenylethylene through solvophobic controlled self-assembly. *Sci. Rep.* **2017,** *7* (1), 42898.

14. Sutar, P.; Suresh, V. M.; Jayaramulu, K.; Hazra, A.; Maji, T. K., Binder driven self-assembly of metal-organic cubes towards functional hydrogels. *Nat. Commun.* **2018,** *9* (1), 3587.

15. Shi, J.; Deng, Q.; Li, Y.; Chai, Z.; Wan, C.; Shangguan, H.; Li, L.; Tang, B., An Aggregation-induced Emission Probe Based on Host–Guest Inclusion Composed of the Tetraphenylethylene Motif and γ-Cyclodextrin for the Detection of α-Amylase. *Chem. Asian J.* **2019,** *14* (6), 847-852.

16. Li, H.; Zhu, L.; Zhu, X.; Zhang, H., Glucose detection via glucose-induced disaggregation of ammonium-modified tetraphenylethylene from polyanion. *Sens. Actuators B Chem.* **2017,** *246*.

17. Li, J.; Liu, K.; Han, Y.; Tang, B. Z.; Huang, J.; Yan, Y., Fabrication of Propeller-Shaped Supra-amphiphile for Construction of Enzyme-Responsive Fluorescent Vesicles. *ACS Appl. Mater. Interfaces* **2016,** *8* (41), 27987-27995.

18. Shustova, N. B.; McCarthy, B. D.; Dincă, M., Turn-On Fluorescence in Tetraphenylethylene-Based Metal–Organic Frameworks: An Alternative to Aggregation-Induced Emission. *J. Am. Chem. Soc.* **2011,** *133* (50), 20126-20129.

19. Yin, G. Q.; Wang, H.; Wang, X. Q.; Song, B.; Chen, L. J.; Wang, L.; Hao, X. Q.; Yang, H. B.; Li, X., Self-assembly of emissive supramolecular rosettes with increasing complexity using multitopic terpyridine ligands. *Nat. Commun.* **2018,** *9* (1), 567.

20. Dong, J.; Zhang, K.; Li, X.; Qian, Y.; Zhu, H.; Yuan, D.; Xu, Q.-H.; Jiang, J.; Zhao, D., Ultrathin two-dimensional porous organic nanosheets with molecular rotors for chemical sensing. *Nat. Commun.* **2017,** *8* (1), 1142.

21. Yu, G.; Zhao, R.; Wu, D.; Zhang, F.; Shao, L.; Zhou, J.; Yang, J.; Tang, G.; Chen, X.; Huang, F., Pillar[5]arene-based amphiphilic supramolecular brush copolymers: fabrication, controllable self-assembly and application in self-imaging targeted drug delivery. *Polym. Chem.* **2016,** *7* (40), 6178-6188.

22. Li, N. N.; Li, J. Z.; Liu, P.; Pranantyo, D.; Luo, L.; Chen, J. C.; Kang, E.-T.; Hu, X. F.; Li, C. M.; Xu, L. Q., An antimicrobial peptide with an aggregation-induced emission (AIE) luminogen for studying bacterial membrane interactions and antibacterial actions. *Chem. Commun.* **2017,** *53* (23), 3315-3318.

23. Hu, Y.; Cao, X.; Guo, Y.; Zheng, X.; Li, D.; Chen, S.-K.; Chen, G.; You, J., An aggregation-induced emission fluorogen/DNA probe carrying an endosome escaping pass for tracking reduced thiol compounds in cells. *Anal. Bioanal. Chem. Res* **2020,** *412* (28), 7811-7817.

24. Zhang, S.; Liu, M.; Tan, L. Y. F.; Hong, Q.; Pow, Z. L.; Owyong, T. C.; Ding, S.; Wong, W. W. H.; Hong, Y., A Maleimide-functionalized Tetraphenylethene for Measuring and Imaging Unfolded Proteins in Cells. *Chem. Asian J.* **2019,** *14* (6), 904-909.

25. Hong, Y.; Häußler, M.; Lam, J. W. Y.; Li, Z.; Sin, K. K.; Dong, Y.; Tong, H.; Liu, J.; Qin, A.; Renneberg, R.; Tang, B. Z., Label-Free Fluorescent Probing of G-Quadruplex Formation and Real-Time Monitoring of DNA Folding by a Quaternized Tetraphenylethene Salt with Aggregation-Induced Emission Characteristics. *Chem. Eur. J.* **2008,** *14* (21), 6428-6437.

26. Lou, X.; Leung, C.; Dong, C.; Hong, Y.; Chen, S.; Zhao, E.; Lam, J.; Tang, B., Detection of adenine-rich ssDNA based on thymine-substituted tetraphenylethene with aggregation-induced emission characteristics. *RSC Adv.* **2014,** *4*.

27. Li, Y.; Yu, H.; Qian, Y.; Hu, J.; Liu, S., Amphiphilic Star Copolymer-Based Bimodal Fluorogenic/Magnetic Resonance Probes for Concomitant Bacteria Detection and Inhibition. *Adv. Mater.* **2014,** *26* (39), 6734-6741.

28. Wang, J.-X.; Chen, Q.; Bian, N.; Yang, F.; Sun, J.; Qi, A.-D.; Yan, C.-G.; Han, B.-H., Sugar-bearing tetraphenylethylene: novel fluorescent probe for studies of carbohydrate–protein interaction based on aggregation-induced emission. *Org. Biomol. Chem.* **2011,** *9* (7), 2219-2226.

29. Li, S.; Langenegger, S. M.; Häner, R., Control of aggregation-induced emission by DNA hybridization. *Chem. Commun.* **2013,** *49* (52), 5835-5837.

30. Zhu, L.; Zhou, J.; Xu, G.; Li, C.; Ling, P.; Liu, B.; Ju, H.; Lei, J., DNA quadruplexes as molecular scaffolds for controlled assembly of fluorogens with aggregation-induced emission. *Chem. Sci.* **2018,** *9* (9), 2559-2566.

31. Zhang, C.; Zhang, T.; Jin, S.; Xue, X.; Yang, X.; Gong, N.; Zhang, J.; Wang, P. C.; Tian, J.-H.; Xing, J.; Liang, X.-J., Virus-Inspired Self-Assembled Nanofibers with Aggregation-Induced Emission for Highly Efficient and Visible Gene Delivery. *ACS Appl. Mater. Interfaces* **2017,** *9* (5), 4425-4432.

32. Saraswathi, S. K.; Karunakaran, V.; Maiti, K. K.; Joseph, J., DNA Condensation Triggered by the Synergistic Self-Assembly of Tetraphenylethylene-Viologen Aggregates and CT-DNA. *Front Chem* **2021,** *9*.

33. Liu, J.; Sheng, J.; Shao, L.; Zheng, Q.; Li, W.; Chen, X.; Mao, L.; Wang, M., Tetraphenylethylene-Featured Fluorescent Supramolecular Nanoparticles for Intracellular Trafficking of Protein Delivery and Neuroprotection. *Angew. Chem. Int. Ed.* **2021,** *60* (51), 26740-26746.

34. Yang, J.; Yu, X.; Song, J.-I.; Song, Q.; Hall, S. C. L.; Yu, G.; Perrier, S., Aggregation-Induced Emission Featured Supramolecular Tubisomes for Imaging-Guided Drug Delivery. *Angew. Chem. Int. Ed.* **2022,** *61* (9), e202115208.

35. Anuradha; La, D. D.; Al Kobaisi, M.; Bhosale, S. V., Right handed chiral superstructures from achiral molecules: self-assembly with a twist. *Sci. Rep.* **2015,** *5* (1), 15652.

36. Li, H.; Zheng, X.; Su, H.; Lam, J. W. Y.; Sing Wong, K.; Xue, S.; Huang, X.; Huang, X.; Li, B. S.; Tang, B. Z., Synthesis, optical properties, and helical self-assembly of a bivaline-containing tetraphenylethene. *Sci. Rep.* **2016,** *6*, 19277-19277.

37. Wang, Y.; Lee, M., Self-Assembly of Tetraphenylethylene-Based Amphiphiles in Aqueous Methanol Solution into Two-Dimensional Chiral Sheets for Enantioselective Sorption. *ChemPlusChem* **2020,** *85* (4), 711-714.

38. Saraswathi, S. K.; Joseph, J., Thymine-Induced Dynamic Switching of Self-Assembled Nanofibers in Diaminotriazine-Functionalized Tetraphenylethylene Derivatives: Implications for One-Dimensional Molecular Devices. *ACS Appl. Nano Mater.* **2022,** *5* (2), 3018-3027.

39. Chakraborty, S.; Ray, D.; Aswal, V. K.; Ghosh, S., Multi-Stimuli-Responsive Directional Assembly of an Amphiphilic Donor–Acceptor Alternating Supramolecular Copolymer. *Chem. Eur. J.* **2018,** *24* (61), 16379-16387.

40. Lee, M.; Lee, S.-J.; Jiang, L.-H., Stimuli-Responsive Supramolecular Nanocapsules from Amphiphilic Calixarene Assembly. *J. Am. Chem. Soc.* **2004,** *126* (40), 12724-12725.

41. Vybornyi, O.; Liu, S.-X.; Häner, R., Stimuli-Responsive Supramolecular Polymers from Amphiphilic Phosphodiester-Linked Azobenzene Trimers. *Angew. Chem. Int. Ed.* **2021,** *60* (49), 25872-25877.

42. Sun, M.; Lee, M., Switchable Aromatic Nanopore Structures: Functions and Applications. *Acc. Chem. Res.* **2021,** *54* (14), 2959-2968.

43. Wang, H.; Lee, M., Switching between Stacked Toroids and Helical Supramolecular Polymers in Aqueous Nanotubules. *Macromol. Rapid Commun.* **2020,** *41* (11), e2000138.

44.   Shen, B.; He, Y.; Kim, Y.; Wang, Y.; Lee, M., Spontaneous Capture of Carbohydrate Guests through Folding and Zipping of Self-Assembled Ribbons. *Angew. Chem. Int. Ed.* **2016,** *55* (7), 2382-2386.

45.   Eder, T.; Stangl, T.; Gmelch, M.; Remmerssen, K.; Laux, D.; Höger, S.; Lupton, J. M.; Vogelsang, J., Switching between H- and J-type electronic coupling in single conjugated polymer aggregates. *Nat. Commun.* **2017,** *8* (1), 1641.

46.   Kamps, A. C.; Cativo, M. H. M.; Fryd, M.; Park, S.-J., Self-Assembly of Amphiphilic Conjugated Diblock Copolymers into One-Dimensional Nanoribbons. *Macromolecules* **2014,** *47* (1), 161-164.

47.   Krishnan, N.; Golla, M.; Thelu, H. V. P.; Albert, S. K.; Atchimnaidu, S.; Perumal, D.; Varghese, R., Self-assembly of DNA–tetraphenylethylene amphiphiles into DNA-grafted nanosheets as a support for the immobilization of gold nanoparticles: a recyclable catalyst with enhanced activity. *Nanoscale* **2018,** *10* (36), 17174-17181.

48.   Rest, C.; Martin, A.; Stepanenko, V.; Allampally, N. K.; Schmidt, D.; Fernández, G., Multiple CH···O interactions involving glycol chains as driving force for the self-assembly of amphiphilic Pd(ii) complexes. *Chem. Commun.* **2014,** *50* (87), 13366-13369.

49.   Kulala Vittala, S.; Joseph, J., Chiral self-assembly of fullerene clusters on CT-DNA templates. *Faraday Discuss.* **2018,** *207* (0), 459-469.

50.   Fan, J. Y.; Valu, K. K.; Woodgate, P. D.; Baguley, B. C.; Denny, W. A. J. A.-c. d. d., Aniline mustard analogues of the DNA-intercalating agent amsacrine: DNA interaction and biological activity. *Anticancer Drug Des.* **1997,** *12 3*, 181-203.

51.   Nair, V. C.; Muthu, C.; Rogach, A. L.; Kohara, R.; Biju, V., Channeling Exciton Migration into Electron Transfer in Formamidinium Lead Bromide Perovskite Nanocrystal/Fullerene Composites. *Angew. Chem. Int. Ed.* **2017,** *56* (5), 1214-1218.

POLYTHYMIDINE ASSISTED ORDERED HIERARCHICAL ASSEMBLY OF DIAMINOTRIAZINE APPENDED TETRAPHENYLETHYLENE AMPHIPHILES
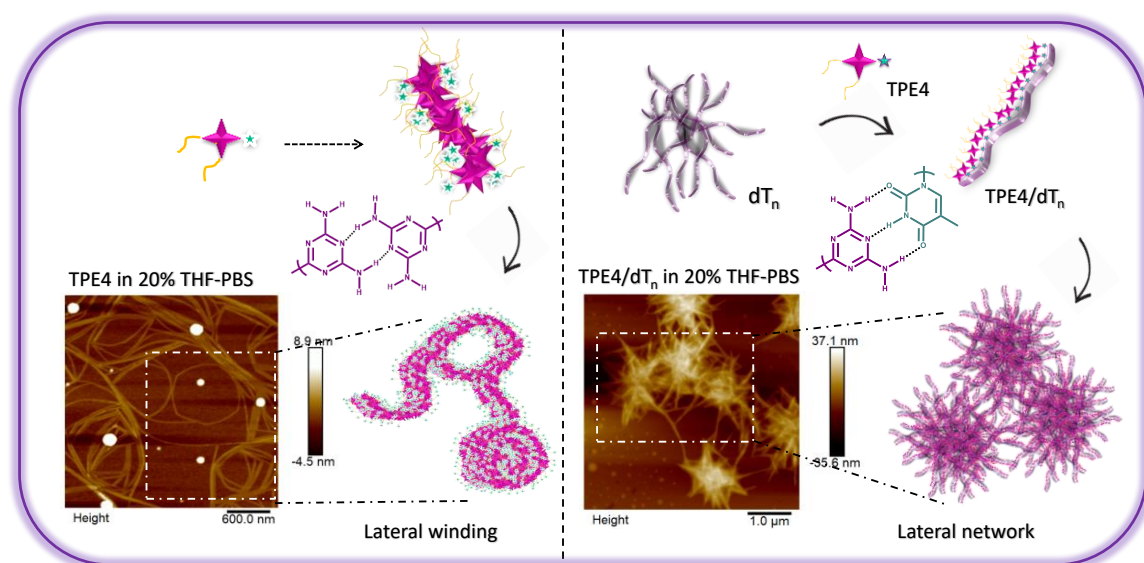
4.1. ABSTRACT

*This chapter demonstrates the formation of hierarchical flower-like structures from diaminotriazine appended TPE derivative (**TPE4**) in aqueous media and its polythymidine assisted ordered assembly through nucleobase recognition. Formation of highly emissive, crystalline flower-like nano- and micro-structures are achieved through polythymidine assisted assembly, and the significant difference in the assembly pathway has been investigated through morphological analyses. The hierarchical self-assembly of **TPE4** alone is primarily guided by hydrophobic interactions to form 1D structures, which undergo lateral association through double self-complementary H-bonding and van der Waals interactions within triethylene glycol chains to form ribbon like structures. Lateral winding of these long, flexible*

*ribbons leads to the formation of nanosheet structures which further stack to form flower-like assemblies. Ordered assembly of **TPE4** can be achieved through the polydeoxythymidine (dT$_n$) assisted templated assembly, by virtue of more stronger triple H-bonding between thymine and diaminotriazine units. Presence of dT$_n$ prevents the initial lateral association of **TPE4** and the templated assembly results in the 1D-organization of amphiphiles on the oligonucleotide strands, which eventually transforms to 2D-network structures through further π-π stacking and van der Waals interactions. The lateral association of more TPE amphiphiles on this network structures result in the formation of nanosheets which further stack to form flower-like assemblies with more ordered **TPE4/dT$_n$** arrangement compared to the initial **TPE4** assembly. Thus, the present studies highlight the possibility of nucleobase recognition to trigger the ordered assembly of small amphiphilic molecules with suitable modifications to follow an entirely different pathway in order to attain highly ordered DNA nanostructures.*

4.2. INTRODUCTION

The very famous DNA double helix, attained by virtue of π-π stacking and H-bonding interactions between purine and pyrimidine nucleobases, draw great attention due to its elegant supramolecular structure. DNA nucleobases with various H-bonding motifs provide several options to make complementary H-bonds with each other and the finite choice significantly determine the ultimate structure of DNA. The standard choice of a double helical structure by DNA primarily relies on canonical Watson-Crick base pairing that strictly follow A-T and G-C combinations.[1] Suitable variations in the arrangement of bases and orientation of H-bonds can lead to the formation of alternative DNA structures like triplexes[2], G-quadruplexes[3], intercalated motifs (i-motifs)[4] *etc*. A triplex DNA structure is typically formed by the

antiparallel orientation of a third strand on a duplex structure through non-canonical Hoogsteen base pairing.[2] Similarly, G-quadruplexes are shaped by the self-association of guanines with each other through Hoogsteen base pairing.[3] In i-motifs, two parallel-stranded duplexes intercalated in an antiparallel orientation and held together by hemi-protonated cytosine-cytosine+ (C:C+) base pair.[4] Thus, the mode of H-bonding interactions has great influence on the final structures of DNA based supramolecular constructs and is highly engaged for the development of various DNA nanostructures.

As inspired from the unique structure of DNA, supramolecular chemists dive into the possibilities of H-bonding interactions to make excellent nanostructures by employing different DNA nucleobase analogues, like melamine, cyanuric acid, barbituric acid, diaminotriazine *etc.*, with similar H-bonding motifs (Figure 4.1A).[5, 6] Among these, the melamine and cynauric acid are generally accepted as best H-bonding partners in supramolecular systems and employed for the generation of several elegant nanostructures with tunable properties.[6-8] The crystal structure of a two dimensional H-bonded molecular construct from this melamine-cyanuric acid partners has been first discovered by Wang *et al.*[9] Later, Whitesides and co-workers identified three sub-motifs in the solid state, namely a) infinite linear tapes, (b) infinite crinkled tapes, and (c) finite cyclic rosette motifs.[10, 11] Sleiman and co-workers, who contributed significantly in the area of DNA nanotechnology, reported the first DNA-analogue hexameric rosette by employing triaminopyrimidine and cyanuric acid based nucleosides.[12] In the following decades, this combination is well-explored to generate plenty of functional assemblies by the design of suitable derivatives.[13, 14] Similar analogues like barbituric acid and diaminotriazine are also

well utilized in the design of supramolecular assemblies based on H-bonding interactions.[14-16] Recently, our group has demonstrated the H-bond directed assembly of diaminotriazine appended TPE derivatives to 1D fibers in dodecane. Further, we have investigated its morphological transformation on co-assembling with an alkylated thymine derivative through nucleobase recognition and it suggests the utility of nucleobase recognition to control and tune the physical and morphological behaviour of TPE-based 1D fibers.[17]

Supramolecular assemblies based on H–bonding interactions often prefer aprotic solvents for the assembly process since these competitive H-bonds are more stable in organic aprotic solvents. Thus, most of the previous reports preferred alkylated derivatives of nucleobase analogues for H-bond based assembly in order to achieve a perfect solubility for the assembly process to occur.[18-20] Instead, the protic solvents serve as a strong competitor for nucleobase analogues in forming H-bonds that weakens the supramolecular assemblies. In the later stages, several efforts have been invested on H-bonded assemblies in aqueous media and it gradually paves way to the incredible supramolecular designs in water.[21, 22] Most of these nucleobase analogues show tendency to form columnar stacks in water through π-π stacking instead of forming H-bonds.[23] But, the extent of H-bond strength in water can be enhanced by providing a proper hydrophobic pocket to save hydrogen bonding motifs from competing water molecules as observed in the case of a DNA double helix. Thus, the supramolecular assembly of nucleobase analogues in aqueous media can be modulated through suitable design of its amphiphilic derivatives. Meijer and co-workers adopted this concept to build a set of DNA-like supramolecular assemblies and first they have demonstrated the formation of a DNA-like nanofiber assembly by the interaction of a novel thymidine-appended bolaamphiphile with

oligoadenylic acids.[24] Furthermore, they have employed the strategy for the templated assembly of chromophores by the H-bonding interactions of diaminotriazine appended naphthalene[25] and oligo(phenylene)vinylene[16] derivatives with oligothymine strands (Figure 4.1B).
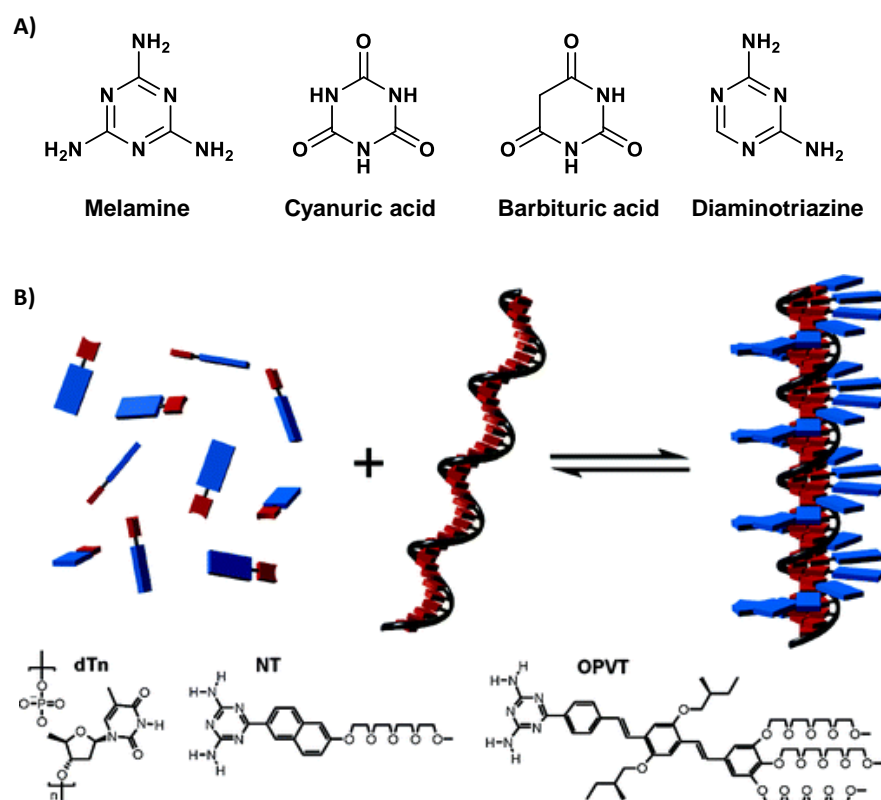
Figure 4.1. A) Molecular structures of nucleobase analogues and B) Schematic representation of ssDNA template assembly of chromophores on oligothymine (dT_n) strands and corresponding molecular structures of dT_n, naphthalene (**NT**) and oligo(phenylene)vinylene (**OPVT**) derivatives (Adapted from reference 16).

Later, the strategy get promoted in the area of DNA nanotechnology, where the interactions of nucleobase analogues with specific, modified and unmodified DNA strands can achieve a library of more versatile DNA nanostructures.[24] One of the important breakthroughs in DNA nanostructure design is reported by Sleiman and co-workers, where they employed cyanuric acid with polyadenine strands to
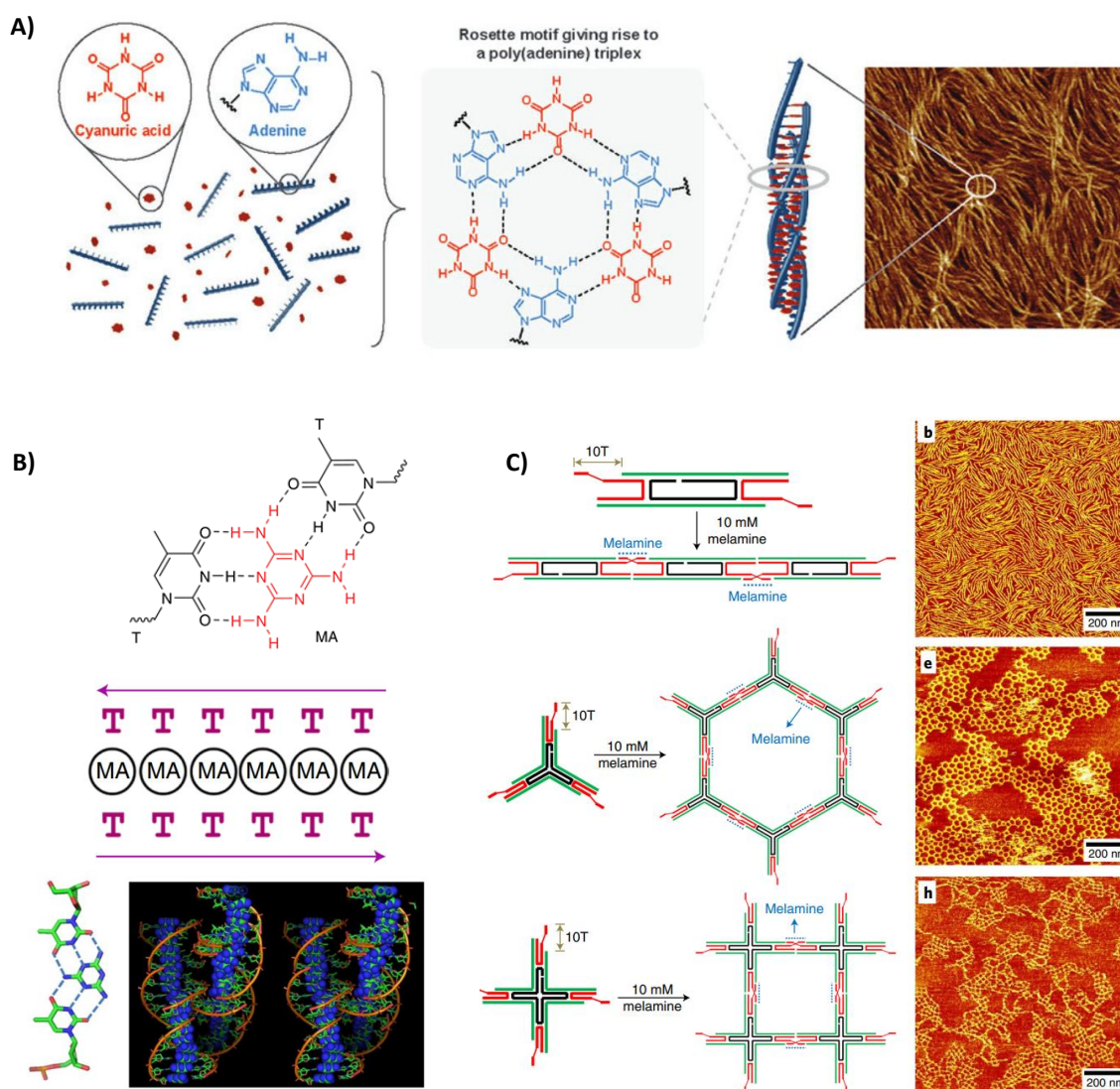
Figure 4.2. A) Schematic representation and AFM images of cyanuric acid mediated assembly of dAn; B) Schematic representations of H-bonding interactions in polythymine-melamine duplex and C) Schematic representations and AFM images of 1D and 2D arrays from melamine mediated DNA self-assembly. (Adapted from reference 26 and 27, respectively).

mediate the co-operative growth of supramolecular polymers to generate DNA nanofibers with high aspect ratio (Figures 4.2A & 4.2B).[26] Subsequently, the same group has demonstrated the association of two poly(T) strands with the assistance of melamine to form antiparallel homoduplexes and well defined nanostructures controlled by the design (Figure 4.2B).[27] These DNA-small molecule assemblies are

more dynamic compared to Watson-Crick base pairing and produce stimuli-responsive, functional DNA nanostructures. A slightly different design strategy has been adopted by Tan and co-workers to assemble long DNA building block to nanoflower-like structures that involve rolling circle replication of a designer template exclusively based on non-canonical base pairing. Further, they have demonstrated the multifunctionality of these DNA nanoflowers in biomedical applications.[28]

Besides the templated assemblies with oligonucleotide strands, simple nucleosides are also amenable to self-assembly in water through H-bonding interactions. Yang and co-workers well-explored the self-assembly of Janus-type pyrimidopyrimidine nucleosides and finally achieved the formation of flower-like structures in water (Figure 4.3). The assembly process follows a two stage mechanism that involve a nucleation process through non-specific H-bonding, followed by a reorganization process to achieve more specific H-bonding interactions.[29]
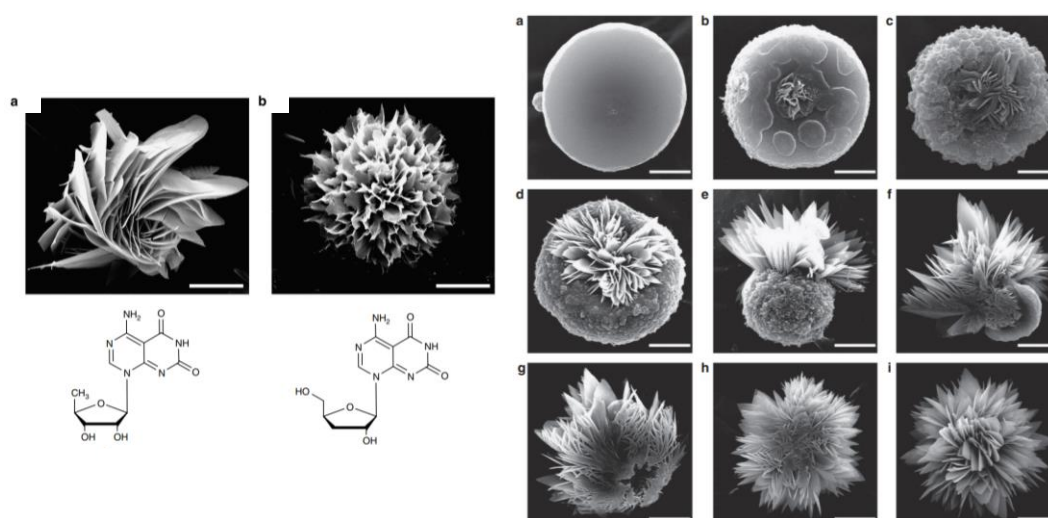
Figure 4.3. SEM images of flower-like assemblies of pyrimido[4,5-d]pyrimidine nucleosides and the formation of flower-like assemblies (Adapted from reference 28).

Hierarchical assemblies of organic small molecules to flower-like superstructures are of great importance due to their potential application in catalysis, superhydrophobic material development, biomedical and optoelectronic applications.[30-32] But, still there are fewer reports on hierarchically assembled organic flower-like structures with tunable properties. The first reported organic flower-like structures are achieved from an alkylated fullerene derivative as a result of π-π interactions and van der Waals interactions in an organic solvent system.[33]
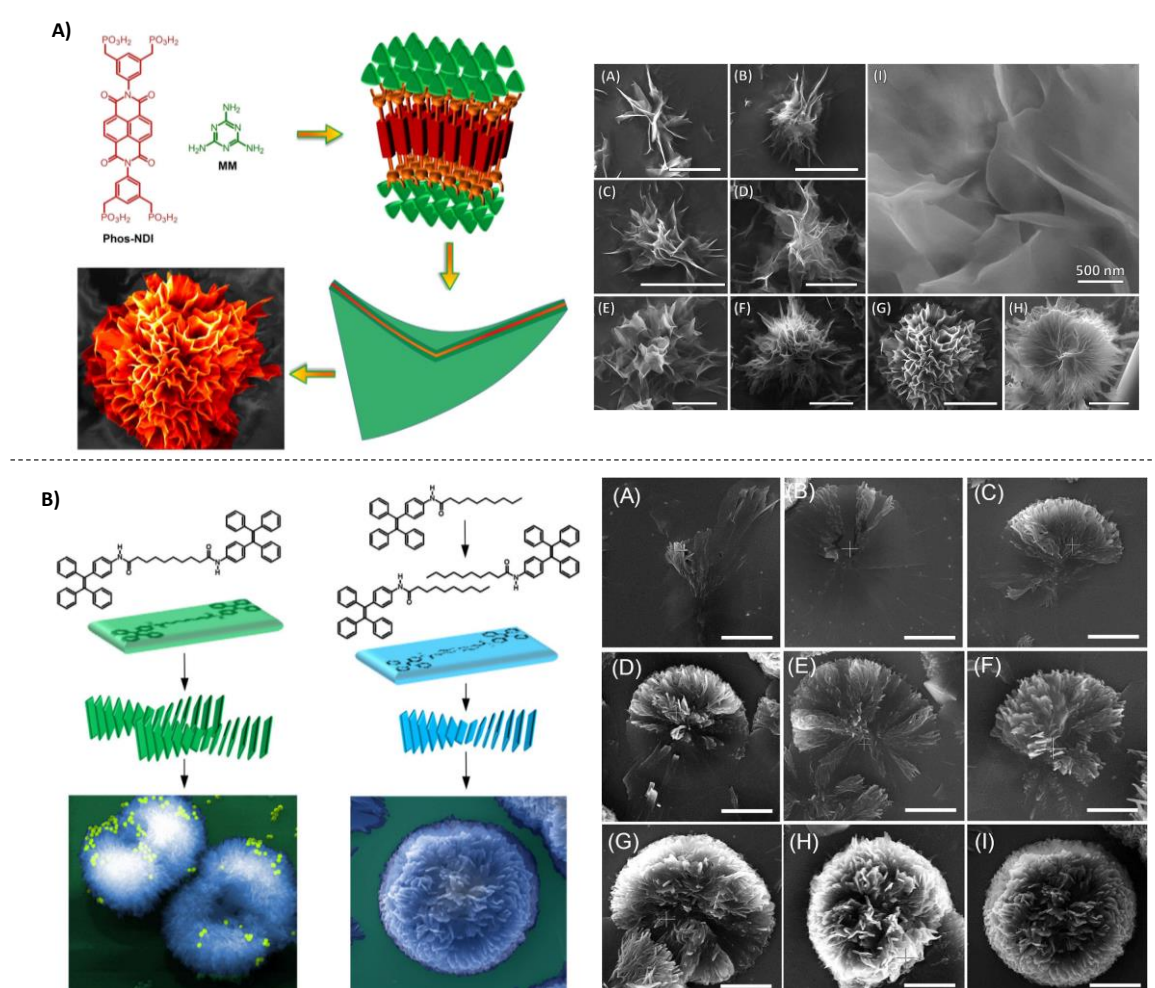
Figure 4.4. Schematic representation of flower-like assembly from A) Phosphonic acid appended naphthalene diimide with melamine and B) Tetraphenylethylene derivatives (Adapted from reference 33 and 34, respectively).

Later, Bhosale *et al.* described the stepwise growth of flower-like structures through the two-component self-assembly of phosphonic acid appended naphthalene diimide and melamine by virtue of π-π and H-bonding interactions in water (Figure 4.4A).[34] Moreover, the same group has reported the solvophobic controlled assembly of tetraphenylethylene derivatives in polar and mixtures of polar and non-polar solvents (Figure 4.4B).[35] In both these examples the flower-like structures are formed by the combined effect of dispersive interactions and H-bonding interactions. But, most of the H-bond directed flower-like structures reported further are mainly discussed the assemblies obtained from non-polar aprotic solvents[36, 37] and there are limited reports on highly ordered flower-like structures from organic small molecules in aqueous media.

In the current chapter, we have demonstrated the formation of flower-like structures through hierarchical arrangement of nanosheets from diaminotriazine appended tetraphenylethylene amphiphiles (**TPE4**) due to self-association in aqueous media. Furthermore, we have attempted the polythymidine assisted ordered reorganisation of **TPE4** amphiphiles through stronger triple H-bonding interactions. The changes in H-bonding pattern in **TPE4/dT$_n$** transformed the assemblies to more extended micrometer sized flower-like structures with high crystalline order. This directional assembly of **TPE4** on polythymidine templates is differentiated from the initial **TPE4** assemblies through AFM, TEM and XRD analysis. Concentration dependent AFM analyses provide more insight into the different morphological pathways for the formation of flower-like structures from **TPE4** and **TPE4/dT$_n$**.

4.3. RESULTS AND DISCUSSION

4.3.1. INTERACTION STUDIES WITH dT_n

Design of diaminotriazine appended TPE derivative (Figure 4.5A) contemplates the idea of nucleobase recognition to generate ordered assemblies in DNA nanostructures. Triethylene glycol chains on both phenyl rings impart hydrophilicity to the molecule and this molecular design prefers to self-assemble in aqueous media, owing to its amphiphilic nature. The synthesis, molecular behaviour and aggregation induced emission characteristics of **TPE4** are already discussed in a previous thesis from our group (synthetic scheme and experimental details adapted from this thesis are also given in "Experimental Section", for the ready reference of the reader).[17] In this Chapter, we are focusing on the polythymidine assisted ordered assemblies of **TPE4** through H-bonding interactions.

4.3.1.1. Spectroscopic analysis

Interaction of **TPE4** amphiphile with dT_n was initially monitored through absorption studies and carried out in 20% THF-PBS with 2mM NaCl. **TPE4** shows typical TPE absorption around 290 nm and 350 nm. **TPE4/dT$_{20}$** hybrid is prepared through a controlled heat-cool process within the temperature range of 10 - 70 ^{o}C. The absorption spectrum of **TPE4/dT$_{20}$** shows significant difference from that of **TPE4** alone and **TPE4** after heat-cool process. As shown in Figure 4.5B, the absorbance shows hypochromism around 350 nm on interaction with dT_{20}, but there are no significant changes in **TPE4** absorption after heat-cool process. Fluorescence emission spectrum of **TPE4** with a λ_{max} at 474 nm, shows an enhanced emission with a slight red shift (λ_{max} = 477 nm) on assembling with dT_{20} as shown in the Figure 4.5C, indicating that TPE rotor get arrested effectively in the hybrid

assembly. The emission enhancement for annealed sample of **TPE4** is very less compared to that of **TPE4/dT$_{20}$** hybrid and is in agreement with the absorption studies.
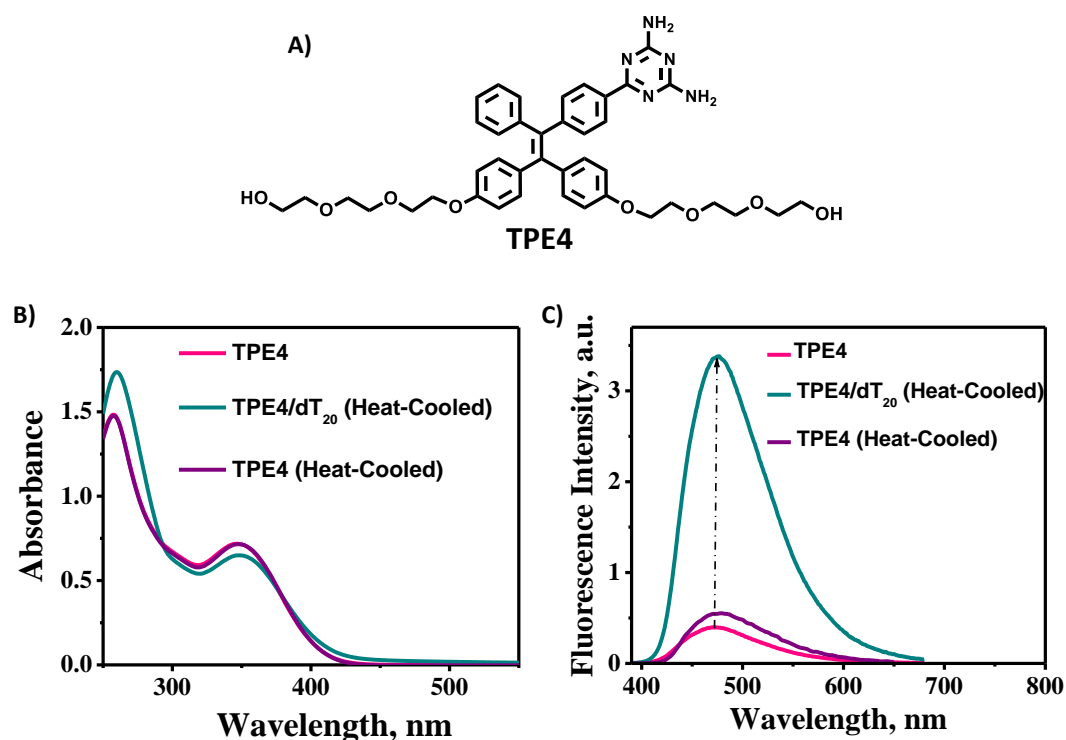
Figure 4.5. A) Molecular structure of **TPE4**; B) Changes in absorption spectra of **TPE4** in 20% THF-PBS, 2 mM NaCl on interaction with dT$_{20}$ after heat-cool and the **TPE4** alone after heat-cool and C) Changes in emission spectra of **TPE4** in 20% THF-PBS, 2 mM NaCl on interaction with dT$_{20}$ after heat-cool and after heat-cool of **TPE4** alone.

4.3.1.2. Morphological analysis

AFM analysis of **TPE4** alone in 20% THF-PBS containing 2 mM NaCl shows the formation of stacked nanosheets (Figure 4.6A). On interaction with dT$_{20}$, **TPE4** forms more extended microflower-like assemblies via ordered stacking of the nanosheets as shown in Figure 4.6B. On the other hand, the heat-cooled sample of **TPE4** forms more extended nanosheets having micrometer lateral dimensions with fewer stacked layers (Figure 4.6C).
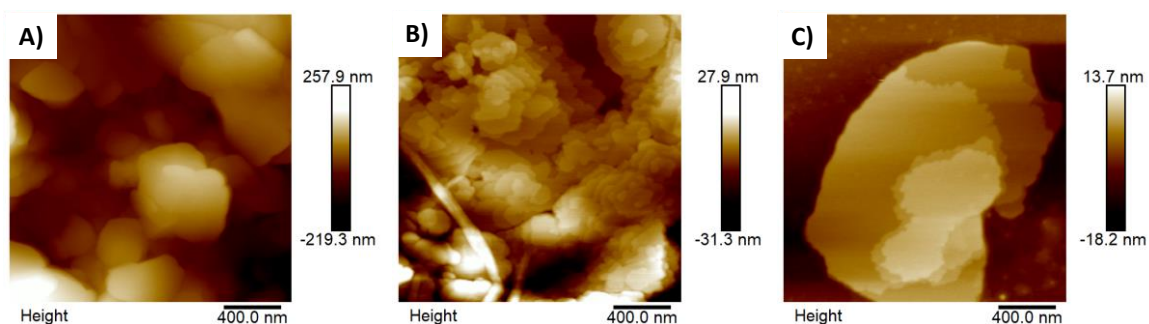
Figure 4.6. AFM images of A) **TPE4**; B) **TPE4/dT$_{20}$** (20 : 1) and C) **TPE4** (Heat-cooled) assemblies in 20% THF-PBS, 2 mM NaCl.

Similarly, TEM analyses also reveal the differential assembly process of **TPE4** and **TPE4/dT$_{20}$** as shown in Figure 4.7. **TPE4** alone shows the presence of stacked nanosheets within 1 μm lateral dimension (Figure 4.7A) and the **TPE4/dT$_{20}$** hybrid shows the formation of more extended flower-like assemblies (Figure 4.7B). The assembled nanosheets in the flower-like structures of **TPE4/dT$_{20}$** hybrids are found to be highly crystalline as evident from the clear lattice fringes in high resolution TEM image and the corresponding FFT pattern (Figure 4.7C), which is not observed in the case of **TPE4** alone assemblies. Moreover, the moderately emissive assemblies of **TPE4** and highly emissive flower-like assemblies of **TPE4/dT$_{20}$** (Figures 4.7D and 4.7E) are distinguished through fluorescence microscopic images, which also confirm the flower-like assembly formation in solution phase itself. Further, the absence and presence of DNA in the respective assemblies of **TPE4** and **TPE4/dT$_{20}$** is confirmed through EDAX analyses, where **TPE4/dT$_{20}$** showed the presence of unique phosphorous peaks corresponding to the phosphate backbone of DNA (Figures 4.8A and 4.8B).
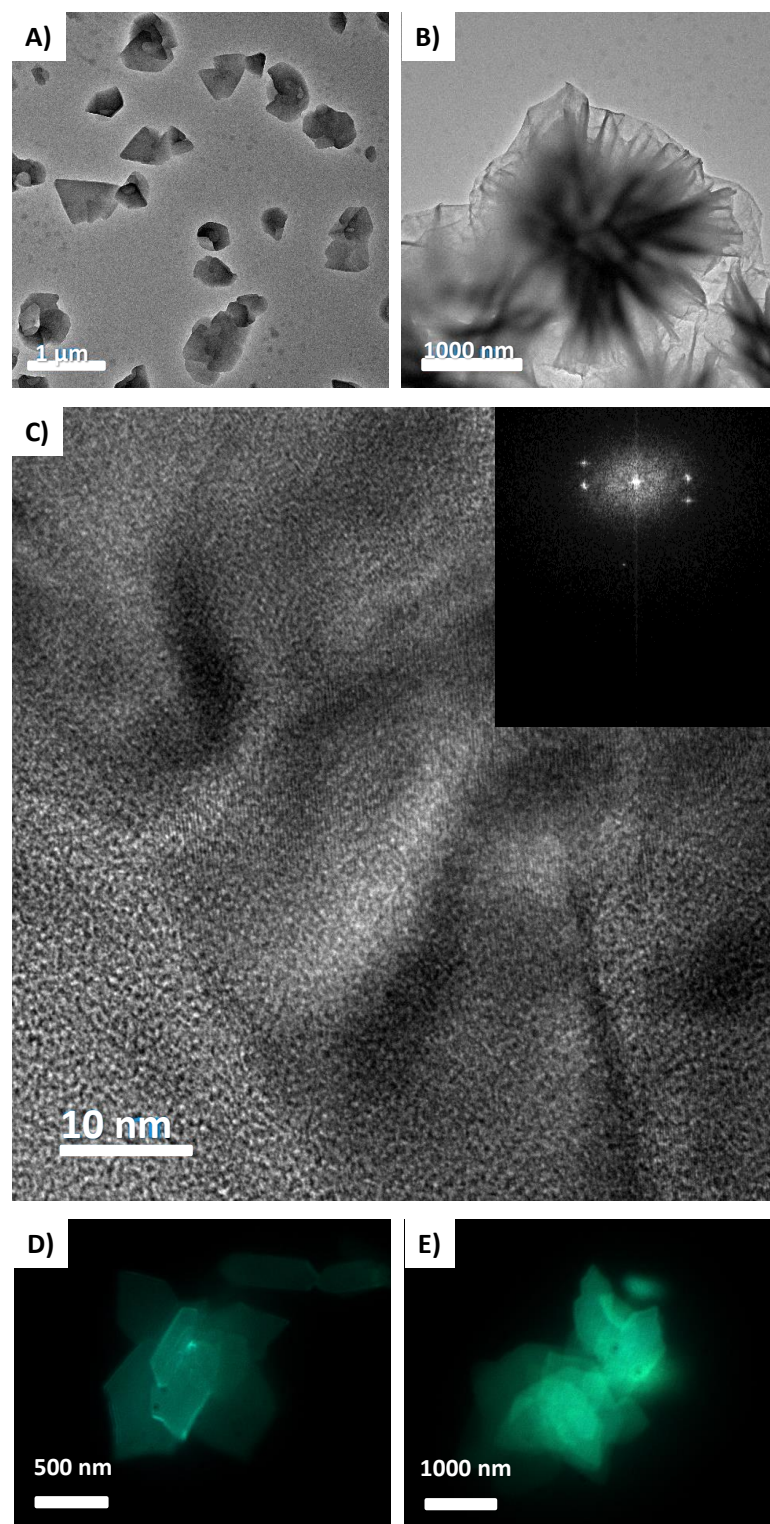
Figure 4.7. TEM images of A) **TPE4** assembly; B) **TPE4/dT$_{20}$** (20:1) assembly in 20% THF-PBS, 2 mM NaCl, C) Magnified TEM image of **TPE4/dT$_{20}$** (20:1) assembly, showing high crystallinity (Inset: Corresponding FFT pattern); D & E) Fluorescence microscopic images of **TPE4** and **TPE4/dT$_{20}$** assembly respectively in 20% THF-PBS, 2 mM NaCl.
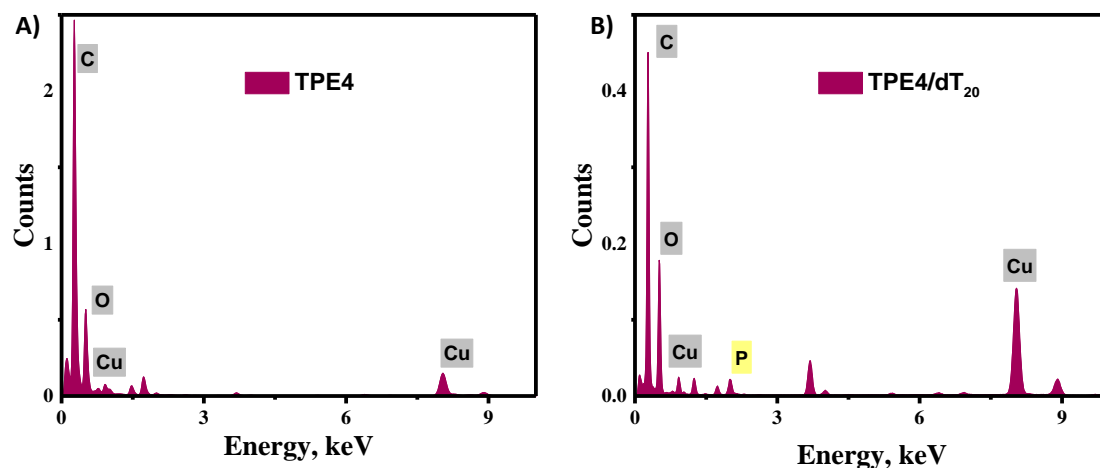
Figure 4.8. EDAX analysis of A) **TPE4** and B) **TPE4/dT$_{20}$** in 20% THF-PBS, 2 mM NaCl

4.3.1.3. XRD analysis

Crystalline nature of these assemblies is further investigated through XRD analyses, which revealed the highly crystalline nature of **TPE4/dT$_{20}$** hybrids compared to both **TPE4** alone and heat-cooled samples of **TPE4** alone.
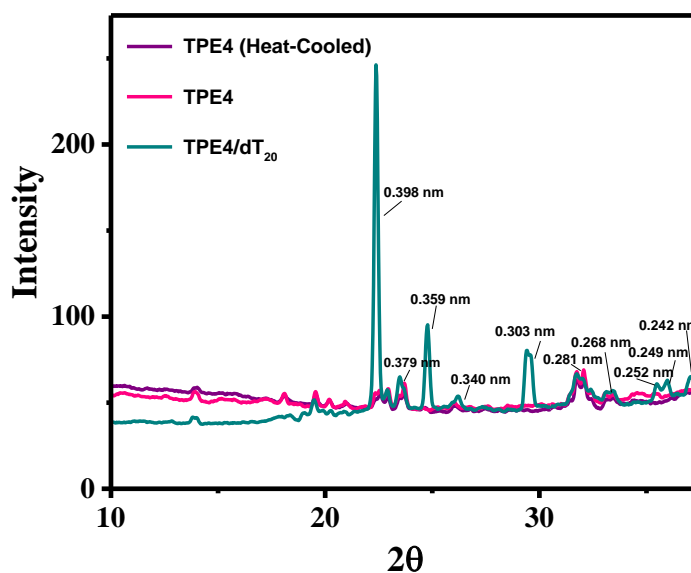
Figure 4.9. XRD spectra of **TPE4** assembly, **TPE4/dT$_{20}$** (20:1) and **TPE4** (Heat-Cooled) in 20% THF-PBS, 2 mM NaCl.

The prominent sharp peaks in **TPE4/dT$_{20}$** hybrids confirm the high crystalline nature of the hybrid assembly compared to that of **TPE4** alone assemblies (Figure 4.9). Besides, the peaks correspond to d-spacing values around 0.2 - 0.3 nm emphasize the role of H-bonding in the assembly processes of **TPE4**.[38] The emergence of new peaks corresponds to d-spacing values of 0.359 nm, 0.303 nm, 0.252 nm, 0.249 nm and 0.242 nm indicate the additional π-π interaction and H-bonding interactions between **TPE4** and thymine nucleobases.[38, 39]

4.3.2. ASSEMBLY PROCESS AND MORPHOLOGICAL PATHWAY

In order to understand the key difference in the assembly processes involved in **TPE4** and **TPE4/dT$_{20}$** assemblies, we have substituted the NaCl salt with MgCl$_2$ salt which might prevent the aggregation to some extent by disturbing the H-bonding interaction[40, 41] and reveal the intermediate steps in the assembly process.

4.3.2.1. Spectroscopic analysis

In order to understand the effect of polythymidine strand length in the assembly process, we have carried out the interaction studies with dT$_{20}$ and dT$_{40}$ strands. Absorption studies show similar results in the case of **TPE4/dT$_{20}$** hybrid in 20% THF-PBS, 1 mM MgCl$_2$ (Figure 4.10A) on comparing with the initial studies with 2 mM NaCl salt. Fluorescence changes are also in agreement with the initial observations. But there is no considerable change observed in **TPE4** absorption and emission on interaction with dT$_{40}$ as shown in Figures 4.10B and 4.10C. In contrast, the CD analysis of **TPE4/dT$_{20}$** and **TPE4/dT$_{40}$** hybrids reveal significant changes in the CD signal compared to that of bare dT$_n$ (Figure 4.10D).
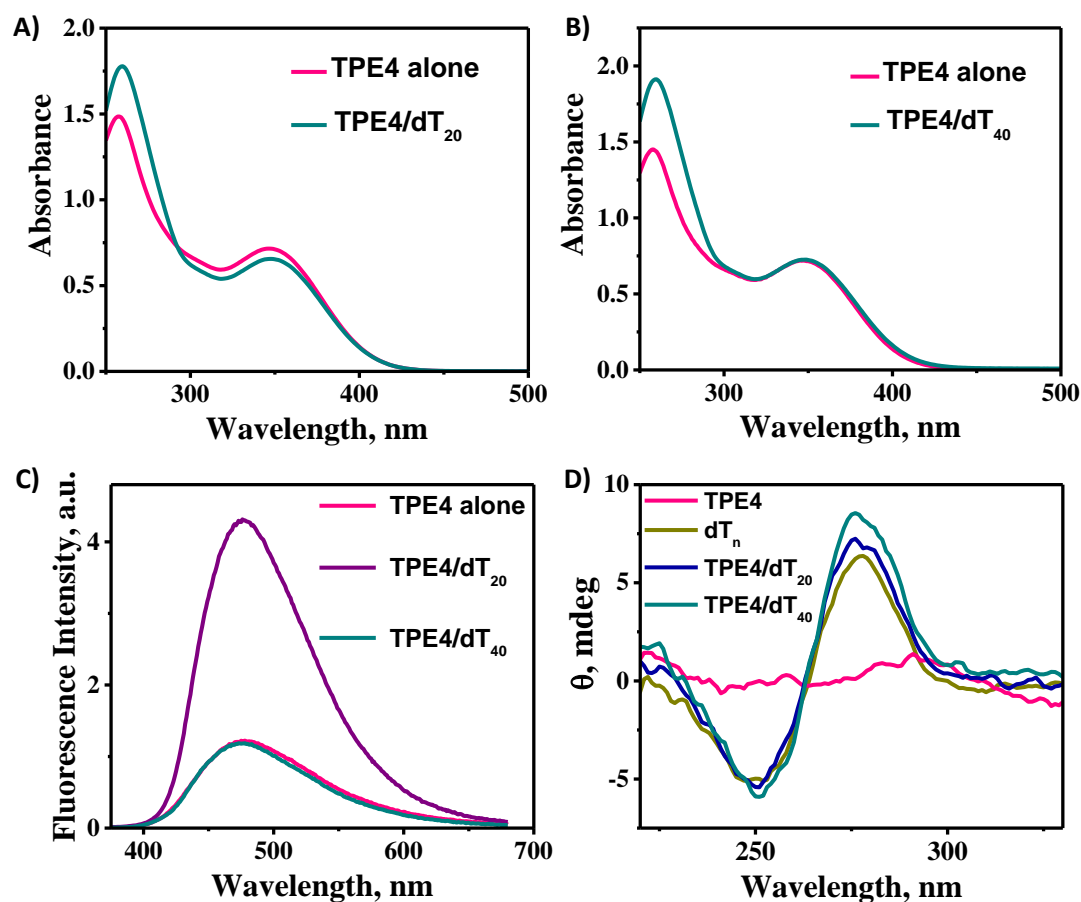
Figure 4.10. Changes in absorption spectra of **TPE4** in 20% THF-PBS with 1 mM MgCl$_2$ on interaction with A) dT$_{20}$ (20:1) and B) dT$_{40}$ (40:1); C) Changes in emission spectra of **TPE4** in 20% THF-PBS, 1 mM MgCl$_2$ on interaction with dT$_{20}$ and dT$_{40}$; D) Changes in the CD signal of dT$_n$ on interaction with **TPE4**.

4.3.2.2. Morphological analysis

AFM analyses of **TPE4** and **TPE4/dT$_{20}$** assemblies provide more insight into the morphological assembly pathways. Figures 4.11A-C and 4.11D-F clearly show each step in the hierarchical assembly of **TPE4** in 20% THF-PBS, 1 mM MgCl$_2$. Nanoribbon-like structures are formed through the lateral association of very long and flexible initially formed 1D structures that eventually undergo lateral winding to form **TPE4** nanosheets. These hierarchically assembled nanosheets further undergo stacking to form flower-like structures. TEM analysis further confirms the lateral

winding of nanoribbon-like structures to form nanosheets (Figures 4.11DG and 4.11H).
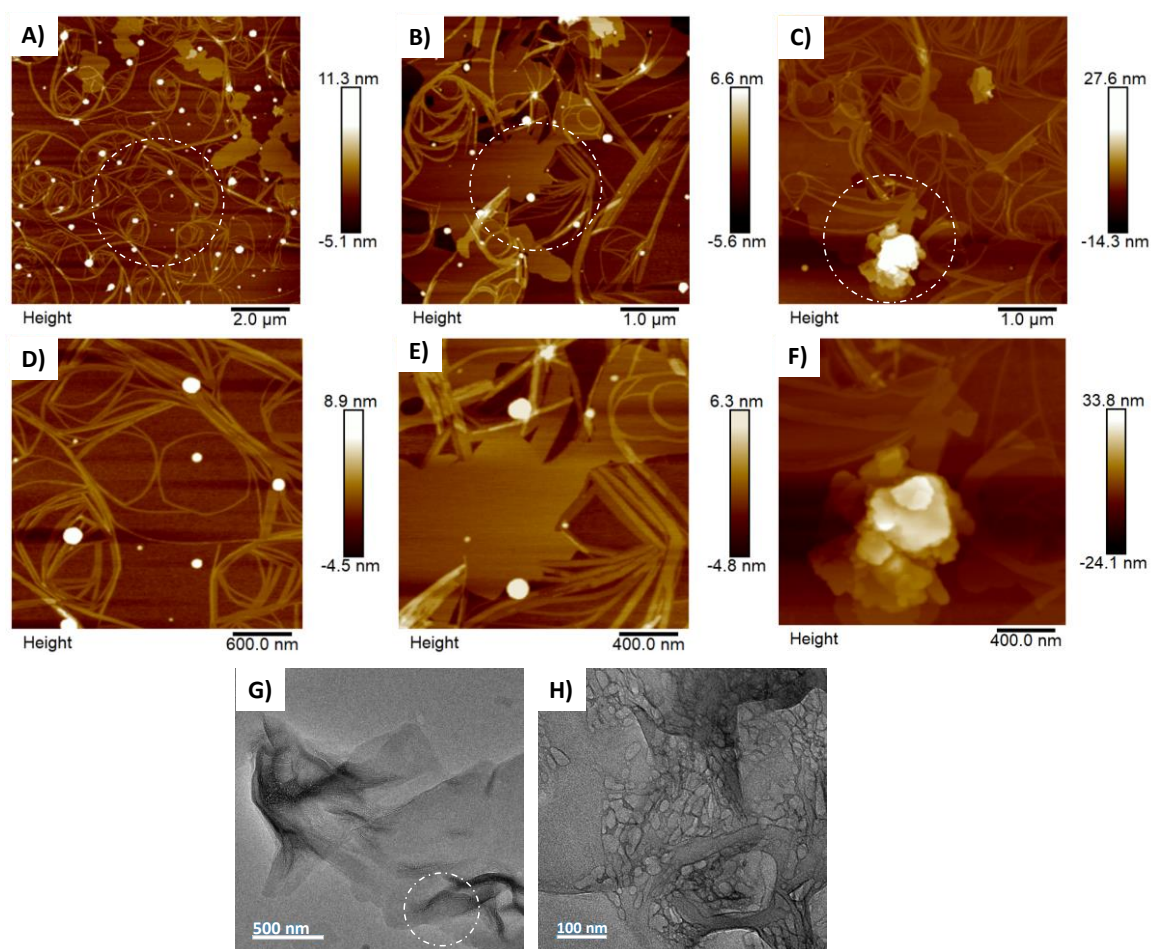
Figure 4.11. A, B & C) AFM images of **TPE4** assembly in 20% THF-PBS, 1 mM $MgCl_2$, showing the formation of nanosheets through lateral winding of ribbon-like structures that eventually forms flower-like assemblies;, D, E & F) Zoomed AFM images of corresponding circled portions. and G & H) Corresponding TEM images.

Morphological analyses of **TPE4/dT$_{20}$** also show the formation of nanosheets and its further stacking. However, the nanosheets are found to be formed through the lateral network formation instead of lateral winding as shown in Figure 4.12A. TEM images also show the formation nanosheet-like morphology from the initial, lateral network structures (Figure 4.12B) and the corresponding SAED pattern reveal the crystalline nature of the hybrid nanosheets (Figure 4.12C). AFM analysis

of **TPE4/dT₄₀**, as shown in Figure 4.12D, which forms more network-like structures and the nanosheets are found to be formed from the network inter-junctions. The observation is further confirmed through TEM analysis (Figures 4.12E and 4.12F) and the magnified TEM image clearly shows the presence of nanonetworks formed from long, rigid 1D structures. The presence of more nanonetwork structures and less formation of nanosheets in **TPE4/dT₄₀** compared to **TPE4/dT₂₀** might be due to the ability of long polythymidine strands to restrict the initial aggregation tendency of **TPE4** molecules and to trigger the template 1D organisation of **TPE4** on long polythymidine strands.
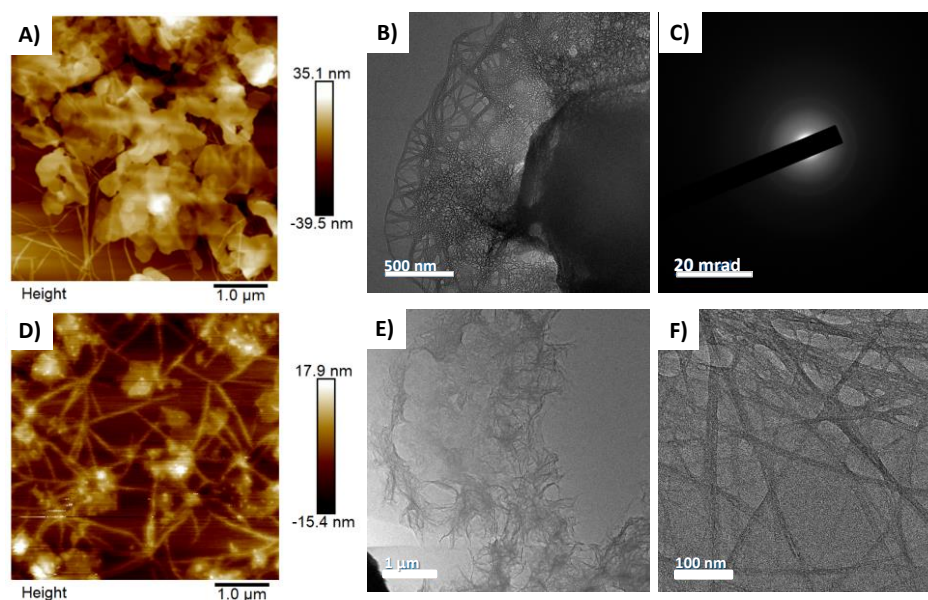
Figure 4.12. A) AFM and B) TEM images of **TPE4/dT₂₀** (20 :1) and C) corresponding SAED pattern; D) AFM, E & F) TEM image and magnified TEM image of **TPE4/dT₄₀** (40 :1).

As a control experiment, we have carried out the morphological analyses of **TPE4/dA₂₀** and **TPE4/dsDNA** in similar conditions. AFM images show the stacked nanosheets that are formed through the lateral association of 1D structures as obvious from Figures 4.13A and 4.13B due to the assembly of **TPE4** alone.
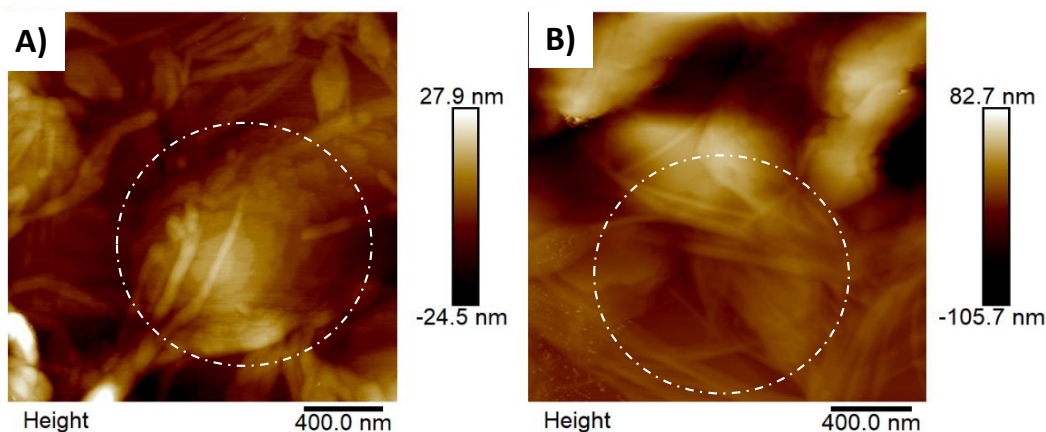
Figure 4.13. AFM images of A) **TPE4/dA$_{20}$** and B) **TPE4/dsDNA** in 20% THF-PBS, 1 mM MgCl$_2$.

4.3.2.3. Concentration dependent studies

In order to confirm the role of polythymidine strands in controlling the self-assembly of **TPE4** and further formation of nanonetwork structures, we have carried out the morphological analysis of **TPE4/dT$_{20}$** hybrids with varying concentration of dT$_{20}$. At a ratio of 20:1, **TPE4/dT$_{20}$** shows the formation of nanosheet-like structures with nanonetwork structures as shown in Figure 4.14A. On the other hand, it shows the formation of more network-like structures and eventual formation of nanosheets from highly interconnected networks with increase in dT$_{20}$ concentration (Figure 4.14B). The morphological results imply that the polythymidine strands prefer to orient the **TPE4** molecules on polythymidine networks in a linearly ordered fashion which further associate laterally to form interconnected networks. Eventually, the highly interconnected network interjunctions get transformed to nanosheet structures which is facilitated by excess **TPE4** molecules in the system.
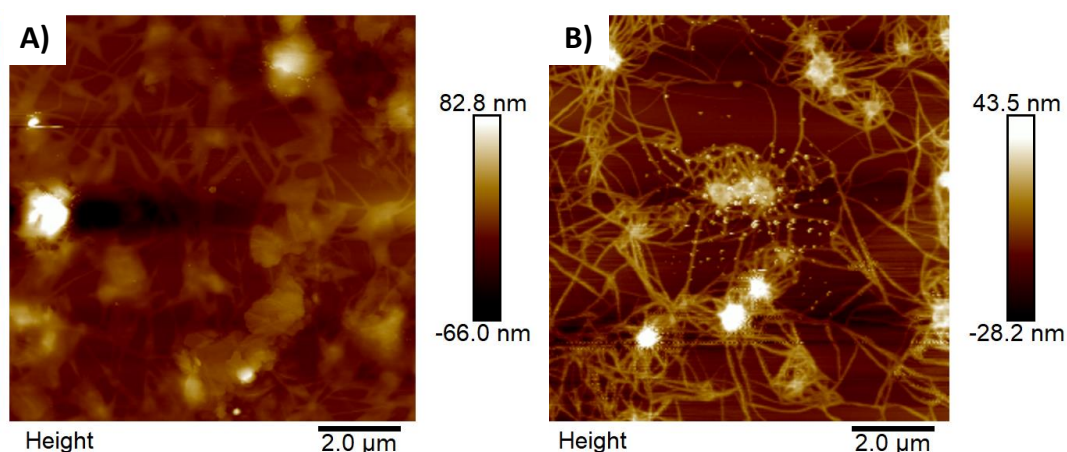
Figure 4.14. AFM images of **TPE4/dT$_{20}$** at various ratios A) 20:1 and B) 20:2.

Further, we have done the morphological studies of **TPE4/dT$_{20}$** with varying concentrations of **TPE4** to validate the above assumption. At higher ratios of **TPE4**, Figure 4.15 clearly shows the lateral association of 1D structures to form long, flexible ribbon-like structures which have a tendency to bend and wind. The tendency for lateral association is getting reduced on decreasing the **TPE4/dT$_{20}$** ratio as shown in Figures 4.15B and 4.15C , and it finally transform to rigid network structures from flexible ribbon-like structures as shown in Figure 4.15D. From these observations, we can conclude that dT$_n$ prevents the initial lateral association of **TPE4** by triggering H-bond directed assembly of **TPE4** on dT$_n$. H-bond directed assembly of **TPE4/dT$_n$** forms 1D structures, which further forms 2D network structures through lateral association of **TPE4** molecules bind to nucleotides through further π-π stacking and van der Waals interactions. Association of excess **TPE4** molecules at the network interjunctions results in the formation of nanosheets and further hierarchical arrangement results in the formation of flower-like structures.
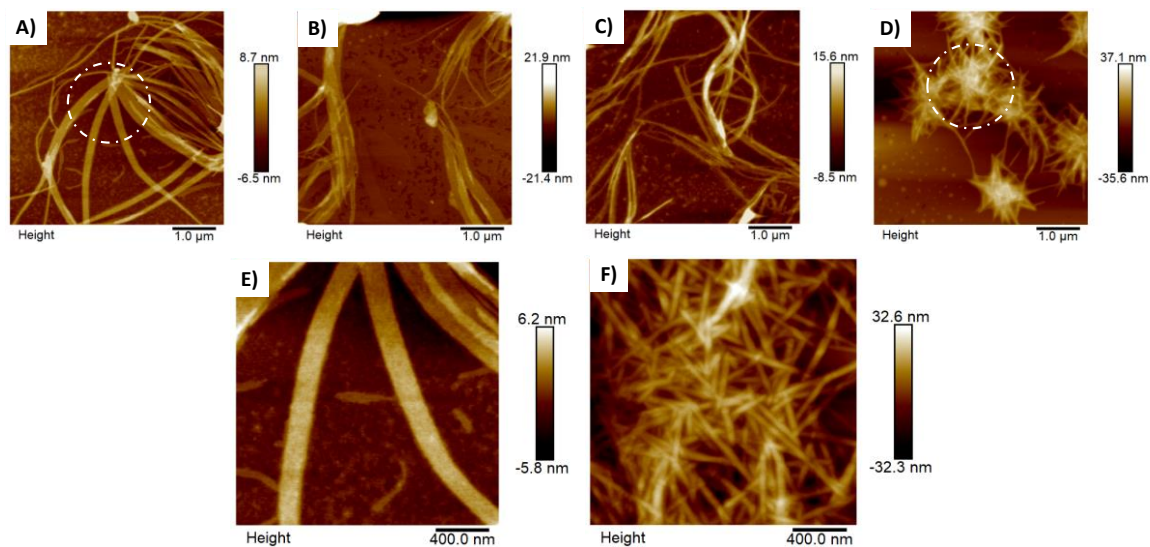
Figure 4.15. AFM images of **TPE4/dT$_{20}$** under various ratios of **TPE4**:dT$_{20}$ A) 30:1, B) 20:1, C) 10:1, D) 2.5:1; Zoomed AFM images of circled portions at **TPE4/dT$_{20}$** ratios of E) 30:1 & F) 2.5:1 in 20% THF-PBS, 1 mM MgCl$_2$

A possible assembly mechanism can be predicted from these results and is shown in Figures 4.16A and 4.16B that include hydrophobic interaction between TPE cores, van der Waals interaction between triethylene glycol chains, intermolecular H-bonding within **TPE4** or between **TPE4** and thymidine units. The delicate balance between these non-covalent interactions brings the molecules together in 20% THF-PBS mixture. The differential assembly processes involved in both **TPE4** assembly and **TPE4/dT$_n$** assembly are mainly based on the hydrophilic - hydrophobic balance in the system and also on nucleobase recognition of diaminotriazine units. In **TPE4** assembly, the 1D structures are initially formed by the hydrophobic interactions within TPE cores in the aqueous media, and it further laterally associates through self-complementary H-bonding within the diaminotriazine units at the surfaces to form ribbon like structures. Further H-bonding interactions and van der Waals interactions promote lateral winding of

these ribbon-like structures to form nanosheets and later stacked to form flower-like structures.
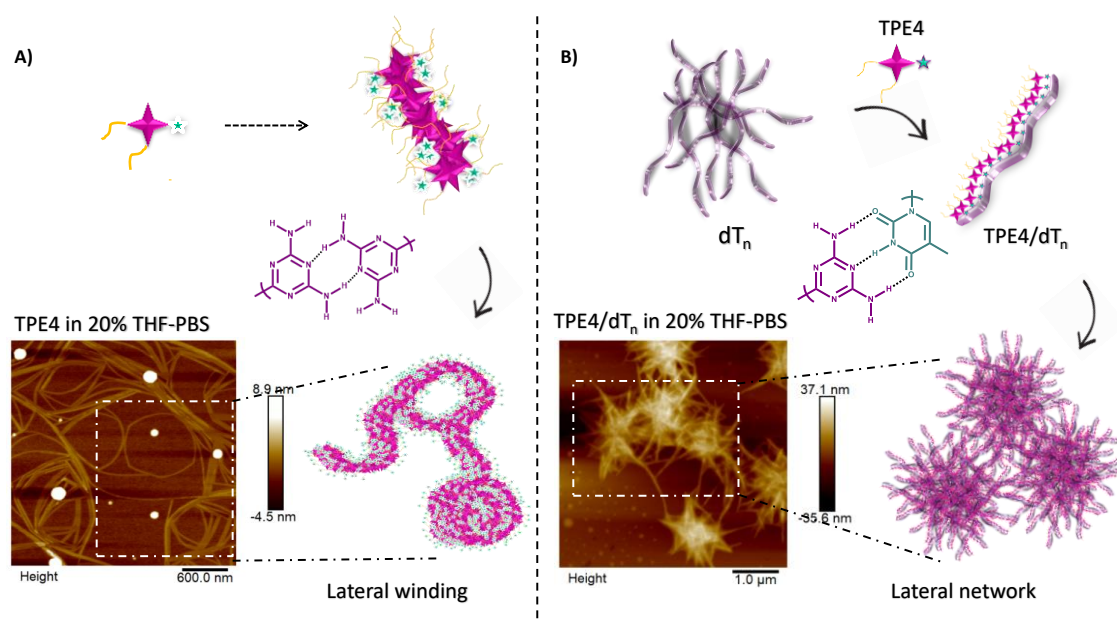
Figure 4.16. Schematic representation of A) **TPE4** assembly, B) **TPE4/dT$_n$** assembly in 20% THF-PBS with the corresponding AFM images showing lateral winding and lateral network formation respectively.

In **TPE4/dT$_n$** assembly, the more effective triple H-bonding interactions between diaminotriazine units and polythymidine strands initially assemble the **TPE4** molecules in an ordered fashion on dT$_n$ templates to form rigid network-like structures and further possible π-π interactions and van der Waals interactions bring **TPE4** molecules together by more interconnections and form nanosheets from the interjunctions. The processes get repeated on top of each nanosheet to form flower-like stacking of nanosheets.

4.4. CONCLUSIONS

In this chapter, we have demonstrated the DNA templated assembly of a diaminotriazine appended TPE derivative with polydeoxythymidine strands. Here, we have utilised the AIE behaviour of TPE and complementary H-bonding

interactions of diaminotriazine and thymine units to form highly emissive, crystalline flower-like structures. The ordered assembly of TPE is achieved in hierarchical flower-like structures by employing the directional H-bonding interaction with polydeoxythymidine templates. The strong and specific triple H-bonding interactions of diaminotriazine and thymine prevent the initial π-π stacking of TPE derivatives in aqueous media. Instead, the polythymidine template helps in the 1D-organisation of TPE derivatives by providing three complementary H-bonding motifs that gradually transform into rigid 2D-network structures through further π-π stacking and van der Waals interactions. The nanosheets formed from these interconnected networks eventually transform into nanosheets, which further stack to form flower-like structures. In conclusion, DNA templated assembly create significant difference in the primary organisation of TPE amphiphiles that in turn affect the entire morphological pathway to promote the growth of highly organised DNA nanostructures.

4.5. EXPERIMENTAL SECTION

4.5.1. MATERIALS AND METHODS

The reagents and solvents were purchased from Sigma-Aldrich, TCI chemicals and Spectrochem chemical suppliers. Synthesis of **TPE4** is achieved through a multi-step synthetic procedure as shown in Scheme 4.1. The 4,4'-(2-(4-bromophenyl)-2-phenylethene-1,1-diyl) diphenol, **(i)** has been synthesized through McMurry coupling using 4,4'-dihydroxybenzophenone and 4-Bromobenzophenone. Subsequent O-alkylation of both hydroxyl groups with 2-(2-(2-bromoethoxy) ethoxy)ethan-1-ol, **(RBr)**yield **(ii)**. Cyanine group has been incorporated in the TPE core by the Bromide to Cyanide conversion using CuCN under reflux condition to yield **(iii)**. Finally, **TPE4**

has been synthesized by the reaction of **(iii)** **with** dicyandiamide and KOH in 2-methoxyethanol. Detailed synthetic procedure of **TPE4** is already reported in a previous thesis.[17]
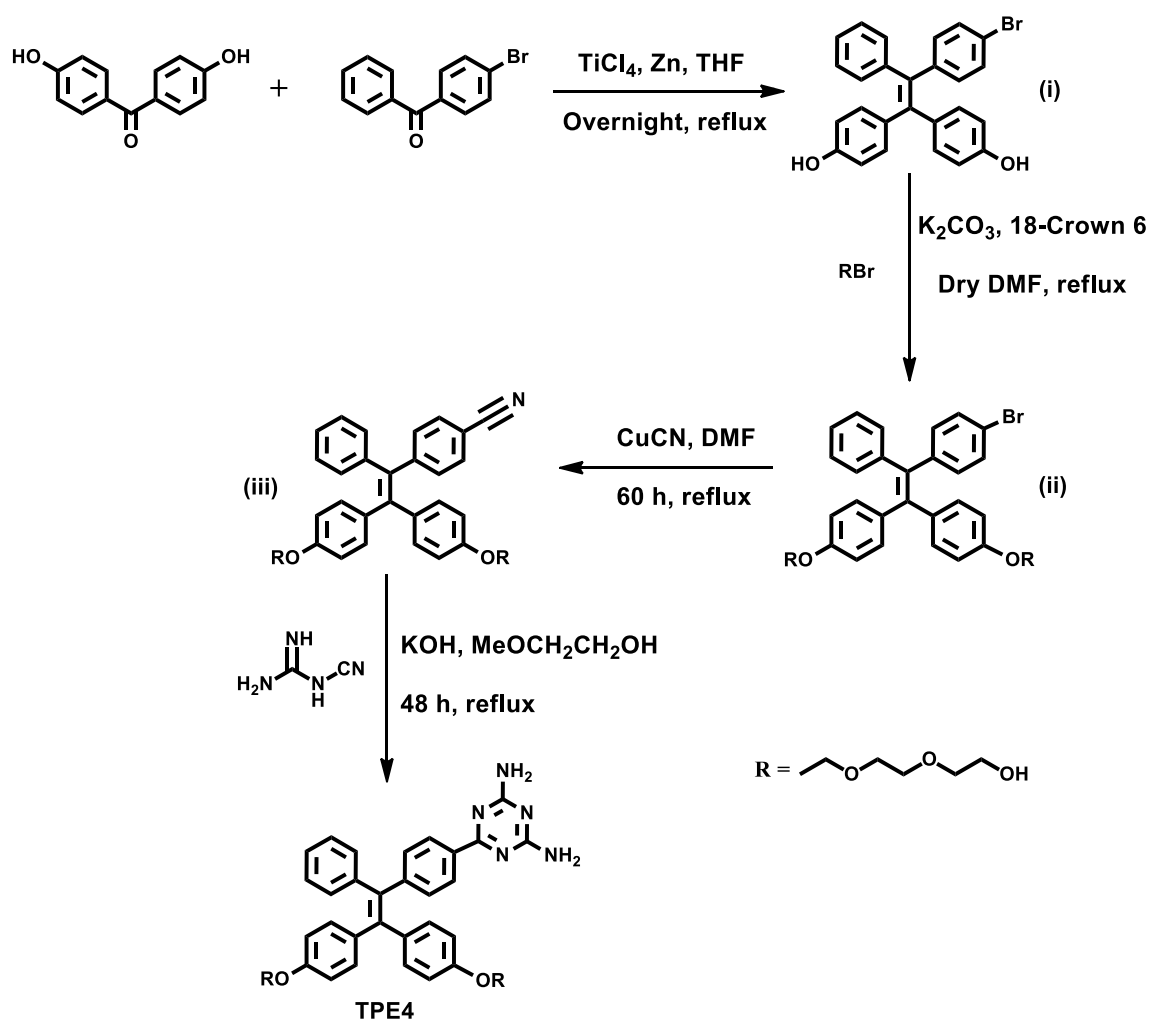
Scheme 4.1. Syntetic scheme of diaminotriazine appended TPE derivative, **TPE4**.

All the experiments have been carried out with 0.5 mM concentration of **TPE4**, unless specified, in 20% THF-PBS with 2 mM NaCl or 1 mM $MgCl_2$ salt. **TPE4/dT$_n$** hybrids were prepared by the addition of required concentration of dT_n to **TPE4** solution and gradual heat-cool process between 70 °C to 10 °C .

4.5.2. SPECTROSCOPIC ANALYSIS

Absorption spectra were monitored with Shimadzu UV-2600 PC UV-Vis spectrophotometer. Emission spectra were recorded using SPEX FLUOROLOG-3 (FL3-221) spectrofluorometer with a slit width of 1.5 at an excitation wavelength of 350 nm. CD analyses were carried out with JASCO J-810 spectropolarimeter having Peltier controlled thermostatic cell holder with an accumulation of 2 and scan speed of 200 nm/min. XRD analyses were performed by XEUSS SAXS/WAXS system using a Genix microsource from Xenocs and the generator was operated at 0.6 mA and 50 kV. FOX2D mirror and two pairs of scatter-less slits from Xenocs were used to collimate the Cu Kα radiation with λ = 1.54 Å. A Mar345 image plate detector and Fit2D software were used to obtain the 2D- WAXS pattern.

4.5.3. MORPHOLOGICAL ANALYSIS

AFM samples were prepared by drop-casting 20 μL of samples to freshly cleaved mica surface. The samples were dried in air overnight and kept in vacuum desiccator prior to analysis. AFM analyses were carried out with a Bruker multimode AFM instrument operating with a tapping mode regime. Micro-fabricated antimony doped Si cantilever tips (Bruker- TESP series) with a resonance frequency of 320 kHz were used. AFM section analysis was performed offline using Nanoscope Analysis 1.5 software. TEM samples were prepared by passing 20 μL of solutions through a carbon-coated Cu grid. HR-TEM analyses were carried out with JEOL JEM-F200 instrument with STEM, EDS and dual EELS at an accelerating voltage of 200 kV. The samples for fluorescence microscopic analyses were dropped on a cleaned glass plate and observed through a Leica DM2500P Optical Microscope equipped with UV

excitation (330-380 nm), violet excitation source (379-420 nm) and DFC 490 camera. All the samples were incubated for 30 minutes prior to drop-casting.

4.6. REFERENCES

1. Watson, J. D.; Crick, F. H. C., Molecular Structure of Nucleic Acids: A Structure for Deoxyribose Nucleic Acid. *Nature* **1953,** *171* (4356), 737-738.

2. Frank-Kamenetskii, M. D.; Mirkin, S. M., Triplex DNA structures. *Annu. Rev. Biochem.* **1995,** *64*, 65-95.

3. Rhodes, D.; Lipps, H. J., G-quadruplexes and their regulatory roles in biology. *Nucleic Acids Res.* **2015,** *43* (18), 8627-8637.

4. Abou Assi, H.; Garavís, M.; González, C.; Damha, M. J., i-Motif DNA: structural features and significance to cell biology. *Nucleic Acids Res.* **2018,** *46* (16), 8038-8056.

5. Cafferty, B. J.; Fialho, D. M.; Khanam, J.; Krishnamurthy, R.; Hud, N. V., Spontaneous formation and base pairing of plausible prebiotic nucleotides in water. *Nat. Commun.* **2016,** *7* (1), 11328.

6. Roy, B.; Bairi, P.; Nandi, A. K., Supramolecular assembly of melamine and its derivatives: nanostructures to functional materials. *RSC Adv.* **2014,** *4* (4), 1708-1734.

7. Zerkowski, J. A.; Seto, C. T.; Whitesides, G. M., Solid-state structures of rosette and crinkled tape motifs derived from the cyanuric acid melamine lattice. *J. Am. Chem. Soc.* **1992,** *114* (13), 5473-5475.

8. Ranganathan, A.; Pedireddi, V. R.; Rao, C. N. R., Hydrothermal Synthesis of Organic Channel Structures: 1:1 Hydrogen-Bonded Adducts of Melamine

with Cyanuric and Trithiocyanuric Acids. *J. Am. Chem. Soc.* **1999,** *121* (8), 1752-1753.

9.   Yi, W.; Bei, W.; Wang, Q. G., Crystal-Structure of Melamine Cyanuric Acid Complex (1-1) Trihydrochloride, Mca3hcl. *J. Cryst. Spectrosc.* **1990,** *20* (1), 79-84.

10.   Zerkowski, J. A.; Macdonald, J. C.; Seto, C. T.; Wierda, D. A.; Whitesides, G. M., Design of Organic Structures in the Solid-State - Molecular Tapes Based on the Network of Hydrogen-Bonds Present in the Cyanuric Acid Melamine Complex. *J. Am. Chem. Soc.* **1994,** *116* (6), 2382-2391.

11.   Seto, C. T.; Whitesides, G. M., Self-Assembly Based on the Cyanuric Acid Melamine Lattice. *J. Am. Chem. Soc.* **1990,** *112* (17), 6409-6411.

12.   Rakotondradany, F.; Palmer, A.; Toader, V.; Chen, B.; Whitehead, M. A.; Sleiman, H. F., Hydrogen-bond self-assembly of DNA-analogues into hexameric rosettes. *Chem. Commun.* **2005,** (43), 5441-5443.

13.   Yagai, S.; Kubota, S.; Unoike, K.; Karatsu, T.; Kitamura, A., Cyanurate-guided self-assembly of a melamine-capped oligo(p-phenylenevinylene). *Chem. Commun.* **2008,** (37), 4466-4468.

14.   Yagai, S.; Kinoshita, T.; Higashi, M.; Kishikawa, K.; Nakanishi, T.; Karatsu, T.; Kitamura, A., Diversification of Self-Organized Architectures in Supramolecular Dye Assemblies. *J. Am. Chem. Soc.* **2007,** *129* (43), 13277-13287.

15.   Yagai, S.; Nakajima, T.; Karatsu, T.; Saitow, K.-i.; Kitamura, A., Phototriggered Self-Assembly of Hydrogen-Bonded Rosette. *J. Am. Chem. Soc.* **2004,** *126* (37), 11500-11508.

16. Janssen, P. G. A.; Vandenbergh, J.; van Dongen, J. L. J.; Meijer, E. W.; Schenning, A. P. H. J., ssDNA Templated Self-Assembly of Chromophores. *J. Am. Chem. Soc.* **2007,** *129* (19), 6078-6079.

17. Ph. D. thesis, DNA-interactions, self-assembly and photophysical properties of DNA three-way junction templated fluorescent silver nanoclusters and functional tetraphenylethylene derivatives, Sajena K. S.; supervised by Dr. Joshy Joseph; University/Institute: Academy of Scientific and Innovative Research (AcSIR), work done at CSIR-NIIST, Trivandrum;

    http://www.vigyangranth.in/getThesisDetails?id=34729.

18. Sessler, J. L.; Wang, R., Self-Assembly of an "Artificial Dinucleotide Duplex". *J. Am. Chem. Soc.* **1996,** *118* (40), 9808-9809.

19. Schall, O. F.; Gokel, G. W., Molecular Boxes Derived from Crown Ethers and Nucleotide Bases: Probes for Hoogsteen vs Watson-Crick H-Bonding and Other Base-Base Interactions in Self-Assembly Processes. *J. Am. Chem. Soc.* **1994,** *116* (14), 6089-6100.

20. Sessler, J. L.; Wang, R., A New Base-Pairing Motif Based on Modified Guanosines. *Angew. Chem. Int. Ed.* **1998,** *37* (12), 1726-1729.

21. Li, C.; Cafferty, B. J.; Karunakaran, S. C.; Schuster, G. B.; Hud, N. V., Formation of supramolecular assemblies and liquid crystals by purine nucleobases and cyanuric acid in water: implications for the possible origins of RNA. *Phys. Chem. Chem. Phys.* **2016,** *18* (30), 20091-20096.

22. Iwaura, R.; Hoeben, F. J. M.; Masuda, M.; Schenning, A. P. H. J.; Meijer, E. W.; Shimizu, T., Molecular-Level Helical Stack of a Nucleotide-Appended Oligo(p-phenylenevinylene) Directed by Supramolecular Self-Assembly with a

Complementary Oligonucleotide as a Template. *J. Am. Chem. Soc.* **2006,** *128* (40), 13298-13304.

23. Sessler, J. L.; Jayawickramarajah, J., Functionalized base-pairs: versatile scaffolds for self-assembly. *Chem. Commun.* **2005,** (15), 1939-1949.

24. Iwaura, R.; Yoshida, K.; Masuda, M.; Ohnishi-Kameyama, M.; Yoshida, M.; Shimizu, T., Oligonucleotide-Templated Self-Assembly of Nucleotide Bolaamphiphiles: DNA-Like Nanofibers Edged by a Double-Helical Arrangement of A–T Base Pairs. *Angew. Chem. Int. Ed.* **2003,** *42* (9), 1009-1012.

25. Janssen, P. G. A.; Jabbari-Farouji, S.; Surin, M.; Vila, X.; Gielen, J. C.; de Greef, T. F. A.; Vos, M. R. J.; Bomans, P. H. H.; Sommerdijk, N. A. J. M.; Christianen, P. C. M.; Leclère, P.; Lazzaroni, R.; van der Schoot, P.; Meijer, E. W.; Schenning, A. P. H. J., Insights into Templated Supramolecular Polymerization: Binding of Naphthalene Derivatives to ssDNA Templates of Different Lengths. *J. Am. Chem. Soc.* **2009,** *131* (3), 1222-1231.

26. Avakyan, N.; Greschner, A. A.; Aldaye, F.; Serpell, C. J.; Toader, V.; Petitjean, A.; Sleiman, H. F., Reprogramming the assembly of unmodified DNA with a small molecule. *Nat. Chem* **2016,** *8* (4), 368-376.

27. Li, Q.; Zhao, J.; Liu, L.; Jonchhe, S.; Rizzuto, F. J.; Mandal, S.; He, H.; Wei, S.; Sleiman, H. F.; Mao, H.; Mao, C., A poly(thymine)–melamine duplex for the assembly of DNA nanomaterials. *Nat. Mater.* **2020,** *19* (9), 1012-1018.

28. Hu, R.; Zhang, X.; Zhao, Z.; Zhu, G.; Chen, T.; Fu, T.; Tan, W., DNA nanoflowers for multiplexed cellular imaging and traceable targeted drug delivery. *Angew. Chem. Int. Ed.* **2014,** *53* (23), 5821-6.

29. Zhao, H.; Guo, X.; He, S.; Zeng, X.; Zhou, X.; Zhang, C.; Hu, J.; Wu, X.; Xing, Z.; Chu, L.; He, Y.; Chen, Q., Complex self-assembly of pyrimido[4,5-d]pyrimidine nucleoside supramolecular structures. *Nat. Commun.* **2014,** *5* (1), 3108.

30. Nakanishi, T.; Michinobu, T.; Yoshida, K.; Shirahata, N.; Ariga, K.; Möhwald, H.; Kurth, D. G., Nanocarbon Superhydrophobic Surfaces created from Fullerene-Based Hierarchical Supramolecular Assemblies. *Adv.Mater.* **2008,** *20* (3), 443-446.

31. Wang, L.; Zhou, Y.; Yan, J.; Wang, J.; Pei, J.; Cao, Y., Organic Supernanostructures Self-Assembled via Solution Process for Explosive Detection. *Langmuir* **2009,** *25* (3), 1306-1310.

32. Zhu, G.; Hu, R.; Zhao, Z.; Chen, Z.; Zhang, X.; Tan, W., Noncanonical Self-Assembly of Multifunctional DNA Nanoflowers for Biomedical Applications. *J. Am. Chem. Soc.* **2013,** *135* (44), 16438-16445.

33. Nakanishi, T.; Ariga, K.; Michinobu, T.; Yoshida, K.; Takahashi, H.; Teranishi, T.; Möhwald, H.; G. Kurth, D., Flower-Shaped Supramolecular Assemblies: Hierarchical Organization of a Fullerene Bearing Long Aliphatic Chains. *Small* **2007,** *3* (12), 2019-2023.

34. Bhosale, R. S.; Al Kobaisi, M.; Bhosale, S. V.; Bhargava, S.; Bhosale, S. V., Flower-like supramolecular self-assembly of phosphonic acid appended naphthalene diimide and melamine. *Sci. Rep.* **2015,** *5* (1), 14609.

35. Salimimarand, M.; La, D. D.; Kobaisi, M. A.; Bhosale, S. V., Flower-like superstructures of AIE-active tetraphenylethylene through solvophobic controlled self-assembly. *Sci. Rep.* **2017,** *7* (1), 42898.

36. Zhang, X.; Nakanishi, T.; Ogawa, T.; Saeki, A.; Seki, S.; Shen, Y.; Yamauchi, Y.; Takeuchi, M., Flowerlike supramolecular architectures assembled from C60

equipped with a pyridine substituent. *Chem. Commun.* **2010,** *46* (46), 8752-8754.

37. Nakanishi, T.; Shen, Y.; Wang, J.; Li, H.; Fernandes, P.; Yoshida, K.; Yagai, S.; Takeuchi, M.; Ariga, K.; Kurth, D. G.; Möhwald, H., Superstructures and superhydrophobic property in hierarchical organized architectures of fullerenes bearing long alkyl tails. *J. Mater. Chem.* **2010,** *20* (7), 1253-1260.

38. Pan, M.-Y.; Hang, W.; Zhao, X.-J.; Zhao, H.; Deng, P.-C.; Xing, Z.-H.; Qing, Y.; He, Y., Janus-type AT nucleosides: synthesis, solid and solution state structures. *Org. Biomol. Chem.* **2011,** *9* (16), 5692-5702.

39. Fonseca Guerra, C.; Bickelhaupt, F. M.; Snijders, J. G.; Baerends, E. J., Hydrogen Bonding in DNA Base Pairs: Reconciliation of Theory and Experiment. *J. Am. Chem. Soc.* **2000,** *122* (17), 4117-4128.

40. Morris, D. L., DNA-bound metal ions: recent developments. *Biomol. Concepts* **2014,** *5* (5), 397-407.

41. Every, A. E.; Russu, I. M., Influence of Magnesium Ions on Spontaneous Opening of DNA Base Pairs. *J. Phys. Chem. B* **2008,** *112* (47), 15261-15261.

ABSTRACT

DNA nanotechnology prevails in engineering functional nanostructures through DNA origami, DNA tile assembly and assembly of DNA amphiphiles. These current technologies rely on the design, synthesis and self-assembly of synthetic and modified oligonucleotides which make it highly expensive and restrict the large scale production of DNA nanostructures. Thus, generation of long-range ordered, functional DNA nanostructures from random, unmodified oligonucleotides is more desirable. In the **First Chapter**, we give a brief introduction on supramolecular assembly strategies and supramolecular DNA assemblies with a general introduction on DNA nanotechnology. Moreover, the chapter discusses the key challenges in this area and highlights the major objectives of the present thesis.

The long range ordered arrangements of functional moieties with nanoscale precision is highly recommended in various optoelectronic applications and is often achieved through various physico-chemical methods. Supramolecular assembly is recognised as a better strategy to achieve precise organization of materials with good programmability. The unique structure of DNA make it a versatile tool in supramolecular assembly for the organisation of small organic molecules, nanoparticles etc. and is made possible through different DNA binding possibilities such as phosphodiester recognition, nucleobase recognition, intercalation, and major and minor groove binding interactions. In the **Second Chapter**, we have utilised electrostatic interactions between the cationic side chain of the amphiphilic fullerene derivative, **FPy** and anionic DNA as a general strategy to make ordered fullerene/DNA nanostructures. The addressability of such nanostructures were demonstrated by incorporating a fluorophore labelled oligonucleotide, which undergo efficient fluorescence quenching via electron transfer between the fluorophore and fullerene units in the assembly (**Chapter 2A**). Further, the generality of this approach was demonstrated in **Chapter 2B** using an anionic polymer, **PSS** which also form ordered nanostructures via electrostatic interactions and exhibit better electron transport properties.

In the **Third Chapter**, the DNA intercalative binding of aniline moiety is employed for the ordered assembly of TPE derivatives (**TPE1**, **TPE2** and **TPE3**) by the suitable design of aniline appended TPE amphiphiles. The hierarchical assembly and DNA assisted reassembly of TPE amphiphiles were investigated in detail and the directional assembly is achieved through the specific binding of aniline appended TPE amphiphiles to DNA. DNA plays a key role in the reassembly process as it alters the hydrophilic-hydrophobic balance in the system. The crystallinity of these TPE assemblies can be modulated appropriately through suitable choice of aqueous media, short or long dsDNAs or by heat-cool process, without significant changes in the ultimate morphology of the assemblies.

In the **Fourth Chapter**, we have demonstrated the DNA templated assembly of a diaminotriazine appended TPE derivative (**TPE4**) with polydeoxythymidine strands by engaging the complementary H-bonding motifs. Ordered assembly of TPE is achieved in hierarchical flower-like structures of **TPE4** by employing the directional H-bonding interaction with polydeoxythymidine templates. The specific H-bonding interactions of diaminotriazine and thymine prevent the initial lateral association of **TPE4** and formation of ribbon-like structures. Instead, the template help in 1D-organisation of **TPE4** which eventually transform into 2D- network structures. This significant difference in the primary organisation of TPE amphiphiles is reflected in the crystallinity of final hierarchical structures and is achieved through the DNA templated assembly involving complementary H-bonding interactions. In summary, we have put forward simple strategies to make DNA nanostructures by the mutually assisted assembly of DNA and small amphiphiles via non-covalent approaches. These strategies make use of the inherent tendency of the amphiphiles to assemble in aqueous media, directed by the unique structural characteristics of DNA. These simple strategies to organise suitably designed small amphiphilic molecules with DNA can significantly contribute to the emerging field of DNA nanotechnology.

List of Publications Emanating from the Thesis

1. **Anjali Bindu Ramesan**, Sandeepa K. Vittala and Joshy Joseph*, DNA condensation and formation of ultrathin nanosheets via DNA assisted self-assembly of an amphiphilic fullerene derivative. *Journal of Photochemistry and Photobiology B: Biology* **2022**, 226, 112352.

2. **Anjali Bindu Ramesan**, Sandeepa K. V., Vibhu Darshan, Dr. K. N. Narayanan Unni* & Dr. Joshy Joseph*, Polymer Assisted Ordered Assembly of Fullerene on Fullerene/Polymer Hybrid with Enhanced Electron Transporting properties (Manuscript under preparation).

3. **Anjali Bindu Ramesan** and Joshy Joseph*, DNA assisted reassembly of tetraphenylethylene amphiphiles to two dimensional crystalline nanostructures in aqueous media (Manuscript under preparation).

List of Publications from Other Related Works

1. Sandeepa K. Vittala, Sajena K. Saraswathi, **Anjali Bindu Ramesan**, and Joshy Joseph*, Nanosheets and 2D-Nanonetworks by Mutually Assisted Self-Assembly of Fullerene Clusters and DNA Three-way Junctions. *Nanoscale adv.*, **2019**, 1, 4158-4165.

Book Chapter

1. **Ramesan, A. B.;** Joseph, J., Chapter 16: Fluorescence-based biosensors for SARS-CoV-2 viral infection diagnostics In *Advanced Biosensors for Virus Detection: Smart Diagnostics to Combat SARS-CoV-2*, Khan, R.; Parihar, A.; Kaushik, A.; Kumar, A., Eds. Academic Press - Elsevier: **2022**.

List of Posters and Papers Presented in Conferences

1. Formation of Ultrathin nanosheets via DNA assisted assembly of amphiphilic fullerene derivative, **Anjali B. R.**, Sandeepa K.V. and Dr. Joshy Joseph. **Paper** pesented for EFCS 2021 at Farook College, Kozhikode, October 29-31. (Received **Best Oral Presentation** Award)

2. Fullerene/Polymer hybrid materials with enhanced electron transporting properties, **Anjali B.R.**, Sandeepa K.V., Vibhu Darshan, K.N. Narayanan Unni and Joshy Joseph. **Poster** presented for National Conference on Recent trends in Materials Science and Technology (NCMST-2020) through Zoom online platform, December 7-9. (Received **Best Poster Presentation** Award)

3. Mutually assisted assembly of fullerene amphiphiles and DNA into nanosheets and DNA-fullerene condensates., **Anjali B.R.**, Sandeepa K.V. and Joshy Joseph. **Paper** presented for NCMST 2019 at IISER, Thiruvananthapuram, December 8.

4. Mutually assisted assembly of fullerene amphiphiles and DNA into nanosheets and DNA-fullerene condensates, **Anjali B.R.**, Sandeepa K.V. and Joshy Joseph. **Poster** presented for ICAFM 2019 at CSIR-NIIST, Thiruvananthapuram, December 10.

5. Mutually assisted assembly of fullerene amphiphiles and DNA into nanosheets and DNA-fullerene condensates., **Anjali B.R.**, Sandeepa K.V. and Joshy Joseph. **Poster** presented for ICEM-14, 2020 at CSIR-NIIST, Thiruvananthapuram, February 7.

6. DNA-Fullerene condensates: A New strategy for ordered self-assembly of amphiphilic fullerenes, **Anjali B.R.**, Sandeepa K.V. and Joshy Joseph. **Poster** presented for Polymer Conference for Young Researchers, 2018 (PCYR'18) at CSIR-NIIST, Thiruvananthapuram, November 17.

7. Ordered assembly of Fullerene Amphiphiles through DNA Condensation, **Anjali B.R.**, Sandeepa K.V. and Joshy Joseph. Poster Presentation at Kerala Science congress 2019 at Fatima Mata National College, Kollam, February 2-3.

8. DNA Assisted Ordered Self-Assembly of Amphiphilic Fullerenes to Nanosheets, **Anjali B.R.**, Sandeepa K.V. and Joshy Joseph. Poster Presentation at MATCON 2019 at CUSAT, Kochi, March 14-16.
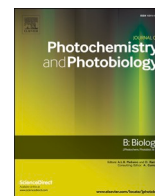
DNA condensation and formation of ultrathin nanosheets via DNA assisted self-assembly of an amphiphilic fullerene derivative

Anjali Bindu Ramesan [a,b], Sandeepa Kulala Vittala [a,b], Joshy Joseph [a,b,*]

[a] *Photosciences and Photonics Section, CSIR-National Institute for Interdisciplinary Science and Technology, Thiruvananthapuram 695 019, India*
[b] *Academy of Scientific and Innovative Research (AcSIR), Ghaziabad 201002, India*

A B S T R A C T

DNA nanotechnology propose various assembly strategies to develop novel functional nanostructures utilizing unique interactions of DNA with small molecules, nanoparticles, polymers, and other biomolecules. Although, well defined nanostructures of DNA and amphiphilic small molecules were achieved through hybridization of covalently modified DNA, attaining precise organization of functional moieties through non-covalent interactions remain as a challenging task. Herein, we report mutually assisted assembly of an amphiphilic fullerene derivative and various DNA structures through non-covalent interactions, which leads to initial DNA condensation and subsequent assembly yielding ordered fullerene-DNA nanosheets. The molecular design of the cationic, amphiphilic fullerene derivative (**FPy**) ensures molecular solubility in the 10% DMSO-PBS buffer system and facile interactions with DNA through groove binding and electrostatic interactions of fullerene moiety and positively charged pyridinium moiety, respectively. The formation of **FPy**/DNA nanostructures were thoroughly investigated in the presence of λ-DNA, pBR322 plasmid DNA, and single and double stranded 20-mer oligonucleotides using UV–visible spectroscopy, AFM and TEM analysis. λ-DNA and pBR322 plasmid DNA readily condense in presence of **FPy** leading to micrometer sized few layer nanosheets with significant crystallinity due to ordered arrangement of fullerenes. Similarly, single and double stranded 20-mer oligonucleotides also interact efficiently with **FPy** and form highly crystalline nanosheets, signifying the role of electrostatic interaction and subsequent charge neutralization in the condensation triggered assembly. However, there is significant differences in the crystallinity and ordered arrangements of fullerenes between these two cases, where longer DNA form condensed structures and less ordered nanosheets while short oligonucleotides lead to more ordered and highly crystalline nanosheets, which could be attributed to the differential DNA condensation. Finally, we have demonstrated the addressability of the assembly using a cyanine modified single strand DNA, which also forms highly crystalline nanosheets and exhibit efficient quenching of the cyanine fluorescence upon self-assembly. These results open up new prospects in the development of functional DNA nanostructures through non-covalent interactions and hence have potential applications in the context of DNA nanotechnology.

1. Introduction

The exciting molecular design of DNA provides room for various sorts of non-covalent molecular interactions such as electrostatic, π-π stacking, hydrophobic interactions etc. Scientific community inquisitively focuses on non-covalent interactions which can alter the secondary and tertiary structures of DNA to make functional DNA nanoarchitectures [1,2]. Unique organization of DNA in nucleosome core particle exists as an inspiring model for the researchers to inquire more into the possible DNA nanostructures [3,4]. Centimeter long DNAs

are closely packed in the micrometer sized nucleosome core particle with the assistance of positively charged histone proteins through electrostatic interaction and is termed as DNA condensation [5]. Cationic lipids [6], polymers [7,8], dendrimers [9], dendrons [10], nanoparticles [11] etc. have been employed for effective DNA condensation and these condensates find applications in templated nanostructure synthesis [12], gene delivery [4,13–15] etc.

The wide opportunities extended by the unique DNA structure have been explored since the emergence of DNA nanotechnology as proposed by Nadrian. C. Seeman [16]. The technology, mainly rely on DNA
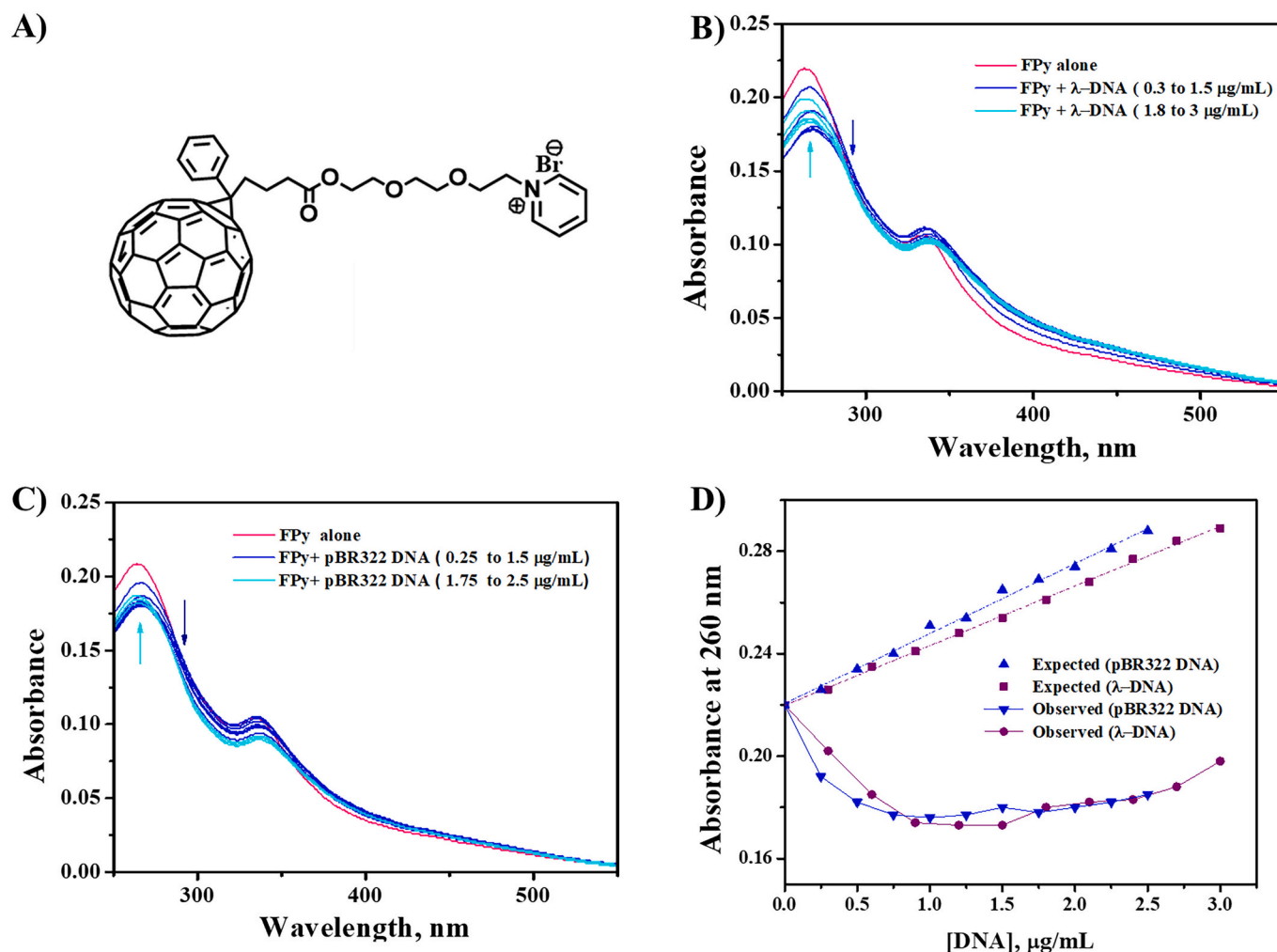
Fig. 1. A) Structure of **FPy**, consisting of cationic pyridinium moiety covalently linked to fullerene through triethylene glycol linkage, which can electrostatically interact with the negatively charged phosphate backbone of DNA, leading to charge neutralization and subsequent DNA condensation; **B)** & **C)** Change in absorption spectra of **FPy** (3 μM) in 10% DMSO-PBS (pH 7.4) with increasing concentration of λ-DNA and pBR322 DNA, respectively. The arrows show the trend of 260 nm absorption with the addition of DNAs in two different concentration ranges; and **D)** Absorption changes at 260 nm in the presence and absence of **FPy** with increasing concentration of λ-DNA and pBR322 DNA. Expected values are sum of absorbance values corresponding to **FPy** and added DNA.

hybridization based assemblies such as tile assembly and DNA origami, contributes well in the field of nanomedicine [17–19] and nano-electronics [20–22]. Small molecule based templated assemblies have emerged in this field to generate functional DNA nanoarchitectures through the co-assembly of suitably designed small functional molecules and DNA, utilizing the benefits of base pairing and other directional and non-directional interactions like π-π stacking, host-guest complexation, electrostatic interactions etc. [23–25] Apart from these initial approaches, an advanced design strategy has been evolved by the amphi-philicity driven self-assembly of DNA amphiphiles with the covalent modification of DNA strands [26–28]. Li and co-workers introduced another approach, a co-ordination driven self-assembly process for the synthesis of DNA nanomaterials with high scalability, tunability and functionality [29]. Even though these methods provide better precision and fine tunability, the materials and methods involved in DNA nano-technology are highly demanding and expensive. Thus, the search for more facile strategies based on directional and non-directional non-co-valent interactions are in progress. For example, Li et al showed self-assembly of poly (T) strands with the help of directional, non-covalent interactions between thymine nucleosides and melamine monomers leading to higly ordered structures with strong mechanical and tunable thermal stabilities [30]. We have reported a non-covalent approach involving non-directional interactions for the formation of

semiconducting DNA nanowires from random, unmodified duplex strands using fullerene nanoclusters as stapler motifs [31]. However, the design of precisely organized functional DNA nanoarchitectures, exclusively involving non-directional interactions is challenging, but highly desirable.

Long range, ordered assembly of chromophores, often achieved through the templated assemblies based on DNA, peptides, polymers, dendrimers etc., outshine the performance of conventional materials in the field of optoelectronics and photovoltaics [32–35]. Among these templates, DNA particularly take advantage of distinct binding possi-bilities such as electrostatic interactions with the phosphate backbone, major/minor groove binding and intercalation provided by its unique structural features [36–38]. Precise ordering in the DNA nanostructure is attained by the action of specific directional interactions such as hydrogen bonding and often require the use of artificial building blocks of DNA [39,40]. Meanwhile, the ordered templated assembly of small functional molecule is less attempted on the basis of non-directional intermolecular interactions like electrostatic interactions. In 2005, Cheng and coworkers achieved the formation of well-ordered fullerene arrays on DNA scaffolds from tile assembly, through the electrostatic interaction of positively charged fullerene molecules and DNA phos-phate backbone. But, it also demands the precise design of DNA scaffolds through directional interactions.
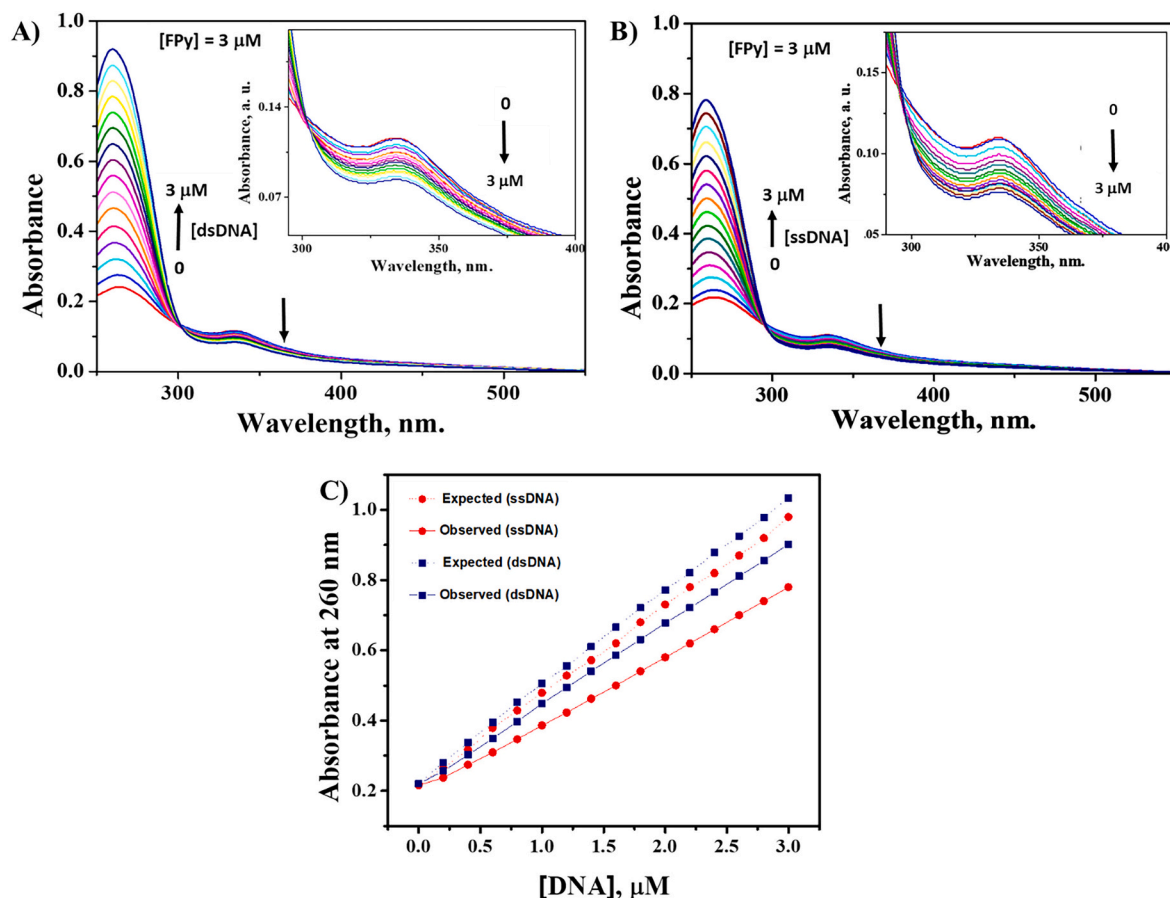
Fig. 2. Change in absorption spectra of **FPy** (3 μM) in phosphate buffer (10 mM; pH 7.4) with increasing concentration of **A)** dsDNA and **B)** ssDNA, **C)** Absorption changes at 260 nm in the presence and absence of **FPy** with increasing concentration of dsDNA and ssDNA. Expected values are sum of absorbance values corresponding to **FPy** and added dsDNA/ssDNA.

Organization of fullerenes is highly desirable in the field of nano-device fabrication due to its unique opto-electronic properties and is realized through different supramolecular assembly approaches [41–43]. Construction of ultrathin fullerene films is generally achieved by different solvent mediated techniques like liquid-liquid interface precipitation and Langmuir-Blodgett technique etc. [44–46] and is further advanced with the design of amphiphilic fullerenes and fullerene-polymer conjugates either through covalent linkages or non-covalent interactions [47–49]. The diverse molecularly ordered structures of fullerenes show high performance in optoelectronic devices such as organic solar cells [25], organic field effect transistors etc. due to its excellent physicochemical and electron transport properties [50]. Herein, we have achieved DNA assisted, long range, ordered assembly of fullerenes leading to micrometer sized ultrathin nanosheets through a facile non-covalent approach using a cationic fullerene amphiphile (**FPy**) and various DNA structures. Longer duplex DNAs such as linear λ-DNA and circular pBR322 plasmid DNA readily condense in presence of **FPy** to form nanosheet structures with sub-micrometer lateral dimensions. On the other hand, short single strand and double strand DNAs form extended nanosheets with significantly higher crystallinity. DNA binding of **FPy** through various non-covalent interactions, subsequent charge neutralization and change in hydrophilicity of **FPy**, possible fullerene-fullerene and fullerene-nucleobase π-π stacking interactions etc. contribute to the assembly of **FPy**/DNA nanosheet structures.

2. Materials and Methods

2.1. Materials

Reagents and materials for synthesis were purchased from Sigma-Aldrich, Alfa Aesar and Spectrochem chemical suppliers. Linear λ-DNA, circular plasmid DNA (pBR322 DNA) and short ssDNAs were purchased from Sigma Aldrich. The 20-mer DNA sequences used in the present studies are DNA1: 5′-CGT CAC GTA AAT CGG TTA AC-3′, DNA2: 5′-GTT AAC CGA TTT ACG TGA CG-3′ and DNA2-Cy3: 5′-Cy3-GTT AAC CGA TTT ACG TGA CG-3′. DNA1/DNA2 forms the duplex DNA (dsDNA) upon annealing while DNA2 and DNA2-Cy3 were used as single strands. The detailed synthesis and characterization of amphiphilic fullerene derivative, **FPy** was previously reported [51].

2.2. DNA Interaction Studies of FPy

For DNA interaction studies of **FPy**, all the experiments were performed in 10% DMSO-PBS mixture (10 mM PBS, 2 mM NaCl). The fullerene derivative was initially dissolved in DMSO and then diluted to obtain appropriate concentrations in 10% DMSO-PBS mixture. DNA interaction studies of **FPy** solutions (3 μM) were carried out in quartz cuvette with a path length of 1 cm. Small aliquots of DNA were added and monitored the absorbance using Shimadzu UV-2600 PC UV–Vis spectrophotometer. The fluorescence emission spectra were recorded on a SPEX FLUOROLOG-3 (FL3-221) spectrofluorimeter. Circular dichroism measurements were performed on a Jasco J-810 spectropolarimeter with a quartz cuvette having 1 mm path length. Fluorescence quenching
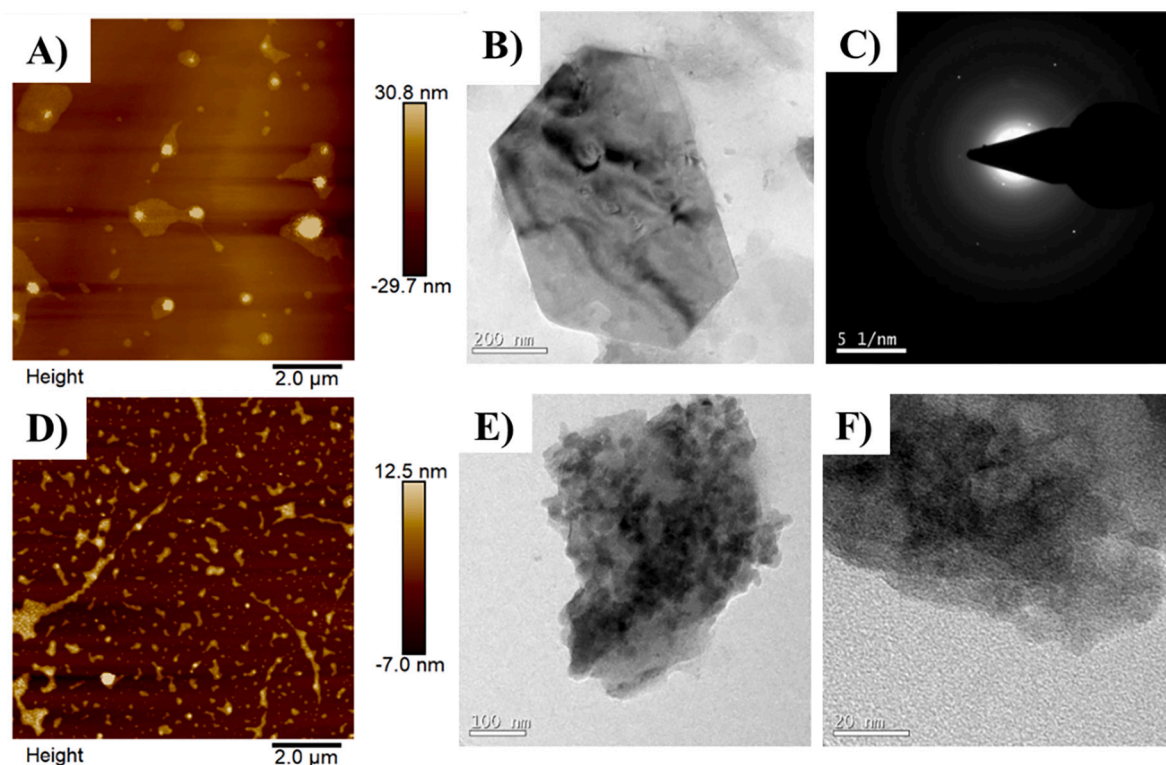
Fig. 3. AFM and TEM images of **A-B**) **FPy**/λ-DNA hybrid and **D-E**) **FPy**/pBR322 DNA hybrid; **C**) SAED pattern of nanosheet obtained from **FPy**/λ-DNA hybrid; **F**) Magnified TEM image of nanosheets obtained from **FPy**/pBR322 DNA.

experiments were done by recording the emission spectra of DNA2-Cy3 (1.5 μM) by adding different equivalence of **FPy**.

2.3. Morphological Analysis of FPy/DNA Hybrids

TEM samples were prepared by mixing DNA and **FPy** in 10% DMSO-PBS mixture with an incubation time of 30 min and dropped on carbon coated Cu grid. HRTEM measurements were carried out by using FEI-Tecnai G2 30, with EDAX at accelerating voltage of 300 kV. Samples were imaged with a Hamamatsu ORCA CCD camera. AFM samples were prepared by mixing DNA and **FPy** in 10% DMSO-PBS mixture with an incubation time of 30 min, dropped on mica surface and dried in air. AFM analyses were carried out with BRUKER MULTIMODE AFM operating with a tapping mode regime and a micro fabricated TiN cantilever tips (NT-MDT-NSG series) with a resonance frequency of 299 kHz and a spring constant of 20 to 80 Nm^{-1}. Confocal imaging was done using a NIKON A1R si spectral confocal microscope (Nikon, Tokyo, Japan) at a wavelength of 561 nm to view the red fluorescence.

3. Results and Discussion

3.1. DNA Interaction Studies

The amphiphilic fullerene derivative, **FPy** (Fig. 1A) has an appended pyridinium moiety which ensures molecular solubility in DMSO and 10% DMSO-PBS buffer and can readily interact with various DNA structures through non-covalent interactions. Fullerene is known to interact with DNA via groove binding while pyridinium moiety can undergo partial intercalation assisted by electrostatic interactions. [13,52,53] We have recently reported effective condensation of Calf Thymus-DNA by **FPy**, assisted by facile DNA interactions of fullerene and pyridinium moieties, leading to charge neutralization and subsequent condensation. [51] In the current article, we are discussing the interaction of **FPy** with various DNA structures such as λ-DNA, pBR322

DNA (plasmid DNA), and single and double stranded 20-mer oligonucleotides, which leads to the formation of significantly crystalline, few layer nanosheets.

Interactions of **FPy** with different DNAs were investigated initially through UV–Visible absorption spectroscopy. In a typical titration experiment, small aliquots of DNA were titrated against 3 μM solution of **FPy** in 10% DMSO-PBS with a maximum 5% dilution. The UV–Visible absorption changes during the titration of **FPy** against λ-DNA and pBR322 DNA are shown in Fig. 1B & 1C. **FPy** has an absorption maximum of 260 nm with a shoulder band around 334 nm. Since DNA bases also strongly absorb around 260 nm, a gradual enhancement of absorption around 260 nm is expected during the titration. On the other hand, both the chromophore interactions with DNA and DNA condensation are known to cause significant hypochromism at the chromophore absorption band and the DNA absorption band at 260 nm due to the enhanced masking of the chromophores [54]. Fig. 1B shows decrease in the absorption around 260 nm up to a λ-DNA concentration of 1.5 μg/mL, followed by a slow and gradual increase in the absorption around 260 nm. Similar observations were made during the titration of pBR322 plasmid DNA to **FPy** solutions (Fig. 1C). The hypochromicity around 260 nm in these cases are affected by the increasing λ-DNA/pBR322 plasmid DNA concentrations and hence a secondary plot of absorbance at 260 nm was used for further analysis which provides a clear picture of the changes in the 260 nm absorption band under the titration conditions (Fig. 1D). Thus we obtained significant hypochromism values of 34% and 36% around 260 nm upon addition of λ-DNA and pBR322 DNA, respectively to **FPy** solutions. The observed large hypochromicity and changes in the DNA absorption around 260 nm could be attributed to the efficient condensation of these DNA structures in the presence of positively charged **FPy** via charge neutralization [51,55,56]. The gradual enhancement of DNA absorption during the final additions could be due to the presence of excess DNA after completion of DNA condensation with available **FPy** molecules. It should be noted that relatively smaller hypochromic perturbations were observed for the fullerene absorption
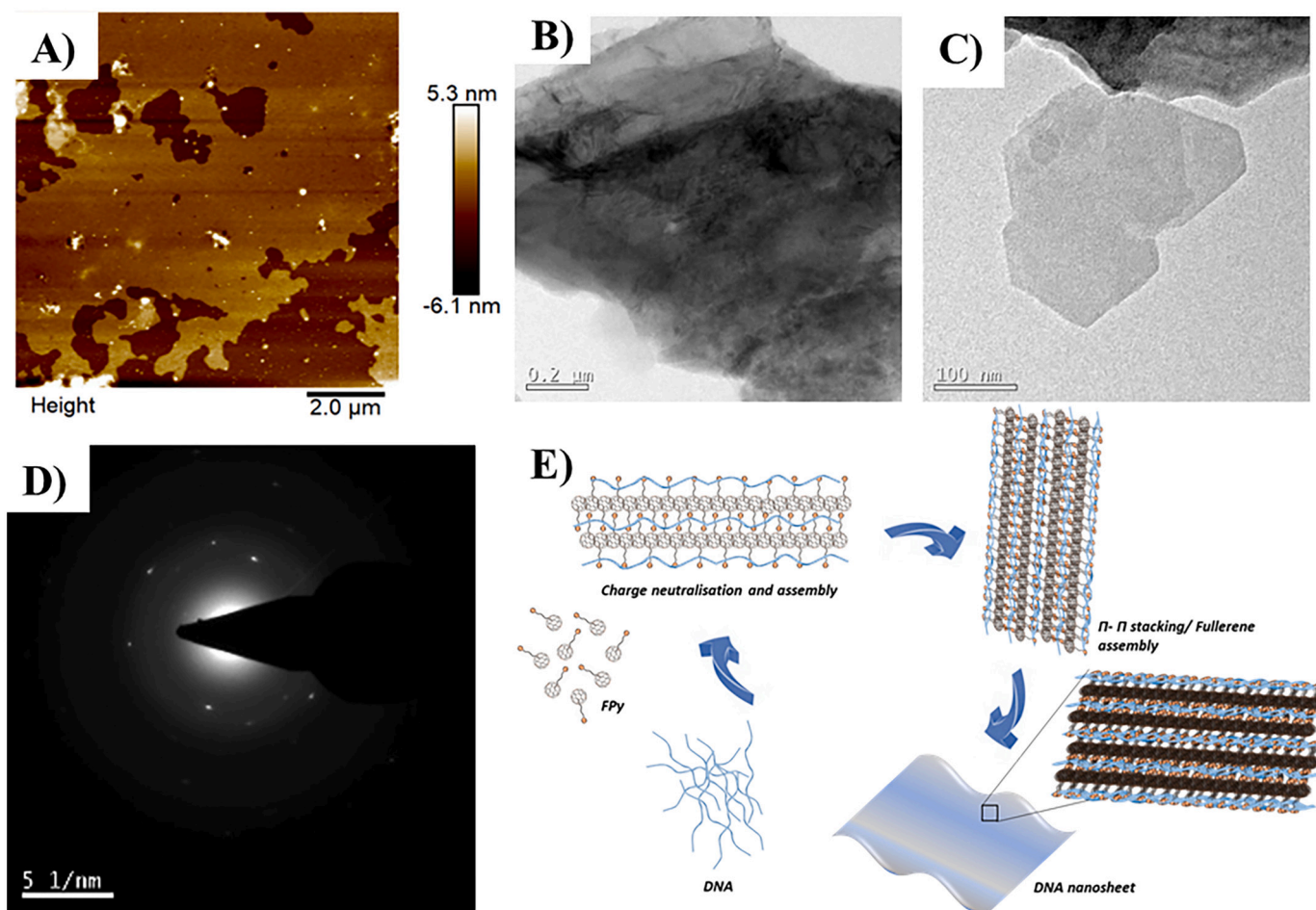
Fig. 4. A) AFM and **B–C)** TEM images of **FPy**/ssDNA hybrid, **D)** the corresponding SAED pattern, **E)** Cartoonic representation of nanosheet formation through **FPy**/ssDNAinteractions.
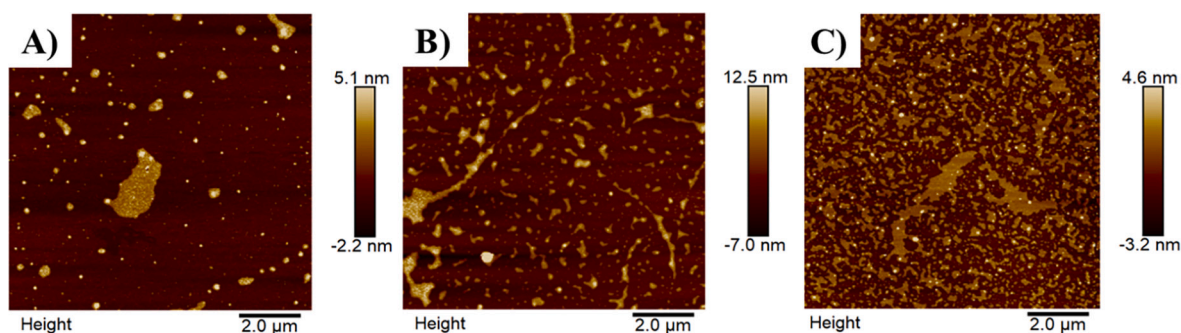

Fig. 5. AFM height image of **FPy**/pBR322 DNA hybrid at different concentration of **FPy; A)** 1 μM; **B)** 3 μM and **C)** 6 μM with constant pBR322 DNA concentration (3 μM).

around 334 nm, as shown in Fig. 1B and C, which are indicative of the interactions between **FPy** and long double strand DNA through non-covalent interactions, such as groove binding and partial intercalation.

In order to understand the role of DNA condensation in generating hierarchical nanostructures, we have investigated the interaction of **FPy** with 20-mer DNA oligonucleotide single and double strands. In principle, due to the short length of the 20-mer single strands and duplex, effective condensation of DNA may not be possible and hence we can differentiate the role of DNA condensation while using these single and double stranded DNA oligonucleotides [57]. Unmodified oligonucleotides (DNA1 & DNA2) were used for these studies, where DNA1/DNA2 form a duplex after annealing and DNA2 alone is used as single strand.

Upon successive addition of 20-mer dsDNA to **FPy**, DNA absorption around 260 nm gradually increased as expected due to overlapping DNA absorption, with a concomitant decrease in the fullerene absorption around 334 nm as shown in Fig. 2A. Similar changes were recorded in the case of ssDNA also (Fig. 2B). In order to understand the hypochromic changes in the case of dsDNA and ssDNA, we have compared the changes around 260 nm with control experiments where similar amounts of dsDNA and ssDNA were added to blank solutions. Analyses using secondary plots (Fig. 2C) revealed the difference in the absorption around 260 nm in both cases (with **FPy** and blank), which clearly showed a maximum hypochromicity of 13% for dsDNA and 20% for ssDNA. The changes in the absorption around 260 nm for λ-DNA/pBR322 DNA and
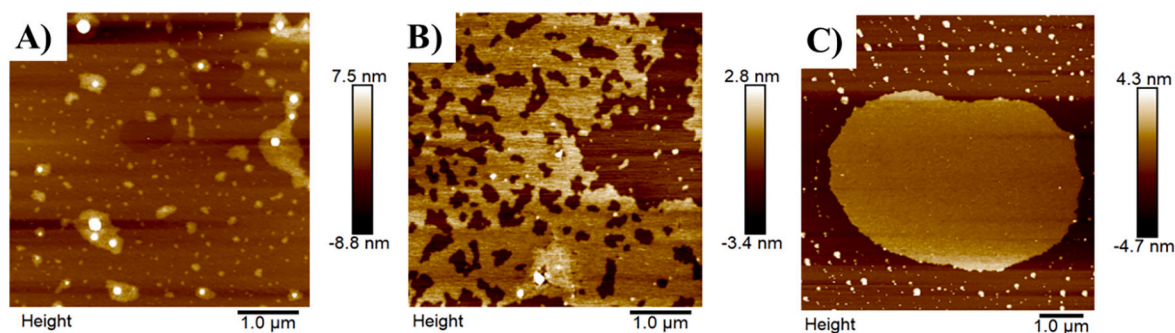
Fig. 6. AFM height image of **FPy**/ssDNA hybrid at different concentrations of **FPy**; **A)** 1 μM; **B)** 3 μM and **C)** 6 μM with constant ssDNA concentration (3 μM).
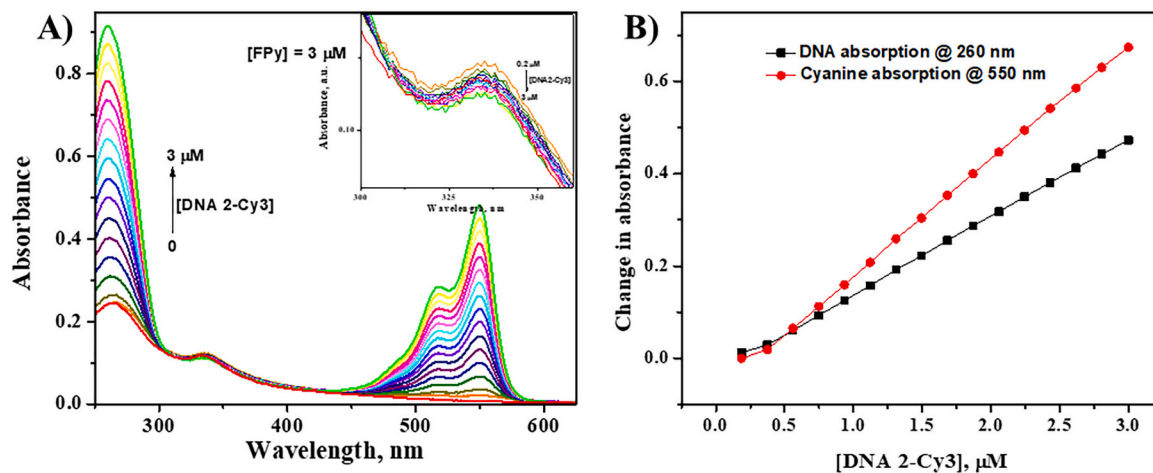

Fig. 7. A) Change in absorption spectra of **FPy** (3 μM) in phosphate buffer (10 mM; pH 7.4) with subsequent addition of DNA2-Cy3 (Inset: Zoomed portion indicating the absorption changes around 334 nm), **B)** Absorption changes at 260 nm (corresponds to DNA) and 550 nm (corresponds to Cyanine) with subsequent addition of DNA2-Cy3 to a fixed concentration of **FPy** (3 μM).

dsDNA are significantly different where we observed large hypochromicity (~36%) due to DNA condensation in the former case whereas only moderate hypochromicity (10–20%) was observed due to DNA binding interactions of fullerene in the latter case. On the other hand, upon increasing the dsDNA and ssDNA concentration, we have observed a maximum hypochromicity of 26% and 34%, respectively at the fullerene absorption band around 334 nm, with an isosbestic point at 302 nm. The observed higher hypochromic changes for the fullerene absorption in these cases are indicative of fullerene self-assembly/aggregation [58] in presence of 20-mer dsDNA/ssDNA. Similarly, the observed UV–Visible absorption changes of **FPy** in presence of dsDNA and ssDNA indicate efficient interactions with both single stranded and double stranded DNA suggestive of the major contribution of electrostatic interactions compared to the groove binding or intercalation. We observed a very small change (ΔTm ~1 °C) in the thermal denaturation studies of dsDNA in presence of **FPy** (Fig. S1) and negligible changes in the CD signals for **FPy**/DNA hybrid at higher **FPy** concentrations (Fig. S2), which further support the electrostatic binding interactions.

3.2. Morphological Studies

Atomic Force Microscopy (AFM) and Transmission Electron Microscopy (TEM) imaging techniques were used for investigating the morphology of various **FPy**/DNA hybrid nanostructures. The long linear λ-DNA (3 μg/mL) on interaction with **FPy** (3 μM) forms nanosheets having thickness around 10 nm and sub-micrometer lateral dimensions as shown in AFM (Fig. 3A) and TEM (Fig. 3B) images. These nanosheets, comprised of several stacked layers of fullerene and DNA, were

significantly crystalline as evident from the selected area electron diffraction (SAED) pattern (Fig. 3C). On the other hand, **FPy** in presence of circular pBR322 DNA (2.5 μg/mL) under similar experimental conditions, showed the formation of aggregated structures of smaller nanosheets having thickness around 6 nm (Fig. 3D–F). In both cases, the initial condensation of the longer DNA by **FPy**, further assist the organization of fullerenes through π-π interactions leading to nanosheet structures composed of DNA and fullerenes.

The AFM and TEM images of the nanosheet structures resulting from the interaction of **FPy** with short dsDNA and ssDNA are shown in Fig. S3 and Fig. 4. Interaction of **FPy** with dsDNA lead to extended nanosheets with lateral dimensions of several micrometers (Fig. S3), in contrast to the more condensed, sub-micrometer structures in the case of longer DNAs. Similarly, **FPy** and ssDNA interact efficiently to form larger and more crystalline nanosheets as evidenced by the AFM, TEM images and SAED pattern (Fig. 4A–D). As discussed earlier, due to the shorter length of the DNA strands, the contribution of DNA condensation is minimum, while charge neutralization via the electrostatic interaction between **FPy** and dsDNA/ssDNA play a major role in the organization of fullerenes and DNA in these nanostructures. Here the nanostructures are majorly guided by the fullerene-fullerene interactions and hence ssDNA with more structural flexibility could lead to more crystalline and extended nanosheets. Further the exposed hydrophobic nucleobases in ssDNA also may be contributing via π-π interactions with fullerenes. These results are in agreement with the UV–Vis titration experiments which predicted efficient interactions of **FPy** with ssDNA leading to extended fullerene/ssDNA assemblies. The presence of ssDNA across these nanostructures was confirmed via EDAX analysis of **FPy**/ssDNA
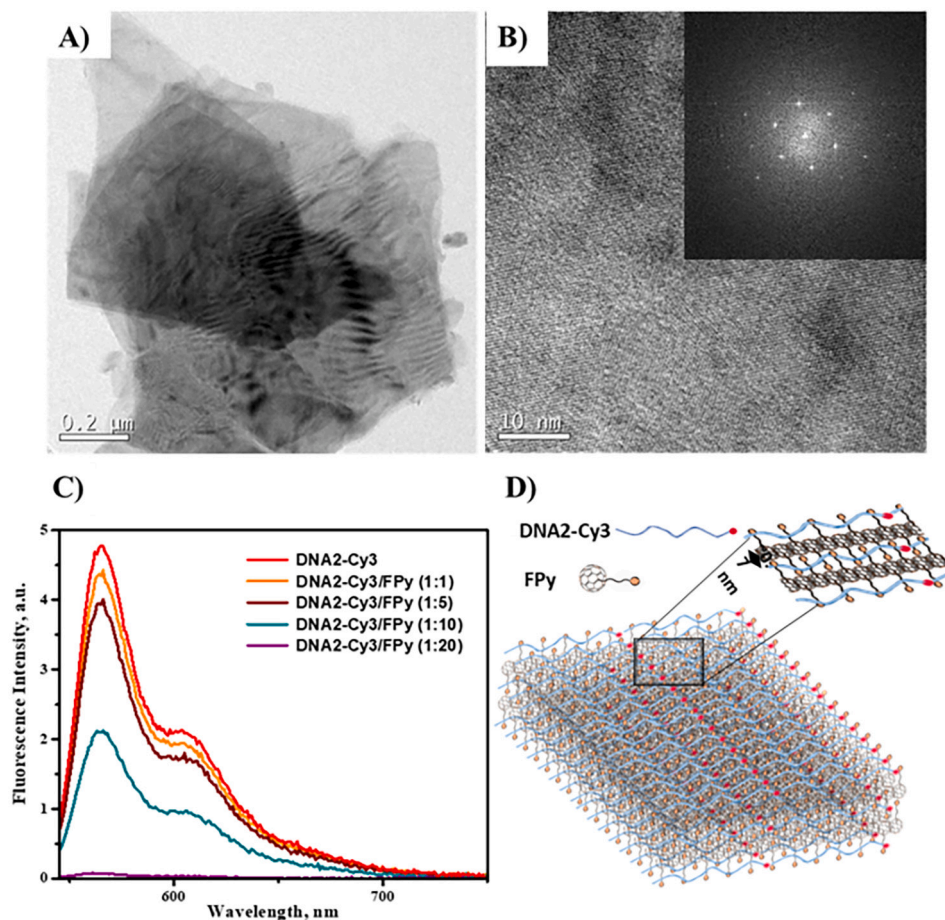
Fig. 8. A) TEM image of nanosheet formed through **FPy**/DNA2-Cy3 interaction, **B)** High resolution TEM image of **FPy**/DNA2-Cy3 hybrid (3 μM**:** 3 μM) (Inset: Corresponding FFT pattern **C)** Fluorescence spectra showing the quenching of DNA2-Cy3 (1.5 μM) emission with gradual addition of **FPy** and **D)** Schematic representation of nanosheets formed through DNA2-Cy3/**FPy**interaction.

hybrid nanosheets (Fig. S4). A cartoonic representation of the possible stacked arrangement of fullerenes and dsDNA/ssDNA is shown in Fig. 4E. Further, we have examined the gradual growth of **FPy**/ssDNA nanosheets with time using AFM analysis (Fig. S5), which showed association of initially formed smaller nanosheets with time, to form larger nanosheets. Although the lateral dimension of nanosheets increase with time, we have not observed extensive layer-by-layer growth of the sheets, which might be due to the excess amount of DNA present in the nanosheet which causes repulsive interaction between the layers, limiting the layer-by-layer growth.

To understand the role of **FPy** in the nanostructure formation, we monitored the concentration dependent growth of nanosheet structures through AFM analyses by varying the concentration of **FPy** from 1 μM to 6 μM with fixed concentrations of different DNAs. For example, Fig. 5 shows the changes of **FPy**/pBR322 DNA hybrid nanostructures with increasing **FPy** concentrations, where considerable increase in the amount of sub-micrometer sized nanosheets were observed, with minor association of the smaller sheets to form larger ones. On the other hand, the change in lateral dimensions of the nanosheets is more noticeable in the case of **FPy**/ssDNA hybrid (Fig. 6), where the initially formed smaller ultrathin nanosheets combine to form large nanosheets with micrometer lateral dimensions at 3 μM **FPy** concentration, and finally to larger nanosheet structures at 6 μM concentration of **FPy,** keeping similar thickness values around ~3 nm (Fig. S6–H). These results demonstrate that formation of ultrathin nanosheets is markedly facilitated by the increase in **FPy** concentrations.

3.3. Addressability of FPy/DNA Hybrid Nanostructures

The mutually assisted assembly of **FPy** and various DNA structures to form significantly crystalline, ordered nanosheets open up the possibility of engineering functional nanostructures with these building blocks. The addressability of these DNA nanostructures via functionalization of the short oligonucleotide strand was demonstrated using a fluorescent probe (Cyanine-3) modified single strand DNA (DNA2-Cy3). The formation of nanosheet structures by the interactions of **FPy** with DNA2-Cy3 was established using UV–Vis spectroscopy, AFM and TEM analyses. Further, we have probed the fluorescence of Cy3 to understand the assembly properties using fluorescence spectroscopy and imaging techniques. Fig. 7A, shows the changes in absorption spectra of **FPy** (3 μM) with increasing concentration of DNA2-Cy3. The changes in absorption at 260 nm corresponding to the combined absorption of **FPy** and DNA and at 550 nm corresponding to the Cy3 absorption are plotted against the concentration of DNA2-Cy3 (Fig. 7B). The decreased slope for the 260 nm band is indicative of the hypochromicity at 260 nm, as observed in the case of **FPy** binding with ssDNA. Morphological analysis of **FPy**/DNA2-Cy3 nanostructures using AFM and TEM techniques show the formation of nanosheets with lateral dimensions in the micrometer range (Fig. 8A–B), very similar to the earlier observed **FPy**/ssDNA nanosheet structures, but with significantly higher crystallinity as evident from the lattice fringes and corresponding Fast Fourier Transform (FFT) patterns. The interaction of hydrophobic Cy3 with fullerene through possible π-π interactions also could be contributing to the ordered arrangement and higher crystallinity of the **FPy**/DNA2-Cy3 nanosheets.

The fluorescence emission properties of DNA2-Cy3 in presence of different concentrations of **FPy** are given in Fig. 8C. Even at very low concentration (1.5 μM) of **FPy**, the fluorescence of DNA2-Cy3 strand showed significant quenching, which could be attributed to possible electron transfer from Cy3 to fullerene facilitated by the ordered assembly of fullerene and Cy3-modified ssDNA [59,60]. At **FPy** concentrations of ~30 μM, corresponding to total charge neutralization (1:20 ratio of DNA2-Cy3 to **FPy**), we observed complete quenching of fluorescence from DNA2-Cy3, which confirmed the **FPy**/ssDNA assembly. Further, the confocal fluorescence images of the assembled **FPy**/DNA2-Cy3 nanosheets (Fig. S7) showed fluorescence from the edges of the nanosheets corresponding to free fluorophores on the edges, whereas the cyanine fluorophores incorporated in the assembly got strongly quenched. Thus, these fluorescence experiments support the hypothesis that the short-oligonucleotides could be functionalized to demonstrate the addressability of **FPy**/DNA nanostructures. Fig. 8D schematically represent the possible ordered assembly of fullerenes and DNA2-Cy3 in these nanosheet structures.

4. Conclusion

In conclusion, we have demonstrated the differential interaction of an amphiphilic fullerene derivative, **FPy** with various DNA structures and the resulting **FPy**/DNA hybrid nanostructures were characterized using AFM and TEM imaging techniques. Longer double strand DNAs such as linear λ-DNA and circular pBR322 plasmid DNA readily condense in presence of **FPy** to form few layer nanosheets with submicrometer lateral dimensions. The assembly in this case is guided by initial DNA condensation and subsequent fullerene-fullerene interactions. On the other hand, **FPy** binds efficiently to shorter DNA strands such as 20-mer dsDNA and ssDNA primarily through electrostatic interactions and subsequent charge neutralization lead to significantly crystalline nanosheets with lateral dimensions in the micrometer range. Since DNA condensation is not facile in this case, binding interactions of amphiphilic **FPy**, subsequent charge neutralization and fullerene-fullerene interactions guide this assembly. In both cases, subtle changes in the hydrophilic-hydrophobic balance of the amphiphilic fullerene derivative upon interactions with DNA play a major role in the self-assembly process. Further, the addressability of the **FPy**/DNA nanostructures were demonstrated using a Cy3-modified ssDNA (DNA2-Cy3), which also forms highly crystalline nanosheets in presence of **FPy** and exhibit strong quenching of Cy3 fluorescence through possible electron transfer interactions with fullerenes in the **FPy**/DNA2-Cy3 assembly. The reported strategy of using amphiphilic fullerene derivatives and various DNA structures to control the assembly properties could find applications in DNA nanotechnology.

Author Statement

Anjali Bindu Ramesan: Methodology, Resources, Acquisition, Analysis, Interpretation of data and Writing- Original draft preparation.

Sandeepa Kulala Vittala: Synthetic Methodology.

Joshy Joseph: Conceptualization, Investigation, Supervision and Manuscript Writing.

Declaration of Competing Interest

There are no conflicts to declare.

Acknowledgements

Appendix A. Supplementary Data

Supplementary data to this article can be found online at https://doi.org/10.1016/j.jphotobiol.2021.112352.

References

[1] R. Hofsass, P. Ensslen, H.A. Wagenknecht, Control of helical chirality in supramolecular chromophore-DNA architectures, Chem. Commun. 55 (2019) 1330–1333.

[2] A. de la Escosura, P.G.A. Janssen, A.P. Schenning, R.J.M. Nolte, J.J.L. M. Cornelissen, Encapsulation of DNA-templated chromophore assemblies within virus protein nanotubes, Angew. Chem. Int. Ed. 49 (2010) 5335–5338.

[3] T. Kikuchi, S. Sato, D. Fujita, M. Fujita, Stepwise DNA condensation by a histone-mimic peptide-coated M12L24 spherical complex, Chem. Sci. 5 (2014) 3257–3260.

[4] S.K. Saraswathi, V. Karunakaran, K.K. Maiti, J. Joseph, DNA condensation triggered by the synergistic self-assembly of tetraphenylethylene-viologen aggregates and CT-DNA, Front. Chem. 9 (2021) 716771.

[5] V.A. Bloomfield, Condensation of DNA by multivalent cations - considerations on mechanism, Biopolymers 31 (1991) 1471–1481.

[6] A. Perico, G.S. Manning, Lamellar cationic lipid-DNA complexes from lipids with a strong preference for planar geometry: a minimal electrostatic model, Biopolymers 101 (2014) 1114–1128.

[7] D.A. Kondinskaia, A.A. Gurtovenko, Supramolecular complexes of DNA with cationic polymers: the effect of polymer concentration, Polymer 142 (2018) 277–284.

[8] E. Haladjova, S. Rangelov, C.B. Tsvetanov, S. Pispas, DNA encapsulation via nanotemplates from cationic block copolymer micelles, Soft Matter 8 (2012) 2884–2889.

[9] D. Kurzbach, C. Velte, P. Arnold, G. Kizilsavas, D. Hinderberger, DNA condensation with spermine dendrimers: interactions in solution, charge inversion, and morphology control, Soft Matter 7 (2011) 6695–6704.

[10] Y. Han, B. Zhu, Y. Chen, Z.S. Bo, Y.L. Chen, Amphiphilic dendrons with a pyrene functional group at the focal point: synthesis, self-assembly and generation-dependent DNA condensation, Polym. Chem. 8 (2017) 4798–4804.

[11] M. Ganguli, J.V. Babu, S. Maiti, Complex formation between cationically modified gold nanoparticles and DNA: an atomic force microscopic study, Langmuir 20 (2004) 5165–5170.

[12] C.M. Wu, W. Liou, H.L. Chen, T.L. Lin, U.S. Jeng, Self-assembled structure of the binary complex of DNA with cationic lipid, Macromolecules 37 (2004) 4974–4980.

[13] C. Klumpp, L. Lacerda, O. Chaloin, T. Da Ros, K. Kostarelos, M. Prato, A. Bianco, Multifunctionalised cationic fullerene adducts for gene transfer: design, synthesis and DNA complexation, Chem. Commun. (2007) 3762–3764.

[14] H. Isobe, W. Nakanishi, N. Tomita, S. Jinno, H. Okayama, E. Nakamura, Gene delivery by aminofullerenes: structural requirements for efficient transfection, Chem. Asian J. 1 (2006) 167–175.

[15] S. Pratihar, Y.V. Suseela, T. Govindaraju, Threading Intercalator-induced nanocondensates and role of endogenous metal ions in decondensation for DNA delivery, ACS Appl. Bio Mater. 3 (2020) 6979–6991.

[16] N.C. Seeman, DNA nanotechnology: novel DNA constructions, Annu. Rev. Biophys. Biomol. Struct. 27 (1998) 225–248.

[17] Q. Hu, H. Li, L. Wang, H. Gu, C. Fan, DNA nanotechnology-enabled drug delivery systems, Chem. Rev. 119 (2018) 6459–6506.

[18] D. Bousmail, P. Chidchob, H.F. Sleiman, Cyanine-mediated DNA nanofiber growth with controlled dimensionality, J. Am. Chem. Soc. 140 (2018) 9518–9530.

[19] H. Atsumi, A.M. Belcher, DNA origami and G-quadruplex hybrid complexes induce size control of single-walled carbon nanotubes via biological activation, ACS Nano 12 (2018) 7986–7995.

[20] X. Wang, C. Li, D. Niu, R.J. Sha, N.C. Seeman, J.W. Canary, Construction of a DNA origami based molecular electro-optical modulator, Nano Lett. 18 (2018) 2112–2115.

[21] T. Bayrak, S. Helmi, J.J. Ye, D. Kauert, J. Kelling, T. Schonherr, R. Weichelt, A. Erbe, R. Seidel, DNA-mold templated assembly of conductive gold nanowires, Nano Lett. 18 (2018) 2116–2123.

[22] K. Tapio, J. Leppiniemi, B.X. Shen, V.P. Hytonen, W. Fritzsche, J.J. Toppari, Toward single electron nanoelectronics using self-assembled DNA structure, Nano Lett. 16 (2016) 6780–6786.

[23] M.B. Avinash, T. Govindaraju, Architectonics: design of molecular architecture for functional applications, Acc. Chem. Res. 51 (2018) 414–426.

[24] M. Pandeeswar, S.P. Senanayak, T. Govindaraju, Nanoarchitectonics of small molecule and DNA for ultrasensitive detection of mercury, ACS Appl. Mater. Interfaces 8 (2016) 30362–30371.

[25] S. Müller, F. Manger, L. Graf von Reventlow, A. Colsmann, H.-A. Wagenknecht, Molecular chromophore-DNA architectures with fullerenes: optical properties and solar cells, Front. Chem. 9 (2021).

[26] S.K. Albert, H.V.P. Thelu, M. Golla, N. Krishnan, S. Chaudhary, R. Varghese, Self-assembly of DNA-oligo(p-phenylene-ethynylene) hybrid amphiphiles into surface-engineered vesicles with enhanced emission, Angew. Chem. Int. Ed. 53 (2014) 8352–8357.

[27] C. Dohno, S. Makishi, K. Nakatani, S. Contera, Amphiphilic DNA tiles for controlled insertion and 2D assembly on fluid lipid membranes: the effect on mechanical properties, Nanoscale 9 (2017) 3051–3058.

[28] S.K. Albert, I. Sivakumar, M. Golla, H.V.P. Thelu, N. Krishnan, K.L.J. Libin, Ashish, R. Varghese, DNA-decorated two-dimensional crystalline nanosheets, J. Am. Chem. Soc. 139 (2017) 17799–17802.

[29] M.Y. Li, C.L. Wang, Z.H. Di, H. Li, J.F. Zhang, W.T. Xue, M.P. Zhao, K. Zhang, Y. L. Zhao, L.L. Li, Engineering multifunctional DNA hybrid nanospheres through coordination-driven self-assembly, Angew. Chem. Int. Ed. 58 (2019) 1350–1354.

[30] Q. Li, J. Zhao, L. Liu, S. Jonchhe, F.J. Rizzuto, S. Mandal, H. He, S. Wei, H. F. Sleiman, H. Mao, C. Mao, A poly(thymine)–melamine duplex for the assembly of DNA nanomaterials, Nat. Mater. 19 (2020) 1012–1018.

[31] S.K. Vittala, S.K. Saraswathi, J. Joseph, Fullerene cluster assisted self-assembly of short DNA strands into semiconducting nanowires, Chem. Eur. J. 23 (2017) 15759–15765.

[32] H. Matsui, M. Ueda, A. Makino, S. Kimura, Molecular assembly composed of a dendrimer template and block polypeptides through stereocomplex formation, Chem. Commun. 48 (2012) 6181–6183.

[33] C.M. Spillmann, I.L. Medintz, Use of biomolecular scaffolds for assembling multistep light harvesting and energy transfer devices, J Photochem Photobiol C: Photochem Rev 23 (2015) 1–24.

[34] L. Rocard, D. Wragg, S.A. Jobbins, L. Luciani, J. Wouters, S. Leoni, D. Bonifazi, Templated chromophore assembly on peptide scaffolds: a structural evolution, Chem. Eur. J. 24 (2018) 16136–16148.

[35] T. Sugimoto, T. Suzuki, S. Shinkai, K. Sada, A double-stranded Helix by complexation of two polymer chains with a helical supramolecular assembly, J. Am. Chem. Soc. 129 (2007) 270–271.

[36] A. D'Urso, A. Mammana, M. Balaz, A.E. Holmes, N. Berova, R. Lauceri, R. Purrello, Interactions of a tetraanionic porphyrin with DNA: from a Z-DNA sensor to a versatile supramolecular device, J. Am. Chem. Soc. 131 (2009) 2046–2047.

[37] T. Nguyen, A. Brewer, E. Stulz, Duplex stabilization and energy transfer in zipper porphyrin–DNA, Angew. Chem. Int. Ed. 48 (2009) 1974–1977.

[38] H. Özhalıcı-Ünal, B.A. Armitage, Fluorescent DNA nanotags based on a self-assembled DNA tetrahedron, ACS Nano 3 (2009) 425–433.

[39] A. Ruiz-Carretero, P.G.A. Janssen, A.L. Stevens, M. Surin, L.M. Herz, A.P.H. J. Schenning, Directing energy transfer in discrete one-dimensional oligonucleotide-templated assemblies, Chem. Commun. 47 (2011) 884–886.

[40] P.G.A. Janssen, S. Jabbari-Farouji, M. Surin, X. Vila, J.C. Gielen, T.F.A. de Greef, M. R.J. Vos, P.H.H. Bomans, N.A.J.M. Sommerdijk, P.C.M. Christianen, P. Leclère, R. Lazzaroni, P. van der Schoot, E.W. Meijer, A.P.H.J. Schenning, Insights into templated supramolecular polymerization: binding of naphthalene derivatives to ssDNA templates of different lengths, J. Am. Chem. Soc. 131 (2009) 1222–1231.

[41] F.K.C. Leung, F. Ishiwari, T. Kajitani, Y. Shoji, T. Hikimi, M. Takata, A. Saeki, S. Seki, Y.M.A. Yamada, T. Fukushima, Supramolecular scaffold for tailoring the two-dimensional assembly of functional molecular units into organic thin films, J. Am. Chem. Soc. 138 (2016) 11727–11733.

[42] Y. Kuramochi, A. Satake, M. Itou, K. Ogawa, Y. Araki, O. Ito, Y. Kobuke, Light-harvesting supramolecular porphyrin macrocycle accommodating a fullerene-tripodal ligand, Chem. Eur. J. 14 (2008) 2827–2841.

[43] V.S. Nair, R.D. Mukhopadhyay, A. Saeki, S. Seki, A. Ajayaghosh, A pi-gel scaffold for assembling fullerene to photoconducting supramolecular rods, Sci. Adv. 2 (2016).

[44] P. Bairi, K. Minami, J.P. Hill, W. Nakanishi, L.K. Shrestha, C. Liu, K. Harano, E. Nakamura, K. Ariga, Supramolecular differentiation for construction of anisotropic fullerene nanostructures by time-programmed control of interfacial growth, ACS Nano 10 (2016) 8796–8802.

[45] S. Das, F. Herrmann-Westendorf, F.H. Schacher, E. Täuscher, U. Ritter, B. Dietzek, M. Presselt, Controlling electronic transitions in fullerene van der Waals aggregates via supramolecular assembly, ACS Appl. Mater. Interfaces 8 (2016) 21512–21521.

[46] R. Krishnan, S.B. Krishnan, B. Balan, K.R. Gopidas, Self-assembly and photoinduced electron transfer in a donor-beta-cyclodextrin-acceptor supramolecular system, J. Chem. Sci. 130 (2018).

[47] X. Zhang, C.-H. Hsu, X. Ren, Y. Gu, B. Song, H.-J. Sun, S. Yang, E. Chen, Y. Tu, X. Li, X. Yang, Y. Li, X. Zhu, Supramolecular [60]fullerene liquid crystals formed by self-organized two-dimensional crystals, Angew. Chem. Int. Ed. 54 (2015) 114–117.

[48] M. Hufnagel, M.-A. Muth, J.C. Brendel, M. Thelakkat, Fullerene-grafted copolymers exhibiting high electron mobility without nanocrystal formation, Macromolecules 47 (2014) 2324–2332.

[49] F. Giacalone, N. Martín, F. Wudl, Fullerene-containing polymers: an overview, in: Fullerene Polymers, 2009, pp. 1–14.

[50] S. Das, M. Presselt, Progress and development in structural and optoelectronic tunability of supramolecular nonbonded fullerene assemblies, J. Mater. Chem. C 7 (2019) 6194–6216.

[51] S.K. Vittala, J. Joseph, Chiral self-assembly of fullerene clusters on CT-DNA templates, Faraday Discuss. 207 (2018) 459–469.

[52] M.H. Alshehri, B.J. Cox, J.M. Hill, C-60 fullerene binding to DNA, Eur. Phys. J. B 87 (2014).

[53] C. Song, Y.Q. Chen, S.J. Xiao, L. Ba, Z.Z. Gu, Y. Pan, X.Z. You, Assembly of fullerene arrays templated by DNA scaffolds, Chem. Mater. 17 (2005) 6521–6524.

[54] Y. Lu, J. Lv, G. Zhang, G. Wang, Q. Liu, Interaction of an anthracycline disaccharide with ctDNA: investigation by spectroscopic technique and modeling studies, Spectrochim. Acta A Mol. Biomol. Spectrosc. 75 (2010) 1511–1515.

[55] V.A. Bloomfield, DNA condensation by multivalent cations, Biopolymers 44 (1997) 269–282.

[56] K. Besteman, K. Van Eijk, S.G. Lemay, Charge inversion accompanies DNA condensation by multivalent ions, Nat. Phys. 3 (2007) 641–644.

[57] V.A. Bloomfield, Condensation of DNA by multivalent cations: considerations on mechanism, Biopolymers 31 (1991) 1471–1481.

[58] D.M. Guldi, H. Hungerbuehler, K.-D. Asmus, Unusual redox behavior of a water soluble malonic acid derivative of C60: evidence for possible cluster formation, J. Phys. Chem. 99 (1995) 13487–13493.

[59] F. Meng, F. Hua, K. Chen, H. Tian, L. Zuppiroli, F. Nüesch, Synthesis of novel cyanine–fullerene dyads for photovoltaic devices, J. Mater. Chem. 15 (2005) 979–986.

[60] J. De Jonghe-Risse, J. Heier, F. Nüesch, J.-E. Moser, Ultrafast charge transfer in solid-state films of pristine cyanine borate and blends with fullerene, J. Mat. Chem. A 3 (2015) 10935–10941.